UNIVERSITEIT GENT

FACULTY OF SCIENCES
DEPARTMENT GEOLOGY AND SOIL SCIENCE

MANIFESTATIONS AND GEOLOGICAL CHARACTERISTICS OF BUBBLE-RELEASING METHANE SEEPS IN THE BLACK SEA, IN THE SW PACIFIC OCEAN AND IN LAKE BAIKAL

LIEVEN NAUDTS

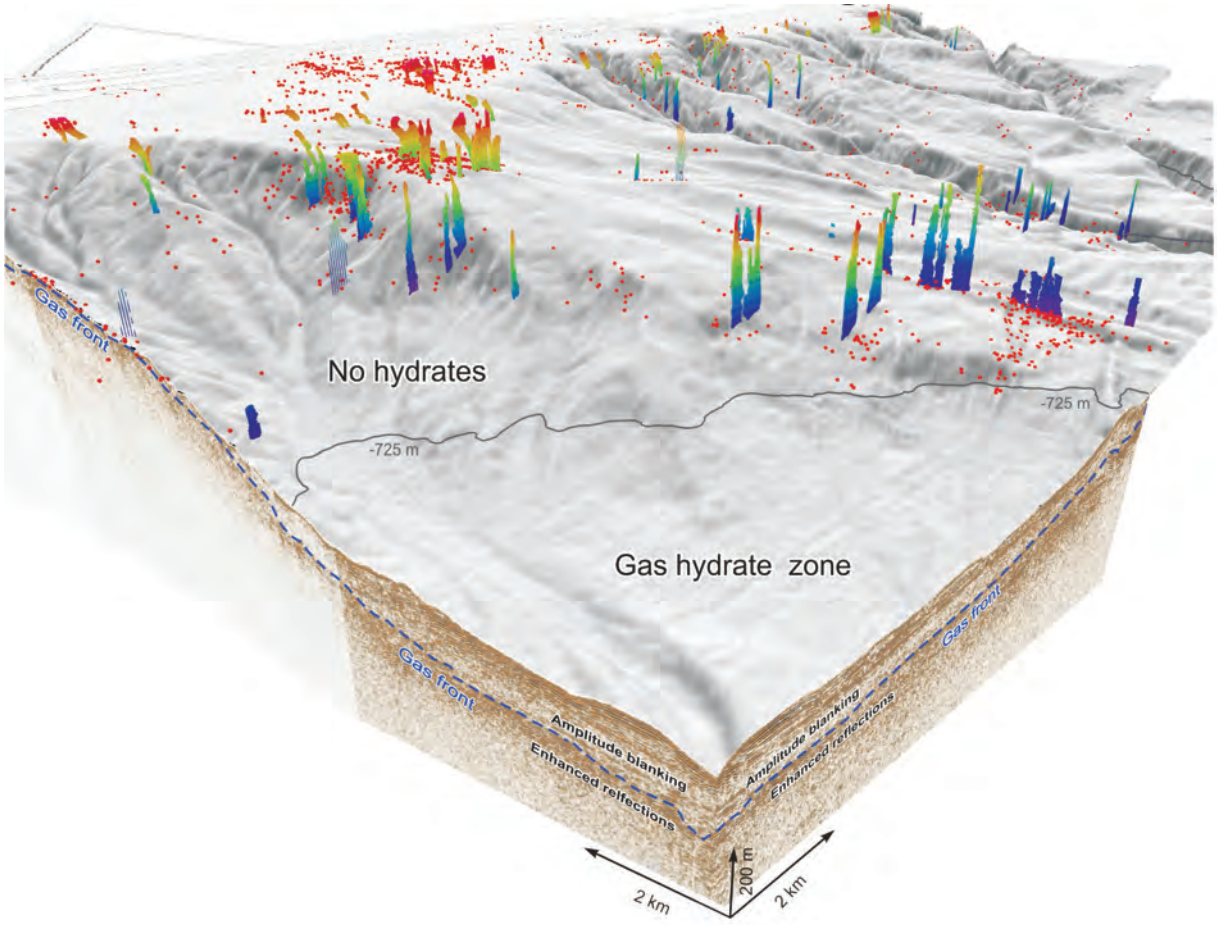

Thesis submitted in partial fulfilment of the requirements for
the degree of Doctor in Sciences, Geology
Academic Year 2009-2010

Faculteit Wetenschappen
VAKGROEP GEOLOGIE EN BODEMKUNDE
RCMG

UNIVERSITEIT GENT

FACULTY OF SCIENCES
DEPARTMENT GEOLOGY AND SOIL SCIENCE

MANIFESTATIONS AND GEOLOGICAL CHARACTERISTICS OF BUBBLE-RELEASING METHANE SEEPS IN THE BLACK SEA, IN THE SW PACIFIC OCEAN AND IN LAKE BAIKAL

MANIFESTATIES EN GEOLOGISCHE KARAKTERISTIEKEN VAN GASBELLEN-PRODUCERENDE METHAANBRONNEN IN DE ZWARTE ZEE, IN DE ZW STILLE OCEAAN EN IN HET BAIKALMEER

LIEVEN NAUDTS

PROMOTER: PROF. DR. MARC DE BATIST
CO-PROMOTER: PROF. DR. JENS GREINERT

FACULTY OF SCIENCES
DEPARTMENT OF GEOLOGY AND SOIL SCIENCE
RESEARCH UNIT RENARD CENTRE OF MARINE GEOLOGY

Thesis submitted in partial fulfilment of the requirements for
the degree of Doctor in Sciences, Geology
Academic Year 2009-2010

Faculteit Wetenschappen

VAKGROEP GEOLOGIE EN BODEMKUNDE

RCMG

To refer to this thesis:
Naudts L., 2010. Manifestations and geological characteristics of bubble-releasing methane seeps in the Black Sea, in the SW Pacific Oceaan and in Lake Baikal, Ph.D. thesis, Ghent University, Ghent, Belgium

Lieven Naudts carried out the presented research as scientific personel in the framework of the EU-funded CRIMEA project (2003-2005) and as an assistent of the Department of Geology and Soil Science (2005-2010). For both mandates the research was carried out at the research unit Renard Centre of Marine Geology of the Ghent University, Ghent, Belgium.

Cover illustration:
3D view showing multibeam bathymetry with detected seeps and two GI-gun seismic profiles in the Dnepr paleo delta, Black Sea (Naudts et al., 2006).

Members of the Reading Committee:

Prof. Dr. Marc De Batist (Ghent University, Belgium): promoter

Prof. Dr. Jens Greinert (NIOZ, The Netherlands –
Guest Professor Ghent University, Belgium): co-promoter

Prof. Dr. Gert J. de Lange (Utrecht University, The Netherlands)

Prof. Dr. Aurélien Gay (Université Montpellier, France)

Members of the Examination Committee:

Prof. Dr. Jean-Pierre Henriet (Ghent University, Belgium): chairman

Prof. Dr. Marc De Batist (Ghent University, Belgium): secretary

Prof. Dr. Jens Greinert (NIOZ, The Netherlands –
Guest Professor Ghent University, Belgium): co-promoter

Prof. Dr. Gert J. de Lange (Utrecht University, The Netherlands)

Prof. Dr. Aurélien Gay (Université Montpellier, France)

Prof. Dr. Rudy Swennen (Katholieke Universiteit Leuven, Belgium)

Prof. Dr. Patric Jacobs (Ghent University, Belgium)

Prof. Dr. Jeffrey Poort (IPGP, France –
Guest Professor Ghent University, Belgium)

ACKNOWLEDGEMENTS - DANKWOORD

Langs deze weg wil ik iedereen bedanken die me de voorbije zeven jaar geholpen en gesteund heeft, of er gewoon was op de juiste plaats, op het juiste moment.

Als eerste wil ik mijn promotor, Marc De Batist, bedanken voor de vele kansen die ik gekregen heb, en voor onze aangename samenwerking de voorbije jaren. Tist, bedankt dat je mijn leefwereld zoveel groter gemaakt hebt dan Lokeren en het Waasland. Bedankt voor je kritische maar steeds opbouwende commentaren met als doel een beter wetenschapper van mij te (proberen) maken. Een dikke merci!!

A second very big influence during the last seven years has been my co-promoter, Jens Greinert. Jens thanks for sharing your knowledge and your drive to get things done! I am sure without you this work would not have been possible!! You and Edna have always been the people who made me feel at home be it in Kiel, Wellington, Gent or on Texel! Herzlichen Dank!

Een andere sterke aanwezige de afgelopen jaren was Jean-Pierre Henriet. Je onnavolgbare levenslust gaf me steeds het gevoel dat alles mogelijk was/is. Bedankt Jean-Pierre en geniet van jouw nieuw leven!

Vervolgens wil ik Jeffrey Poort bedanken om me in contact te brengen met Baikal, heatflow en gas hydraten. Jeffrey, jij bent ook diegene die me Rusland en alles wat Russisch is, heeft leren kennen. Jij hebt me ook getoond dat je op een rustige manier toch een duidelijke mening kunt hebben, dit zowel op wetenschappelijk als op sociaal en menselijk vlak. Het feit dat we sinds jouw vertrek uit het RCMG nog steeds contact hebben, en dit zowel professioneel als vriendschappelijk, zegt heel veel!!

Since my research is based on the data acquired during many international expeditions, I want to thank all captains, crew members and participants I worked and lived with for their hard work, for allowing a safe return to the harbor and just for having a good time (ships: R.V. Vodyanitskiy, R.V. Vereshchagin, R.V. Titov, R.V. Sonne, R.V. La Licorne, R.V.I.B. Nathaniel B. Palmer and R.V. Belgica).

Of all the people I have ever been on expedition with my biggest gratitude goes out to Oleg Khlystov! Oleg, we have been on 5 different Baikal expeditions; on land, on water, on ice and even underwater! Thank you for getting all the expedition going, for your hard work during the expeditions and for bringing my Russian language skills to a higher level. I would also like to thank you and your family for sharing your home with me! Thanks Oleg, Sveta, Katya and Rita for making me feel at home in Irkutsk. Furthermore I would like to thank all new friends I made in Irkutsk, Moscow and St.-Petersburg during the last years. A special thanks goes out to Andrey Habuev, Alexey Krylov, Oleg Belousov, Kolya, Vladimir Slobodyan, Alexey Guruliev, Marina Kulikova and all other Russians who made my stay in Russia pleasant and unforgettable. Спасибо большое!!!

I would also like to thank our Japanese colleagues for the nice collaboration on Lake Baikal. Thanks, Hitoshi Shoji, Shinya Nishio, Akihiro Hachikubo, Masato Kida and Hirotsugu Minami. 本当にありがとうございます

Before exploring Lake Baikal, I have spent 12 weeks on the Black Sea in 2003 and 2004. It has been a while but I didn't forget how nice the CRIMEA expeditions were. We did good science and lots of friendships were forged. Research expeditions should always be like this! I would like to thank Oliver Schmale, Lyobomir Dimitrov, Atanas Vassiliev, Dan McGinnis, Christian Holzner, Jan Klerkx, Rolf Kipfer, Stan Beaubien, Oleg Kravchuk, Vladimir Popovichev, Dimitry Evtushenko, Yuriy Artemov, Sergey Gulin, Viktor Egorov, Liza Logvina, Manuella Delalande, Joerg Bialas, Peter Linke, Laurent Bergonzini, Matthias Haeckel, Marilena Calarco, Martin Piper, Peter Staelens, Jeffrey Poort, Jeroen Vercruysse, Marc De Batist, Sonia Papili, Pieter Van Rensbergen, Koen De Rycker and so many others for these fantastic expeditions.

The last couple of years, research expeditions at RCMG have been focused around our small yellow unmanned submarine robot, ROV Genesis aka SUZEE! I was fortunate to join SUZEE on cruises off New Zealand and around the Antarctic Peninsula! For the cruise on R.V. Sonne I would like to thank

Andrew “Cartoonman” Thurber, Kerstin Kröger, Kristin Krieger, Ruth Martin, Jens Schneider, Jens Greinert, Edna Huetten, Dethlev Cordts, Kevin Faure, Matthias Marquardt, Marlene Bausch and others for making us Belgians feel welcome on this German cruise, for teaching me how to play fussball and for the fantastic road trip afterwards. And of course Jeffrey Poort, Dries Boone and Marc De Batist are thanked for experiencing this cruise with me.

I also would like to thank the people who I have spent this last winter with, sailing around the Antarctic Peninsula on R.V.I.B. Nathaniel B. Palmer. Thank you for bearing my presence the last two months before the almighty dissertation deadline. A big thanks goes out to Craig Smith, Doug Fox and David Honig for the entertaining and hydrated fussball matches. I also like to thank the following people who got me going when it was most needed; Caroline Lavoie, Sarah Park, Yuribia Munoz, Laura Grange, Maria Stenzel, Maria Vernet, Paul Huckins, Dmitriy Tizon, Andy Nun, Tony, Daniel Powers, Jeremy Lucke, Buzz Scott, Mike McCormick, Adam Jenkins, Kim Roe, Debra Tillinger, Alejandra, Mike Lewis, Katleen Gavahan, Sheldon Blackman, Lindsey Ekern, Greg Balco, Erin Pettit, Ross Hein, Matthias Cape, Martin Truffer, Bruce Huber, Scott Ishman, Amy Leventer, Stephany Brachfeld, Ted Scambos, Ronald Ross, Eugene Domack and others. A very special thanks to Dries Boone and Katrien Heirman who kept my head above water during this two-month-during ordeal! I will never forget this!

Besides these large-scale expeditions, I also enjoyed smaller cruises like the multibeam mapping of Lake Geneva. Thanks to Vincent Sastre, Philippe Arpagaus, Flavio Anselmetti, Walter Wildi and of course Jens Greinert for making this a nice, successful and very enjoyable expedition.

In addition to expeditions, scientists also go to conferences, therefore I would like to thank people who have stimulated me in seep research and were fun to hang out with. Thank you Alan Judd, Martin Holvand, Dan Orange, Ira Leifer, Katja Heeschen, Vas Kitidis, Alina Stadnitskaia, Tatyana Matveeva, Tom Lorenson and so many others!!

Ik wil ook alle collega’s en vrienden van het RCMG bedanken voor de aangename werksfeer en de gezellige momenten buiten de werkuren. Aangezien ik zeven jaar aan dit doctoraat heb gewerkt, heb ik velen zien komen en gaan. Veel collega’s, die ondertussen ex-collega’s zijn geworden, zijn super belangrijk geweest tijdens de beginjaren van dit doctoraat. Eerst en vooral een dikke merci aan Rob Hus die me sterk geholpen heeft tijdens mijn licentiaatsthesis en tijdens de daaropvolgende IWT-aanvragen. Rob, was ook diegene die samen met o.a. Johan De Grave en Vanessa Coisne me reeds liet proeven van de Russische geneugten. Hij en Johan introduceerden me in het minivoetbal en zorgden er voor dat ik terug begon te sporten na het basketbal. Ook onvergetelijk waren Ben De Mol, Francois Charlet, Yannick Imbo, Pieter Van Rensbergen, Veerle Huvenne en de nog steeds aanwezige David Van Rooij. Deze mensen waren de eerste doctoraatsstudenten die ik leerde kennen, en zij hebben daardoor mijn visie op wetenschap en op de wereld erbuiten mee bepaald. Een speciale merci voor Peter Staelens met wie ik een studententijd beleefde nadat ik afgestudeerd was…onvergetelijk! Andere mensen die ik wil bedanken, en die spijtig genoeg reeds verdwenen zijn uit het RCMG, zijn Els Verfaillie, Samuel Deleu, Isabelle Du Four, Julie Reveillaud, Vera Van Lancker en Kristien Schelfaut. Ik wil natuurlijk alle huidige collega’s bedanken; Marcske, Tine, Koen, Andres, Anita, Javiera, Rindert, Lies en Sonja. En in het bijzonder, de “puntje drie” of “.3” mensen, voor de stoomafblazende discussies aan de overkant, merci Dries, Jeroen, Wim, Matthias, Hans, Maarten, Mieke, Katrien en Jasper. Wie ik natuurlijk niet mag vergeten bedanken zijn Mieke Mathys, Davy Depreiter en Anneleen Foubert. Mieke, Davy en Anneleen bedankt dat jullie kunnen samenleven hebben met mij in een bureau en voor de instandhouding van de Lokeren/Waasland connectie binnen het RCMG.

Daarnaast wil ik ook nog de andere (ex-)collega’s en vrienden bedanken die ik leerde kennen binnen de S8 en binnen UGent; Stijn De Schepper, Kenneth Mertens, Johan De Grave, Thijs Vandenbroucke, Laura D’ heer, Lot Cole, Johan Reyns, Geraldine Nolf, Griet van Waes, Heleen Vanneste, Mieke Thierens, Wim Malfait, Frederik “Elvis” Goethals, Eva De Boever, Thomas Verleye, Tim Debacker, Lois Maignien, Cedric Corteel, Koen Verhoeven, Stijn Glorie, Jan Dewanckele, Veerle

Cnudde, Stephen Louwye, Jacques Verniers, Patric Jacobs, en zoveel andere proffen, doctoraatstudenten, thesisstudenten (Claudia, Elke, Joke, Joris, Lies, Maud, Michael, Myriam, Nele T., Nele V., Robbert, etc.) en (mede)studenten voor de toffe excursies, de Friday Beers, en voor de interessante gesprekken,… die mijn verblijf de afgelopen 15 jaar in de S8 onvergetelijk gemaakt hebben.

Verder wil ik nog mijn vrienden bedanken die, ondanks mijn veelvuldige afwezigheid, ervoor gezorgd hebben dat ik nog een leven had buiten de wetenschap en de S8. Dries, Bram, Wim en Kristof bedankt voor de amusante etentjes! Bjorn en Koen, merci voor onze late/vroege uitstapjes met als hoogtepunt het weekendje Berlijn! Evy, Wim, Stan en Stijn bedank ik voor de leuke quizzen en de lopers, jullie voor de maandelijkse etentjes. De heroïsche koerstochten en mountainbike weekends in de Vlaamse en Waalse Ardennen en in de Vogezen met de fietsersbende zou ik voor geen geld willen gemist hebben. Ook de minivoetbal met de G8 en GEO's zorgde voor de nodige ontspanning. Hopelijk vind ik na dit doctoraat terug de tijd om te komen shotten.

Ten slotte, wil ik de belangrijkste mensen in mijn leven bedanken. Eerst en vooral bedank ik mijn vader. Pa, je hebt er altijd voor gezorgd dat ik kon doen wat ik wou doen. Je hebt er voor gezorgd dat ik kon studeren en blijven studeren ondanks dat het er op sommige momenten niet zo rooskleurig uitzag. Je was er steeds tijdens alle moeilijke momenten. Ook bedankt voor de werken in ons huis, ook toen ik er niet was. Naast mijn pa, wil ik ook mijn zus Annick en haar vriend Louk bedanken, die mij gesteund hebben op allerlei manieren en op alle mogelijke momenten. Verder dank ik ook alle andere Naudtskes!!

Griet, mijn werk en dit doctoraat heeft de voorbije jaren en vooral dit laatste jaar het grootste deel van ons leven opgeëist. Ik besef dat het niet vanzelfsprekend was dat ik tijdens de laatste 9 maand gedurende 5 maand op campagne geweest ben. En toen ik thuis was moest ik tijdens het weekend en 's avonds ook nog aan dit doctoraat werken. Ik ben zeer blij dat we ondanks alles samen door deze moeilijke periode geraakt zijn. Ik kan je niet genoeg bedanken voor je steun!!!! Ik wil ook jouw familie (Agnes, Filip, Bart, Els, Tine, Pepijn, Floor, Rien, Bram, Koen en Beryl) en jouw vrienden bedanken die jou en mij gesteund hebben de laatste jaren!

Bedankt iedereen! Ook de mensen die ik vergeten ben en misschien niet met naam genoemd heb! Ik wil dit gerust goedmaken met een Duvel!

Lieven
Oostakker
maart 2010

SUMMARY

Bubble-releasing methane seeps, often referred to as gas seeps or cold seeps, are locations at the seafloor or lakebed where gas, mainly methane, is transferred as a free gas phase (bubbles) from the sediments into the overlying water column. Methane release occurs widespread in the world oceans and can be found on active and passive continental margins ('cold seeps') and at the ocean spreading centers ('hot vents'). Gas seeps have engendered a substantial research effort worldwide because of their potential impact on the geosphere, the biosphere, the hydrosphere and the atmosphere. They can support unique endemic ecosystems of highly diverse organisms (bacteria, tube worms, clams, etc.) associated with authigenic carbonate or barite precipitation. Seeps also have an important economical value because they can be indications for shallow or deep hydrocarbon reservoirs. Recently substantial research has been carried out to better understand and assess the contribution of methane emission from marine and lacustrine cold seeps to the geological and global atmospheric methane budget. Given that methane is a very strong greenhouse gas, a correct assessment of these budgets is needed to better understand and scale the impact human activities have on the global atmospheric methane budget and consequently on global climate change. The amount of methane released by seeps, at the seafloor, into the water column and possibly into the atmosphere is strongly variable and largely unknown. The main problem in obtaining reliable regional and global estimates is the uncertainty in the actual area of active seepage and the temporal variability of the seepage intensity and activity. Until the distribution and activity of methane seeps is better understood, seeps should not be neglected as an atmospheric methane source.

Over the last seven years, we have studied cold seep sites around the world at different geological settings to understand which are the main geological controls affecting gas-bubble release and to see if there are differences in seepage-control related to these distinct geological and plate-tectonic environments. Seeps were studied in the NW Black Sea (a passive continental margin), in the SW Pacific Ocean (an active continental margin) and in Lake Baikal (a rift lake). In all three cases the presence or absence of seepage is directly or indirectly related to gas hydrates. This study was mainly based on hydro-acoustic investigations (single- and multibeam, side scan sonar, seismics), sea-floor observations (ROV, submersible, TV-sled) and sediment sampling.

The first study area, the Dnepr paleo-delta on the continental margin of the northwestern Black Sea is well-known for the abundant presence of shallow gas and gas seeps and is probably one of the most active seep sites in the world. We studied the relation between the spatial distribution of methane seeps, sea-floor morphology and subsurface structures based on detailed multibeam, seismic and hydro-acoustic water-column investigations. This study was carried out within the EU-funded CRIMEA project that focused on the transfer of methane from the seafloor through the water column and into the atmosphere from submarine high-intensity methane seeps in the Black Sea. During the CRIMEA expeditions almost 3000 individual seeps were detected on echosounding records in the Dnepr paleo-delta. All seeps are located in the transition zone between the continental shelf and slope, in water depths of -66 to -825 m. The integration of geophysical data indicated that the seeps are not randomly distributed, but are concentrated in specific locations. The depth limit for 99.5% of the detected seeps coincides with the phase boundary of pure methane hydrate at -725 m water depth. This suggests that gas hydrates, where stable, can act as a buffer for the upward migration of methane gas and prevent seepage of methane bubbles into the water column. Higher up on the margin, gas seeps occur preferentially in particular morphological and geological contexts. On the continental slope and shelf, fluid flow is focused by the occurrence of a widespread impermeable sediment cover. As a result seeps are concentrated on crests of sedimentary ridges, in the vicinity of canyons, near submarine landslides or along filled channels. This subsurface focusing was observed on seismic data that show the presence of a distinct "gas front" within the sea-floor sediments that locally domes up to the seafloor where gas bubbles were detected in the water column. On the continental shelf 600 active bubble-releasing seeps were detected in water depths ranging from -72 m to -156 m, often in association with pockmarks. The seeps systematically occur in areas with a higher-than-average acoustic backscatter response on side scan sonar and multibeam recordings. Based on integrations of all datasets (geophysics, grain-size distribution, geochemistry), we suggest

that the observed relation is the result of ongoing seepage and the precipitation of methane-derived authigenic carbonates (MDACs) in the sediment. The MDACs lead to the self-sealing of fluid pathways by carbonate clogging, followed by relocation of the fluid pathways and seeps around the cemented, impermeable areas. Our analysis shows that backscatter data can be used as a proxy for seep densities to extrapolate methane fluxes from the seabed. The complete integration of all data sets indicates that the spatial distribution of methane seeps in the Dnepr paleo-delta is mainly controlled by the gas-hydrate stability zone (GHSZ), by morphology, by the underlying stratigraphy and by sediment properties.

In the SW Pacific Ocean east of New Zealand, several visual observations and measurements of physical properties were performed with a ROV (Remotely Operated Vehicle) and other video-guided platforms at two seep sites on the Hikurangi Margin; Faure Site and LM-3. This research was carried out during the 'New Vents' SO191 cruise during which the activity and distribution of seep sites on the gas-hydrate-bearing Hikurangi Margin were subjected to a highly detailed interdisciplinary study. The ROV allowed first ever visual observations of bubble-releasing seeps at the Hikurangi Margin. At Faure Site, bubble release was monitored during several dives, up to periods of 20 minutes. During the ROV-2 dive, this resulted in the observation of six outbursts, each lasting one minute at a three minute interval. These violent outbursts were accompanied by the displacement and resuspension of sediment grains and the formation of small depressions showing what is possibly an initial stage of pockmark formation. During subsequent dives at this bubble site, bubble release was rather constant and the previously observed outbursts could no longer be witnessed. The bubble release rates at Faure Site (5-190 Hz) varied within minutes to hours, leading to variations in average mole flow rates per outlet of 0.018-7.019 mol of methane per minute. At LM-3, the strongest manifestation of seep activity was a large carbonate platform covered by seep fauna (*Bathymodiolus* sp. mussels, *Calyptogena* sp. shells and *Lamellibrachia* sp. tube worms). Bubble activity near this platform was less prominent than at Faure Site. Our observations suggest that the two seep environments result from different types of methane release; mainly by bubble release at Faure Site and rather by diffusive release at LM-3. We propose a conceptual model that explains the differences in methane-releasing mechanisms and resulting seep environments based on differences in the depth of the base of the GHSZ (BGHSZ) and the different tectonic histories of both seep areas.

A third studied seep area is Lake Baikal. It is the only fresh-water basin in the world with inferred and sampled gas hydrates making this rift lake a unique, tectonically active area to study gas hydrates and gas seeps. The distribution and origin of shallow gas seeps occurring at the crest of the Posolsky Bank have been studied based on the integration of detailed seismic, multibeam and hydro-acoustic water-column investigations. In total 65 acoustic flares, indicating gas-bubble release at the lake floor (seepage), have been detected within the 630 km^2 area of the Posolsky Bank. All seeps are located on the Posolsky Fault scarp near the crest of the Posolsky Bank or on similar locations in water depths of -43 m to -332 m. Our seismic data image bottom-simulation reflections (BSRs), which are indicative for the presence of gas hydrates, occurring in water depths up to -300 m. This is much shallower than the previously reported -500 m water depth. Calculations for hydrate stability, heat flow and topographic effect based on the BSR occurrences and multibeam bathymetry allowed inferring a methane-ethane gas mixture and heat-flow values for which gas hydrates could be stable in the lake sediments at the given ambient conditions. None of the seeps associated with the Posolsky Bank have been detected within this newly established gas-hydrate stability zone. Our observations and data integration suggest that the seeps at the crest of Posolsky Bank occur where gas-bearing strata are cut off by the Posolsky Fault. These gas-bearing layers could be traced down the Posolsky Bank to below BGHSZ, suggesting that the detected seeps on the crest of the Posolsky Bank are mainly fed by gas coming from below the BGHSZ.

For all study areas, our observations and results clearly indicate that the geological control on gas bubble release at the sea or lake bed is strongly affected by the regional geological setting, by the occurrence and stability of gas hydrates and other stratigraphic, sedimentary and morphological factors.

SAMENVATTING

Gasuitsijpelingen of gasbellen-producerende methaanbronnen zijn locaties op de zee- of meerbodem waar gas, voornamelijk methaan, vrijkomt als bellen. Momenteel is er een grote wetenschappelijke interesse voor dergelijke gasuitsijpelingen aangezien ze een sterke invloed kunnen uitoefenen op de geosfeer, de biosfeer, de hydrosfeer en de atmosfeer. Methaanbronnen worden vaak gekenmerkt door unieke endemische ecosystemen en methaanafgeleide carbonaatafzettingen. Methaanbronnen zijn ook economisch belangrijk, aangezien ze de aanwezigheid van zowel diepe als ondiepe koolwaterstofreservoirs kunnen aangeven. Omdat methaan een zeer sterk broeikasgas is, is het belangrijk om te bepalen hoeveel methaan afkomstig van mariene en lacustriene gasuitsijpelingen terechtkomt in de atmosfeer. Op die manier kan de invloed van de menselijke activiteit op de hoeveelheid broeikasgas en dus op de klimaatsverandering beter ingeschat worden. Recente studies tonen aan dat de hoeveelheid methaan die vrijkomt bij methaanbronnen en eventueel in de atmosfeer terechtkomt zeer variabel en grotendeels ongekend is. Het grootste probleem hierbij is de onzekerheid betreffende de grootte van een methaanbrongebied, het aantal methaanbronnen binnen dit gebied en de intensiteit en activiteit van die methaanbronnen. Zolang de verspreiding en de activiteitsgraad van methaanbronnen niet beter gekend is, mogen methaanbronnen zeker niet worden verwaarloosd als belangrijke bron van atmosferisch methaan.

Gedurende de voorbije zeven jaar werden in het kader van dit doctoraatsonderzoek gasbellen-producerende methaanbronnen wereldwijd bestudeerd. De bedoeling was om na te gaan welke de belangrijkste geologische factoren zijn die het voorkomen van methaanbronnen bepalen, en dit voor verschillende geologische omgevingen. Tevens werd er onderzocht of het verschil in geologische en plaattektonische context een invloed heeft op deze factoren. Methaanbronnen werden bestudeerd in de noordwestelijke Zwarte Zee (een passieve continentale rand), in de zuidwestelijke Stille Oceaan ten oosten van Nieuw-Zeeland (een actieve continentale rand) en in het Baikalmeer in Siberië (een continentaal riftmeer). Deze studie was voornamelijk gebaseerd op hydro-akoestisch/geofysisch onderzoek (met *single-* en *multibeam*, *side scan sonar*, seismiek), op visuele waarnemingen van de zeebodem (met *ROV*, duikboot, video frame) en op sedimentstaalnames.

Het eerste studiegebied, de Dnepr paleo-delta gelegen op de continentale rand van de noordwestelijke Zwarte Zee, is bekend wegens het overvloedig voorkomen van gas en gasuitsijpelingen. Het is waarschijnlijk één van de meest actieve methaanbrongebieden ter wereld. De relatie tussen de verspreiding van de methaanbronnen, de zeebodemmorfologie en de ondergrondse structuren werd bestudeerd. Deze studie werd uitgevoerd binnen het door de EU gefinancierde CRIMEA project dat onderzocht hoeveel methaan, afkomstig van methaanbronnen in de Zwarte Zee, via de waterkolom in de atmosfeer terechtkomt. Tijdens de CRIMEA campagnes werden bijna 3000 methaanbronnen ontdekt in de Dnepr paleo-delta op basis van *single-beam* opnames. De methaanbronnen bevinden zich in waterdieptes van -66 tot -825 m, en meerbepaald in de overgangszone van het continentale plat naar de continentale helling. De integratie van de geofysische gegevens heeft aangetoond dat de methaanbronnen niet willekeurig voorkomen, maar voornamelijk geconcentreerd zijn op specifieke locaties. Daarbij heeft 99.5% van de methaanbronnen een dieptelimiet van -725 m, die samenvalt met de faseovergang van zuiver methaanhydraat. Dit suggereert dat gashydraten, indien ze stabiel zijn, kunnen fungeren als een buffer voor de opwaartse migratie van methaangas, en dat hun aanwezigheid tevens het vrijkomen van methaanbellen in de waterkolom verhindert. Hoger op de helling komen gasuitsijpelingen voornamelijk voor in gebieden met bepaalde morfologische en geologische kenmerken. Op de continentale helling en plat, wordt de vloeistofstroming in de ondergrond bepaald door het algemeen voorkomen van een ondoordringbare sedimentlaag. Deze laag zorgt ervoor dat de methaanbronnen geconcentreerd voorkomen op toppen van sedimentaire ruggen, in de nabijheid van canyons, nabij onderzeese aardverschuivingen of langs gevulde paleokanalen. Het voorkomen van ondergrondse vloeistofstromingen werd afgeleid op basis van seismische opnames die een duidelijk "gas front" in de sedimenten weergeven. Dit gas front benaderd de zeebodem op locaties waar methaanbronnen voorkomen. Op het continentaal plat komen 600 methaanbronnen voornamelijk voor ter hoogte van *pockmarks* (kleine depressies). Methaanbronnen komen stelselmatig voor op delen van de zeebodem met een hogere akoestische backscatterwaarde zichtbaar op *side scan sonar* en *multibeam* opnames. De beschikbare datasets

tonen aan dat de relatie tussen methaanbronnen en backscatter enkel het resultaat is van het langdurig vrijkomen van methaan en de daarmee geassocieerde vorming van methaanafgeleide carbonaatafzettingen in de ondergrond. De carbonaten zorgen voor het afsluiten van de ondergrondse vloeistofstroming waardoor methaanbronnen voorkomen juist buiten de ondoordringbare carbonaatgecementeerde gebieden. Aangezien de akoestische backscatterwaarde van de zeebodem evenredig is met het aantal aanwezige methaanbronnen, kan de backscatterwaarde gebruikt worden om het totaal aantal methaanbronnen binnen een gebied te bepalen. Dit is zeer nuttig om na te gaan hoeveel methaan er aan de zeebodem en mogelijks in de atmosfeer vrijkomt. Voor de Dnepr paleo-delta heeft de volledige integratie van de gegevens aangetoond dat de ruimtelijke verspreiding van methaanbronnen voornamelijk wordt bepaald door de gashydraat-stabiliteitzone (GHSZ), door de morfologie, door de onderliggende stratigrafie en door de sedimenteigenschappen.

In de zuidwestelijke Stille Oceaan ten oosten van Nieuw-Zeeland werden er, aan de hand van een onderwaterrobot of ROV (*Remotely Operated Vehicle*) en andere videogeleide instrumenten, visuele observaties en metingen van fysische eigenschappen uitgevoerd. Dit gebeurde ter hoogte van Faure site en LM-3. Dit onderzoek werd uitgevoerd tijdens de 'New Vents' SO191 campagne waarbij de activiteit en de verspreiding van methaanbronnen op de gashydraathoudende Hikurangi Rand onderworpen werd aan een zeer gedetailleerde interdisciplinaire studie. De ROV zorgde voor de allereerste visuele waarneming van gasbellen-producerende methaanbronnen ter hoogte van de Hikurangi Rand. De methaanbronnen ter hoogte van Faure Site werd tijdens meerdere duiken waargenomen gedurende periodes tot 20 minuten. Tijdens de ROV-2 duik kon men zes uitbarstingen van telkens een minuut waarnemen, en dit om de drie minuten. Deze uitbarstingen gingen gepaard met de verplaatsing van sedimentdeeltjes en de vorming van kleine depressies (*pockmarks*). Tijdens de daaropvolgende duiken ter hoogte van de Faure Site, bleek het vrijkomen van bellen eerder constant te zijn en konden de eerder waargenomen uitbarstingen niet meer geobserveerd worden. Ter hoogte van LM-3 werd de aanwezigheid van methaanbronnen aangeduid door een groot carbonaatplatform, bedekt met methaangerelateerde fauna (mosselen, schelpenresten en borstelwormen). Het vrijkomen van gasbellen was hier eerder beperkt. Deze bevindingen suggereren dat het verschil tussen beide methaanbrongebieden het gevolg is van het op een verschillende manier vrijkomen van methaan; voornamelijk door bellen in Faure Site en eerder via diffusie in LM-3. De verschillende mechanismen voor het vrijkomen van methaan en de geassocieerde verschillende omgevingen (fauna en carbonaten) zijn wellicht het gevolg van een verschil in waterdiepte en de daarmee geassocieerde dikte van de onderliggende hydraatlaag, en het verschil in tektonische geschiedenis van beide methaanbrongebieden.

Het derde studiegebied met methaanbronnen is het Baikalmeer in Siberië. Dit is het enige zoetwaterbekken in de wereld waar tot op heden gashydraten bemonsterd zijn of waar hun aanwezigheid werd afgeleid van seismische opnames. Hier werd de verspreiding en de oorsprong van ondiepe methaanbronnen op de top van de Posolsky Bank, een gekanteld breukblok, bestudeerd. In totaal werden er 65 methaanbronnen ontdekt in een gebied van 630 km^2. De methaanbronnen bevinden zich op de Posolsky breukwand op waterdieptes tussen -43 m en -332 m. Op de seismische opnames zijn bodemsimulerende reflecties (BSRs) zichtbaar die de mogelijke aanwezigheid van gashydraten aanduiden op waterdieptes tot -300 m. Berekening op basis van BSRs en multibeam bathymetrie toont aan dat enkel gassen met een bepaalde methaan-ethaan compositie stabiele hydraten kunnen vormen in de sedimenten van de Posolsky Bank, dit gezien de lokale ondergrondse druk en temperatuur. De data-integratie suggereert dat de methaanbronnen op de Posolsky Bank voornamelijk gevoed worden door gas dat aanwezig is onder de basis van de GHSZ. Dit gas migreert langs gekantelde permeabele lagen van de bank tot de breukwand waar het gas vrijkomt.

Voor alle studiegebieden kan duidelijk gesteld worden, op basis van de observaties en resultaten, dat de verspreiding en activiteit van gasbellen-producerende methaanbronnen sterk beïnvloed worden door de regionale geologische omgeving, door de aanwezigheid en stabiliteit van gashydraten en door andere stratigrafische, sedimentaire en morfologische factoren.

TABLE OF CONTENTS

Acknowledgements - Dankwoord **5**
Summary **9**
Samenvatting **11**
Table of contents **13**
List of figures **17**
List of tables **24**
List of abbreviations **25**

Chapter 1
Introduction **27**
1.1. Background 27
1.2. Study objectives 33
1.3. Geological setting 33
1.3.1 Black Sea – Dnepr paleo-delta 33
1.3.2. SW Pacific Ocean – Hikurangi Margin 35
1.3.3. Lake Baikal – Posolsky Bank 36
1.4. Methods 38
1.4.1. Water-column data 39
1.4.2. Seafloor data 40
1.4.3. Subsurface data 42
1.5. Project framework 42
1.6. Thesis outline 43
References 44

Chapter 2
Geo- and hydro-acoustic manifestations of shallow gas and gas seeps in the Dnepr paleo-delta, northwestern Black Sea **51**
2.1. Background 51
2.2. Dnepr paleo-delta 51
2.3. High-resolution reflection seismic data 52
2.4. Shallow gas 54
2.5. Gas hydrates 58
2.6. Gas seeps 59
2.7. Concluding remarks 62
Suggested reading 62
Acknowledgements 63
Additional information 63

Chapter 3
Geological and morphological setting of 2778 methane seeps in the Dnepr paleo-delta, northwestern Black Sea **65**
Abstract 65
Keywords 65
3.1. Introduction 66
3.2. Study area 66
3.3. Data and Methods 69

3.3.1. Water-column data *69*
3.3.2. Seafloor data *69*
3.3.3. Subsurface data *69*
3.4. Observations and results 71
3.4.1. Morphology *71*
3.4.1.1. Shelf 72
3.4.1.2. Slope 73
a) Western mass-wasting dominated area *73*
b) Eastern deposition-dominated area *73*
c) Central divide *75*
3.4.2. Seep locations *75*
3.4.3. Gas hydrate and free gas occurrences *76*
3.4.4. Seep relation to morphology and subsurface structure *78*
3.4.4.1. Continental shelf 78
3.4.4.2. Continental slope 78
3.5. Discussion 80
3.5.1. Pockmarks *80*
3.5.2. Crests of sedimentary ridges *84*
3.5.3. Canyons *84*
3.5.4. Submarine landslides *84*
3.5.5. Terrace *85*
3.5.6. Controls on seep distribution *85*
3.6. Conclusions 87
Acknowledgements 87
Additional information 87
References 88

Chapter 4
Anomalous seafloor backscatter patterns in methane venting areas, Dnepr paleo-delta, NW Black Sea **93**
Abstract 93
Keywords 93
4.1. Introduction 94
4.2. Study area 95
4.3. Methods and data 97
4.3.1. Single-beam echosounding and seep detection *97*
4.3.2. Multibeam mapping *97*
4.3.3. Side-scan sonar imaging and subbottom profiling *97*
4.3.4. Pore-water and grain-size analysis *97*
4.3.5. Visual seafloor observations *99*
4.4. Observations and results 99
4.4.1. Backscatter anomalies, seafloor morphology and seep distribution *99*
4.4.2. Seismic observations *100*
4.4.3. Pore-water and grain-size analysis *102*
4.4.4. Visual seafloor observations *105*
4.5. Discussion 105
4.5.1. Bacterial mats, carbonates and their relation to seep distribution *105*

4.5.2. Controls on acoustic seafloor backscatter *108*
4.5.3. Backscatter, seep distribution and subsurface integrative model *110*
4.6. Conclusions 111
Acknowledgements 112
Additional information 112
References 112

Chapter 5
Active venting sites on the gas-hydrate-bearing Hikurangi Margin, Off New Zealand: Diffusive- versus bubble-released methane **117**
Abstract 117
Keywords 117
5.1. Introduction 118
5.2. Study area 118
5.3. Methods and data 121
5.3.1. Single-beam seep detection *121*
5.3.2. Multibeam mapping *121*
5.3.3. Visual observations *121*
ROV 'GENESIS' 121
OFOS, TV-MUC and TV-G 122
5.3.4. Measurements of physical properties *122*
5.4. Observations and results 122
5.4.1. Regional seafloor observations *122*
5.4.1.1. Northern Rock Garden: LM-3 122
5.4.1.2. Western Rock Garden: Faure Site 122
5.4.2. Local seafloor observations *123*
5.4.2.1. LM-3 123
5.4.2.2. Faure Site 126
5.4.2.3. Methane bubble-release rates 130
5.4.3. Thermal measurements *132*
5.5. Discussion 133
5.5.1. Differences in seep environment: diffusive versus bubble-released methane *133*
5.5.2. Temporal variations in bubble-release activity *134*
5.5.3. An integrative seep model *136*
5.6. Conclusions 138
Acknowledgements 138
Additional information 139
References 139

Chapter 6
Stratigraphic and structural controls on the location of active methane seep on Posolsky Bank, Lake Baikal **145**
Abstract 145
Keywords 145
6.1. Introduction 146
6.2. Study area 146
6.3. Methods and data 149

6.3.1. Single-beam echosounding and seep detection *149*
6.3.2. Multibeam bathymetry *150*
6.3.3. Seismic subbottom data *150*
6.4. Observations and results 151
6.4.1. Lake-floor morphology *151*
6.4.2. Stratigraphic framework *152*
6.4.3. Gas seep distribution *154*
6.4.4. Indications for shallow gas and gas-hydrate occurrence *154*
6.5. Discussion 155
6.5.1. Gas-hydrate stability, heat flow and topographic effect *155*
6.5.2. Fluid flow and seep distribution model 157
6.6. Conclusions 159
Acknowledgements 159
Additional information 159
References 160

Chapter 7
Final discussion **163**
7.1. Global occurrence of bubble-releasing seeps 163
7.2. Subsurface controls on the distribution of bubble-releasing seeps 163
7.2.1. Fluid sources *163*
7.2.1. Fluid migration modes, triggers and rates *169*
7.2.2. Fluid migration within the gas-hydrate stability zone *173*
7.2.3. Fluid migration outside of the gas-hydrate stability zone *175*
7.2.4. Faults versus sediments; which is the primary conduit/seal related to bubble-releasing seeps? *176*
7.3. Seafloor manifestations associated with bubble-releasing seeps 177
7.3.1. Chemosynthetic communities *177*
7.3.2. Methane-derived authigenic carbonates *178*
7.3.3. Seafloor morphology *179*
7.4. Fate of methane released at bubble-releasing seeps 181
References 182

Chapter 8
Conclusions **193**
Future perspectives 194

Appendices
Appendix A: List of publications A1-A7
Appendix B: List of research expeditions B1-B2

LIST OF FIGURES

Figure 1.1. Schematic diagram indicating the role of methane and methane release in the carbon cycle (after Judd and Hovland, 2007). 27

Figure 1.2. A. Diagram showing the relative contributions from various sources of methane to the global atmospheric methane budget. The total atmospheric methane budget is estimated to be 600 Tg of CH_4 yr^{-1} of which 71.7% has an anthropogenic source and 28.3% a natural source Note the absence of methane seeps as a possible source (IPCC, 2001b; Kvenvolden and Rogers, 2005). B. Diagram showing the relative contributions from various geological methane sources (Etiope and Klusman, 2002; Etiope and Milkov, 2004; Judd and Hovland, 2007; Etiope, 2009). 28

Figure 1.3. Worldwide distribution of bubble-releasing seeps (red dots) and gas seepage indicators (bacterial mats, authigenic carbonates, ice streamthroughs, etc.) (yellow dots). Where seeps as well as the seep indicators are present; they are indicated by red dots (after Judd and Hovland, 2007). 29

Figure 1.4. A general overview of the subsurface- and water-column features associated with gas-bubble release as witnessed in the Gulf of Mexico where gas-bubble release is associated with oil leakage (Jean Whelan, WHOI). 29

Figure 1.5. A. An overview map of all locations on Earth with recovered gas hydrates (red circles) and inferred gas hydrates (yellow circles). B. Estimated thickness of the gas-hydrate stability zone in the world's oceans (Krey et al., 2009). 30

Figure 1.6. A. An overview of the chemical reactions that take place at the seabed-water column transition zone as a result of the anaerobic oxidation of methane (AOM). Note that a difference in methane flux leads to different chemosynthetic fauna's and that AOM is strongly associated with authigenic carbonate formation (Suess, 2010). B. A schematic overview of the anaerobic oxidation of methane and its resulting chemical species (Judd and Hovland, 2007). 31

Figure 1.7. Tectonic map of the Black Sea region with indication of the Dnepr paleo-delta study area. (Abbreviations: NDO—North Dobrogea Orogen, SCO—South Crimea Orogen, PDD—Pre-Dobrogea Depression, NKD—North Kilia Depression, KaD—Karkinit Depression, KaR—Kalamit Ridge, HD—Histria Depression, SD—Sorokin Depresion, KTD—Kerci–Taman Depression, KD—Nijna–Kamciisk Depression, ATD—Adjaro–Trialet Depression, TB—Taupse Basin, SSR—Suvorov–Snake Island Ridge, KR—Kramski Ridge, AR—Azov Ridge, BR—Bubkin Ridge (after Dinu et al., 2005). 34

Figure 1.8. Overview map of the Black Sea with indications of seep locations, mud volcanoes and sampled gas hydrates (after Egorov et al., 1998; Naudts et al., 2006; Judd and Hovland, 2007; Popescu et al., 2007). 35

Figure 1.9. Tectonic map of the Hikurangi Margin with indication of the Rock Garden study area. The white trusts represent the principle deformation front, the major active faults are shown in black and the thickness (km) of the trench-fill turbidites is also indicated (after Lewis et al., 1998; Barnes et al., in press). 36

Figure 1.10. Overview map of the Hikurangi Margin with indications of seep locations (red dots), gas seepage indicators (yellow dots) and sampled gas hydrates (black triangles) (Greinert et al., in press). 37

Figure 1.11. Tectonic map of Lake Baikal with indication of the Posolsky Bank study area (Klerkx et al., 2006). (Abbreviations: SDAZ—Selenga Delta Accommodation Zone; ARAZ—Academician Ridge Accommodation Zone). 38

Figure 1.12. Overview map of Lake Baikal with indications of seep locations (red dots), gas seepage indicators (black dots), mud volcanoes (yellow dots) and sampled gas hydrates (orange triangles) (Granin and Granina, 2002; Klerkx et al., 2006; Schmid et al., 2007). 39

Figure 1.13. Overview of the main datasets used in this study. 41

Figure 2.1. Location of Dnepr paleo-delta in the northwestern Black Sea with indication of major structures, deep faults, oil and gas fields and seep locations. 52

Figure 2.2. A. High-resolution seismic reflection survey lines and outlines for Figs. 2.4.-2.9. (see Fig. 2.1. for location). B. Ship track with hydro-acoustically detected seeps (see Fig. 2.1. for location). 53

Figure 2.3. Single-beam echogram showing typical hydro-acoustic manifestations of rising methane bubbles (flares) in the Dnepr paleo-delta. 54

Figure 2.4. Different shallow gas signatures showing different behaviors on 5 kHz pinger data (see Fig. 2.2.A. for location). 55

Figure 2.5. Comparison of “gas fronts” visible on 5 kHz data and sparker data (see Fig. 2.2.A. for location). 56
Figure 2.6. 3D view showing the depth variation of the “gas front” as a depth map overlain by an isopach map (depth of the “gas front” below the seafloor) together with the used 5 kHz seismic profiles (see Fig. 2.2.A. for location). Gas seeps were mainly detected where the gas front approaches the seafloor within a couple of meters. 57
Figure 2.7. GI-gun reflection profile showing a BSR/gas front in the GHSZ. Inset A shows the inverse polarity of the BSR. 59
Figure 2.8. 3D view showing the depth variation of the BSR/“gas front” together with the detected seeps and two GI gun profiles (see Fig. 2.2.A. for location). 60
Figure 2.9. 3D view showing relation between shallow gas features on 5 kHz data, multibeam bathymetry overlain by color-coded multibeam backscatter data and single-beam seep locations (see Fig. 2.2.A. for location). 61

Figure 3.1. Location map of the Dnepr paleo-delta study area with indication of deep structures, major faults and seep locations in the northwestern Black Sea (Robinson et al., 1996; Egorov et al, 1998). Inset shows the bathymetry of the study area in greater detail, with indication of faults, mud diapirs, area with observed BSR and the Dnepr Canyon (after Lüdmann et al., 2004). 68
Figure 3.2. Swath bathymetry map (30 m grid) acquired during the 2003 and 2004 CRIMEA cruises with all newly detected seeps plotted as black dots. Gaps in the multibeam coverage were filled in by data from the 2004 METROL cruise. The outlines of the areas covered by Figs. 3.6., 3.9., 3.10., 3.11. & 3.12. is indicated as well as the viewing direction of Fig. 3.5. and the location of the profile used in Fig. 3.7. Inset A shows the track lines of the seismic data (GI-gun, sparker and 5 kHz) acquired within the study area and the seismic and echosounder profiles shown in this manuscript are also indicated. Inset B gives an overview of the ship tracks sailed during the 2003 and 2004 CRIMEA cruises and along which hydro-acoustic seep detection was performed (seeps locations are plotted as black dots). 70
Figure 3.3. Hydro-acoustic image ("flare") of several methane bubble trains rising towards the sea surface at a seep site at -200 m water depth. The image consists of a succession of pings over a certain time interval. The tilted arrows show the rise of isolated bubbles. The bubbles clearly cross the oxic–anoxic interface at -90 m water depth. The other backscatter signals above this depth correspond to fish, jelly fish and larvae. The vertical acoustic anomalies (a) are caused by the parallel running multibeam system. 71
Figure 3.4. Map of the study area with indication of the major geomorphological regions and canyons. Seep locations are plotted as black dots. The scarps of the submarine landslides are emphasized by dashed lines and the position of two chimney fields is indicated by 2 horizontal arrows (1: Michaelis et al., 2002; 2: CRIMEA cruise 2004). 72
Figure 3.5. Oblique view of grey-shaded bathymetry map of the upper part of the study area with indication of different geomorphological features (see Fig. 3.2. for location). Seeps locations are plotted as black dots. The scarps of the submarine landslides are emphasized by dashed lines and the position of the 2 chimney fields is indicated by 2 arrows (1: Michaelis et al., 2002; 2: CRIMEA cruise 2004). Seep clusters are evident at the crest of sedimentary ridges, at submarine landslides, along canyons, on the shelf and at the terrace at -200 m water depth. 73
Figure 3.6. Plan view of grey-shaded bathymetry map of the shelf and the dune area (5 m grid) overlain by bathymetric contours (see Fig. 3.2. for location). The four elongated depressions are marked by a transparent white mask. The inset shows an oblique view of the intensive seep site at -92 m water depth characterized by pockmarks. Seep positions are plotted as black dots. On the 5 kHz profiles AB and CD (see Fig. 3.2.A. for location) the updoming gas front (dotted white line) underneath the seep positions (arrows) is clearly visible. Seeps are located at the margins of filled channels and not above them. 74
Figure 3.7. A multi-channel GI-gun profile (see Figs. 3.2. for location) from the GHOSTDABS project (Lüdmann et al., 2004) clearly indicates that the rather unusual morphology of the central divide has been inherited from a series of underlying, buried channel-levee systems. The two parallel channels within the central divide are formed probably due to differential compaction of the underlying channel sediments, which resulted in the two channels with central ridge morphology. Also notice the presence of the Dnepr Canyon. 75

Figure 3.8. Oblique view of grey-shaded bathymetry map (see Fig. 3.2.A for location), seep locations plotted as red dots and some seeps are shown as 3D flares. Seeps are abundant upslope of the GHSZ, delineated by the -725 m contour line. The two crossing GI-gun profiles clearly show that the gas front, i.e. the top of the free gas in the subsurface as indicated by the enhanced reflections, domes up to the surface outside the GHSZ, where gas bubbles were detected in the water column. The graph in the lower left corner shows the seep distribution versus depth with clear seep clusters at -92, -200 and at -650 m water depth, just outside the GHSZ. 77

Figure 3.9. Map showing the depth of the gas front beneath the seafloor (see Fig. 3.2. for location), as mapped on 5 kHz profiles, overlain by bathymetric contours. The map emphasizes that gas seeps (white dots) are present where the gas front approaches the seafloor. Bubbles were detected where the gas front comes within 25 m of the surface. For the abundant seeps sites at the terrace (inset A) and the shelf (inset B) this is < 10 m. 79

Figure 3.10. Oblique view of grey-shaded bathymetry map of a sediment ridge in the mass-wasting dominated area and of a sediment ridge in the deposition-dominated area overlain by bathymetric contours (see Fig. 3.2. for location). Both ridges are characterized by seeps (black dots) along their crests. The 5 kHz profiles (see Fig. 3.2.A. for location) crossing the ridges show that at both ridges the gas front domes up to the crest of the ridges where seeps (arrows) were detected and that the sediment cover thins out towards the crest. The gas front (dotted lines) follows the base of the sediment cover. 81

Figure 3.11. Oblique view of grey-shaded bathymetry map of the area affected by submarine landslides (see Fig. 3.2. for location) with indication for the major geomorphological regions, overlain by bathymetric contours. The 5 kHz profile (see Fig. 3.2.A. for location) and the 3D image show the difference in location of seeps (black dots or arrows) on scarps of the submarine landslides in the western mass-wasting area and seeps within the submarine landslides in front of detached sediment ridges in the eastern deposition-dominated area. The -725 m water depth contour line, marking the border of the GHSZ, is located at the base of both submarine landslide areas. 82

Figure 3.12. Oblique view of grey-shaded bathymetry map of the terrace seep site (see Fig. 3.2. for location), with indication the major geomorphological regions, overlain by bathymetric contours. The sparker profile AB (see Fig. 3.2.A. for location) shows that seeps (black dots or arrows) are detected where the gas front domes up to the seafloor and that no gas seeps are detected above a filled channel. The perpendicular 5 kHz (see Fig. 3.2.A. for location) profile shows the same gas front-seep relation. The inset clearly shows that the gas front can only dome up to the surface where the sediment cover diminishes or is breached by mass-wasting at the flanks. During the 2004 METROL cruise this 5 kHz profile was used as a base for coring. Sand was cored at the seep sites and clay or fine sediments were retrieved outside the seep sites from the parallel-stratified sediment cover. 83

Figure 3.13. Combining model of the supposed fluid migration in the subsurface and its expression at the seafloor surface. The 3D block diagram based on the bathymetric data, seep positions and subsurface data presenting a model for the seep distribution in the Dnepr paleo-delta for the shallow-water seep sites (top) and the deep-water seep sites, with submarine landslides and gas hydrates (bottom). 86

Figure 4.1. A. The location of the study area in the NW Black Sea with seeps (black dots) and acquired multibeam data (Egorov et al., 1998; Naudts et al., 2006). B. The multibeam bathymetry of the shelf with dunes, pockmarks (transparent white masks) and seeps (see Fig. 4.1.A. for location). C. Oblique view on the multibeam bathymetry of the high-intensity seep and pockmark site at -92 m water depth (after Naudts et al., 2006) (see Fig. 4.1.B. for location). D. Side-scan sonar mosaic of the studied area with indication for the multi-cores (MC: 4, 7, 8, 9), 5 kHz seismic lines (SB 1-3: dashed white lines) and video lines (white lines) and seeps (see Fig. 4.1.B. for location). 96

Figure 4.2. A. Multibeam-derived backscatter map overlain with bathymetric contours, detected seep locations (black dots), positions of multi-core stations and outlines for Figs. 4.3., 4.7. and 4.9. (see Fig. 4.1.B. for location). Furthermore the positions of the high-backscatter (HBS) and low-backscatter (LBS) swaths used in Figure 4.10. are indicated by the solid bold lines. B. Graph showing the distribution of the number of seeps with respect to their backscatter values, both, as a histogram and cumulative percentage curve (full line). The second cumulative percentage curve (dashed line) shows the distribution of all backscatter values recorded in the shown study 98

area. Arrows a-a' show that 74 % of all seeps occur in the high-backscatter areas above 0 BU, thus within only 33 % of the studied area. Arrows b-b' show that 75 % of all seeps with the lowest backscatter values occur below 2 BU.

Figure 4.3. 3D view of the multibeam bathymetry overlain with the color-coded backscatter data, bathymetric contours and seep locations (black dots) (for location, see Fig. 4.2.A.). Pockmarks are characterized by high- to very-high-backscatter values with seeps located on their margins. The sediment dunes have higher backscatter values on the ENE flanks. 100

Figure 4.4. Three 5 kHz subbottom profiles SB1, SB2 and SB3 (C, F and I) with their respective multibeam-derived backscatter profiles (A, D and G) and side-scan sonar images (B, E and H) (for location see Fig. 4.1.D.). Shallow gas fronts (dashed white line) occur at medium- and high-backscatter areas associated with seeps (arrows), whereas deep gas fronts occur at low-backscatter areas without seeps. Bubbles recorded as noise in the water column on the subbottom data (SB 1 & 2) sometimes blank out the side-scan sonar recordings (see NE of SB1)(Fig. 4.4.B.).The extent of SB2 shown in Figure 4.8. is indicated. 101

Figure 4.5. Pore-water data from multi-cores taken at different backscatter intensity sites. MC 4 was taken at an actively bubbling high-backscatter site. MC 7-9 are taken from areas with backscatter values ranging from low- to very-high-backscatter values. Values at -1 cm depth are water samples taken from the core liner above the sediment surface (for locations see Figs. 4.1.D. and 4.2.). 102

Figure 4.6. Grain-size data from multi-cores taken at different backscatter intensity sites shown as histograms and cumulative percentage curves for each centimeter of the uppermost 5 cm. MC 4 was taken at an actively bubbling high-backscatter site. MC 7-9 are taken from areas with backscatter values ranging from low- to very-high-backscatter values (for locations see Figs. 1D and 2). 103

Figure 4.7. Screenshots captured from the JAGO dive 852 video (for outline of dive area see Fig. 4.2A) A-E: Bacterial mats of different sizes surrounding black venting holes all or not associated with bubble release (arrows) or carbonate structures. G-I: Semi-buried to fully-exposed carbonate structures, all or not associated with bacterial mats. J-L: Seafloor depression (pockmark) with rough, probably carbonate-cemented, edges and with a small bacterial mat on the bottom surrounded by Tunicates. Bubble release was observed on the right of the bacterial mat (arrow). 104

Figure 4.8. Screenshots taken during the OFOS video lines shown in Figure 4.9., characterizing the study-area seafloor (for scale see the 10 by 10 cm shackles). A: Usual flat, shell-covered, seafloor. B-E: Bacterial mats of different sizes. F-I: Carbonate formations showing up as solitary buildups with small bacterial mats or as rough, carbonate-cemented, seafloor. 106

Figure 4.9. Multibeam backscatter map overlain with bathymetric contours (for location see Fig. 4.2.A.), seep locations (black dots) and the outline of seismic profile SB2 (see Fig. 4.1.D. and Fig. 4.4.). Visually observed bacterial mats are indicated by black markers along the offset-corrected OFOS video lines (white lines). Bacterial mats occur solely at high to very-high-backscatter areas. 107

Figure 4.10. Comparison of two multibeam swaths from one multibeam line, one recorded in a high-backscatter area (full line) and one from a low- to medium-backscatter area (dotted line). A. The raw depth for both swaths (see Fig. 4.2.A. for location). B. The raw amplitude for both swaths within a cloud representing all amplitudes recorded during the particular multibeam line. C. The incidence angle for each beam of both swaths. D. Normalized backscatter values for both swaths. 109

Figure 4.11. Overview model of the supposed fluid migration in the subsurface, carbonate formation with seep relocation and the acoustic seafloor backscatter expression. ① A. Gas-bubble release from black venting holes. B. Bacterial-mat formation around the black venting holes. C-D. Precipitation of methane-derived authigenic carbonates underneath bacterial mats with subsequent relocation or termination of seepage. E. Semi-buried to fully exposed methane-derived authigenic carbonate structures. F. Bacterial mats with limited gas-bubble release and associated with chemosynthetic communities (e.g. Tunicates). All mentioned features can occur in association with or without pockmark formation. ② Acoustic seafloor backscatter expression resulting from the seep distribution and associated features. Filled channels, blocking fluid migration, are characterized by low backscatter values (LBS) and the absence of seeps. Locations with active seepage and ongoing authigenic carbonate precipitation show up as medium- to high-backscatter areas (MBS), whereas those with advanced, massive carbonate precipitation and at present less or no seep activity show up as very high to maximum backscatter areas 111

(VHBS).

Figure 5.1. Location map of the Hikurangi Margin, east of New Zealand's North Island, with acquired multibeam data (Greinert et al., this issue) and indication of the area with observed BSRs (black dashed line) and major tectonic features with the white lines indicating the deformation front (Lewis et al., 1998; Henrys et al., 2003; Barnes et al., this issue). Outline for Fig. 5.2. is also given. Land topography is derived from Shuttle Radar Topography Mission (SRTM) data. The bathymetry data is courtesy of NIWA. 119

Figure 5.2. Multibeam bathymetry of Rock Garden (30 m grid) with indications of the known seep sites, video tracks (black lines) and acoustic flare locations (white dots) (see Fig. 5.1. for location) (Greinert et al., this issue). The possible depth limit for the GHSZ is indicated by the -630 m and -710 m isobaths (Faure et al., 2006). A. Multibeam bathymetry map of the LM-3 area with indications of ROV (red), TV-G (yellow) and OFOS tracks (black), flares (white dots) and the track line of the echosounder and seismic recordings (a-a') (black dashed line). Outline for Fig. 5.6. is also indicated. B. Multibeam bathymetry map of the area around Faure Site with indications of ROV (red), TV-MUC (yellow) and OFOS video tracks (black), flares (white dots) and the track lines of the echosounder (b-b') and seismic recording (c-c') (black dashed lines). Outline for Fig. 5.8. is also indicated. 120

Figure 5.3. A. Seafloor observations along NW-SE orientated OFOS-2 track over the northern part of Rock Garden, crossing the LM-3 site (for location see Fig. 5.2.). B. Zoom of the OFOS-2 track over the LM-3 site. C. Video mosaic created with ADELIE software from the OFOS-2 video sequence over the LM-3 site. Video mosaic shown in C corresponds to the track shown in B. 123

Figure 5.4. Stills taken during the OFOS video tracks shown in Figs. 5.2., 5.3. and 5.5. as a characterization of the seafloor in Rock Garden. A. Authigenic carbonate platform with live *Bathymodiolus* sp. mussels at LM-3. B. *Calyptogena* sp. shell hash with some *Bathymodiolus* sp. mussels at the LM-3 site. The darker patch referred to as 'rain drop site' is an area with ampharetid polychaetes (Sommer et al., this issue). C. Coral rubble. D. Chemoherm and bioturbated soft sediments. E. Presumed carbonate platform with *Calyptogena* sp. shells and a tubeworm from the area west of the Faure Site. F. Semi-indurated outcrops at the Faure Site. G. Boulders H. Rocky outcrop from the slide scarp west of the Faure Site. 124

Figure 5.5. A. Seafloor observations along W-E orientated OFOS-1 track over the western part of Rock Garden, crossing Faure Site (for location see Fig. 5.2.). B. Seafloor observations along NE-SW orientated OFOS-1a track over the western part of Rock Garden, crossing Faure Site (for location see Fig. 5.2.). The crossing point of the two tracks is indicated in A and B. 125

Figure 5.6. Seafloor observation maps at the LM-3 site. A. Multibeam bathymetry map with the ROV, OFOS and TV-G tracks. B. Sediment-type distribution. C. *Bathymodiolus* sp. distribution within the fauna distribution D. *Calyptogena* sp. shell hash distribution within the fauna distribution. E. *Lamellibrachia* sp. distribution within the fauna distribution. F. Distribution of sponges and soft tissue corals within the fauna distribution. B-F have multibeam backscatter as background. 126

Figure 5.7. Stills taken from ROV-4, ROV-5 and TV-G-17 deployments at LM-3. A. Side view of the authigenic carbonate platform surrounded by a *Calyptogena* sp. hash. B. Top of the carbonate platform with live *Bathymodiolus* sp. mussels. C. Side view of the carbonate platform with abundant *Lamellibrachia* sp. tubeworms. D. One of the multiple depressions/bioturbations observed at LM-3. E. Bubbling seep observed in-between shell hashes during ROV-4. F. Bubbling seep observed during TV-G-17. 127

Figure 5.8. Seafloor observation maps at Faure Site with multibeam bathymetry (A and C) or backscatter (B) as background. A. Overview of the BIGO-04 and FLUFO-04 lander positions and ROV, OFOS and TV-MUC tracks. B. Sediment-type distribution. C. Fauna distribution. 128

Figure 5.9. Stills taken from ROV deployments at Faure Site. A. Side view of a strongly eroded outcrop. B. Close-up of the transition between the bioturbated sandy sediments and the outcrop shown in Fig. 5.9A. C. Bioturbated sandy sediments with depression-hill morphology. D. BIGO-04 lander visited during ROV-6 dive with in front bubble-releasing seeps. E. Alignment of bubble-releasing outlets at a 'rain drop site'. F. Bottom-water sampling at one of the active seeps seen in Fig. 5.9.E. 129

Figure 5.10. A. Bubble-release rates at Faure Site observed during the different ROV dives. The assumed bubble size is also indicated between brackets. B. Flow rates and mole flow rates 131

estimated for methane bubbles and based on bubble sizes and release rates given in Fig. 5.10A. Flow rate and mole flow rate (for methane) based on the bubble sizes and release rates given in A. During ROV-2 dive, bubbles sizes were ca. 9 mm and 6 mm, during the outbursts and the regular periods respectively. C. Still from ROV-2 during an outburst. D. Still from ROV-2 during a regular period. E. Schematic map showing the dive tracks, seep locations (red dots) and the locations of seep observation.

Figure 5.11. Bottom-water and sediment temperature measured during ROV-5 at LM-3. Stills A to F show the different locations where sediment temperatures were measured with the ROV-mounted THP sensor. A-A'. Top of the platform, in a live *Bathymodiolus* sp.bed. B. Sandy seafloor with *Calyptogena* sp. shell fragments. C. Depression with a depth of ca. 20 cm. D. Dark reduced sediment on a hill feature. E. *Calyptogena* sp. shell hash F. A 'Rain drop site' with ampharetid polychaetes (Sommer et al., this issue). This location was characterized by a negative sediment-temperature anomaly (see graph Fig. 5.11.). 132

Figure 5.12. Proposed seep model for Faure Site and LM-3 to explain the differences in methane-releasing mechanism (bubble versus diffusive) and resulting seep environments based on difference in depth, subsurface depth of the BGHSZ/BSR and observed seafloor features. 137

Figure 6.1. Location map of the study area in Lake Baikal with indications for regional faults, Baikal Basins, mountain ranges, rivers and area with observed bottom simulation reflections (BSRs) (Golmshtok et al., 2000). The location of seeps (red stars), mud volcanoes (black triangles), ice streamthroughs (yellow dots) and the BDP-97 drill hole is also indicated (Granin and Granina, 2002; Klerkx et al., 2006; Schmid et al., 2007). The location on Planet Earth, the view directions for Figs. 6.2.A. & 2.B. and outline for Fig. 6.3. are also indicated. The map is constructed by compiling SRTM-derived topography data with bathymetry data from Lake Baikal (INTAS Project 99-1669 Team, 2002) and multibeam bathymetry data (Naudts et al., submitted). 147

Figure 6.2. 3D views of Lake Baikal and Posolsky Bank with indication for the most prominent features. The view directions (A and B) are indicated on Fig. 6.1. The images are constructed by compiling SRTM-derived topography data with bathymetry data from Lake Baikal (INTAS Project 99-1669 Team, 2002) and multibeam bathymetry data (Naudts et al., submitted). 148

Figure 6.3. Multibeam bathymetry map of the Posolsky Bank overlain by bathymetric contours, detected seep locations (red dots), acquired sparker and echosounder profiles (respectively red and yellow dashed lines) and main faults (black dashed lines) (see Fig. 6.1. for location). Location of BDP-99 drill hole is also indicated together with depth contour of -370 m which forms the theoretical boundary of the GHSZ for pure methane hydrate (blue area) (Sloan, 1998). 149

Figure 6.4. Echogram from the central seep area on the scarp of the Posolsky Bank (for location see Fig. 6.8.) where rising bubbles are hydro-acoustically detected as „flares". The other backscatter signals in the water column probably correspond to fish. 150

Figure 6.5. Pictures of gas bubbles being trapped underneath and within the frozen lake surface above seep sites at Posolsky Bank (pictures courtesy of N. Granin). The lower-right picture shows gas bubbles reaching the lake surface at a seep site close to the Selenga Delta (picture courtesy of V. Kapitanov). 151

Figure 6.6. 3D view of multibeam bathymetry overlain by bathymetric contours and seep locations, plotted as red dots or shown as 3D flares in combination with sparker profile SELE029 (for location see Fig. 6.3.). Seeps occur at the crest of the Posolsky Bank upslope of the GHSZ, delineated by the -370 m blue contour line. No seeps have been detected near the Posolsky Bank within the GHSZ. On the seismic profile, strong acoustic attenuation in combination with dispersed enhanced reflections can be seen along one reflection. This reflection is interpreted as the TGBL. Seeps occur where the TGBL is cut off by the Posolsky Fault. The graph in the lower right corner shows the seep distribution versus depth with a clear seep cluster at -40 to -100 m water depth and no seeps in water depths greater than -340 m. 152

Figure 6.7. Seismic sparker profiles CONT031 (AB) and SELE023 (CD) where the TGBL can be traced from the seeps at the crest of the Posolsky Bank to below the BGHSZ. The BGHSZ shows up as a series of enhanced reflections. The location of BDP-99 well is also indicated. For locations of both profiles see Fig. 6.3. 153

Figure 6.8. 3D view of multibeam bathymetry overlain with bathymetric contours and with seep locations plotted as red dots or shown on an echogram in combination with three sparker 155

profiles. The top of the gas-bearing layer (TGBL) is shown as depth color-coded surface. This surface starts from or above the seeps positions at the scarp of the Posolsky Bank and can be traced down the Posolsky Bank to below the BSR or BGHSZ.

Figure 6.9. Bathymetric contour map of the Posolsky Bank area, showing the modeled topographic correction on background regional heat flow caused by the relief of the Posolsky Bank. 156

Figure 6.10. Proposed seep model for the Posolsky Bank gas seeps. 158

Figure 7.1. The locations of our study areas (indicated by white stars) within the worldwide distribution of bubble-releasing seeps (red dots) and gas seepage indicators (bacterial mats, authigenic carbonates, ice streamthroughs, etc.) (yellow dots). Where seeps as well as the seep indicators are present; they are indicated by red dots (after Judd and Hovland, 2007). 167

Figure 7.2. Overview of the fluid sources, the fluid types, the fluid pathways, the fluid flow rates and the numbers of seeps for the three study areas, shown relatively to each other as indicated by the arrows. The figure shows that the Hikurangi accretionary margin and the Dnepr paleo-delta are the two end-members for most fluid flow characteristics. 172

Figure 7.3. Overview of the models explaining fluid flow, the distribution of seeps and the associated seafloor/lake floor manifestations for the different study areas. 180

LIST OF TABLES

Table 5.1. Overview of average bubble-release rates, flow rates and mole flow rates (CH_4) of seeps observed at Rock Garden (this study) in comparison with published data from seeps around the world. Values in between brackets are calculated based on provided data and where needed, the SiBu-GUI was used to calculate (mole) flow rates (Greinert and McGinnis, 2009). 135

Table 7.1. Overview of all known bubble-releasing seep sites in the world with indication of water depth, tectonic setting and associated features. 164

ABBREVIATIONS

AOM: anaerobic oxidation of methane

ARAZ: Academician Ridge Accommodation Zone

BGHSZ: base of the gas-hydrate stability zone

BDP: Baikal Drilling Project

BRZ: Baikal Rift Zone

BSR: bottom-simulating reflection

BU: backscatter unit

CBB: Central Baikal Basin

CRIMEA: contribution of high-intensity gas seeps in the Black Sea to methane emission to the atmosphere

CTD: conductivity-temperature-depth sensor

GHSZ: gas-hydrate stability zone

HBS: high-backscatter area

LBS: low-backscatter area

LM-3: Lewis and Marshall seep site 3

MBS: medium-backscatter area

MC: multi-core

MDAC: methane-derived authigenic carbonate

NBB: North Baikal Basin

OFOP: ocean floor observation protocol

OFOS: ocean floor observation system

ROV: remotely operated vehicle

SB: subbottom profile

SBB: South Baikal Basin

SDAZ: Selenga Delta Accommodation Zone

SRB: sulfate-reducing bacteria

TGBL: top of the gas-bearing layer

THP: thermoprobe temperature sensor

TV-G: TV-guided grab

TV-MUC: TV-guided multi-core

TWTT: two-way travel time

USBL: ultra-short baseline

VHBS: very-high-backscatter area

CHAPTER 1

Introduction

This chapter gives a general overview of the background and importance of bubble-releasing methane seeps and thus the relevance of this thesis. Furthermore the aim of this thesis, the geological setting of the three study areas, the used methods, the project framework as well as the outline of the thesis are briefly discussed. More detailed information about the items dealt with in the introduction is provided in the 'introduction', 'study area', 'data and methods' sections of the subsequent chapters. Whereas the introduction is intended as a brief overview more detailed background information is given and integrated with the results in the 'final discussion' chapter.

1.1. Background

Bubble-releasing seeps, often referred to as gas seeps or cold seeps, are locations at the sea or lake floor where gas, mainly methane (CH_4), is transferred as a free gas phase (bubbles) from the sediments into the overlying water column. Over the last decades, methane release has become a very important scientific, economic and even political issue. The release of methane, a major component of the global carbon cycle, strongly affects the atmosphere, the biosphere, the hydrosphere and the geosphere (Fig. 1.1.) (Judd, 2003; Judd and Hovland, 2007). Furthermore methane is becoming an increasingly important energy resource.

Methane is a very important greenhouse gas with 21-23 times the global warming potential as the same mass of carbon dioxide and it accounts for 20% of the greenhouse forcing since the mid 1700's (Lelieveld et al., 1998; IPCC, 2001b). Strong changes in atmospheric methane concentrations and coupling with changes in atmospheric temperatures are well-known from ice cores for the last 650 kyr (Petit et al., 1999; Spahni et al., 2005; IPCC, 2007b). Since pre-industrial times, atmospheric methane concentration has more than doubled to

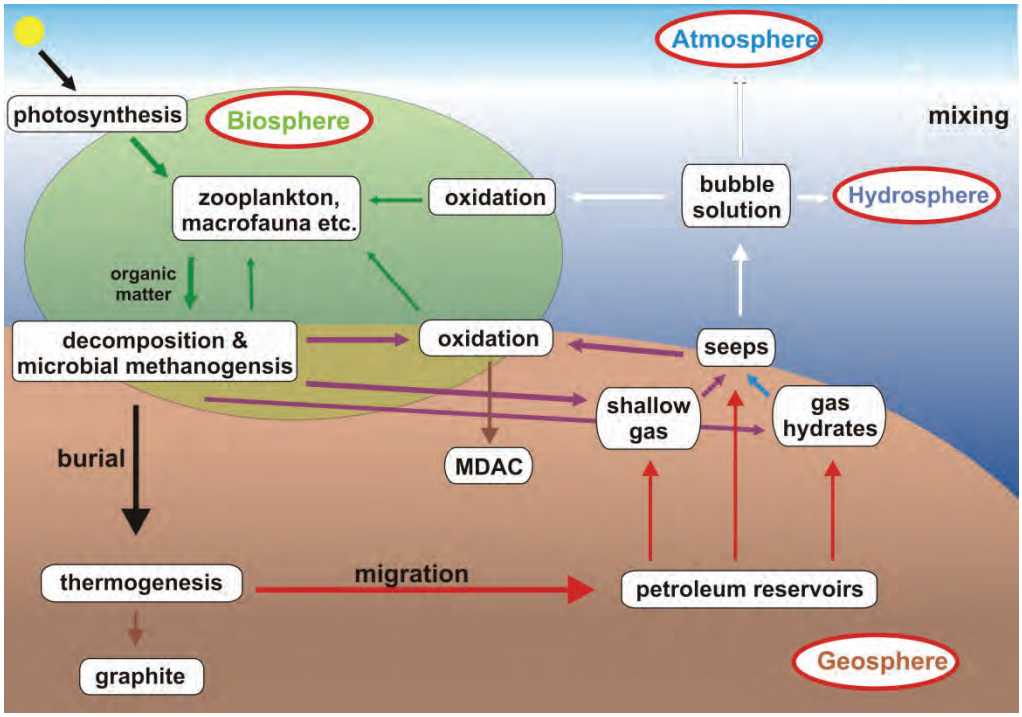

Figure 1.1. Schematic diagram indicating the role of methane and methane release in the carbon cycle (after Judd and Hovland, 2007).

unprecedented high values, due to increasing emissions from anthropogenic sources (livestock, rice paddies, etc.) (Fig. 1.2.A.) (Wuebbles and Hayhoe, 2002; IPCC, 2007b). The total global methane budget is well-known but the strength of each source and sink and their trends are not (IPCC, 2007a). Therefore a correct assessment of natural methane sources (wetlands, oceans, etc.) and sinks is essential to better evaluate the human impact on global atmospheric methane concentration and consequently on global climate change (Fig. 1.2.A.)(IPCC, 2001a; IPCC, 2007a).

Until recently only gas hydrates were considered as a major geological source for atmospheric methane. Destabilizing these ice-like compounds of gas and water present in the ocean sediments could be one of the explanations for the rapid warming episodes during the Earth's history (Dickens et al., 1997; Dickens, 2001; IPCC, 2001b; Etiope, 2009). It is only very recently that other geological methane sources, mainly offshore seeps, have been regarded as possible important contributors to atmospheric methane (IPCC, 2007b) (Fig. 1.2.B.). Before, these sources were regarded negligible, as indicated by their absence in Fig. 1.2.A. (IPCC, 2001b). Current estimates of global methane emissions into the atmosphere from marine bubble-releasing seeps vary between 0.4 and 48 Tg yr^{-1}, with 20 Tg yr^{-1} being a conservative estimate (Judd, 2004; Judd and Hovland, 2007; Etiope, 2009). A comparison with other geological methane sources shows that bubble-releasing methane seeps should be regarded as one of the major natural sources of atmospheric methane (Figs. 1.2.A. and 1.2.B.). However until now the amount of methane released at seeps is still largely unknown. There is a need to obtain correct estimates about the actual area of active seepage and the temporal variability of the seepage intensity and activity. Until the distribution and activity of methane seeps is better understood, seeps should not be neglected as an atmospheric methane source. Judd and Hovland (2007) give a very good overview of and references to this topic. They also indicate the reluctance of atmospheric

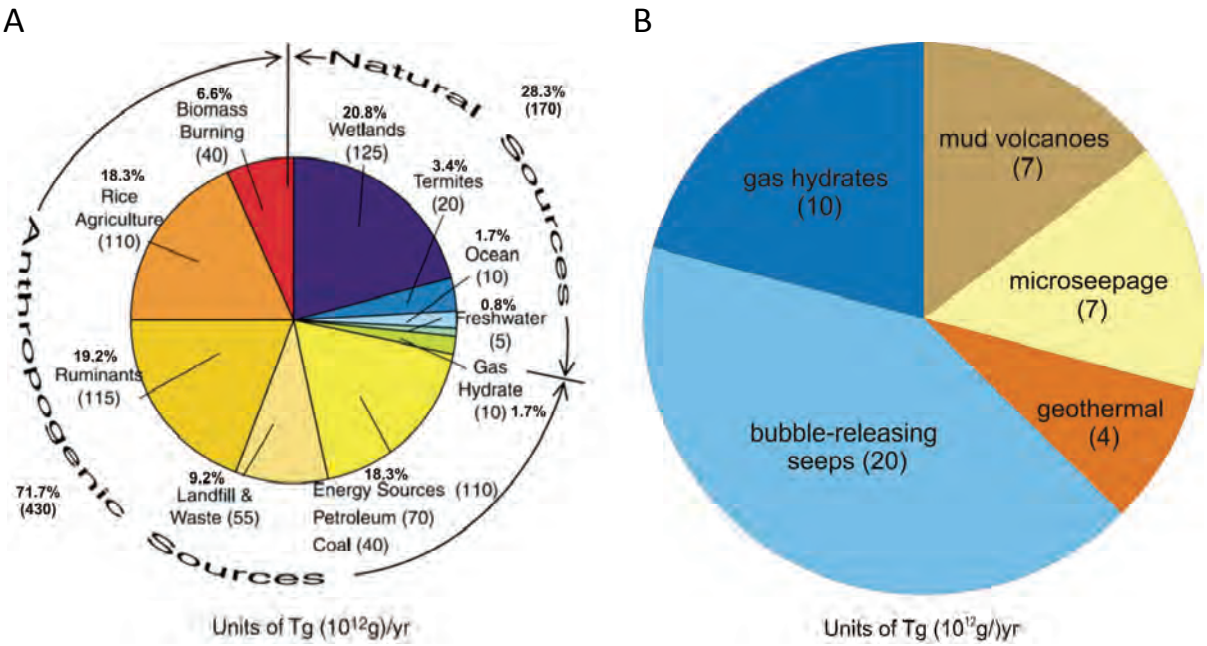

Figure 1.2. A. Diagram showing the relative contributions from various sources of methane to the global atmospheric methane budget. The total atmospheric methane budget is estimated to be 600 Tg of CH_4 yr^{-1} of which 71.7% has an anthropogenic source and 28.3% a natural source Note the absence of methane seeps as a possible source (IPCC, 2001b; Kvenvolden and Rogers, 2005). **B.** Diagram showing the relative contributions from various geological methane sources (Etiope and Klusman, 2002; Etiope and Milkov, 2004; Judd and Hovland, 2007; Etiope, 2009).

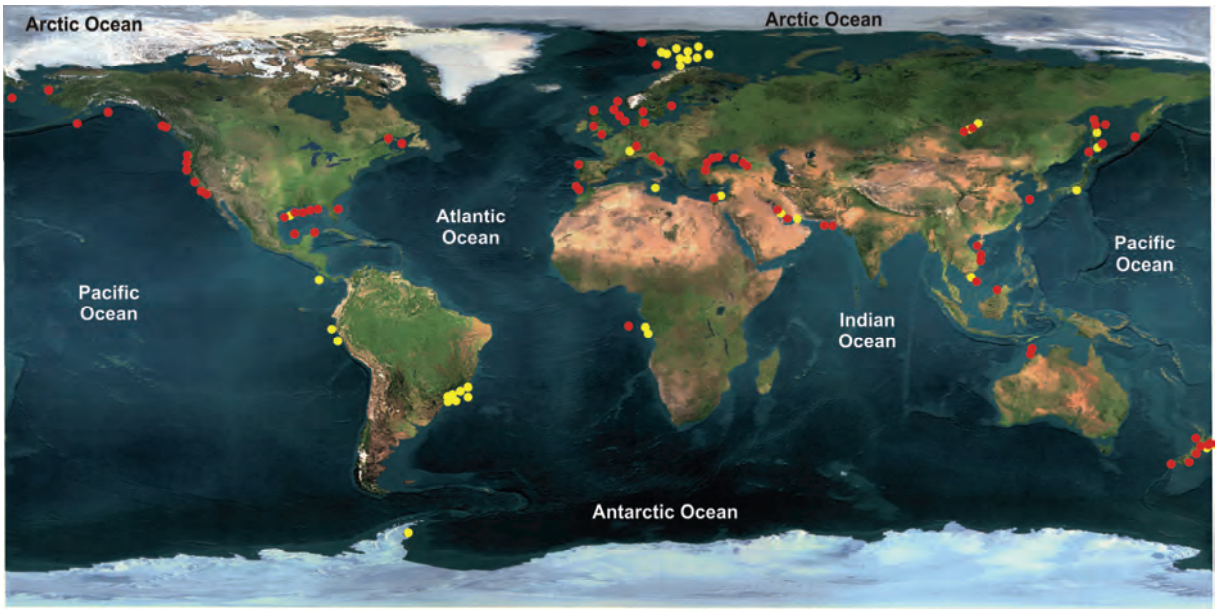

Figure 1.3. Worldwide distribution of bubble-releasing seeps (red dots) and gas seepage indicators (bacterial mats, authigenic carbonates, ice streamthroughs, etc.) (yellow dots). Where seeps as well as the seep indicators are present; they are indicated by red dots (after Judd and Hovland, 2007).

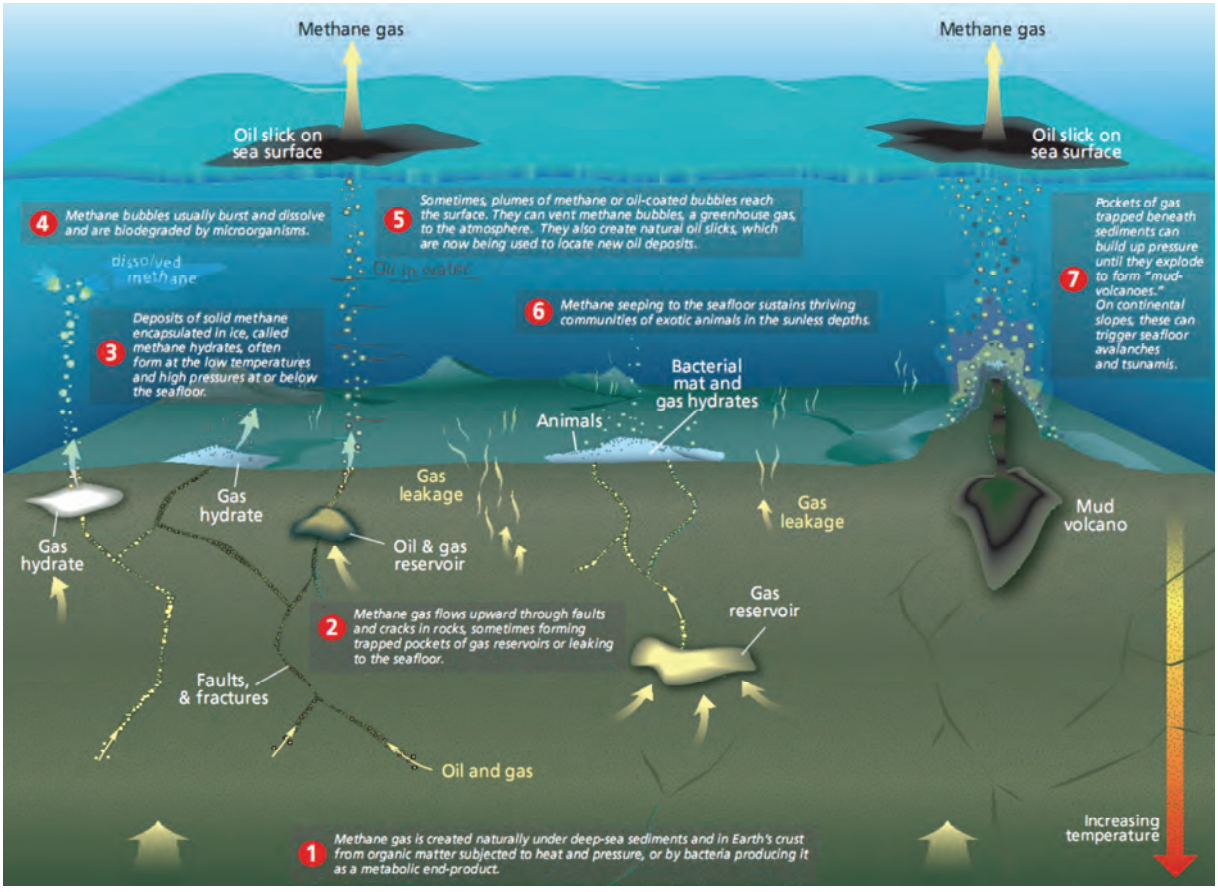

Figure 1.4. A general overview of the subsurface- and water-column features associated with gas-bubble release as witnessed in the Gulf of Mexico where gas-bubble release is associated with oil leakage (Jean Whelan, WHOI).

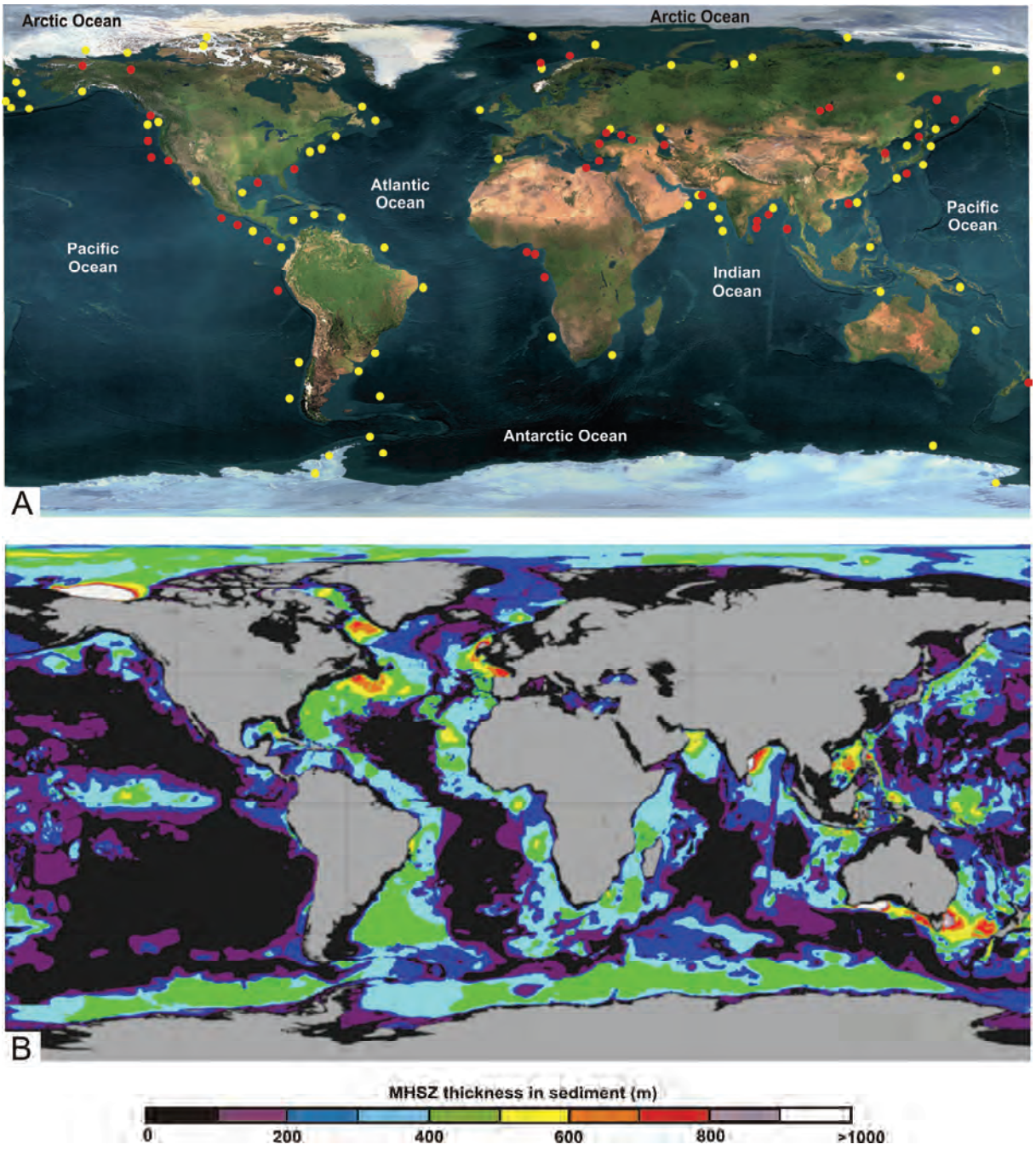

Figure 1.5. A. An overview map of all locations on Earth with recovered gas hydrates (red circles) and inferred gas hydrates (yellow circles). B. Estimated thickness of the gas-hydrate stability zone in the world's oceans (Krey et al., 2009).

modelers to take into account the existence of these geological sources and processes. This alone is already an indication that there is a strong need to study and understand this natural release of methane and the processes involved.

Recent literatures shows that methane seeps and related features occur worldwide from coastal areas to the deep ocean trenches at all possible oceanographic and plate tectonic settings (Fig. 1.3.) (Judd, 2003; Judd and Hovland, 2007). However most seep sites occur at continental margins where organic-rich sediments accumulate and methane is formed. microbially from methanogenesis of organic material or thermogenically resulting from catagenesis of organic material at depth and at higher temperatures (Figs. 1.1. and 1.4.)

(Whiticar, 1999; Judd and Hovland, 2007). The migration of methane and other fluids through the sediments towards the seabed is related to the buoyancy of methane and/or to overpressure generated at depth. During the migration towards the seabed, dissolved and/or free methane gas can be stored in the sediments due to structural or stratigraphic traps (Fig. 1.4.). The largest methane reservoirs present in the ocean's sediments are solid methane hydrates (Fig. 1.5.). These crystalline structures consisting of gas and water can only form and be stable under high-pressure and low-temperature conditions with substantial amounts of gas and water. It is believed that there is more carbon stored in methane hydrates than in all other fossil fuels combined (Fig. 1.5.) (Henriet and Mienert, 1998; Paull and Dillon, 2001; Max et al., 2006; Sloan and Koh, 2007). If pressure and temperature conditions change, gas hydrates can dissociate and hereby support gas seeps at the seafloor and enhance sediment destabilization (Bouriak et al., 2000; Bünz et al., 2005). When methane and other

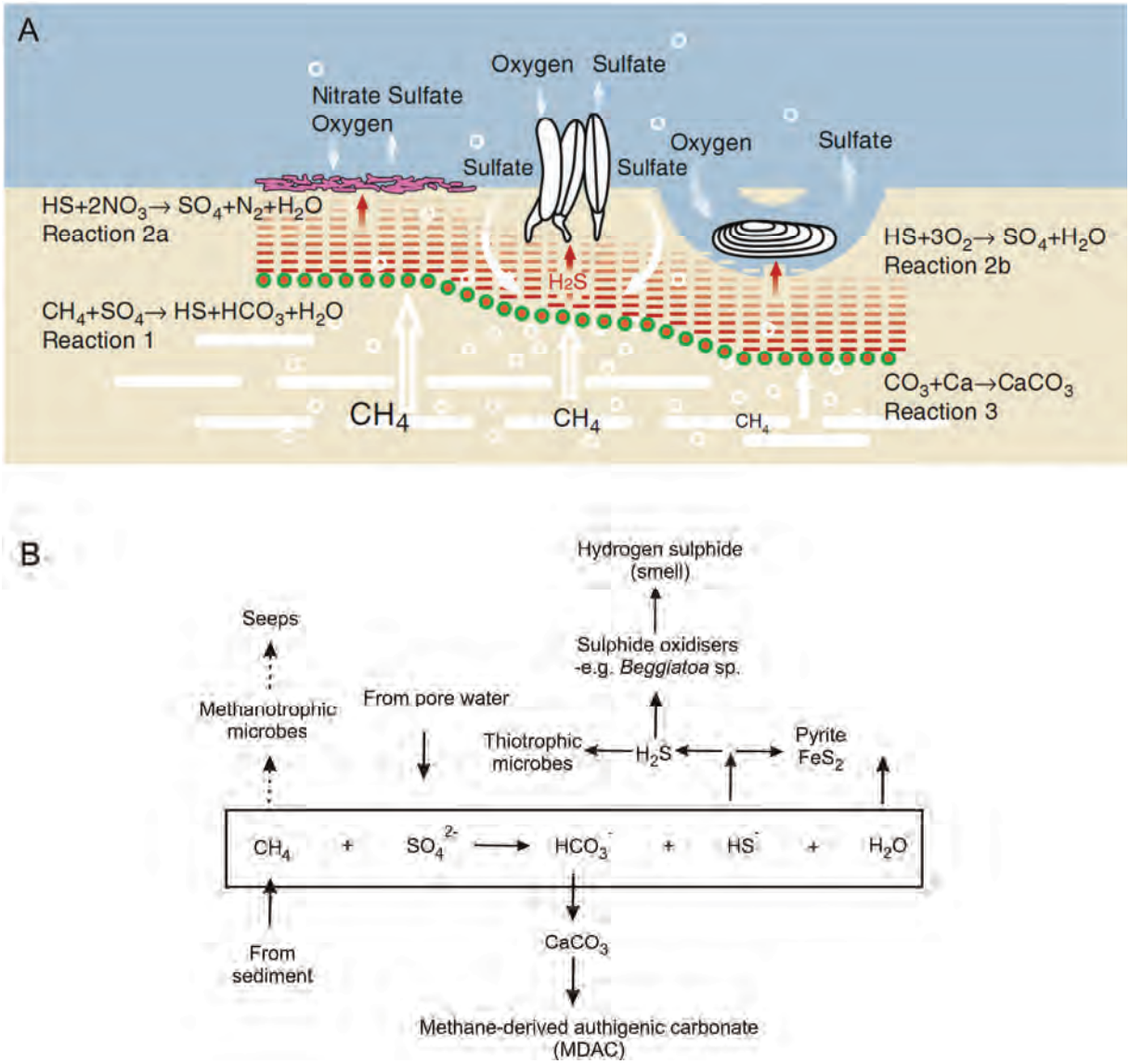

Figure 1.6. A. An overview of the chemical reactions that take place at the seabed-water column transition zone as a result of the anaerobic oxidation of methane (AOM). Note that a difference in methane flux leads to different chemosynthetic fauna's and that AOM is strongly associated with authigenic carbonate formation (Suess, 2010). **B.** A schematic overview of the anaerobic oxidation of methane and its resulting chemical species and methane-related products (Judd and Hovland, 2007).

fluids are released at the seabed after migration through the sediments, their origin as well as their formation depth and the possible followed migration pathways can be deducted from the carbon isotopes ($\delta^{13}C_{CH_4}$) and hydrogen isotopes (δD_{CH_4}) of the released methane (Whiticar, 1999; Judd and Hovland, 2007). Other isotope ratios, e.g. from Sr, B, Li, I, etc., or geothermometers like the lithium-magnesium ratio can also help to indicate the source depth and the followed migration pathway of the fluids released at the seafloor (Aloisi et al., 2004).

Generally, dissolved methane present in pore waters of the near-surface sediments gets completely oxidized by consortia of methane-oxidizing archaea and sulfate-reducing bacteria in anaerobic environments or by the aerobic activity of bacteria (Figs. 1.4. and 1.6.) (Reeburgh et al., 1993; Boetius et al., 2000; Boetius and Suess, 2004; Sommer et al., 2006). As a result of the bacterial activity, seeps can support unique endemic ecosystems of marine organisms (bacteria, tubeworms, clams, etc.) which are strongly related to the flux of dissolved methane, as shown in Fig. 1.6. (see chapters 4, 5 and 7) (Boetius, 2000; Suess, 2010).

Another strong seabed manifestation of high methane fluxes and the associated anaerobic oxidation of methane (AOM) is the precipitation of methane-derived authigenic carbonates (MDACs) or authigenic barites (Boetius, 2000; Greinert et al., 2001; Michaelis et al., 2002; Greinert et al., 2002; Suess, 2010). As shown in Fig. 1.6., MDACs are formed as the product of Ca (and/or Mg) and the bicarbonate resulting from AOM present in the pore waters or bottom waters. Since these carbonates result from AOM, MDACs also have typical carbon isotopes ($\delta^{13}C_{CH_4}$) (see chapters 4, 5 and 7) (von Rad et al., 1996; Judd and Hovland, 2007). Based on their typical geochemistry, fossil MDACs can even provide evidence of fluid flow and AOM in areas where fluid flow only occurred in geological times and has ceased a long time ago (Campbell et al., 2008; De Boever et al., 2009). By the formations of carbonate hardgrounds, seeps can also support non-chemosynthetic organisms.

It is only where fluid flow is focused, mainly at bubble-releasing seeps, that methane can pass the benthic AOM filter and can be released into the water column (Figs. 1.4. and 1.6.) (Judd, 2003). Besides the chemosynthetic fauna and the authigenic carbonates, focused fluid flow leads in some cases to peculiar seabed features like mud volcanoes, pockmarks, etc. These features are all related to seabed fluid flow and possibly with bubble release, nevertheless their genesis can be completely different (Judd and Hovland, 2007).

Methane seepage and the associated features are clearly widespread and diverse, but the activity of seepage is also very variable and transient. Seepage activity changes over short (minutes to days) related to e.g. tides or currents or even over long time scales (years to glacial/interglacial) related to e.g. eustatic sealevel changes (Leifer et al., 2004; Greinert, 2008). The activity and the amount of methane released at the seafloor are also strongly related to the methane sources and the fluid flow pathways and vice versa (see chapters 5 and 7).

Besides the wide variety of scientific interests, the release of methane at the seafloor and the associated features can be economically valuable as potential indicators of deeper hydrocarbon reservoirs. Furthermore the presence of seeps and shallow gas reservoirs pose a threat to offshore constructions, affecting seafloor stability and possibly destroying drilling rigs, pipelines etc (Judd and Hovland, 2007).

It is clear that bubble-releasing seeps and seabed fluid flow are very interesting in various ways and attracted the attention of a variety of scientists and people from industry. Notwithstanding the large amount of studies focusing on gas seeps, their distribution, activity and controls are still largely unknown. A better understanding of these controls, activity and the distribution of seeps, especially bubble-releasing seeps which are the pinnacle of focused fluid flow, would allow more correct assessments of atmospheric methane input from seeps, the fauna associated with seeps and could help to find new energy resources.

1.2. Study objectives

The major objective of this study is to determine the main geological controls on gas-bubble release to better evaluate the distribution of seeps and their associated features. This study should form a solid base for methane flux calculations and for exploration of new hydrocarbon resources. Therefore several seep areas around the world, occurring in different geological settings, have been studied and are compared based on the integration of hydro-acoustic investigations (single- and multibeam echosounding, side scan sonar, seismics), seafloor observations (ROV, submersible, TV-sled) and grainsize-, geochemical- and thermal analyses. Seeps were studied in the NW Black Sea (a passive continental Margin), in the SW Pacific Ocean (an active continental margin) and in Lake Baikal (a rift lake) to see if there are clear differences in control on seepage related to these distinct geological environments. Besides the overall geological and structural setting the main focus was on the role gas hydrates, methane-derived authigenic carbonates, faults and sediment type play in controlling seep distribution.

The main questions posed are:

1) What are the different geological controls on seep distribution, on a basin-wide scale, on kilometer scale and on meter scale?
2) Do seeps occur at certain seafloor morphologies or at certain water depths? Which are these morphologies and how do they relate to the seep distribution, seep activity and to the associated fauna's?
3) Do gas hydrates act as a buffer, a source or a sink for methane and how do hydrates relate to the distribution of bubble-releasing seeps?
4) Can faults be regarded as the main geological features controlling seeps on a kilometer to meter scale? Or is the type of sediment and/or the stratigraphic build up and geometry more important in focusing subsurface fluid migration and the release of gas bubbles at the seafloor?
5) What is the spatial relation between bubble release and other seep-related manifestations at the seafloor and shallow subsurface, e.g. chemosynthetic fauna, authigenic methane-derived carbonates, etc.)?

1.3. Geological setting

1.3.1. Black Sea – Dnepr paleo-delta

The Black Sea is a large semi-enclosed marginal basin surrounded by alpine mountain chains (the Greater Caucasus, Pontides, Southern Crimea, and Balkanides) (Fig. 1.7.). The only connection it has with the world oceans is via the Bosporus Strait through the Marmara Sea, the Dardanelles and the Mediterranean Sea. The Black Sea was formed via back-arc spreading during the Early, Cretaceous-Early Paleogene associated with the subduction of the Neo-Tethys below the Balcanides-Pontides volcanic Arc. (Robinson et al., 1996; Dinu et al., 2005). The Black Sea consists of two large basins, the Western Black Sea Basin and the Eastern Black Sea Basinseparated by the Andrusov Ridge. Sediment thickness in the Black Sea varies from 19 km in the Western Black Sea, 5-6 km on the Andrusov Ridge and 12 km in the Eastern Black Sea (Tugolesov et al., 1985). Since the Eocene, the Black Sea region has changed to a dominantly compressional environment (Nishishin et al., 2003). The study area, the Dnepr paleo-delta, is located on the continental margin of the northwestern Black Sea, above the Kalamit Ridge where the top of the Cretaceous lies at depths of less than 1 km (Fig. 1.7.) (Robinson et al., 1996).

There is no direct evidence for large petroleum reservoirs below the study area; however several oil and gas fields are being produced in the vicinity of the Dnepr paleo-delta (Fig. 2.1.) (Dinu et al., 2005; Popescu et al., 2007). In the Black Sea, the Maykop formation of Middle to Upper Eocene age is the chief hydrocarbon source that feeds numerous mud volcanoes in

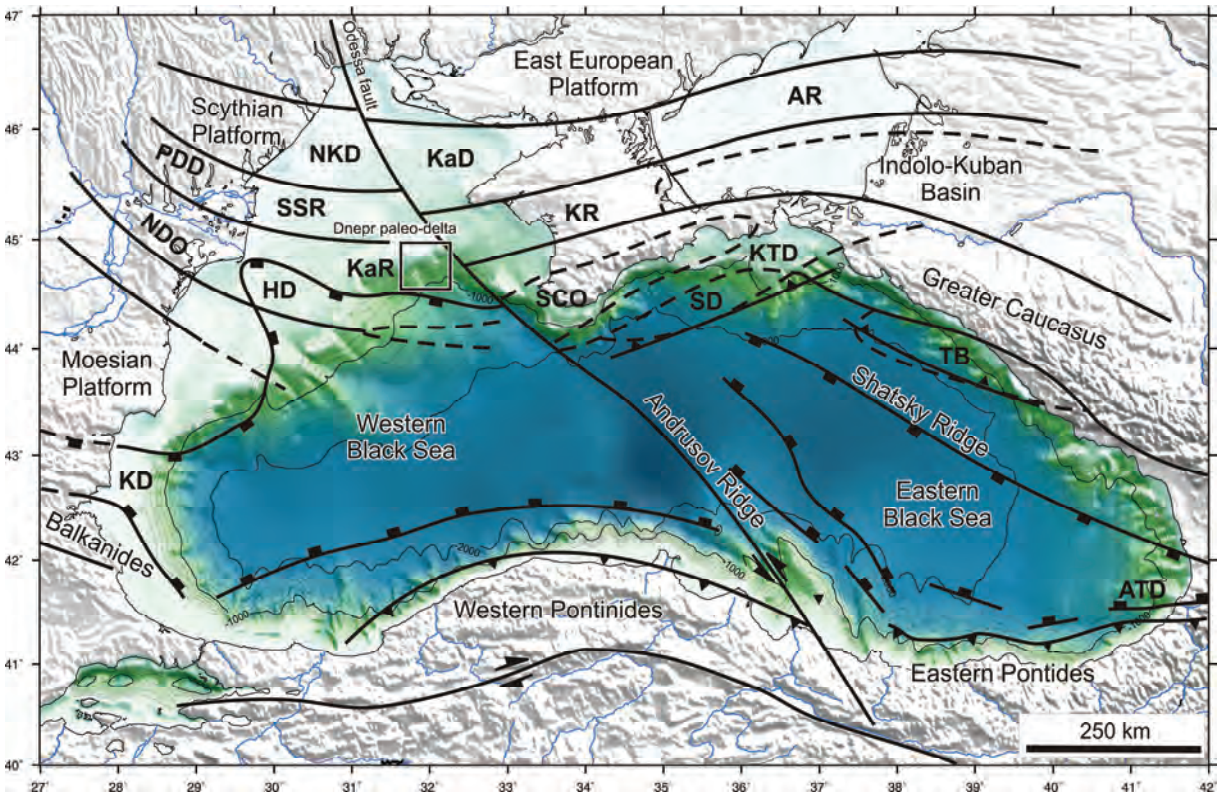

Figure 1.7. Tectonic map of the Black Sea region with indication of the Dnepr paleo-delta study area. (Abbreviations: NDO—North Dobrogea Orogen, SCO—South Crimea Orogen, PDD—Pre-Dobrogea Depression, NKD—North Kilia Depression, KaD—Karkinit Depression, KaR—Kalamit Ridge, HD—Histria Depression, SD—Sorokin Depresion, KTD—Kerci-Taman Depression, KD—Nijna-Kamciisk Depression, ATD—Adjaro-Trialet Depression, TB—Taupse Basin, SSR—Suvorov–Snake Island Ridge, KR—Kramski Ridge, AR—Azov Ridge, BR—Bubkin Ridge (after Dinu et al., 2005).

the deeper basins (Fig. 1.8.) (Robinson et al., 1996; Bohrmann et al., 2003; Kruglyakova et al., 2004). In the Dnepr paleo-delta however, the methane seeps are probably sourced by Holocene organic-rich sediments deposited during successive sea-level lowstands when the main inflowing rivers, Dnepr and Dnestr, deposited organic-rich material hundreds of kilometers beyond their present mouths forming shelf-edge deltas at the present-day shelf break. After the last sea-level lowstand water level rose, leading to fresh-water outflow from and salt-water inflow into the Black Sea through the Bosporus. As a result of density differences and the absence of complete water-column mixing, the Black Sea became the biggest anoxic basin in the world, covering an area of 423,000 km^2, with favorable conditions for preserving organic material and generating hydrocarbons. Microbial degradation of the organic-rich sediments present in the paleo-deltas has led to the formation of shallow gas associated with prolific gas seepage at the seabed at various shelf-break locations in the Black Sea (Fig. 1.8.). The seeps in the Dnepr paleo-delta are associated with a variety of authigenic carbonate build-ups formed by the anaerobic oxidation of microbial methane (Luth et al., 1999; Peckmann et al., 2001; Thiel et al., 2001; Amouroux et al., 2002; Michaelis et al., 2002). The presence of gas hydrates in the study area is indicated by bottom-simulating reflections (BSRs) on seismic data from -700 m water depth (Lüdmann et al., 2004; Zillmer et al., 2005).

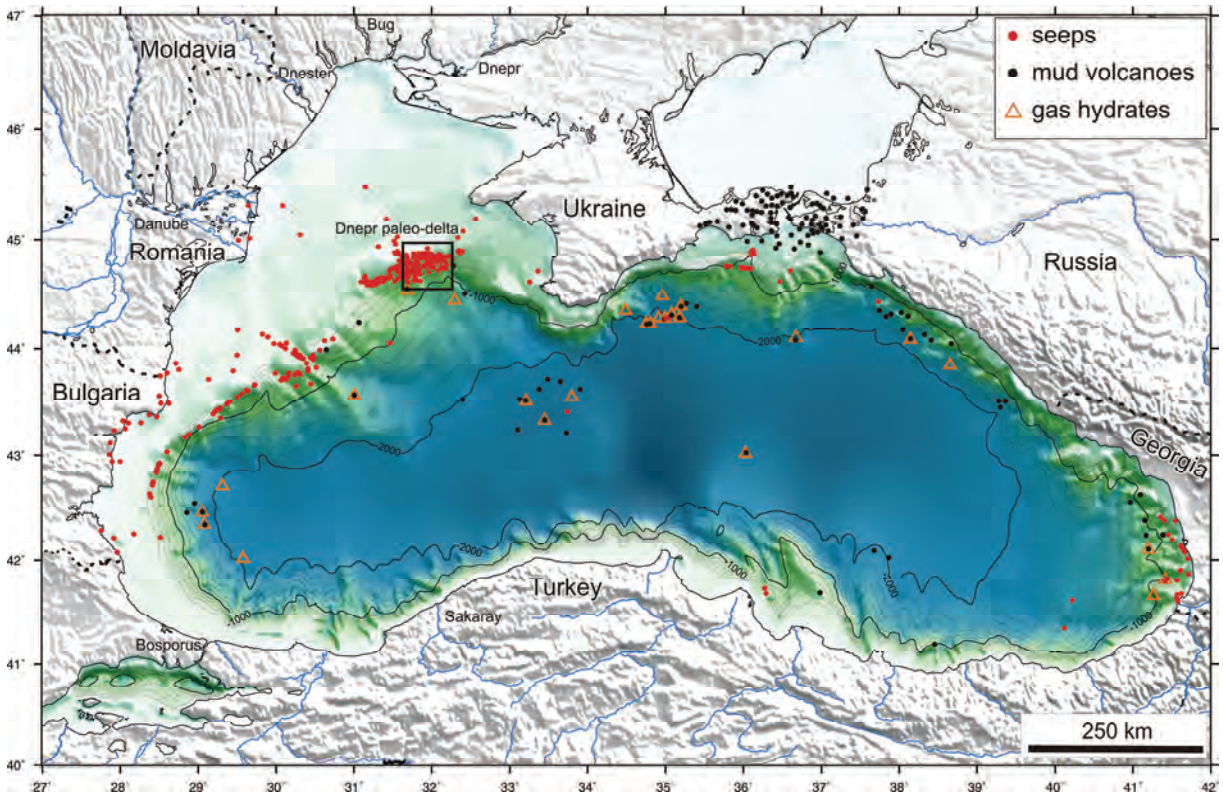

Figure 1.8. Overview map of the Black Sea with indications of seep locations, mud volcanoes and sampled gas hydrates (after Egorov et al., 1998; Naudts et al., 2006; Judd and Hovland, 2007; Popescu et al., 2007).

1.3.2. SW Pacific Ocean – Hikurangi Margin

The Hikurangi Margin in the SW Pacific Ocean on the eastside of the New Zealand's North Island is an active accretionary margin formed by the westward oblique subduction of the Pacific Plate underneath the Australian Plate at a convergence rate of about 40-50 mm/yr (Fig. 1.8.) (Barnes et al., 2010). The 25 Myr old Hikurangi Margins forms the southern end of the Tonga-Kermadec-Hikurangi subduction zone. The Rock Garden study area is positioned above a 3 km high subducted seamount which has strongly deformed and uplifted this part of the Hikurangi Margin (Pecher et al., 2005; Barnes et al., 2010). This area can be regarded as the transition zone between the classic frontal accretionary system in the south and the steeper margin associated with tectonic erosion and subducting seamounts in the north (Barnes et al., 2010). Laterally the Hikurangi Margin can be divided in a western part with an imbricated foundation of pre-subduction accretionary wedge of mainly scraped off Pliocene – Pleistocene trench-fill turbidites. The boundary between these two units may be significant for the distribution of the different seeps sites at the Hikurangi Margin (Fig. 1.10.) (Lewis and Marshall, 1996; Barnes et al., 2010). The Hikurangi Margin comprises six seep areas with a total of 32 seep sites detected by visual or acoustic observations or by sampling of seep fauna or authigenic carbonates (Fig. 1.10.) (Lewis and Marshall, 1996; Greinert et al., 2010). Almost all discovered seeps on the Hikurangi Margins occur within or on the edge of the gas-hydrate stability zone. The presence of gas hydrates on the Hikurangi Margin is indicated by the widespread occurrence of BSRs on seismic data from -650 m water depth (Henrys et al., 2003; Pecher et al., 2010). Notwithstanding the widespread occurrence, gas hydrates have only been sampled at three seep sites (Fig. 1.10.) (Greinert et al., 2010). Hydrates have not yet been retrieved in the Rock Garden study area, although BSRs occur at shallow subsurface depth and even pinch out near the ridge crest. Some of these sites, e.g. the studied Faure Site,

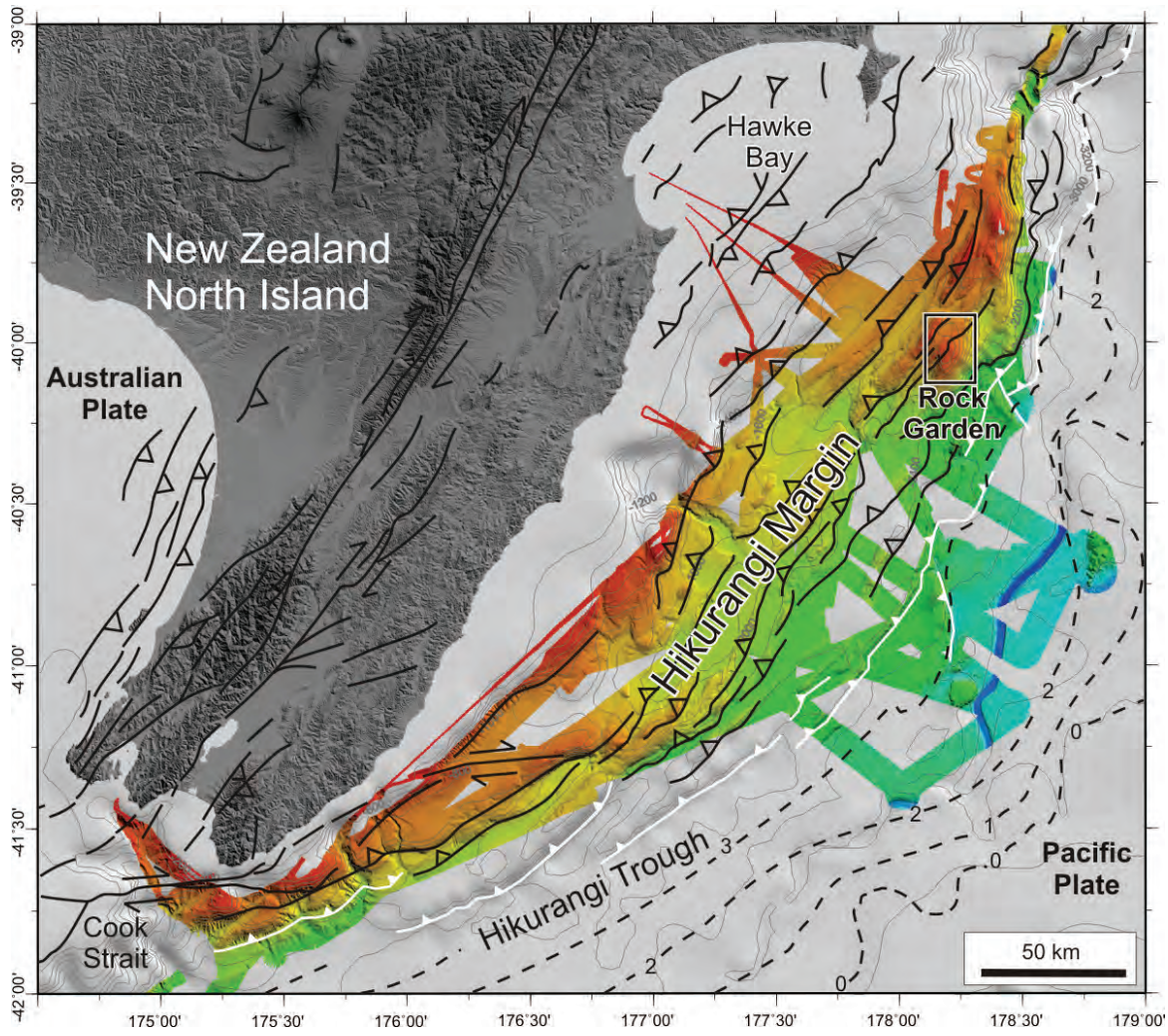

Figure 1.9. Tectonic map of the Hikurangi Margin with indication of the Rock Garden study area. The white trusts represent the principle deformation front, the major active faults are shown in black and the thickness (km) of the trench-fill turbidites is also indicated (after Lewis et al., 1998; Barnes et al., 2010).

are associated with seepage and/or submarine landslides (Pecher et al., 2005; Faure et al., 2006). As for other seep sites in the Hikurangi Margin, deep reaching fractures play an important role in the distribution of seeps in the Rock Garden area (Crutchley et al., this issue).

1.3.3. Lake Baikal – Posolsky Bank

Lake Baikal is a rift lake in Southern Siberia which occupies the three central depressions of the Baikal Rift Zone (BRZ); the Southern, the Central and the Northern Baikal Basins (SBB, CBB & NBB) (Fig. 1.11.). The lake has a maximum depth of -1637 m and it holds 20% of the world's liquid surface fresh water which makes it the deepest lake and the largest lake with regard to volume in the world. The rifting of the BRZ started ca. 30-35 Ma ago as a result of the India-Eurasia collision and is still active at an extension rate of about 4-5 mm/yr (Tapponnier and Molnar, 1979; Petit et al., 1997; Calais et al., 1998; Petit et al., 1998). The three basins are separated by two structural highs; the Selenga Delta Accommodation Zone (SDAZ) between the SBB and the CBB, and the Academician Ridge Accommodation Zone (ARAZ) between the CBB and NBB. The three Baikal Basins have a clear asymmetric geometry with large displacement faults at their western borders and small normal faults at their eastern borders (Fig. 1.1.)

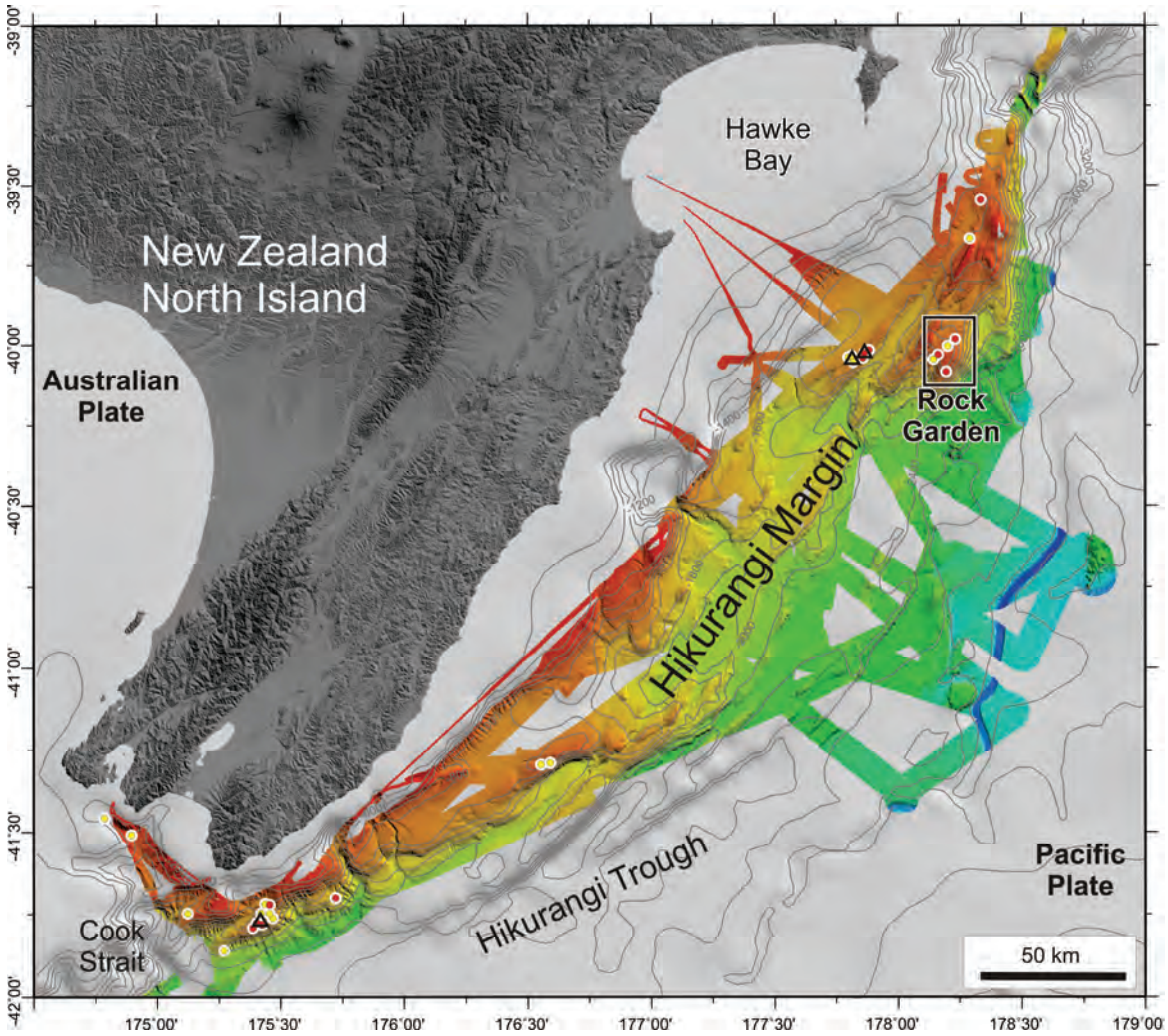

Figure 1.10. Overview map of the Hikurangi Margin with indications of seep locations (red dots), gas seepage indicators (yellow dots) and sampled gas hydrates (black triangles) (Greinert et al., 2010).

(Hutchinson et al., 1992; Mats, 1993; Scholz et al., 1993). Sediment thickness in the basins varies between 4.4 km in NBB, over 7 km in SBB to 7.5 km in the CCB (Kontorovich et al., 2007). The study area, the Posolsky Bank fault block, is located near the Posolsky Fault which is an eastern segment of the Obruchevsky Fault that marks the western margin of the SBB (Fig. 1.11.). The Posolsky Bank structurally belongs to the SDAZ (Scholz and Hutchinson, 2000; Bezrukova et al., 2005; Charlet et al., 2005).

The presence of seeps in Lake Baikal was already described in ancient records reporting on areas with absent ice cover in winter ('ice streamthroughs'), abundant fish deaths and observation of bubbles at the lake surface (Fig.1.12.) (Granin and Granina, 2002). Since the observation of BSRs on seismic recordings and the subsequent sampling of deep hydrates during the Baikal Drilling Project (BDP-97), methane seeps, oil seeps and gas-hydrate-bearing mud volcanoes have been discovered on many locations in the SBB and the CBB (Fig. 1.12.) (e.g. Hutchinson et al., 1991; Golmshtok et al., 1997; Vanneste et al., 2001; Williams et al., 2001; Klerkx et al., 2003; Matveeva et al., 2003; Khlystov, 2006; Klerkx et al., 2006). All mud volcanoes occur at locations with an anomalous shallow BSR near major faults. Geothermal fluid pulses along these large faults are believed to have led to hydrate destabilization and source the mud volcanoes (Vanneste et al., 2001; De Batist et al., 2002; Van Rensbergen et al., 2002; Vanneste et al., 2002; Klerkx et al., 2006). Notwithstanding the occurrence of gas-bubble release at some of the

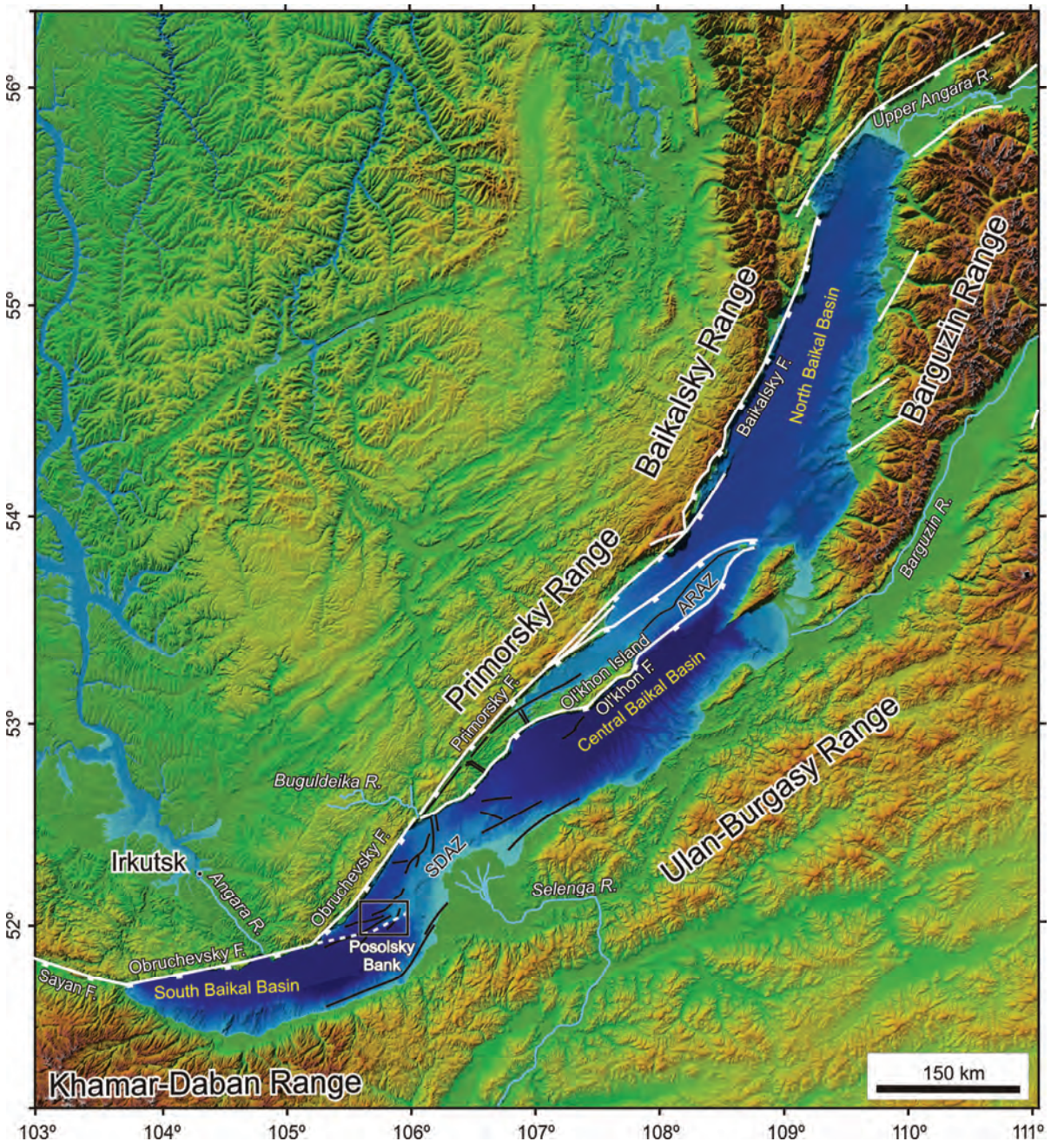

Figure 1.11. Tectonic map of Lake Baikal with indication of the Posolsky Bank study area (Klerkx et al., 2006). (Abbreviations: SDAZ—Selenga Delta Accommodation Zone; ARAZ—Academician Ridge Accommodation Zone).

mud volcanoes, a majority of the methane seeps occur outside of the gas-hydrate stability zone near deltas or canyons (Granin and Granina, 2002). The seeps on the Posolsky Bank are unique since they occur on the scarp of a tilted fault block, outside of the GHSZ. Furthermore, the released methane has a mixed microbial-thermogenic origin with a small ethane admixture (Kalmychkov et al., 2006).

1.4. Methods

Since the release of gas bubbles and its associated features are often associated with disturbances of the natural environment they cause different anomalies in a variety of datasets. To better understand the distribution of and the controls on gas-bubble releasing seeps different datasets have been integrated. This includes water-column data, seafloor data

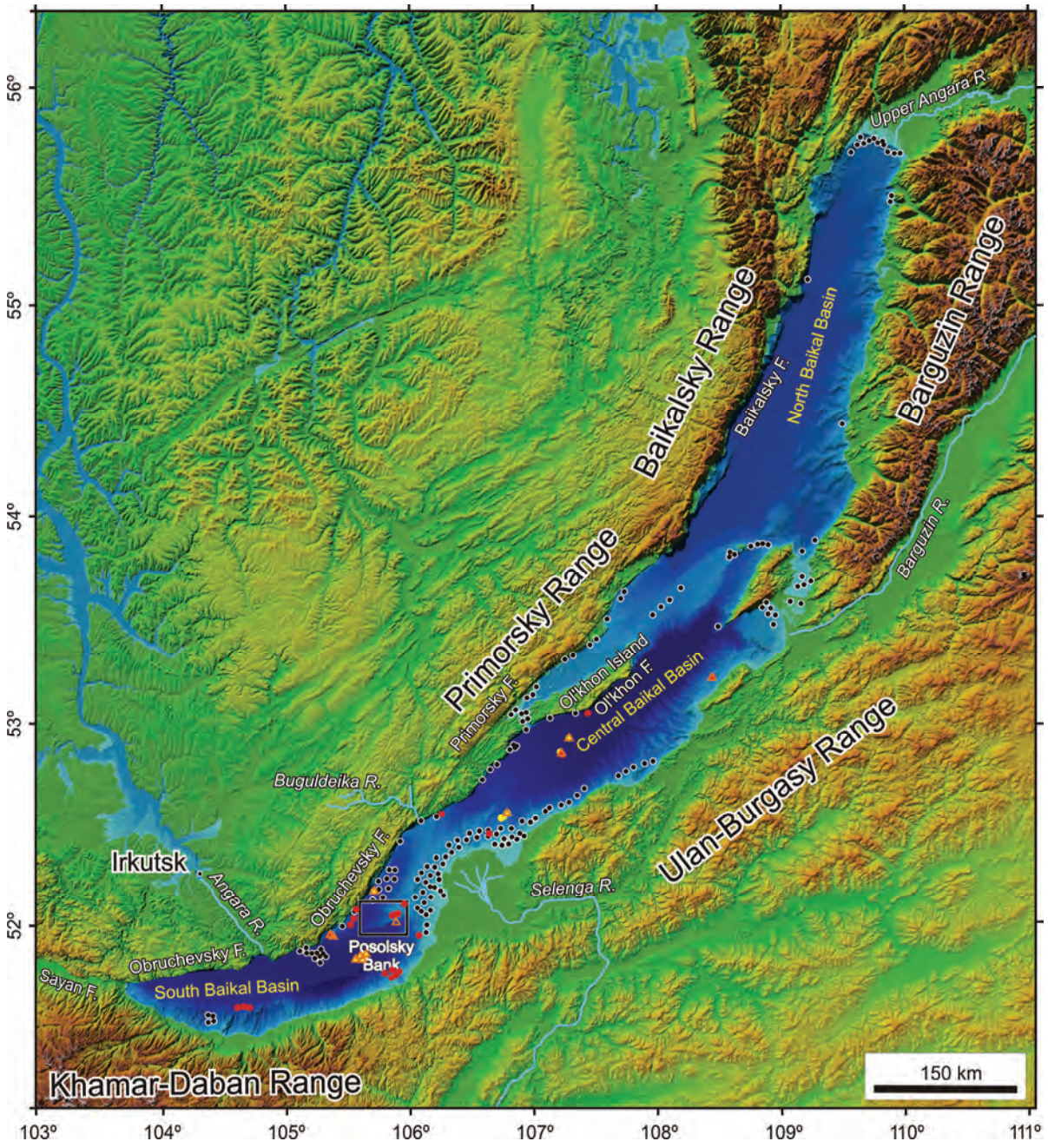

Figure 1.12. Overview map of Lake Baikal with indications of seep locations (red dots), gas seepage indicators (black dots), mud volcanoes (yellow dots) and sampled gas hydrates (orange triangles) (Granin and Granina, 2002; Klerkx et al., 2006; Schmid et al., 2007).

and subsurface data. This study mainly used acoustic methods since they are strongly affected by the occurrence of free gas in different media.

1.4.1. Water-column data

The hydro-acoustic water-column data is the essential dataset for this study, since the high impedance contrast between free gas and water allows the detection and positioning of gas-bubble release from the seafloor into the water column over vast areas in a limited time span (Greinert et al., 2006; Artemov et al., 2007). Bubbles in the water column have been detected with single-beam echosounders in all three study areas (Fig. 1.13.). On such echosounder records the rising bubbles form

acoustic anomalies that are commonly referred to as "flares".

On the Black Sea a hull-mounted SIMRAD EK500 dual-frequency (38-120 kHz) split-beam echosounder was used which operates with a total beam width of 7°. Bubble detection on the Hikurangi Margin was performed with two echosounder systems a SIMRAD EK500 using 12 and 27 kHz and a SIMRAD ES60 using 38 kHz. On Lake Baikal also two different echosounder systems were used; a FURUNO-1000 and a FURUNO-1100, both operating at 28 kHz. All these systems are able to detect rising bubbles with sizes ranging from mm to cm scale (see chapters 2-6).

Flares were even observed on high-resolution seismic data (5 kHz). Visual observation of seeps in the Black Sea was also performed with a submersible and video sled (Fig. 1.13.). On the Hikurangi Margin gas bubbles were detected with the forward-looking sonar (325-675 kHz) installed on the ROV and by visual ROV observations (Fig. 1.13.) (see chapters 2-6).

From all the used methods, seep detection by the use of echosounders is the most effective since a large area can be covered even during deployment of other gear. Furthermore, very small bubbles can be detected, which are visually sometimes hard to indentify. Visual observations have the advantage of being able to pinpoint the bubble-releasing location on the seafloor with a higher accuracy than what can be achieved by echosounders. They also allow monitoring of the seep activity, accurate flux determinations and observations of seep-related seafloor manifestations. But deployments of ROVs or submersibles are much more cumbersome and the area covered on the seafloor is much smaller.

1.4.2. Seafloor data

Since active seep sites are often associated with typical seafloor morphologies, with chemosynthetic faunal communities or with authigenic methane-derived carbonates, they are relatively easy to be observed by a wide range of seafloor observations, even at instances without active release of bubbles. For this study two different types of seafloor data were used: acoustic seafloor data from multibeam and side-scan sonar measurements and visual seafloor observations done with a ROV, with a submersible, with a video sled or with other TV-guided equipment (Fig. 1.13.).

On the Black Sea and on Lake Baikal a 50 kHz SeaBeam 1050 swath system was used that was operated with 120° swath, transmitting and receiving 108 beams of 3° by 3° beam angle. At the Hikurangi Margin different, lower frequency systems were used adapted to the larger water depth. The used multibeam systems were the SIMRAD EM120 which operates at 20 kHz with 191 beams of 2° by 2° beam angle and the SIMRAD EM 300 which operates at 30 kHz with 135 beams of 2° by 2° beam angle. Besides obtaining the water depth, all used multibeam systems were able to record the raw backscatter data which gave extra information about the nature of the seafloor near the seep sites (e.g. presence of MDACs, etc.). In the Black Sea, backscatter seafloor data was also obtained by side-scan sonar measurement with the SONIC-3 sonar system (30 kHz). In case of the Black Sea, the results from the multibeam system was more useful than the data obtained from the side-scan sonar, since the multibeam backscatter data is correctly positioned at the seafloor, which is not the case for the side-scan sonar data, even with the side-scan data having a larger theoretic horizontal resolution than the multibeam backscatter data (0.5 m by 0.5 m versus 5 m by 5 m) (see chapters 2-6).

The visual observation techniques discussed in section 1.4.1. have also been used for seafloor observations. From all used visual observations techniques it is clear that the ROV and submersible are most suited for detailed long-term (minutes to hours) observation of seeps and the surrounding seafloor. Video sleds and other TV-guided equipment have the advantage of being less complicated and are ideal for making transects but they normally don't have the capability of sampling gas or rocks (see chapters 2-6).

As for the water-column observations, large seafloor observations are best done with acoustic methods which are able to cover a lot of ground in rather small time spans. Possible interesting areas indicated by the acoustic observations can then be inspected by visual

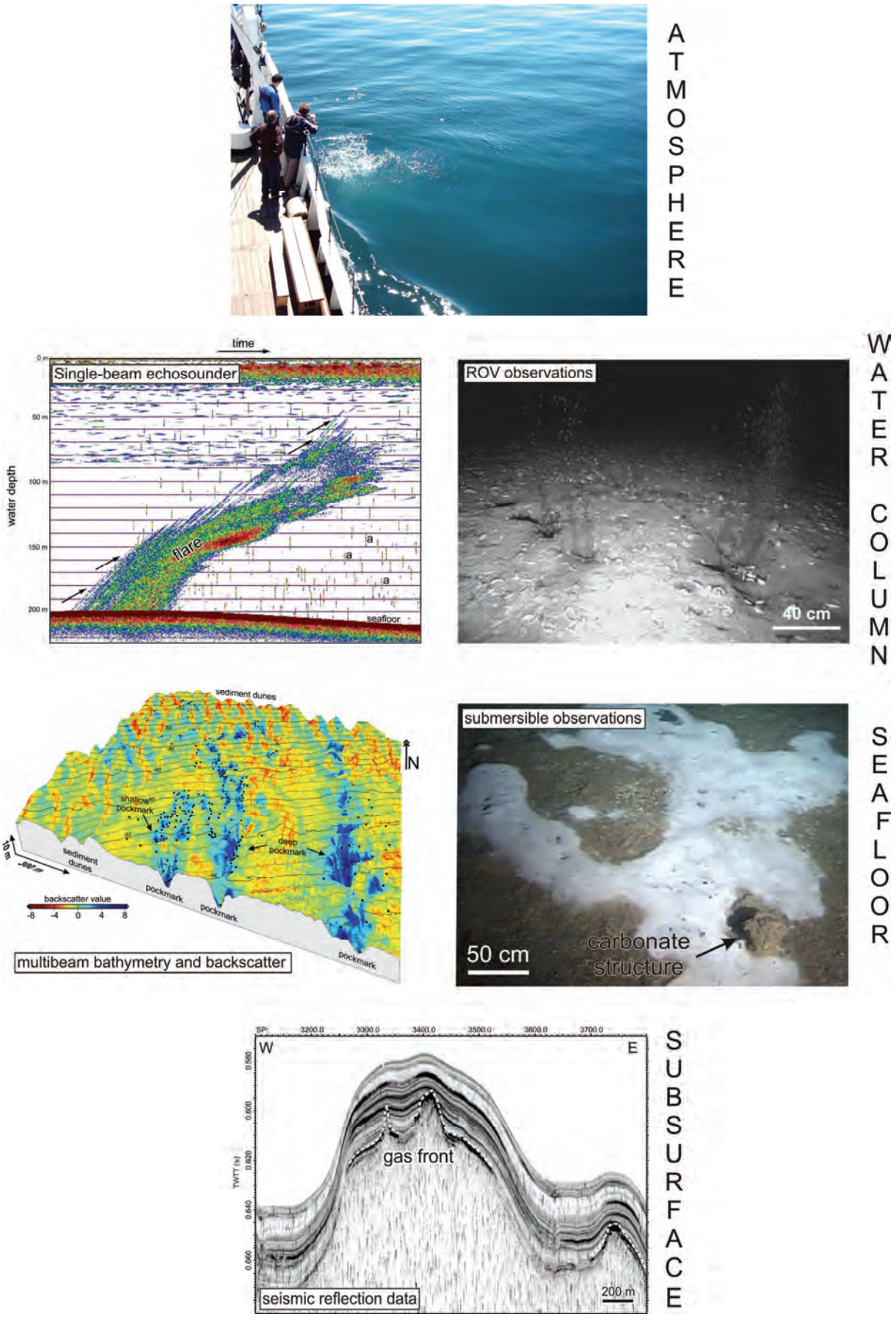

Figure 1.13. Overview of the main datasets used in this study.

seafloor observations which allow very detailed seafloor characterization.

1.4.3. Subsurface data

The presence of seep sites on the seafloor is often indicated by shallow gas in the subsurface. Different kinds of seismic reflection data has been used to image the presence, the behavior and the kind (i.e. free gas versus hydrate) of shallow gas in the subsurface (Fig. 1.13.). In the Black Sea, sediment coring was undertaken to investigate possible correlations between high-backscatter patches on multibeam data, seep occurrences and shallow gas. For the Lake Baikal study, seismic reflection data was used to make calculations for heat flow and hydrate stability.

Four types of seismic reflection data were acquired using four different sources (5 kHz pinger, SIG-sparker, CENTIPEDE sparker and GI-gun) each within a different frequency range showing different aspects of the subsurface geology and shallow gas distribution. The very shallow was investigated using a deeptow 5 kHz pinger with a theoretical resolution of 30 cm, for a maximum penetration of 35 ms two-way travel time (TWTT). To achieve a bit more penetration, single-channel reflection data were collected with a SIG and with a CENTIPEDE sparker source with a passive surface streamer with 10 hydrophones. The SIG has a central frequency of 500-700 Hz and a theoretical resolution of 1 m, for a maximum penetration of 200-300 ms TWTT. Whereas the CENTIPEDE has a central frequency of 1100-1200 Hz and a theoretical resolution of 70 cm, for a maximum penetration of 100 ms TWTT. Possible hydrate reservoirs in the Black Sea were visualized with multi-channel seismic data acquired with a GI-gun source (central frequency of 150 Hz) and a passive surface streamer with 16 hydrophone groups. The theoretical vertical resolution of the GI-gun data is 6 m and the maximum penetrations is 600 ms TWTT.

As indicated in the previous paragraph each seismic source has its own characteristics, sources with higher frequency have higher resolutions and are more affected by shallow gas, whereas sources with a lower frequency have lower resolutions but are able to visualize the deeper subsurface even with the presence of near surface shallow gas. A nice comparison of the different seismic reflection techniques and its application for shallow gas detection is given in chapter 2, as well as in chapter 3, 4 and 6.

1.5. Project framework

The datasets obtained for this study came from the EC-FP5 project CRIMEA (Black Sea), the New Vents SO191 cruise (New Zealand), several BELSPO and INTAS projects and an FWO “Krediet aan Navorsers” project (Lake Baikal).

Dnepr paleo-delta (Black Sea)

The EC-FP5 project CRIMEA (“Contribution of high-intensity gas seeps in the Black Sea to methane emission to the atmosphere”) (2003-2006) studied and quantified the transfer of methane emitted at bubble-releasing seeps at the seafloor through the water column and into the atmosphere. This RCMG-UGENT coordinated project focused on the Dnepr paleo-delta area and the Dvurechenskiy mud volcano area in the Ukrainian Part of the Black Sea. As RCMG-UGENT, we were responsible for the geological characterization of the seep areas; e.g. subsurface methane sources, the migration pathways and controls on seep distribution. The results obtained in the Dnepr paleo-delta are described in CHAPTER 2-4 (Naudts et al., 2006; Naudts et al., 2008; Naudts et al., 2009)

Hikurangi Margin (SW Pacific Ocean)

The SO191 expedition to the Hikurangi Margin (2007) was funded by the Federal Ministry of Education and Research (Germany) in the framework of the COMET project within the R&D program GEOTECHNOLOGIEN (grant 03G0600D and 03G0191A). The ROV work during the SO191 cruise was co-funded by FWO Flanders. The purchase of the ROV was possible thanks to an Impulsfinanciering of the Special Research Fund of Universiteit Gent. The SO191 expedition focused on seeps and associated gas hydrates at the Hikurangi Margin to better understand the role of methane in the global biogeochemical cycle. The results obtained with the ROV and other TV-guided gear in the Rock

Garden area of the Hikurangi Margin are described in CHAPTER 5 (Naudts et al., 2010).

Posolsky Bank (Lake Baikal)

The data studied from Lake Baikal were obtained within the framework of the BELSPO-project "Gas hydrates and gas seeps in Lake Baikal" (1998-2001), the BELSPO-project "Gas hydrates and gas seeps in Lake Baikal (Phase 2)" (2001-2003), the INTAS-project "Assessment and evaluation of gas hydrates in Lake Baikal" (1998-2000), the INTAS-project "A new bathymetric computer map of Lake Baikal" (2000-2002), the INTAS-project "MULTISGAS - Multidisciplinary study of natural gas seeps in Lake Baikal" (2002-2004) and the FWO project Krediet aan Navorsers L. Naudts “Detailkartering van actieve methaanbronnen, moddervulkanen en gashydraten in het Baikalmeer door middel van multibeam-bathymetrie” (2009). All of these projects had mainly the goal to assess the distribution of gas hydrates, mud volcanoes and seeps in Lake Baikal. For this study all available data within the Posolsky Bank area was combined to understand the present seep sites, as described in CHAPTER 7 (Naudts et al., submitted).

1.6. Thesis outline

The thesis consists of a general introduction chapter, followed by a result part consisting of five chapters which are followed by a discussion/conclusion part consisting of two chapters. The first four chapters of the result part (CHAPTER 2 - CHAPTER 5) have been published in international peer-reviewed journals; the remaining CHAPTER 6 is submitted. Since each of these chapters has been published individually an overlap regarding introductions and methodologies is unavoidable; this however allows the separate reading of each chapter. A number of other relevant papers published during the time of this study can be found in the publication list added in appendix A. Since a large time of this study has been spend on research expeditions, an overview is given in appendix B.

CHAPTER 2 gives an overview of shallow gas, gas-hydrate occurrence and bubble-releasing seeps and their detection by geophysical methods. Taking into account the used methods and datasets this chapter can be seen as an introduction chapter to CHAPTER 3-6. This chapter has been published as: *Naudts, L., De Batist, M., Greinert, J., Artemov, Y., 2009. Geo- and hydro-acoustic manifestations of shallow gas and gas seeps in the Dnepr paleo-delta, northwestern Black Sea. The Leading Edge 28, 1030-1040.*

CHAPTER 3 reports on the large scale geological controls on seep distribution in the Dnepr paleo-delta, northwestern Black Sea. This chapter gives also an overview of different seafloor morphologies that are associated with bubble-releasing seeps in the Black Sea and other seep areas. The almost 3000 detected seeps in this area, makes the Dnepr paleo-delta one of the largest known seep areas in the world. This chapter is published as: *Naudts, L., Greinert, J., Artemov, Y., Staelens, P., Poort, J., Van Rensbergen, P., De Batist, M., 2006. Geological and morphological setting of 2778 methane seeps in the Dnepr paleo-delta, northwestern Black Sea. Mar. Geol. 227, 177-199.*

CHAPTER 4 focuses on the shelf area of the Dnepr paleo-delta seep area discussed in CHAPTER 3, more precisely on the relation between high acoustic seafloor backscatter and the associated local distribution of seeps. Analyses of geophysical, geochemical and seafloor observations identified methane-derived authigenic carbonates as the being the main cause for the enhanced backscatter and associated seeps distribution. This chapter is published as: *Naudts, L., Greinert, J., Artemov, Y., Beaubien, S.E., Borowski, C., De Batist, M., 2008. Anomalous seafloor backscatter patterns in methane venting areas, Dnepr paleo-delta, NW Black Sea. Mar. Geol. 251, 253-267.*

CHAPTER 5 looks at two different seafloor manifestations of bubble-releasing seeps on the Hikurangi Accretionary Margin, east of New Zealand’s North Island. Seafloor observations made by a ROV and other TV-guided gear

integrated with seismic and geochemical data allowed explaining the differences between the two seeps sites in regard to the depth of the gas-hydrate stability zone and the tectonic history. This chapter is published as: *Naudts, L., Greinert, J., Poort, J., Belza, J., Vangampelaere, E., Boone, D., Linke, P., Henriet, J.P., De Batist, M., 2010. Active venting sites on the gas-hydrate-bearing Hikurangi Margin, Off New Zealand: Diffusive- versus bubble-released methane. Mar. Geol.272, 233-250.*

CHAPTER 6 deals with bubble-releasing seeps in the rift-lake environment of Lake Baikal. The seeps on the Posolsky Fault Scarp near the crest of the Posolsky Fault Block are fed by gas coming from below the gas-hydrate stability zone. The fault associated with the seepage rather cuts off the gas-bearing layers than acts as a fluid conduit. This chapter is submitted as: Naudts, L., Khlystov, O., Granin, N., Chensky, A., Poort, J., De Batist, M., submitted. *Stratigraphic and structural controls on the location of active methane seep on Posolsky Bank, Lake Baikal.* Mar. Pet. Geol.

CHAPTER 7 integrates all findings discussed in the previous chapters with published data from other bubble-releasing seep site in the world to come up with the similarities and differences in geological controls on the distribution of seeps. This chapter also discusses if these similarities or differences are related to the specific geological setting.

CHAPTER 8 gives an overview of the final conclusions and raises some questions which have originated from this study.

References

Aloisi, G., Drews, M., Wallmann, K., Bohrmann, G., 2004. Fluid expulsion from the Dvurechenskii mud volcano (Black Sea) - Part I. Fluid sources and relevance to Li, B, Sr, I and dissolved inorganic nitrogen cycles. Earth Planet. Sci. Lett. 225, 347-363.

Amouroux, D., Roberts, G., Rapsomanikis, S., Andreae, M.O., 2002. Biogenic Gas (CH4, N2O, DMS) Emission to the Atmosphere from Near-shore and Shelf Waters of the North-western Black Sea. Estuarine, Coastal Shelf Sci. 54, 575-587.

Artemov, Y.G., Egorov, V., Polikarpov, N., Gulin, S.B., 2007. Methane emission to the hydro- and atmosphere by gas bubble streams in the Dnieper paleo-delta, the Black Sea. Reports of the Natl. Acad. of Sci. of Ukraine 5, 110-116.

Barnes, P.M., Lamarche, G., Bialas, J., Henrys, S., Pecher, I., Netzeband, G.L., Greinert, J., Mountjoy, J.J., Pedley, K., Crutchley, G., 2010. Tectonic and geological framework for gas hydrates and cold seeps on the Hikurangi subduction margin, New Zealand. Mar. Geol. 272, 26-48.

Bezrukova, E., Bukharov, A., Bychinsky, V., Fedenya, S., Gelety, V., Goreglyad, A., Gorokhov, I., Gvozdkov, A., Ivanov, E., Kalmychkov, G., Kawai, T., Kerber, E., Khakhaev, B., Khomutova, M., Khursevich, G., Kochukov, V., Krainov, V., Kravchinsky, V., Kudryashov, N., Kulagina, N., Kuzmin, M., Letunova, P., Levina, O., Ochiai, S., Pevzner, L., Prokopenko, A., Solotchin, P., Tanaka, A., Tkachenko, L., Williams, D., Yamaguchi, J., 2005. A new Quaternary record of regional tectonic, sedimentation and paleoclimate changes from drill core BDP-99 at Posolskaya Bank, Lake Baikal. Quat. Int. 136, 105-121.

Boetius, A., Ravenschlag, K., Schubert, C.J., Rickert, D., Widdel, F., Gieseke, A., Amann, R., Jorgensen, B.B., Witte, U., Pfannkuche, O., 2000. A marine microbial consortium apparently mediating anaerobic oxidation of methane. Nature 407, 623-626.

Boetius, A., Suess, E., 2004. Hydrate Ridge: a natural laboratory for the study of microbial life fueled by methane from near-surface gas hydrates. Chem. Geol. 205, 291-310.

Bohrmann, G., Ivanov, M., Foucher, J.P., Spiess, V., Bialas, J., Greinert, J., Weinrebe, W., Abegg, F., Aloisi, G., Artemov, Y., Blinova, V., Drews, M., Heidersdorf, F., Krabbenhoft, A., Klaucke, I., Krastel, S., Leder, T., Polikarpov, I., Saburova, M., Schmale, O., Seifert, R., Volkonskaya, A.,

Zillmer, M., 2003. Mud volcanoes and gas hydrates in the Black Sea: new data from Dvurechenskii and Odessa mud volcanoes. Geo-Mar. Lett. 23, 239-249.

Bouriak, S., Vanneste, M., Saoutkine, A., 2000. Inferred gas hydrates and clay diapirs near the Storegga Slide on the southern edge of the Voring Plateau, offshore Norway. Mar. Geol. 163, 125-148.

Bünz, S., Mienert, J., Vanneste, M., Andreassen, K., 2005. Gas hydrates at the Storegga Slide: Constraints from an analysis of multicomponent, wide-angle seismic data. Geophysics 70, B19-B34.

Calais, E., Lesne, O., Deverchere, J., San'kov, V., Lukhnev, A., Miroshnitchenko, A., Buddo, V., Levi, K., Zalutzky, V., Bashkuev, Y., 1998. Crustal deformation in the Baikal rift from GPS measurements. Geophys. Res. Lett., 4003-4006.

Campbell, K.A., Francis, D.A., Collins, M., Gregory, M.R., Nelson, C.S., Greinert, J., Aharon, P., 2008. Hydrocarbon seep-carbonates of a Miocene forearc (East Coast Basin), North Island, New Zealand. Sediment. Geol. 204, 83-105.

Charlet, F., Fagel, N., De Batist, M., Hauregard, F., Minnebo, B., Meischner, D., Sonic Team, 2005. Sedimentary dynamics on isolated highs in Lake Baikal: evidence from detailed high-resolution geophysical data and sediment cores. Global Planet. Change 46, 125-144.

Crutchley, G., Pecher, I.A., Gorman, A.R., Henrys, S.A., Greinert, J., this issue. Seismic imaging of gas conduits beneath seafloor seep sites in a shallow marine gas hydrate province, Hikurangi Margin, New Zealand. Mar. Geol.

De Batist, M., Klerkx, J., Van Rensbergen, P., Vanneste, M., Poort, J., Golmshtok, A.Y., Kremlev, A.A., Khlystov, O.M., Krinitsky, P., 2002. Active hydrate destabilization in Lake Baikal, Siberia? Terra Nova 14, 436-442.

De Boever, E., Birgel, D., Thiel, V., Muchez, P., Peckmann, J., Dimitrov, L., Swennen, R., 2009. The formation of giant tubular concretions triggered by anaerobic oxidation of methane as revealed by archaeal molecular fossils (Lower Eocene, Varna, Bulgaria). Palaeogeogr Palaeoclimatol Palaeoecol 280, 23-36.

Dickens, G.R., 2001. The potential volume of oceanic methane hydrates with variable external conditions. Org. Geochem. 32, 1179-1193.

Dickens, G.R., Castillo, M.M., Walker, J.C.G., 1997. A blast of gas in the latest Paleocene: Simulating first-order effects of massive dissociation of oceanic methane hydrate. Geology 25, 259-262.

Dinu, C., Wong, H.K., Tambrea, D., Matenco, L., 2005. Stratigraphic and structural characteristics of the Romanian Black Sea shelf. Tectonophysics 410, 417-435.

Egorov, V., Luth, U., Luth, C., Gulin, M.B., 1998. Gas seeps in the submarine Dnieper Canyon, Black Sea: acoustic, video and trawl data. In: U. Luth, C. Luth and H. Thiel (Editors), MEGASEEPS Gas Explorations in the Black Sea, Project Report. Zentrum für Meres- und Klimaforschung der Universität Hamburg, Hamburg, pp. 11-21.

Etiope, G., 2009. Natural emissions of methane from geological seepage in Europe. Atmos. Environ. 43, 1430-1443.

Etiope, G., Klusman, R.W., 2002. Geologic emissions of methane to the atmosphere. Chemosphere 49, 777-789.

Etiope, G., Milkov, A.V., 2004. A new estimate of global methane flux from onshore and shallow submarine mud volcanoes to the atmosphere. Environ. Geol. (Berlin) V46, 997-1002.

Faure, K., Greinert, J., Pecher, I.A., Graham, I.J., Massoth, G.J., De Ronde, C.E.J., Wright, I.C., Baker, E.T., Olson, E.J., 2006. Methane seepage and its relation to slumping and gas hydrate at the Hikurangi margin, New Zealand. N. Z. J. Geol. Geophys. 49, 503-516.

Golmshtok, A.Y., Duchkov, A.D., Hutchinson, D.R., Khanukaev, S.B., Elnikov, A.I., 1997. Estimations of heat flow on Baikal from seismic data on the lower boundary of the gas hydrate layer. Geol. Geofiz. 38, 1677-1691.

Granin, N.G., Granina, L.Z., 2002. Gas hydrates and gas venting in Lake Baikal. Russian Geology and Geophysics 43, 589-597.

Greinert, J., 2008. Monitoring temporal variability of bubble release at seeps: The hydroacoustic swath system GasQuant. Journal of Geophysical Research-Oceans 113, 20.

Greinert, J., Artemov, Y., Egorov, V., De Batist, M., McGinnis, D., 2006. 1300-m-high rising bubbles from mud volcanoes at 2080m in the Black Sea: Hydroacoustic characteristics and temporal variability. Earth Planet. Sci. Lett. 244, 1-15.

Greinert, J., Lewis, K.B., Bialas, J., Pecher, I.A., Rowden, A., Bowden, D.A., De Batist, M., Linke, P., 2010. Methane seepage along the Hikurangi Margin, New Zealand: Overview of studies in 2006 and 2007 and new evidence from visual, bathymetric and hydroacoustic investigations. Mar. Geol. 272, 6-25.

Henriet, J.P., Mienert, J., 1998. Gas hydrates: relevance to world margin stability and climate change, Geological Society special publication 137. Geological Society, London, UK. 338 pp.

Henrys, S.A., Ellis, S., Uruski, C., 2003. Conductive heat flow variations from bottom-simulating reflectors on the Hikurangi margin, New Zealand. Geophys. Res. Lett. 30, 1065–1068.

Hutchinson, D.R., Golmshtok, A.J., Zonenshain, L.P., Moore, T.C., Scholz, C.A., Klitgord, K.D., 1992. Depositional and Tectonic Framework of the Rift Basins of Lake Baikal from Multichannel Seismic Data. Geology 20, 589-&.

Hutchinson, D.R., Golmshtok, A.Y., Scholz, C.A., Moore, T.C., Lee, M.W., Kuz'min, M., 1991. Bottom simulating reflector in Lake Baikal. Eos Trans. Am. Geophys. Union, 307.

IPCC, 2001a. Climate Change 2001: Synthesis Report. A Contribution of Working Groups I, II, and III to the Third Assessment Report of the Intergovernmental Panel on Climate Change. Cambridge University Press, Cambridge, United Kingdom and New York, NY, USA. 398 pp.

IPCC, 2001b. Climate Change 2001: The Scientific Basis. Contribution of Working Group I to the Third Assessment. Cambridge University Press, Cambridge, United Kingdom and New York, NY, USA. 881 pp.

IPCC, 2007a. Changes in Atmospheric Constituents and in Radiative Forcing. In: S. Solomon et al. (Editors), Climate Change 2007: The Physical Science Basis. Contribution of Working Group I to the Fourth Assessment Report of the Intergovernmental Panel on Climate Change Cambridge University Press, Cambridge, United Kingdom and New York, NY, USA

IPCC, 2007b. Couplings Between Changes in the Climate System and Biogeochemistry. In: S. Solomon et al. (Editors), Climate Change 2007: The Physical Science Basis. Contribution of Working Group I to the Fourth Assessment Report of the Intergovernmental Panel on Climate Change. Cambridge University Press, Cambridge, United Kingdom and New York, NY, USA.

Judd, A., Hovland, M., 2007. Seabed fluid flow: the impact on geology, biology and the marine environment. Cambridge University Press, Cambridge. 475 pp.

Judd, A.G., 2003. The global importance and context of methane escape from the seabed. Geo-Mar. Lett. 23, 147-154.

Judd, A.G., 2004. Natural seabed gas seeps as sources of atmospheric methane. Environ. Geol. (Berlin) 46, 988-996.

Kalmychkov, G., Egorov, A., Kuz'min, M., Khlystov, O., 2006. Genetic types of methane from Lake Baikal. Doklady Earth Sciences 411, 1462-1465.

Khlystov, O.M., 2006. New findings of gas hydrates in the Baikal bottom sediments. Russian Geology and Geophysics 47, 972-974.

Klerkx, J., De Batist, M., Poort, J., Hus, R., Van Rensbergen, P., Khlystov, O., Granin, N., 2006. Tectonically controlled methane escape in Lake Baikal, Advances in the Geological Storage of Carbon Dioxide, pp. 203-219.

Klerkx, J., Zemskaya, T.I., Matveeva, T.V., Khlystov, O.M., Namsaraev, B.B., Dagurova, O.P., Golobokova, L.P., Vorob'eva, S.S., Pogodaeva, T.P., Granin, N.G., Kalmychkov, G.V., Ponomarchuk, V.A., Shoji, H., Mazurenko, L.L., Kaulio, V.V., Solov'ev, V.A., Grachev, M.A., 2003. Methane hydrates in deep bottom sediments of Lake Baikal. Doklady Earth Sciences 393A, 1342-1346.

Kontorovich, A.E., Kashirtsev, V.A., Moskvin, V.I., Burshtein, L.M., Zemskaya, T.I., Kostyreva, E.A., Kalmychkov, G.V., Khlystov, O.M., 2007. Petroleum potential of Baikal deposits. Russian Geology and Geophysics 48, 1046-1053.

Krey, V., Canadell, J.G., Nakicenovic, N., Abe, Y., Andruleit, H., Archer, D., Grubler, A., Hamilton, N.T.M., Johnson, A., Kostov, V., Lamarque, J.F., Langhorne, N., Nisbet, E.G., O'Neill, B., Riahi, K., Riedel, M., Wang, W.H., Yakushev, V., 2009. Gas hydrates: entrance to a methane age or climate threat? Environ. Res. Lett. 4, 6.

Kruglyakova, R.P., Byakov, Y.A., Kruglyakova, M.V., Chalenko, L.A., Shevtsova, N.T., 2004. Natural oil and gas seeps on the Black Sea floor. Geo-Mar. Lett. V24, 150-162.

Kvenvolden, K.A., Rogers, B.W., 2005. Gaia's breath--global methane exhalations. Mar. Pet. Geol. 22, 579-590.

Leifer, I., Boles, J.R., Luyendyk, B.P., Clark, J.F., 2004. Transient discharges from marine hydrocarbon seeps: spatial and temporal variability. Environ. Geol. (Berlin) 46, 1038-1052.

Lelieveld, J., Crutzen, P.J., Dentener, F.J., 1998. Changing concentration, lifetime and climate forcing of atmospheric methane. Tellus, Ser. B. 50, 128-150.

Lewis, K.B., Collot, J.-Y., Lallem, S.E., 1998. The dammed Hikurangi Trough: a channel-fed trench blocked by subducting seamounts and their wake avalanches (New Zealand-France GeodyNZ Project). Basin Res. 10, 441-468.

Lewis, K.B., Marshall, B.A., 1996. Seep faunas and other indicators of methane-rich dewatering on New Zealand convergent margins. N. Z. J. Geol. Geophys. 39, 181-200.

Lüdmann, T., Wong, H.K., Konerding, P., Zillmer, M., Petersen, J., Flüh, E., 2004. Heat flow and quantity of methane deduced from a gas hydrate field in the vicinity of the Dnieper Canyon, northwestern Black Sea. Geo-Mar. Lett. V24, 182-193.

Luth, C., Luth, U., Gebruk, A.V., Thiel, H., 1999. Methane gas Seeps Along the Oxic/Anoxic Gradient in the Black Sea: Manifestations, Biogenic Sediment Compounds and Preliminary Results on Benthic Ecology. Mar. Ecol. 20, 221-249.

Mats, V.D., 1993. The Structure and Development of the Baikal Rift Depression. Earth-Sci. Rev. 34, 81-118.

Matveeva, T.V., Mazurenko, L.L., Soloviev, V.A., Klerkx, J., Kaulio, V.V., Prasolov, E.M., 2003. Gas hydrate accumulation in the subsurface sediments of Lake Baikal (Eastern Siberia). Geo-Mar. Lett. 23, 289-299.

Max, M.D., Johnson, A.H., Dillon, W.P., 2006. Economic geology of natural gas hydrate. Springer, Dordrecht, The Netherlands. 341 pp.

Michaelis, W., Seifert, R., Nauhaus, K., Treude, T., Thiel, V., Blumenberg, M., Knittel, K., Gieseke, A., Peterknecht, K., Pape, T., Boetius, A., Amann, R., Jorgensen, B.B., Widdel, F., Peckmann, J., Pimenov, N.V., Gulin, M.B., 2002. Microbial Reefs in the Black Sea Fueled by Anaerobic Oxidation of Methane. Science 297, 1013-1015.

Naudts, L., De Batist, M., Greinert, J., Artemov, Y., 2009. Geo- and hydro-acoustic manifestations of shallow gas and gas seeps in the Dnepr paleodelta, northwestern Black Sea. The Leading Edge 28, 1030-1040.

Naudts, L., Greinert, J., Artemov, Y., Beaubien, S.E., Borowski, C., De Batist, M., 2008. Anomalous sea-floor backscatter patterns in methane venting areas, Dnepr paleo-delta, NW Black Sea. Mar. Geol. 251, 253-267.

Naudts, L., Greinert, J., Artemov, Y., Staelens, P., Poort, J., Van Rensbergen, P., De Batist, M., 2006. Geological and morphological setting of 2778 methane seeps in the Dnepr paleo-delta, northwestern Black Sea. Mar. Geol. 227, 177-199.

Naudts, L., Greinert, J., Poort, J., Belza, J., Vangampelaere, E., Boone, D., Linke, P., Henriet, J.P., De Batist, M., 2010. Active venting sites on the gas-hydrate-bearing Hikurangi Margin, Off New Zealand: Diffusive- versus bubble-released methane. Mar. Geol. 272, 233-250.

Naudts, L., Khlystov, O., Granin, N., Chensky, A., Poort, J., De Batist, M., submitted. Stratigraphic and structural controls on the location of active methane seep on Posolsky Bank, Lake Baikal. Mar. Pet. Geol.

Nishishin, A.M., Korotaev, M.V., Ershov, A.V., Brunet, M.F., 2003. The Black Sea basin: tectonic history and Neogene-Quaternary rapid subsidence modelling. Sediment Geology, 149-168.

Paull, C.K., Dillon, W.P., 2001. Natural gas hydrates: occurence, distribution and detection. Geophysical Monograph 124. American Geophysical Union, Washington D.C., USA. 315 pp.

Pecher, I.A., Henrys, S.A., Ellis, S., Chiswell, S.M., Kukowski, N., 2005. Erosion of the seafloor at the top of the gas hydrate stability zone on the Hikurangi Margin, New Zealand. Geophys. Res. Lett. 32.

Pecher, I.A., Henrys, S.A., Wood, W.T., Kukowski, N., Crutchley, G.J., Fohrmann, M., Kilner, J., Senger, K., Gorman, A.R., Coffin, R.B., Greinert, J., Faure, K., 2010. Focussed fluid flow on the Hikurangi Margin, New Zealand -- Evidence from possible local upwarping of the base of gas hydrate stability. Mar. Geol. 272, 99-113.

Peckmann, J., Reimer, A., Luth, U., Luth, C., Hansen, B.T., Heinicke, C., Hoefs, J., Reitner, J., 2001. Methane-derived carbonates and authigenic pyrite from the northwestern Black Sea. Mar. Geol. 177, 129-150.

Petit, C., Burov, E., Deverchere, J., 1997. On the structure and mechanical behaviour of the extending lithosphere in the Baikal rift from gravity modeling. Earth Planet. Sci. Lett. 149, 29-42.

Petit, C., Koulakov, I., Deverchere, J., 1998. Velocity structure around the Baikal rift zone from teleseismic and local earthquake traveltimes and geodynamic implications. Tectonophysics 296, 125-144.

Petit, J.R., Jouzel, J., Raynaud, D., Barkov, N.I., Barnola, J.M., Basile, I., Bender, M., Chappellaz, J., Davis, M., Delaygue, G., Delmotte, M., Kotlyakov, V.M., Legrand, M., Lipenkov, V.Y., Lorius, C., Pepin, L., Ritz, C., Saltzman, E., Stievenard, M., 1999. Climate and atmospheric history of the past 420,000 years from the Vostok ice core, Antarctica. Nature 399, 429-436.

Popescu, I., Lericolais, G., Panin, N., De Batist, M., Gillet, H., 2007. Seismic expression of gas and gas hydrates across the western Black Sea. Geo-Mar. Lett. 27, 173-183.

Reeburgh, W.S., Whalen, S.C., Alperin, A.J., 1993. The role of methylotrophy in the global methane budget. In: J.A. Murrel and D.P. Kelley (Editors), Microbial Growth on C-1 Compounds. Intercept, Andover, Uk, pp. 1-14.

Robinson, A.G., Rudat, J.H., Banks, C.J., Wiles, R.L.F., 1996. Petroleum geology of the Black Sea. Mar. Pet. Geol. 13, 195-223.

Schmid, M., De Batist, M., Granin, N.G., Kapitanov, V.A., McGinnis, D.F., Mizandrontsev, I.B., Obzhirov, A.I., Wuust, A., 2007. Sources and sinks of methane in Lake Baikal: A synthesis of measurements and modeling. Limnol. Oceanogr. 52, 1824-1837.

Scholz, C.A., Hutchinson, D.R., 2000. Stratigraphic and structural evolution of the Selenga Delta Accommodation Zone, Lake Baikal Rift, Siberia. Int. J. Earth Sci. 89, 212-228.

Scholz, C.A., Klitgord, K.D., Hutchinson, D.R., Ten Brink, U.S., Zonenshain, L.P., Golmshtok, A.Y., Moore, T.C., 1993. Results of 1992 seismic reflection experiment in Lake Baikal. Eos Trans. Am. Geophys. Union 74, 469-470.

Sloan, E.D., Koh, C.A., 2007. Clathrate hydrates of natural gases. CRC Press, Boca Raton, USA. 721 pp.

Sommer, S., Pfannkuche, O., Linke, P., Luff, R., Greinert, J., Drews, M., Gubsch, S., Pieper, M., Poser, M., Viergutz, T., 2006. Efficiency of the benthic filter: Biological control of the emission of dissolved methane from sediments containing shallow gas hydrates at Hydrate Ridge. Global Biogeochem. Cycles 20.

Spahni, R., Chappellaz, J., Stocker, T.F., Loulergue, L., Hausammann, G., Kawamura, K., Fluckiger, J., Schwander, J., Raynaud, D., Masson-Delmotte, V., Jouzel, J., 2005. Atmospheric Methane and Nitrous Oxide of the Late Pleistocene from Antarctic Ice Cores. Science 310, 1317-1321.

Suess, E., 2010. Marine Cold Seeps. In: K.N. Timmis (Editor), Handbook of Hydrocarbon and Lipid Microbiology. Springer-Verlag, Berlin Heidelberg, pp. 187-203.

Tapponnier, P., Molnar, P., 1979. Active faulting and cenozoic tectonics of the Tien-Shan, Mongolia and Baykal Regions. J. Geophys. Res. 84, 3425-3459.

Thiel, V., Peckmann, J., Richnow, H.H., Luth, U., Reitner, J., Michaelis, W., 2001. Molecular signals for anaerobic methane oxidation in Black Sea seep carbonates and a microbial mat. Mar. Chem. 73, 97-112.

Tugolesov, D.A., Gorshkov, A.S., Meisner, L.B., Solovev, V.V., Khakhalev, E.M., 1985. Tectonics of Mezo-Cenozoic deposits of the Black Sea basin. Nedra, Moscow.

Van Rensbergen, P., De Batist, M., Klerkx, J., Hus, R., Poort, J., Vanneste, M., Granin, N., Khlystov, O., Krinitsky, P., 2002. Sublacustrine mud volcanoes and methane seeps caused by dissociation of gas hydrates in Lake Baikal. Geology 30, 631-634.

Vanneste, M., De Batist, M., Golmshtok, A., Kremlev, A., Versteeg, W., 2001. Multi-frequency seismic study of gas hydrate-bearing sediments in Lake Baikal, Siberia. Mar. Geol. 172, 1-21.

Vanneste, M., Poort, J., De Batist, M., Klerkx, J., 2002. Atypical heat-flow near gas hydrate irregularities and cold seeps in the Baikal Rift Zone. Mar. Pet. Geol. 19, 1257-1274.

von Rad, U., Rosch, H., Berner, U., Geyh, M., Marchig, V., Schulz, H., 1996. Authigenic carbonates derived from oxidized methane vented from the Makran accretionary prism off Pakistan. Mar. Geol. 136, 55-77.

Whiticar, M.J., 1999. Carbon and hydrogen isotope systematics of bacterial formation and oxidation of methane. Chem. Geol. 161, 291-314.

Williams, D.F., Kuzmin, M.I., Prokopenko, A.A., Karabanov, E.B., Khursevich, G.K., Bezrukova, E.V., 2001. The Lake Baikal drilling project in the context of a global lake drilling initiative. Quat. Int. 80-81, 3-18.

Wuebbles, D.J., Hayhoe, K., 2002. Atmospheric methane and global change. Earth-Sci. Rev. 57, 177-210.

Zillmer, M., Flueh, E.R., Petersen, J., 2005. Seismic investigation of a bottom simulating reflector and quantification of gas hydrate in the Black Sea. Geophys. J. Int. 161, 662-678.

CHAPTER 2

Geo- and hydro-acoustic manifestations of shallow gas and gas seeps in the Dnepr paleo-delta, northwestern Black Sea

Lieven Naudts, Jens Greinert, Yuriy Artemov, Marc De Batist

2.1. Background

Shallow gas has been a topic of major interest to academic and industrial researchers worldwide and this within different scientific fields. Shallow gas occurs in a depth window between 0 m and 1000 m below the seafloor. It consists mainly of microbial-formed or thermogenic methane or a combination of both, sometimes with a limited admixture of higher hydrocarbons (propane, butane, etc.). The main interest from the oil and gas industry in shallow gas is because of the possible hazard it poses during drilling, as it can lead to blow-outs and seafloor instability affecting seafloor-based constructions. Besides this, shallow gas can also be an important tool to localize deeper economically valuable hydrocarbon resources and reservoirs. Also in academic research, shallow gas has become a major study object over the last decennia drawing the attention of geologists, geophysicists, microbiologists, geochemists, oceanographers, etc. Shallow gas and seabed fluid flow are global phenomena, which play a fundamental role in various natural processes that affect the geosphere, the biosphere, the hydrosphere and the atmosphere. In order to study the possible effects of shallow gas and seabed fluid flow, it is important to understand the processes and parameters that control its distribution and presence in the subsurface. High-resolution reflection seismics is the main tool that has traditionally been used to determine the presence of free gas in the shallow sediments, and to infer the possible geological controls on its distribution (e.g. impermeable sediment layers) as well as the associated fluid pathways (e.g. faults, permeable sediment layers, diapirs). In some cases, shallow gas is able to migrate and to reach the seafloor, where gas (free and/or dissolved) might be released into the water column. Since locations of gas release, i.e. gas seeps, at the seafloor often have a distinct morphological expression (e.g. pockmarks, mud volcanoes, ridges); they can easily be detected on high-resolution reflection seismic data, single-beam and multibeam echosounding data and side-scan sonar recordings. In this paper, we present an overview of some of the characteristics and seismic signatures of shallow free gas on different types of high-resolution seismic reflection data. We also discuss the factors that control the distribution of shallow gas and gas seeps in the Dnepr paleo-delta, northwestern Black Sea.

2.2. Dnepr paleo-delta

The Dnepr paleo-delta area is located on the continental margin of the northwestern Black Sea, west of the Crimea Peninsula (Fig. 2.1.). Structurally, the Dnepr paleo-delta is situated on the transition zone between the Scythian Platform and the Karkinit Trough in the north, the Shtormavaya Graben, the Kalamit Ridge and the Western Black Sea Basin in the south (Fig. 2.1.). The Western Black Sea Basin formed during the late Cretaceous in a back-arc setting above the northward subducting Tethys Ocean, close to the southern margin of Eurasia. The continental margin west of the Crimea Peninsula consists of Late Paleozoic to Mesozoic basement rocks covered by thick Cenozoic sediments with a thickness of at least 2 km (Robinson et al., 1996).

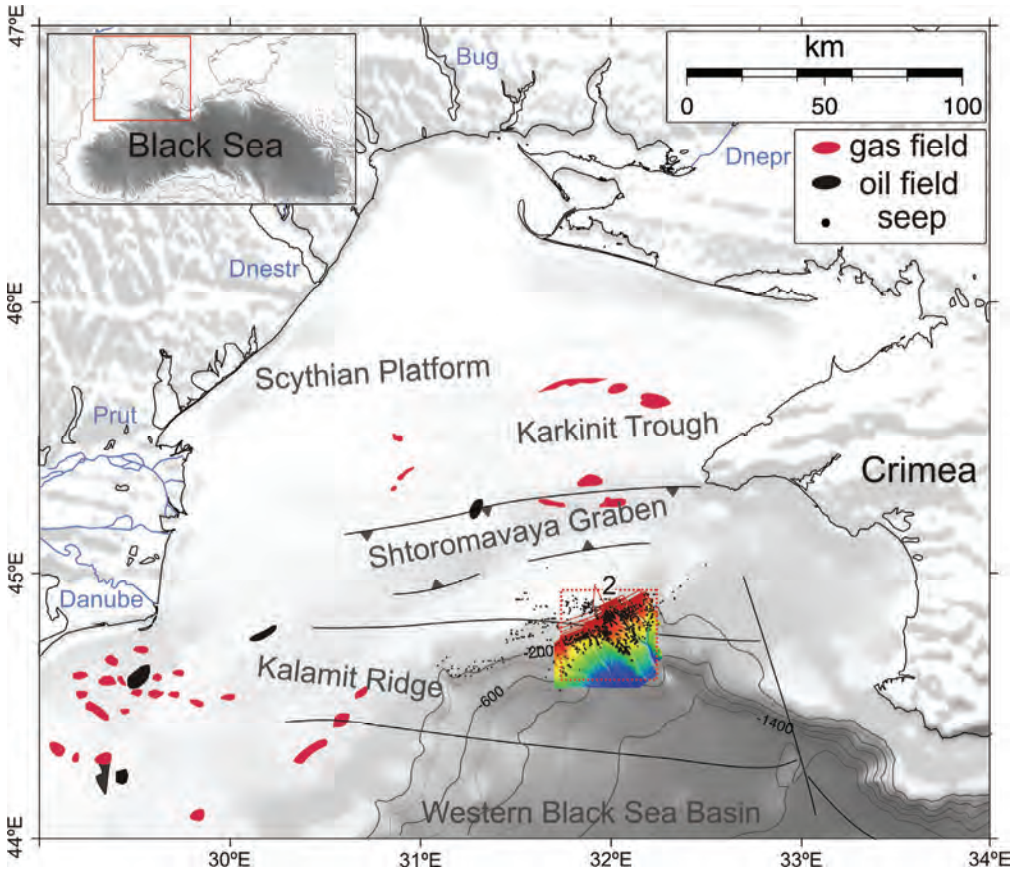

Figure 2.1. Location of Dnepr paleo-delta in the northwestern Black Sea with indication of major structures, deep faults, oil and gas fields and seep locations.

Nowadays the northwestern Black Sea is dominated by a rather wide shelf (60-200 km) with a shelf break at 120 to 170 m water depth and canyon systems with large deep-sea fan complexes which mainly developed during sealevel lowstands. During several successive lowstands the main inflowing rivers, Dnepr and Danube, deposited organic-rich material hundreds of kilometers beyond their present mouths forming shelf-edge deltas at the present-day shelf break. The Dnepr paleo-delta is one of these shelf-edge deltas, in which microbial degradation of the organic-rich sediments has led to the formation of shallow gas associated with prolific gas seepage at the seabed. The presence of the shallow gas and gas seeps in the Dnepr paleo-delta already received a lot of attention from different European-funded research projects. The data shown here were acquired during the EU-funded CRIMEA project (2003-2006).

2.3. High-resolution reflection seismic data

Three different types of seismic reflection data were acquired using three different sources (5 kHz pinger, SIG-sparker and GI-gun) (Fig. 2.2.A), each within a different frequency range to extract the best possible information about the underlying geology and shallow gas distribution. The very shallow subsurface was investigated using a deeptow 5 kHz pinger, which was mounted in a towfish together with a side-scan sonar (SONIC-3). The towfish was towed at 50-200 m above the seafloor. The theoretical resolution (i.e. Rayleigh criterion) is 30 cm, for a maximum penetration of 35 ms. In total 590 km of 5 kHz data were recorded. To achieve deeper penetration, single-channel reflection seismic data were collected with a SIG sparker source (central frequency of 500-700 Hz) and an active

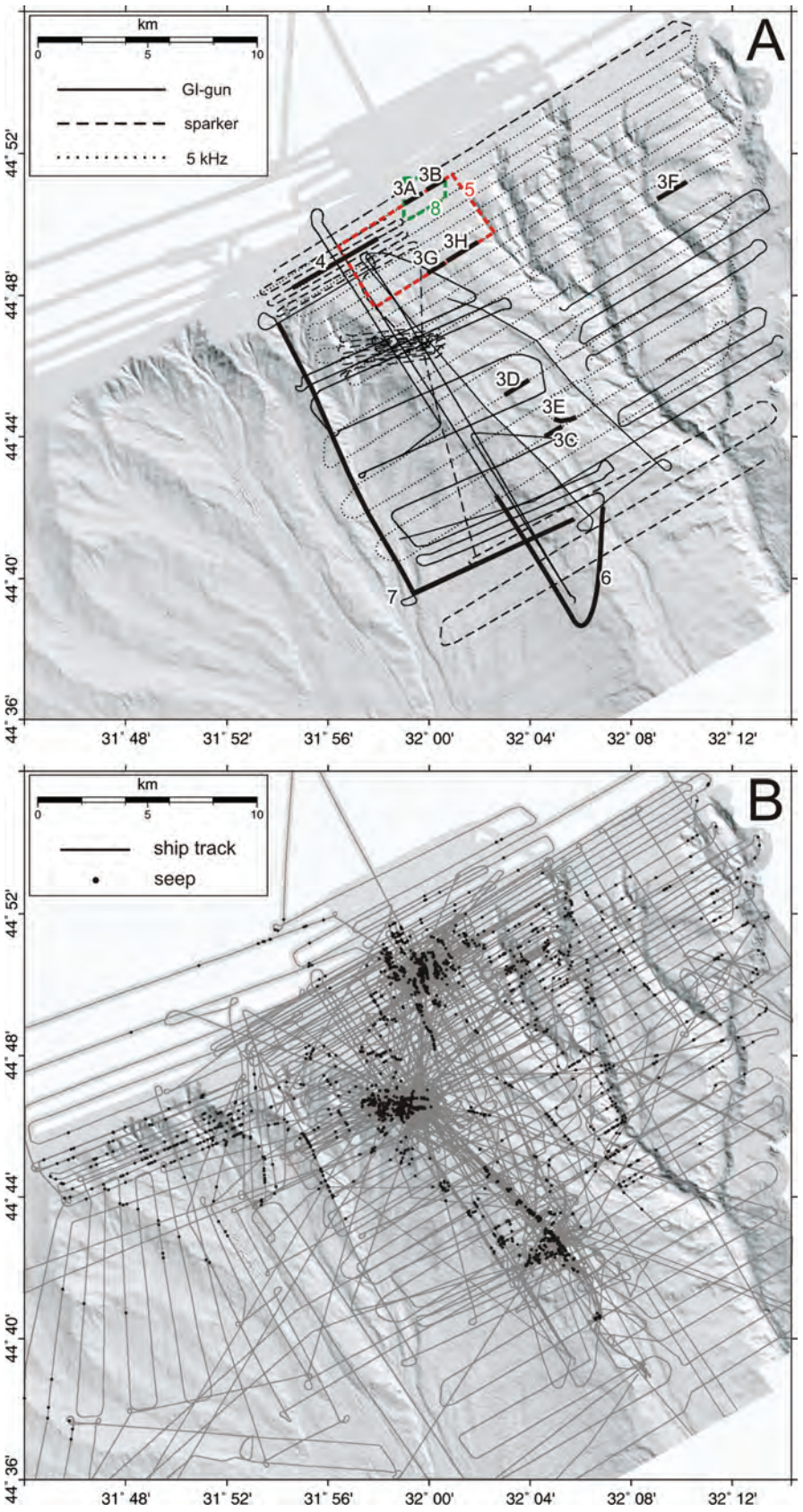

Figure 2.2. A. High-resolution seismic reflection survey lines and outlines for Figs. 2.4.-2.9. (see Fig. 2.1. for location). **B**. Ship track with hydro-acoustically detected seeps (see Fig. 2.1. for location).

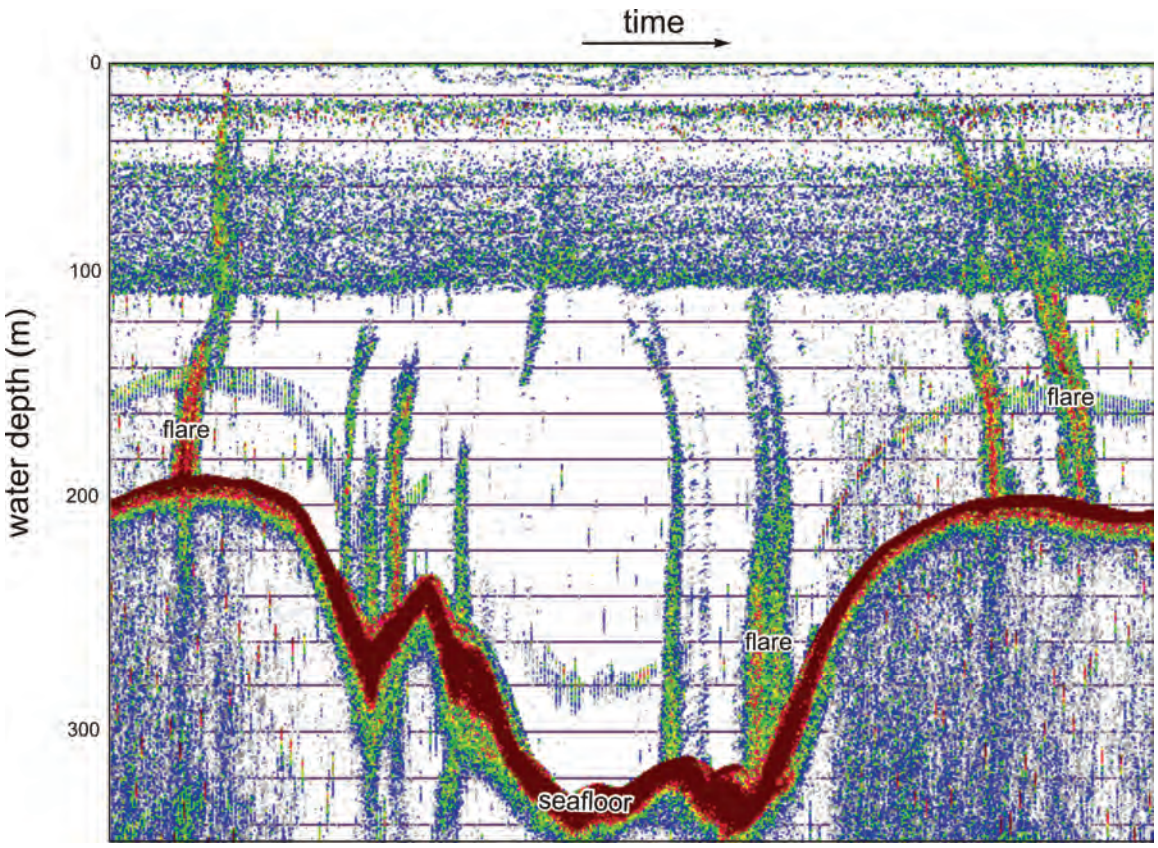

Figure 2.3. Single-beam echogram showing typical hydro-acoustic manifestations of rising methane bubbles (flares) in the Dnepr paleo-delta.

single-channel surface streamer with 10 hydrophones. The theoretical vertical resolution is 1 m and the maximum penetration is 100 ms. 330 km of sparker data were recorded. For visualizing possible gas hydrate reservoirs and major depositional units, also multi-channel seismic data were acquired with a GI-gun source (central frequency of 150 Hz; maximum shooting interval of 8 s) and a passive surface streamer with 16 hydrophone groups. The theoretical vertical resolution is 6 m and the maximum penetration is 600 ms. Multi-channel data were recorded over a total length of 665 km. Data processing involved frequency filtering, velocity analysis, NMO correction, stacking and deconvolution. Interpretation and analysis of the three types of seismic data was carried out with the Kingdom Suite software package. In addition to the acquisition of seismic reflection data, single-beam echosounding was performed for seep detection (i.e. for the detection of gas bubbles released in the water column) using a hull-mounted SIMRAD EK-500 dual-frequency (38 and 120 kHz) split-beam echosounder (Figs. 2B and 2.3). Seabed features related to gas venting and the presence of shallow gas were additionally imaged by a combination of multibeam echosounding, using a 50 kHz SEABEAM 1050 system, and side-scan sonar imaging, using the 30 kHz SONIC-3 deep-water sonar.

2.4. Shallow gas

The presence of shallow gas strongly influences the mechanical and acoustic properties of the sediment (increased sound attenuation, acoustic energy scattering, affecting sound velocity, etc.). Therefore geo-acoustic methods, like seismic reflection profiling, are significantly affected by the presence of shallow gas and are therefore very well-suited for the detection of gas in the sediments. Even very small concentrations of gas in the pore space (0.5% gas by volume)

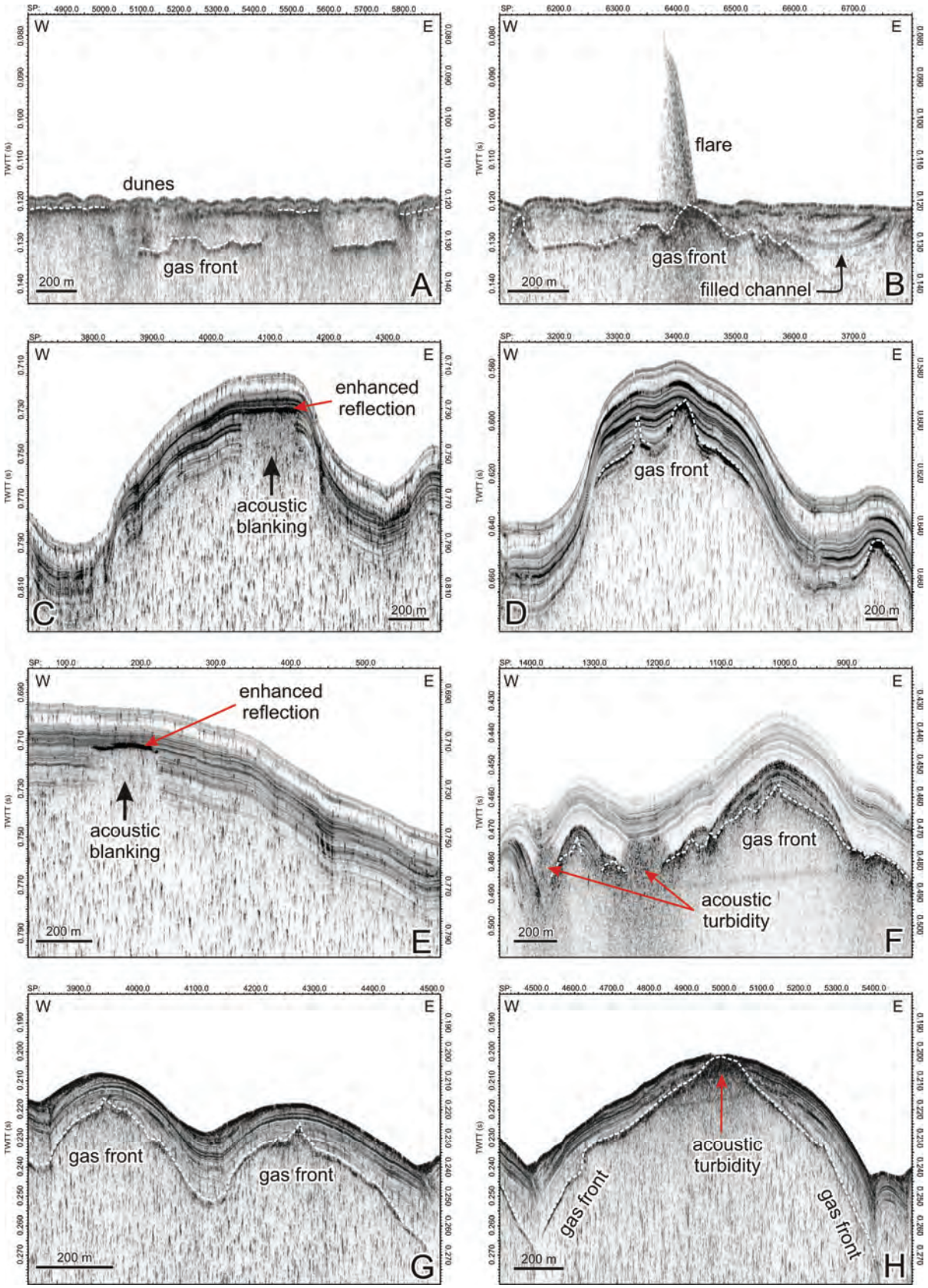

Figure 2.4. Different shallow gas signatures showing different behaviors on 5 kHz pinger data (see Fig. 2.2.A. for location).

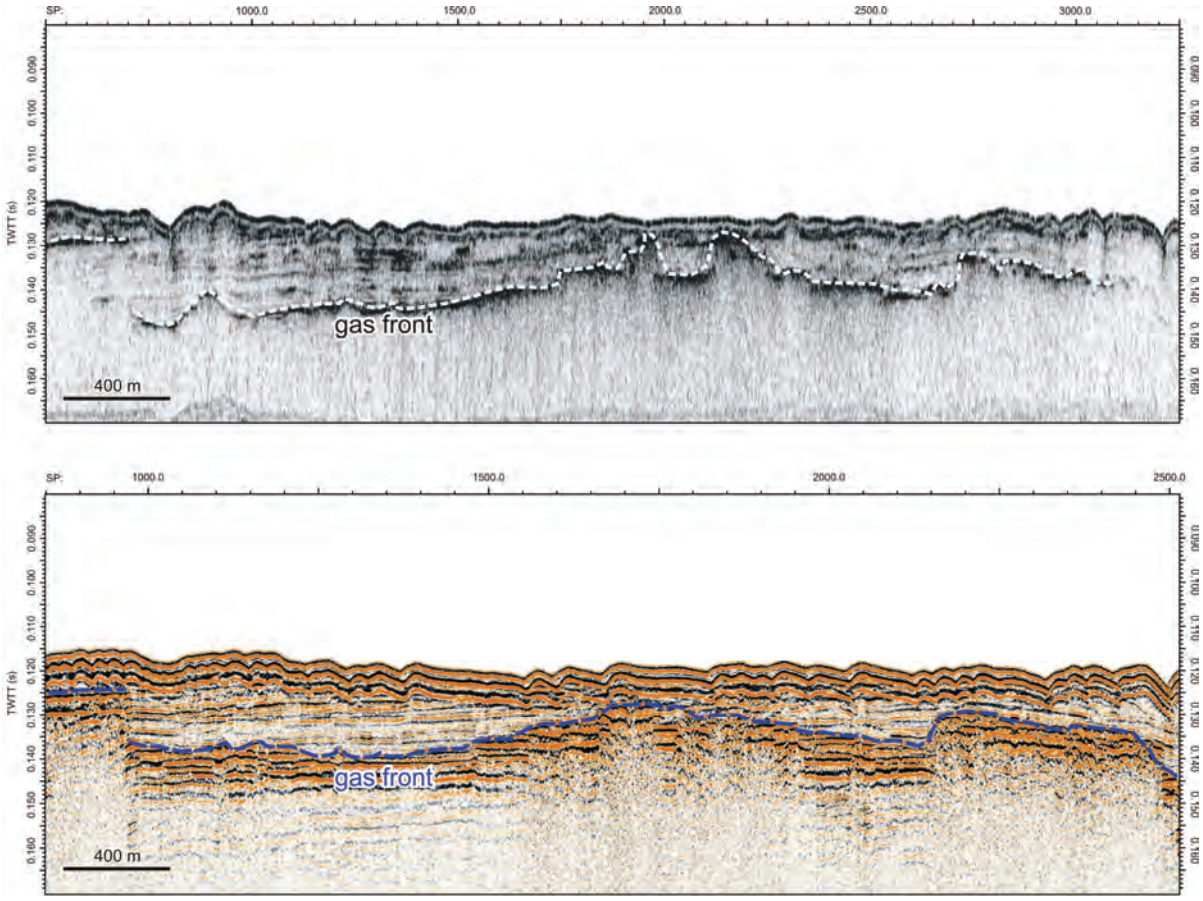

Figure 2.5. Comparison of "gas fronts" visible on 5 kHz data and sparker data (see Fig. 2.2.A. for location).

already lead to a variety of shallow gas signatures on most types of high-resolution reflection seismic data (Figs. 2.4.-2.9.) (Judd and Hovland, 2007). The most common types of seismic disturbances related to gas-bearing sediments are "enhanced reflections" and "acoustic turbidity", both often in combination with "acoustic blanking" (Fig. 2.4.). "Enhanced reflections" on high-resolution reflection data are the analogues of "bright spots" on low-frequency industrial data (Figs. 2.4.C. and 2.4.E.). They are characterized by anomalously high amplitude and are interpreted to be caused by the accumulation of (minor amounts of) free gas below a certain horizon. This gas accumulation causes a negative impedance contrast across that horizon, and the subsequent large-amplitude, phase reversed reflection on seismic data. "Acoustic turbidity" shows up on seismic data as a dark smear that sometimes cross-cuts the normal stratigraphy and completely masks all reflections below (Fig. 2.4.). "Acoustic turbidity" results from the attenuation (absorption and scattering) of the acoustic energy by the presence of gas bubbles within the sediment. The term "gas front" is often used for the top of the "acoustic turbidity" and associated gas features and is therefore interpreted as the upper limit of the free gas zone within the sediment (Fig. 2.4.). This interpretation is clearly supported by Fig. 2.4.B., on which the gas front can be seen to dome up to the seafloor and where a "flare", a hydro-acoustic water-column anomaly caused by rising bubbles, is observed on the 5 kHz data. Since higher frequencies are more strongly attenuated, the 5 kHz pinger data provides the most valuable information about the depth variations of the shallow gas present in the sediments (Figs. 2.4.-2.6. and 2.9.). Comparison between the 5 kHz data and sparker data (lower frequency) over a same area confirms that even if both types of seismic data clearly portray the gas front and its lateral depth variations, the 5 kHz data provide a higher-resolution image of the subsurface (Fig. 2.5.). The later is of course

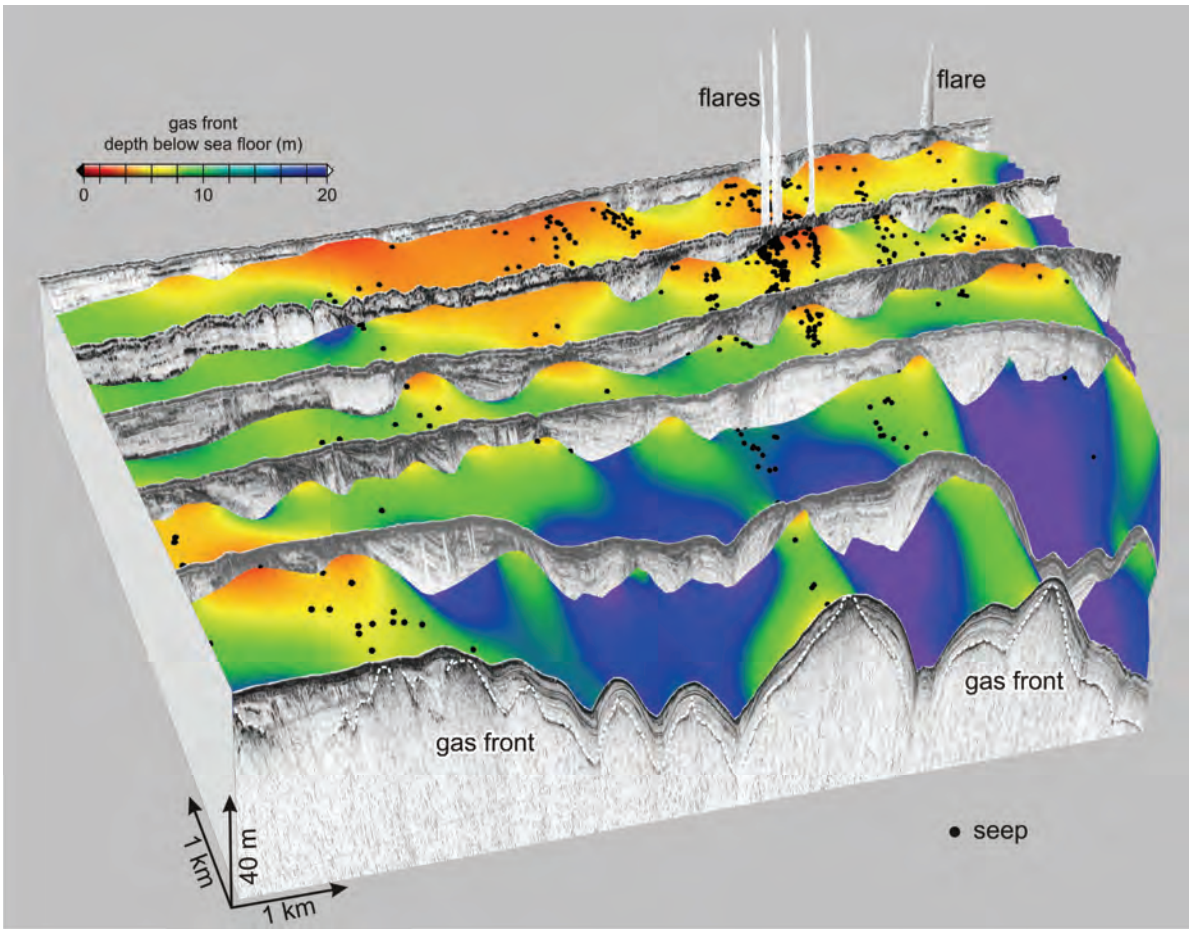

Figure 2.6. 3D view showing the depth variation of the gas front as a depth map overlain by an isopach map (depth of the gas front below the seafloor) together with the used 5 kHz seismic profiles (see Fig. 2.2.A. for location). Gas seeps were mainly detected where the gas front approaches the seafloor within a couple of meters.

expected from a higher-frequency source. On the 5 kHz data, the gas front shows up as a single, strong reflection, whereas on the sparker data the gas front rather appears as a combination of enhanced reflections. The comparison also shows that the sparker data only provide very little extra information of the deeper subsurface, less than would be expected from its lower frequency. The quality of these sparker data suffered significantly from a combination of several acquisition parameters (e.g. high vessel speed, engine noise, etc). The free gas within the sediments strongly attenuates the acoustic signal for both sources. Acoustic attenuation is largest when the acoustic frequency matches the resonant frequency of the bubbles, which stands in relation to the bubble size. The data suggest that a wide range of bubbles sizes occurs within the sediments imaged by the two seismic sources. However, the observation depth of the gas front is very similar for both methods. Both datasets show the presence of distinct “gas fronts”, laterally strongly varying in depth and locally doming up towards the seafloor. The areas of “gas-front” updoming coincide with seep locations as observed by hydro-acoustics. By combining the gas front surface from the 5 kHz data with the seafloor surface, a “depth-to-gas-front” map was produced, which illustrates the strong “gas front-versus-seep” relationship that was observed on the seismic profiles (Fig. 2.6.). The majority of the seeps occur where the gas front approaches the seafloor within a couple of meters (Fig. 2.6.). The behavior or the depth variations of the “gas fronts” seem erratic at first, but a closer examination shows that “gas fronts” tend to dome up towards the seafloor at morphologic highs. Furthermore, “gas fronts” have the tendency to stay below the

sedimentary infill of incised channels and only come up to the seafloor at the margins of these filled paleo-channels (Fig. 2.4.B.). Naudts et al. (2006) (CHAPTER 3) integrated the geophysical seismic data with multibeam data and coring information. Their results showed that the distribution and migration of gas near the seafloor in the Dnepr paleo-delta is predominantly controlled by stratigraphic and sedimentary factors, and not by faults as might be expected. In the Dnepr paleo-delta, along-strata and across-strata variations in grain-size distributions and consequent changes in permeability seem to be the main controlling factors on shallow gas migration and accumulation outside the gas-hydrate stability zone (GHSZ).

2.5. Gas hydrates

Shallow gas within the sediments does not only occur as free gas (bubbles) or in dissolved form in sediment pore waters. It can also be trapped in crystalline, ice-like compounds composed of water and gas. These compounds are gas hydrates which are only stable at specific high-pressure and low-temperature conditions. In the marine environment, these conditions can generally be found at water depths of over 300-500 m, depending on bottom-water temperatures and gas composition. The GHSZ is also limited to a certain depth below the seafloor because of the geothermally-induced rise in subsurface temperature with depth. Besides the P-T conditions, also the amount of available gas and water in the pore spaces needs to be high enough to sustain gas-hydrate growth and to keep hydrates stable. Marine gas hydrates have attracted massive attention from scientists and decision makers over the last decades, because they represent a possible energy resource as well as a geohazard. When P-T conditions change, gas hydrates can become unstable and dissociate. This can lead to sediment destabilization, submarine landsliding and possibly the generation of tsunamis. The dissociation of methane hydrates involves the release of large amounts of methane, which is a very strong greenhouse gas. If this methane would reach the atmosphere, it would strongly affect global climate.

In the northwestern Black Sea, methane gas hydrates are theoretically stable only below water depths of -725 m due to the relatively high bottom-water temperatures of 8.9°C. Hydrate stability calculation was done based on presumed average open-ocean pore-water salinity in the sedimentary column of 35 ppt (Naudts et al., 2006). During the CRIMEA expeditions no gas hydrates were sampled by sediment coring in the Dnepr paleo-delta. However, based on seismic reflection profiling the presence of gas hydrates in the subsurface can be inferred geophysically from anomalous reflections. These reflections mimic the seafloor topography and are therefore referred to as bottom-simulating reflections (BSRs). The subsurface depth of the BSRs often corresponds to the lower P-T controlled boundary of the GHSZ, and is usually referred to as the base of the gas-hydrate stability zone (BGHSZ). Since BSRs mimic the seafloor, they often crosscut the reflections of the normal subhorizontal stratigraphy, making BSRs easy to identify. BSRs occur typically above high-amplitude reflections with a reverse negative phase polarity and underlie low-amplitude blanked reflections. Generally, it is assumed that the seismic signatures of BSRs are the result of relatively dense hydrate-bearing layers with high acoustic velocity overlying gassy sediments with low acoustic velocity. Deep drilling through BSRs have shown that BSRs can occur without the presence of hydrates in the subsurface and vice versa (Judd and Hovland, 2007).

Our GI-gun data also exhibit a BSR-like event, which is located at the calculated sub-bottom depth of the BGHSZ (Figs. 2.7.-2.8.). This BSR displays a number of characteristics of a typical BSR (i.e. low amplitudes above, enhanced reflections below, cross-cutting the stratigraphy, reverse polarity), but instead of appearing as a distinct, single reflection, the BSR on our data is expressed as a transition from high-amplitude (gas-enhanced) reflections below and low-amplitude (blanked) reflections above (Figs. 2.7.-2.8.). Such seismic response is attributed to the relatively high frequency of the seismic signal and to the acquisition lay-out with relatively short offsets (Naudts et al., 2006).

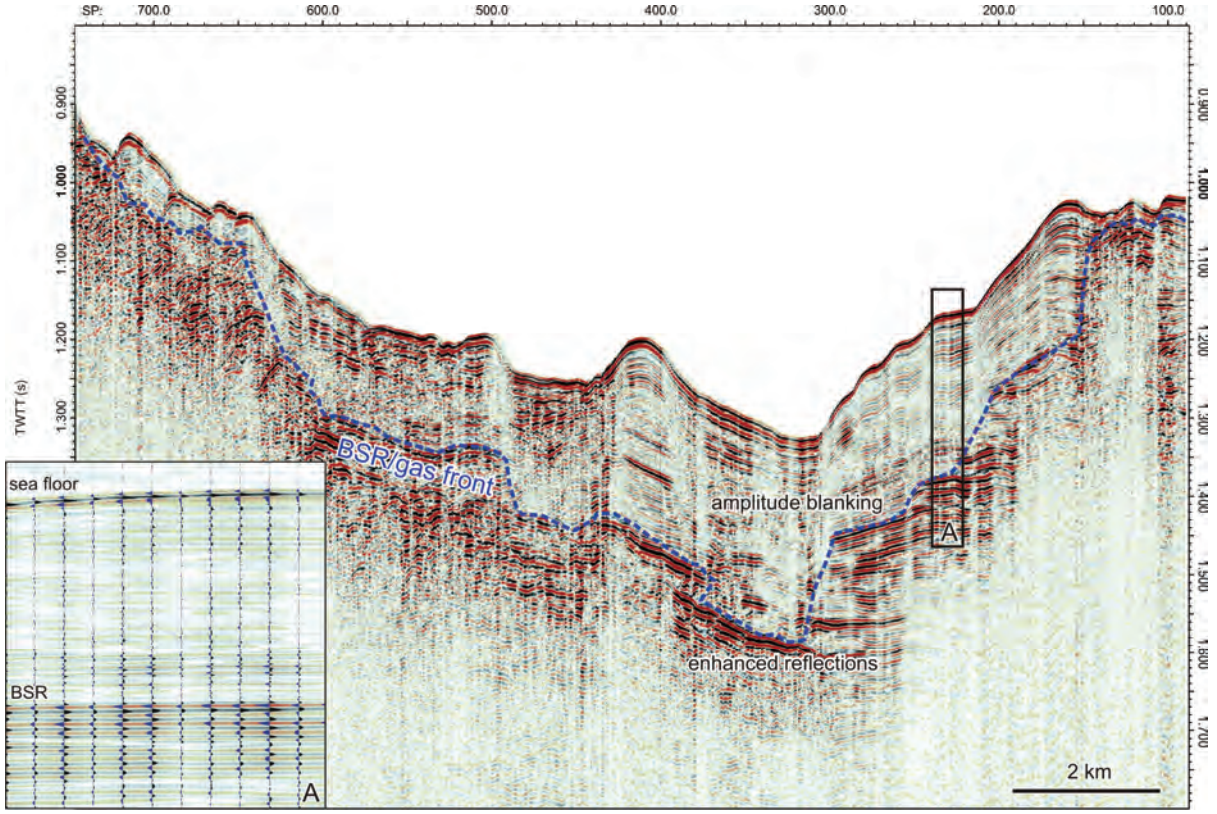

Figure 2.7. GI-gun reflection profile showing a BSR/gas front in the GHSZ. Inset A shows the inverse polarity of the BSR.

Seismic velocity analyses conducted within the CRIMEA project confirmed that the high-amplitude reflections correspond to low-velocity gas-bearing horizons. Seismic inversion revealed that there is 38±10% hydrate in the pore space at BSR depth, where the porosity is 57 % (Zillmer et al. 2005). Since the high-amplitude reflections below the BSR are caused by sedimentary strata containing free gas, we can also interpret the BSR as a gas front (Figs. 2.7.-2.8.). Where the BSR approaches the seafloor, close to -725 m water depth, gas bubbles were detected in the water column (Fig. 2.8.), similarly to what was observed for the gas front outside of the GHSZ (Figs. 2.4. and 2.6.). It is important to realize that the physical processes controlling the depth of the free gas inside and outside the GHSZ are completely different, i.e. gas hydrates versus grain-size distribution. Nevertheless, sometimes it is hard to distinguish the transition from a "hydrate-controlled gas front" to a "grain-size-controlled gas front" (Fig. 2.8.) without having information about the extent of the GHSZ. In any case, our data clearly suggest that for the Dnepr paleo-delta, gas hydrates present in the sediments are a major factor controlling shallow gas migration and accumulation within the GHSZ.

2.6. Gas seeps

Gas seeps are locations where gas bubbles escape from the seafloor in the overlying water column. They are the ultimate prove, in addition to the geophysical detection of shallow gas, that gas is present in the subsurface. The detection and localization of seeps is generally performed by means of echosounders, which detect gas bubbles in the water column due to the contrast in acoustic impedance between water and free gas in the bubbles (Figs. 2.2.B. and 2.3.). Seeps often have a distinct geomorphologic expression (e.g. pockmarks, mud volcanoes), which means that they can also easily be detected on high-resolution reflection seismic data, on single-

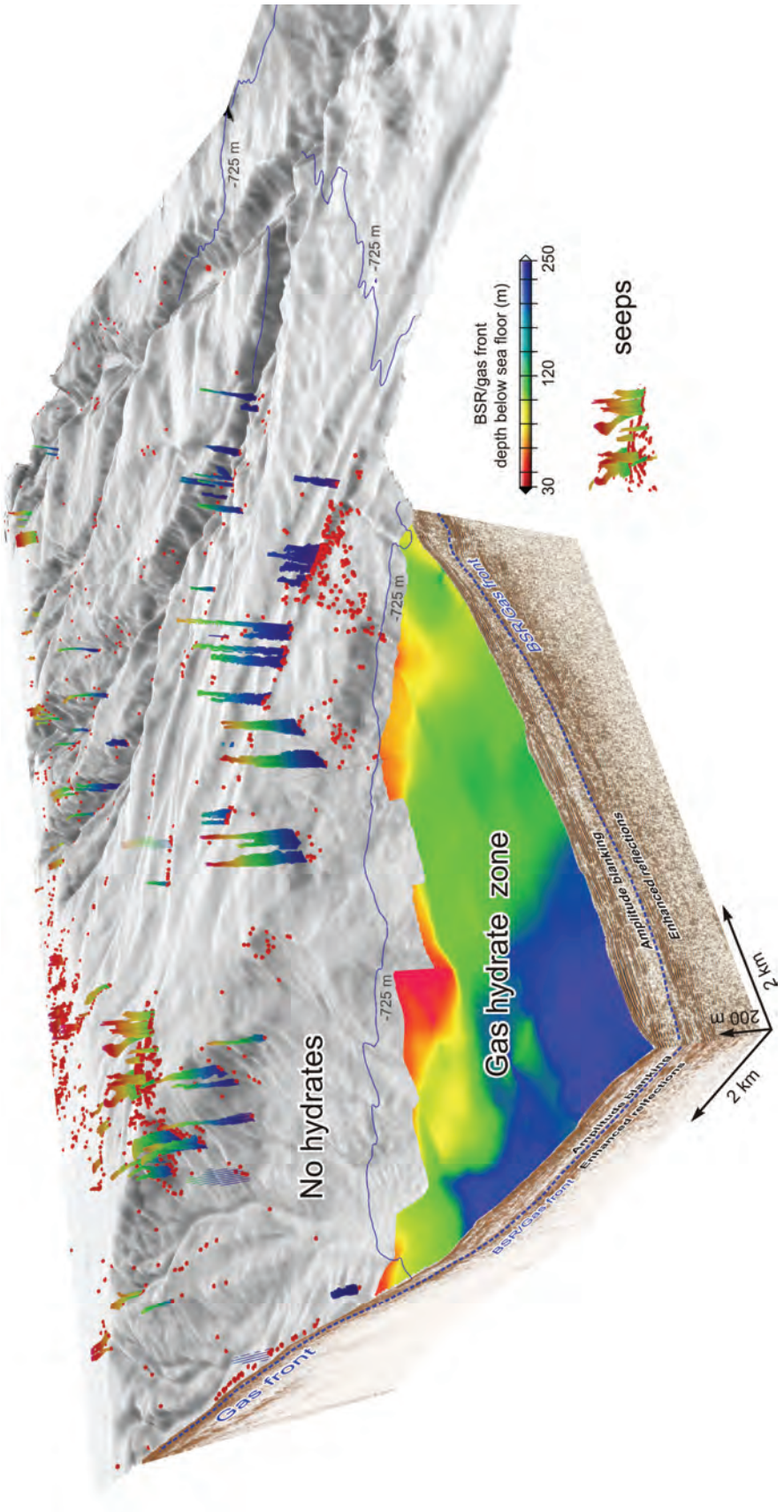

Figure 2.8. 3D view showing the depth variation of the BSR/gas front together with the detected seeps and two GI gun profiles (see Fig. 2.2.A. for location).

beam and multibeam echosounding data and on side-scan sonar recordings. The delineation of seep sites on the seafloor often arises from the detection of anomalously high acoustic backscatter on side-scan sonar or multibeam echosounder recordings. High-acoustic backscatter can be caused by abrupt changes in seafloor relief or by the enhanced acoustic impedance or roughness contrast between certain regions of the seafloor and their surroundings. At methane seeps, this contrast is primarily caused by the presence of methane-derived authigenic carbonates (MDACs), chemosynthetic "cold seep" communities (e.g. clams, tube worms), gas bubbles or gas hydrates in the sediment. The variety and the uniqueness of these seep-related features at the seafloor made seep research to be a stand-alone (academic) research topic (Judd and Hovland, 2007). Recently, several studies have addressed the question of how gas seeps -methane seeps in particular- contribute to atmospheric methane concentrations and to the composition of the world ocean, and how they could affect global warming and the carbon cycle.

During the CRIMEA project, almost 3000 active bubble-releasing seeps were hydro-acoustically detected within an area of 1540 km^2 in the Dnepr paleo-delta (Figs. 2.2.B. and 2.3.) (Naudts et al., 2006). The distribution of these seeps is not random, but the seeps are concentrated in specific locations. Most remarkable is the almost complete absence of seeps in the GHSZ. As much as 95.5 % of the detected seeps have a depth limit that coincides with the phase boundary of pure methane hydrate at -725 m water depth (Fig. 2.8.). This suggests that gas hydrates not only control the distribution of subsurface gas, but also act as an effective seal and sink for methane, which prevents upward migration of methane gas and its release into the water column. Elsewhere, seeps generally occur in association with e.g. pockmarks on the continental shelf, along crests of sedimentary ridges, at bottoms, flanks and margins of canyons and associated with submarine landslides on the continental slope (Figs. 2.8.-2.9.) (Naudts et al., 2006). At all these sites, outside of the GHSZ, stratigraphy and sediment properties are the main factors

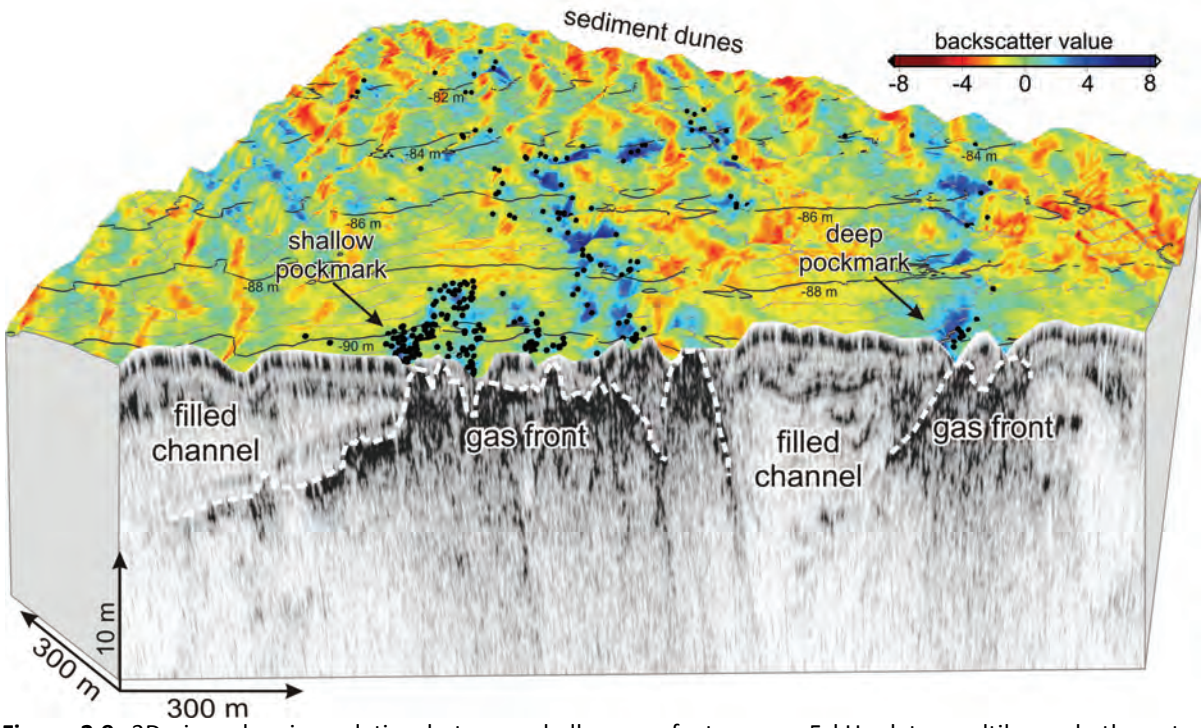

Figure 2.9. 3D view showing relation between shallow gas features on 5 kHz data, multibeam bathymetry overlain by color-coded multibeam backscatter data and single-beam seep locations (see Fig. 2.2.A. for location).

controlling the distribution of shallow gas and gas seeps, resulting in focused fluid flow and gas seepage in association with well-defined seafloor morphologies.

The highest abundance of seeps in the Dnepr paleo-delta was detected on the continental shelf in water depths ranging from -72 m to -156 m, where they commonly occur in association with up to 3 m deep, elongated, large (up to 100 m wide and 500 m long) pockmarks. Sediment-filled channels control the depth of the gas front, which is only able to dome up at the edges of these filled channels. This is also where seeps occur (Fig. 2.9.). For the shelf region, these sediment-filled channels thus appear to be an important controlling factor on shallow-gas migration and gas-seep distribution. However, the multibeam backscatter data indicates an additional factor controlling shallow gas migration and seep distribution on the shelf of the Dnepr paleo-delta. The data show that seeps and a very shallow gas front are associated with pockmarks and with anomalously-high acoustic multibeam backscatter (Fig. 2.9.). Strikingly, the seeps do not occur at maximum high-backscatter values or in the deepest pockmarks, but they seem to occur preferentially in the surrounding medium- to high-backscatter areas, often in shallow pockmarks. Naudts et al. (2008) (CHAPTER 4) examined the cause of these backscatter anomalies and their relation with gas seepage by integrating the multibeam backscatter data with 5 kHz pinger, multibeam bathymetry, hydro-acoustic seep detection, visual observations, sediment and pore-water data. This revealed that the backscatter anomalies are caused by the presence of methane-derived authigenic carbonates (MDACs) in the seafloor sediments, and it allowed to rule out alternative explanations, such as irregular pockmark morphology, grain-size distribution or subsurface gas bubbles (Naudts et al., 2008). The methane-derived carbonates are the result of the anaerobic oxidation of methane (AOM) by a consortium of sulfate-reducing bacteria and methane-oxidizing archaea, which utilize the methane dissolved in the sediment pore water and the sulfate available in the sea water. AOM results in the formation of sulfide and bicarbonate, giving way to sulfide-oxidizing bacterial mats at the seafloor and MDAC formation near the seafloor (Judd and Hovland, 2007). The absence of active seeps in areas with the highest backscatter values was explained as a result of longtime AOM-induced carbonate formation that leads to (self-)sealing of fluid pathways by carbonate clogging, followed by a relocation of the fluid/gas pathways around the cemented, impermeable areas. For the shelf of the Dnepr paleo-delta, MDAC formation controls, on a (sub-)meter scale, gas migration in the very shallow subsurface and the subsequent seep distribution (Naudts et al., 2008).

2.7. Concluding remarks

The integration of different geo- and hydro-acoustic datasets allowed us to determine the presence and distribution of shallow gas, gas hydrates in the subsurface and gas seeps at the seafloor in the Dnepr paleo-delta, northwestern Black Sea. Furthermore, integration of the geo- and hydro-acoustic datasets with non-acoustic data, such as visual observations and sediment cores, enabled us to identify the main controls on shallow-gas migration and gas-seep distribution in our study area. These controls comprise the presence of gas hydrates, continental slope morphology, stratigraphy and sediment properties (e.g. grain size), the presence of shelf-incised channels and the precipitation of methane-derived authigenic carbonates, each operating in different sub-environments and at a different spatial scale.

Suggested reading

The “bible” of shallow gas, gas hydrates and gas seeps is the textbook “Seabed fluid flow: the impact on geology, biology and the marine environment” by Judd and Hovland (Cambridge University Press, 2007). More detailed information about the data and results presented here can be found in “Geological and morphological setting of 2778 methane seeps in the Dnepr paleo-delta, northwestern Black Sea” by Naudts et al. (Marine Geology, 2006) and “Anomalous sea-floor backscatter patterns in methane venting areas, Dnepr paleo-delta, NW

Black Sea" by Naudts et al. (Marine Geology, 2008).

Acknowledgements

We thank the captain and the crew of the 58th and 60th cruise of RV Professor Vodyanitskiy for their hard work and their hospitality and L-3 communications ELAC Nautik for their superior and fast support. This study was carried out in the framework of the CRIMEA project (http://www.CRIMEA-info.org) (EC project EVK-2-CT-2002-00162). We also thank the SONIC Team for the pleasant collaboration and the collection of the pinger and side-scan sonar data. SMT (Kingdom Suite) and IVS (Fledermaus) are acknowledged for the academic licenses. Finally, we thank Gabor Tari and Michal Nemcok, the guest editors of this special issue, for the invitation to publish this paper in TLE.

Additional information

Lieven Naudts processed and interpreted the datasets, wrote the manuscript and made all figures. Lieven Naudts also assisted with the data acquisition during the 12 weeks of expedition on RV Vodyanitskiy in 2003 and 2004. Co-authors helped by reviewing the manuscript and/or by providing the datasets. For the processing of the multibeam data assistance was given by Jens Greinert. For processing of the seismic data assistance was given by Peter Staelens.

CHAPTER 3

Geological and morphological setting of 2778 methane seeps in the Dnepr paleo-delta, northwestern Black Sea

Lieven Naudts, Jens Greinert, Yuriy Artemov, Peter Staelens, Jeffrey Poort, Pieter Van Rensbergen, Marc De Batist

Abstract

The Dnepr paleo-delta area in the NW Black Sea is characterized by an abundant presence of methane seeps. During the expeditions of May-June 2003 and 2004 within the EU-funded CRIMEA project, detailed multibeam, seismic and hydro-acoustic water-column investigations were carried out to study the relation between the spatial distribution of methane seeps, seafloor morphology and subsurface structures.

2778 new methane seeps were detected on echosounding records in an area of 1540 km^2. All seeps are located in the transition zone between the continental shelf and slope, in water depths of -66 to -825 m. The integration of the different geophysical datasets clearly indicates that methane seeps are not randomly distributed in this area, but are concentrated in specific locations.

The depth limit for the majority of the detected seeps is -725 m water depth, which corresponds more or less with the stability limit for pure methane hydrate at the ambient bottom temperature (8.9° C) in this part of the Black Sea. This suggests that, where gas hydrates are stable, they play the role of buffer for the upward migration of methane gas and thus prevent seepage of methane bubbles into the water column.

Higher up on the margin, gas seeps are widespread, but accurate mapping illustrates that seeps occur preferentially in association with particular morphological and subsurface features. On the shelf the highest concentration of seeps is found in elongated depressions (pockmarks) above the margins of filled channels. On the continental slope where no pockmarks have been observed, seepage occurs along crests of sedimentary ridges. There, seepage is focussed by a parallel-stratified sediment cover that thins out towards the ridge crests. On the slope, seepage also appears in the vicinity of canyons (bottom, flanks and margins) or near the scarps of submarine landslides where mass-wasting breaches the fine-grained sediment cover that acts as a stratigraphic seal. The seismic data show the presence of a distinct “gas front”, which has been used to map the depth of the free gas within the seafloor sediments. The depth of this gas front is variable and locally domes up to the seafloor. Where the gas front approaches the seafloor, gas bubbles were detected in the water column. A regional map of the subsurface depth of the gas front emphasises this “gas front - versus - seep” relationship.

The integration of all data sets indicates that the spatial distribution of methane seeps in the Dnepr paleo-delta is mainly controlled by the gas-hydrate stability zone as well as by stratigraphic and sedimentary factors.

Keywords

Methane seeps; seismic; gas front; gas hydrates; pockmarks; canyons; sedimentary ridges; methane-derived carbonate cementation; Dnepr paleo-delta; Black Sea

3.1. Introduction

Gas seeps are widespread in the oceans and can be found on both active and passive continental margins ('cold seeps') and at ocean spreading centers ('hot vents') (Judd, 2003).
Cold seeps and gas seeps in general have engendered a substantial research effort worldwide because of their potential impact on the geosphere, the biosphere, the hydrosphere and the atmosphere (Judd, 2003). They can support unique endemic ecosystems of marine organisms (bacteria, tube worms, clams, etc.) associated with authigenic carbonate or barite precipitation (Hovland et al., 1985; Boetius et al., 2000; Greinert et al., 2001; Greinert et al., 2002; Michaelis et al., 2002). Furthermore, seeps have an important economical value because they can be indications for shallow or deep hydrocarbon accumulations. These are not only interesting as possible energy sources but also have a large influence on the geotechnical properties of sediments and thus on the stability of the seabed. Shallow hydrocarbon reservoirs can also lead to blow-outs when reached during drilling operations (Sills and Wheeler, 1992). Recently, intensive research has focused on how gas seeps, methane seeps in particular, contribute to atmospheric methane concentrations and to the composition of the world oceans, and how they could affect global warming and the carbon cycle (Judd et al., 1997; Judd et al., 2002).

Seepage occurs where fluid flow is focused and where flux rates exceed utilizations rates allowing methane to pass through the seabed into the water column (Judd, 2003). However, under normal conditions, most of the methane will be oxidized by consortia of sulfate-reducing bacteria and methane-oxidizing archaea in anaerobic environments or by the aerobic activity of bacteria (Reeburgh et al., 1993; Boetius et al., 2000; Michaelis et al., 2002). Fluid migration can occur via conduits, such as fault zones, stratigraphic layers and mud diapirs (Hovland and Curzi, 1989; Moore et al., 1991), or by geomorphologically focused flow (Orange and Breen, 1992; Orange et al., 1994). This can be through diffusion of dissolved gas or by means of free-gas bubbles. Gas can also be a part of a gas-hydrate system (Kvenvolden, 1993). If pressure and/or temperature conditions change, gas hydrates can dissociate and hereby support gas seeps at the seafloor and result in sediment destabilization (Bouriak et al., 2000; Bünz et al., 2005).

With the recent increasing interest in gas seeps, detection tools and methods have been developed and adapted to discover and investigate seep sites. In addition to echosounder and high-resolution seismic recordings, multibeam and side-scan sonar have been used to detect gas seepage and shallow gas (Judd and Hovland, 1992; Wever et al., 1998). These methods are not only able to detect changes in morphology related to gas seepage (e.g. pockmarks, mud volcanoes) but also to detect changes in backscatter strength, which can provide strong indications for the presence of, for example, authigenic carbonates that are common at cold seeps (Greinert et al., 2001; Campbell et al., 2002). ROV's, submarines and CTD's have been used for groundtruthing, mapping and sampling seafloor seeps (Suess et al., 2001; Orange et al., 2002; Johnson et al., 2003; Paull et al., 2005). Recent work also paid attention to the subsurface with a focus on seismic subbottom signatures and indications of shallow gas (acoustic turbidity, enhanced reflections, acoustic blanking, etc.) and possible conduits (faults, diapirs, etc.), which can be indirect indications for seepage at the seafloor (Judd and Hovland, 1992; Orange and Breen, 1992; Yun et al., 1999; Garcia-Gil et al., 2002; Van Rensbergen et al., 2002; Krastel et al., 2003).

In this paper we present the discovery of thousands of active methane seeps detected directly with an adapted scientific split-beam echosounder. We were able to pinpoint the exact location of all seeps and to integrate the seep locations with the acquired multibeam and geophysical datasets to explain the observed seep distribution in relation to the geology and morphology.

3.2. Study area

The Dnepr paleo-delta area is located on the continental margin of the northwestern Black Sea, west of the Crimea Peninsula (Fig. 3.1.). The

area is well known for the abundant presence of shallow gas and gas seeps (Polikarpov et al., 1989; Polikarpov et al., 1992; Egorov et al., 1998; Popescu and De Batist, 2004). Structurally, this part of the Black Sea forms the transition zone between the Scythian Platform and the Karkinit Trough in the north, the Shtormavaya Graben, the Kalamit Ridge and the Western Black Sea Basin in the south (Robinson et al., 1996; Nikishin et al., 2003) (Fig. 3.1.). The Western Black Sea Basin was formed during the late Cretaceous in a back-arc setting above the northward subducting Tethys Ocean, close to the southern margin of Eurasia (Robinson et al., 1996). The continental margin west of the Crimea Peninsula consists of Late Paleozoic to Mesozoic basement rocks covered by thick Cenozoic sediments (>2 km) (Finetti et al., 1988).

The northwestern Black Sea is dominated by a rather wide shelf (60-200 km) with a shelf break at -120 m to -170 m water depth and canyon systems with large deep-sea fan complexes, mainly developed during sealevel lowstands (Winguth et al., 2000; Popescu et al., 2001). The main canyon systems in the western Black Sea are the Danube and Dnepr Canyons, each with their own typical morphology. The well-studied Danube Canyon (Popescu et al., 2001; Popescu et al., 2004) differs from the Dnepr Canyon and other, smaller canyons because it indents the shelf over a distance of 26 km and has an unidirectional development. The Dnepr Canyon only starts from the shelf edge and deeply incises the upper slope (Wong et al., 2002). Both canyon systems are likely to have formed by sediment flows along the axial thalweg causing sediment failures along the channel margins. These sediment failures are probably also influenced by gas-related instability and by deep faulting (Popescu et al., 2004). The deep-sea fans, related to these canyon systems, are fed by sediment input from the Danube River (Central Europe) and the Dnepr, Dnestr and Bug Rivers (Eastern Europe). At present the Dnepr, Dnestr and Bug discharge their sediment loads into a lagoonal system separated from the Black Sea by beach barriers, and only a small fraction of the suspended load reaches the sea (Winguth et al., 2000). During the last lowstand the Dnepr and Danube flowed hundreds of kilometers beyond there present mouths depositing organic-rich material and forming shelf-edge deltas at the present-day shelf break (Ryan et al., 1997). After the last sealevel lowstand water level rose, leading to fresh-water outflow from and salt-water inflow into the Black Sea through the Bosporus. As a result of density differences and the absence of complete water-column mixing, the Black Sea became the biggest anoxic basin in the world, with favorable conditions for preserving organic material and generating hydrocarbons (Jorgensen et al., 2004). A well-pronounced oxycline at about 90 m separates the upper oxic from the deeper, permanently sub-oxic and anoxic water masses. So it is not surprising that the shelf-edge deltas and adjacent areas of the northwestern Black Sea are characterized by shallow gas and gas seeps that release methane of microbial origin (Polikarpov et al., 1989; Polikarpov et al., 1992; Egorov et al., 1998; Amouroux et al., 2002; Michaelis et al., 2002; Popescu and De Batist, 2004).

The Dnepr paleo-delta area is the most prolific seep area of the northwestern Black Sea margin and possibly one of the most active in the World (Hornafius et al., 1999). The methane seeps in this area were first registered on echosounder recordings by Polikarpov et al. in 1989. Later studies discovered more seeps (Polikarpov et al., 1992; Egorov et al., 1998) as well as the presence of carbonate buildups formed by anaerobically oxidized methane in an anoxic environment at -230 m water depth (Luth et al., 1999; Peckmann et al., 2001; Thiel et al., 2001; Michaelis et al., 2002). Gas seeps occur in the oxic as wel as in the anoxic zone over a wide depth range from -35 to -785 m (Egorov et al., 1998). This part of the northwestern Black Sea margin is dominated by the presence of the Dnepr Canyon and the Dnepr Fan. The Dnepr Fan starts at a water depth of about -300 m and it consist of several vertically stacked, laterally displaced channel-levee systems, deposited during water-level lowstands. Generally, the channel floors are covered by coarse-grained deposits and flanked by finer-grained levee and overbank sediments deposited during overflow of the canyons. The area east of the Dnepr Fan is characterized by drift sedimentation, whereas to the west, mass-wasting and mass-transport deposition is prominent (Wong et al., 2002).

Southwest of the Dnepr Canyon a bottom-simulating reflection (BSR) has been observed on seismic recordings between -700 and -1350 m water depth (Inset Fig. 3.1.) (Lüdmann et al., 2004; Zillmer et al., 2005). Commonly, a BSR is a high-amplitude reflection that runs sub-parallel

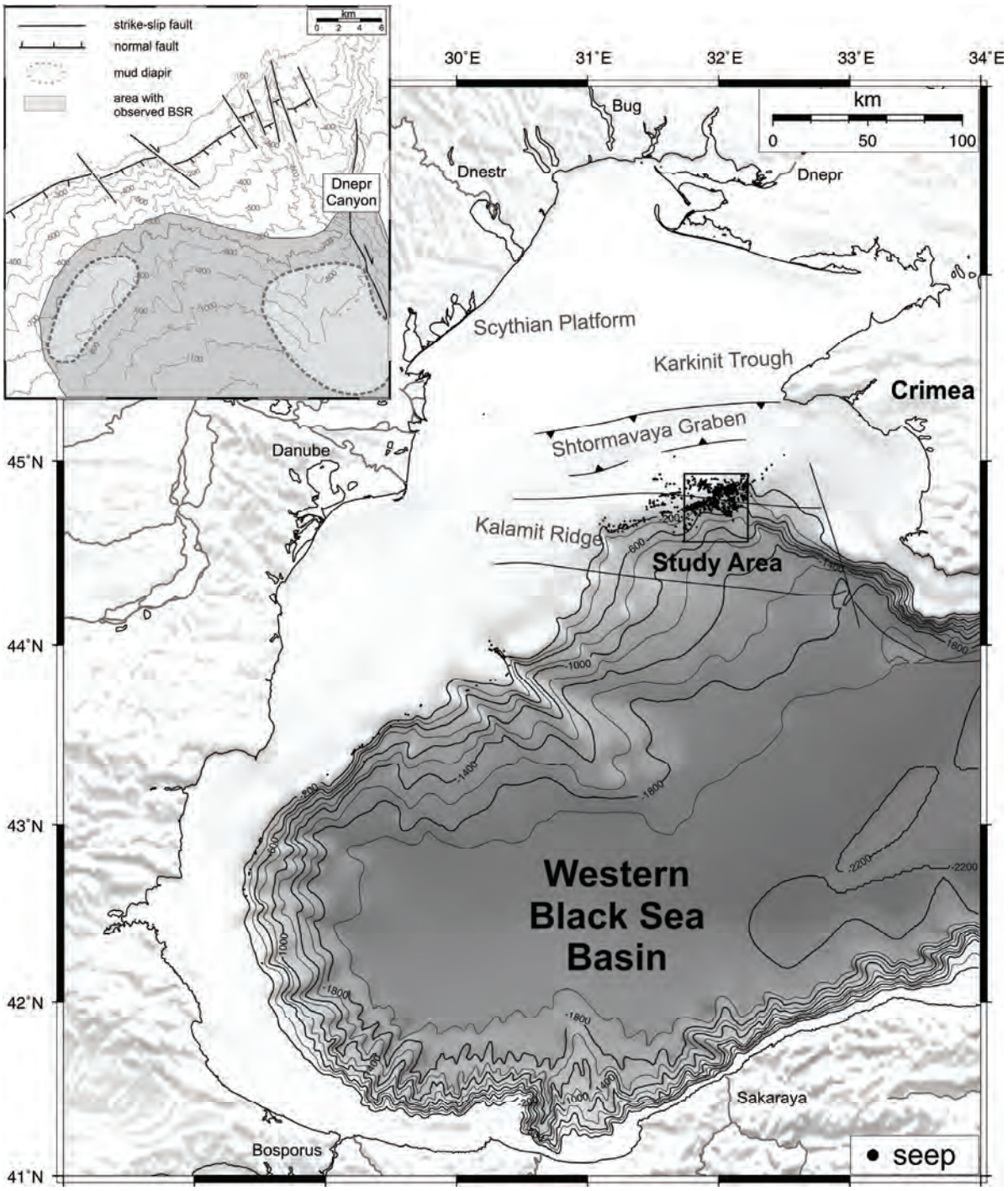

Figure 3.1. Location map of the Dnepr paleo-delta study area with indication of deep structures, major faults and seep locations in the northwestern Black Sea (Robinson et al., 1996; Egorov et al, 1998). Inset shows the bathymetry of the study area in greater detail, with indication of faults, mud diapirs, area with observed BSR and the Dnepr Canyon (after Lüdmann et al., 2004).

to the seafloor reflection, has a polarity that is opposite to that of the seafloor reflection and occasionally crosscuts the sediment stratification (Kvenvolden, 1998). BSRs mark the temperature- and pressure-controlled base of the gas-hydrate stability zone (BGHSZ) and are therefore commonly regarded as an indirect indication for the presence of gas hydrates.
The seismic studies by Lüdmann et al. (2004) also revealed the presence of possible faults and mud diapirs in the Dnepr paleo-delta area (Fig. 3.1.).

3.3. Data and Methods

The data presented in this paper were gathered during the 58th (May-June 2003) and 60th (May-June 2004) cruise of RV Professor Vodyanitskiy. We combine and integrate hydro-acoustic water-column data, hydro-acoustic seafloor data and seismic subsurface data (Fig. 3.2.) to obtain better insight in the geological and morphological characterization of the discovered seep sites.

3.3.1. Water-column data

Hydro-acoustic water-column data was recorded with a hull-mounted SIMRAD EK500 dual-frequency (38 and 120 kHz) split-beam echosounder. This system operates with a total beam width of 7°. Due to the high impedance contrast between water and free gas, gas-bubble seepage in the water column can be acoustically detected and shows up as “acoustic flares” on echograms (Fig. 3.3.). Such a flare can comprise one single bubble stream or can be a conjugation of different bubble streams or seeps within the footprint of the echosounder. The WaveLens software package (by Y. Artemov) was used to trace and locate the origin of the bubble streams, i.e. the exact position of the seeps at the seafloor, based on gas-bubble backscatter strength. Video footage of the seafloor, collected by OFOS (Ocean Floor Observation System), confirmed the accuracy of the seep positioning and the nearly full coverage at the major seep sites. During the two cruises, a total length of 5261 km echosounder tracks was recorded within the 1540 km^2 study area (Fig. 3.2.B.).

3.3.2. Seafloor data

Regional bathymetric mapping of the study area was performed with a mobile 50 kHz swath system (SeaBeam 1050). This system operates with 126 beams (width 1.5° by 3° beam angle and 120° swath) and it was motion-compensated by an OCTANS 3000 motion sensor. Sound-velocity profiles were acquired via CTD casts and the sound velocity at the transducers was continuously measured. Data acquisition was managed with Hydrostar Online and the data processing was carried out with HDPEdit and HDPPost. Fine editing of the data by deleting bad data points was done with Fledermaus (6.1.2), which was also used for the visualization of the merged data sets. During the two cruises an area of 1540 km^2 was covered in water depths from -57 to -1248 m (Fig. 3.2.). Gaps in the multibeam coverage were filled in by data acquired during the 2004 METROL cruise (Poseidon cruise P317/3) with the same swath system (SeaBeam 1050) as used during the CRIMEA cruises. All grids shown in this paper have a cell size of 30 m, except when specifically mentioned otherwise.

3.3.3. Subsurface data

Three different types of seismic data were acquired (GI-gun, sparker and 5 kHz subbottom profiler) (Fig. 3.2.A.), each within a different frequency range to extract the best possible information about the underlying geology.

A first set of single-channel seismic data were acquired with a GI-gun source (central frequency of 150 Hz; maximum shooting interval of 8 s) and an active surface streamer with 10 hydrophones. The raw signal was analog filtered (70-200 Hz) and recorded on a Delph-2 system. The theoretical vertical resolution is 6 m and the maximum penetration is 600 ms TWTT. Single-channel GI-gun data were recorded only during the first cruise and this over a total length of 664

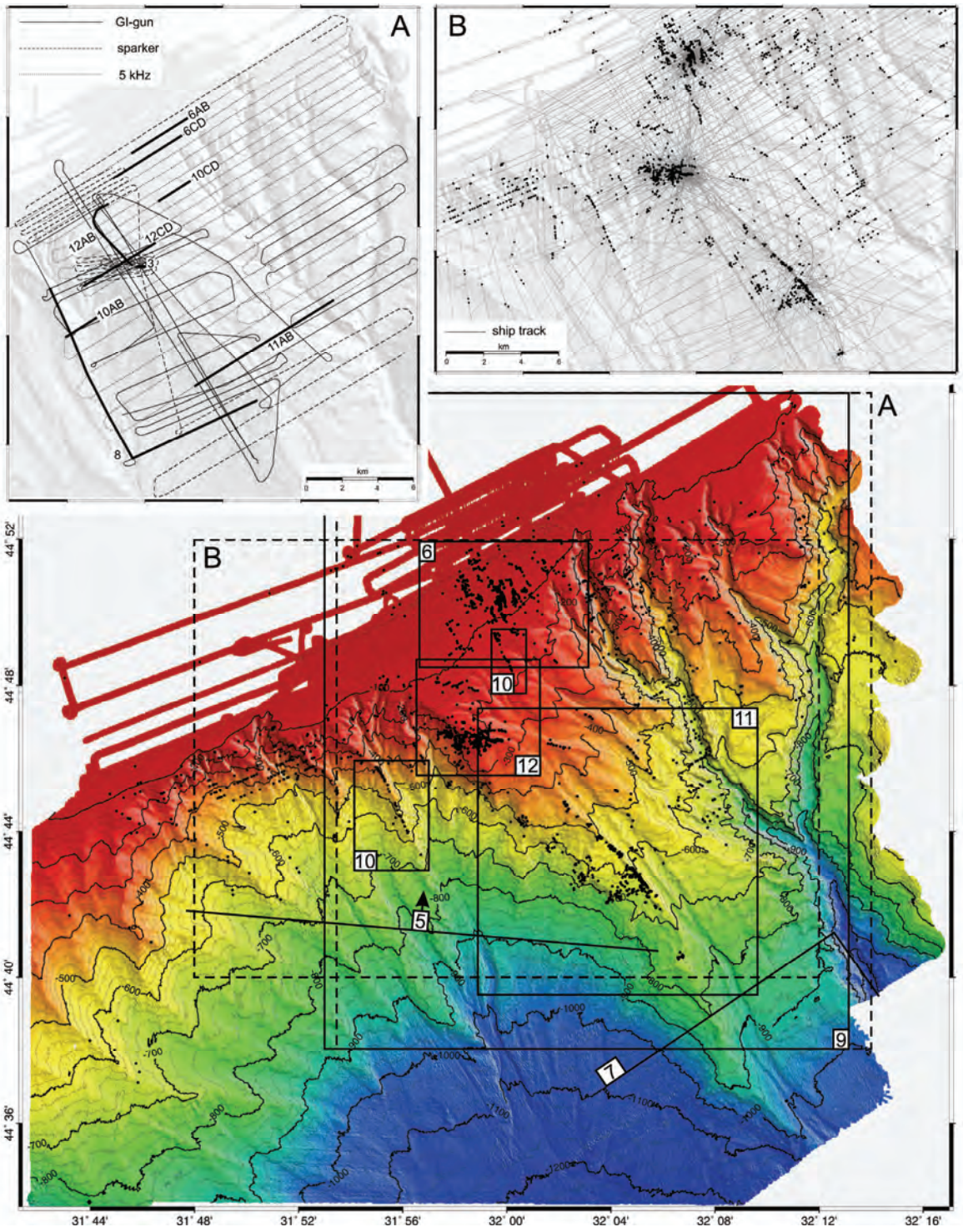

Figure 3.2. Swath bathymetry map (30 m grid) acquired during the 2003 and 2004 CRIMEA cruises with all newly detected seeps plotted as black dots. Gaps in the multibeam coverage were filled in by data from the 2004 METROL cruise. The outlines of the areas covered by Figs. 3.6., 3.9., 3.10., 3.11. and 3.12. is indicated as well as the viewing direction of Fig. 3.5. and the location of the profile used in Fig. 3.7. Inset A shows the track lines of the seismic data (GI-gun, sparker and 5 kHz) acquired within the study area and the seismic and echosounder profiles shown in this manuscript are also indicated. Inset B gives an overview of the ship tracks sailed during the 2003 and 2004 CRIMEA cruises and along which hydro-acoustic seep detection was performed (seeps locations are plotted as black dots).

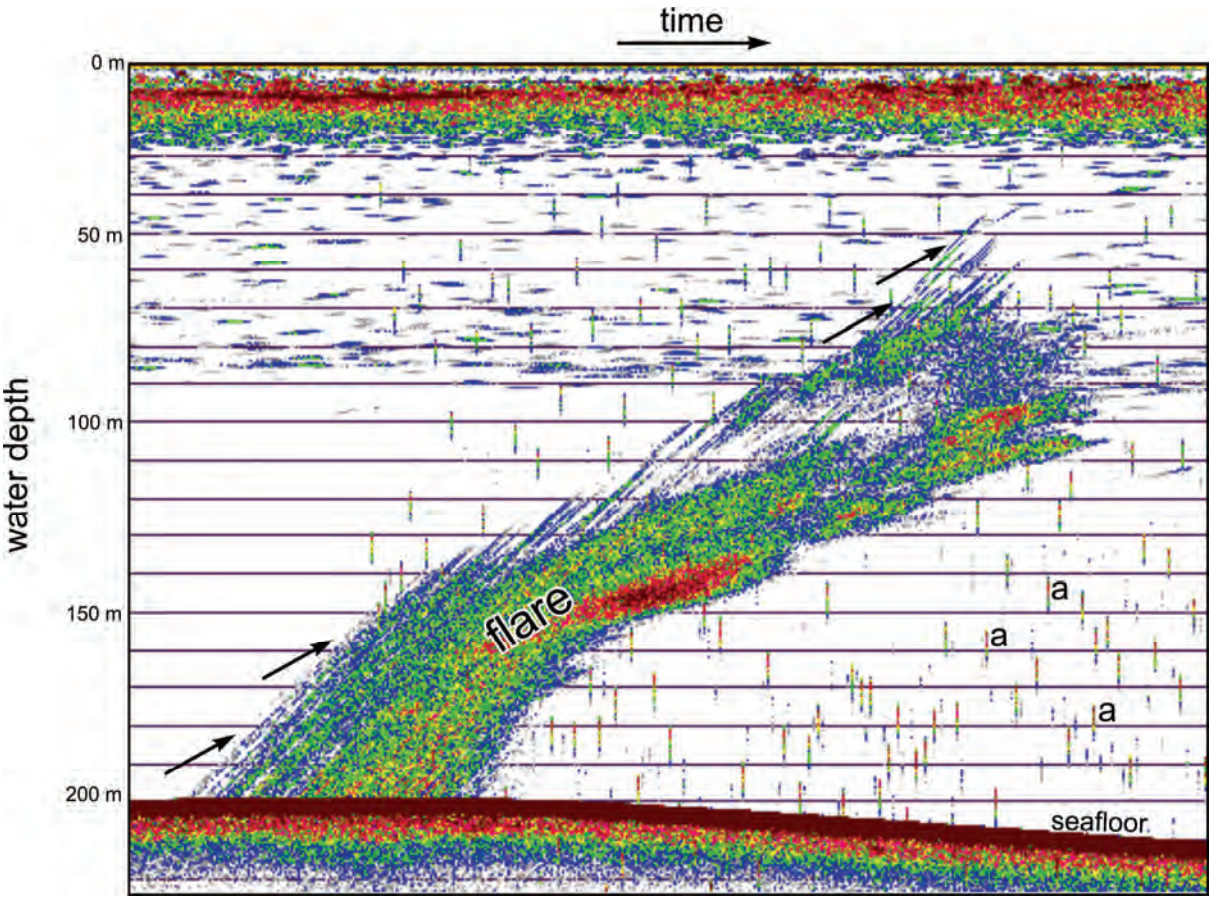

Figure 3.3. Hydro-acoustic image ("flare") of several methane bubble trains rising towards the sea surface at a seep site at -200 m water depth. The image consists of a succession of pings over a certain time interval. The tilted arrows show the rise of isolated bubbles. The bubbles clearly cross the oxic–anoxic interface at -90 m water depth. The other backscatter signals above this depth correspond to fish, jelly fish and larvae. The vertical acoustic anomalies (a) are caused by the parallel running multibeam system.

km. A second set of single-channel seismic data were collected with a SIG sparker source (central frequency of 500-700 Hz) and an active surface streamer with 10 hydrophones. The analog signal was bandpass-filtered (200-2000 Hz) and recorded on a Delph-2 system. The theoretical vertical resolution is 1 m and the maximum penetration is 100 ms TWTT. During the 2003 cruise, 332 km of sparker data were recorded.

Subbottom profiling data were shot with a 5 kHz profiler system (Sonic-3), which was mounted in a tow fish with a fish-track underwater-navigation system and a pressure sensor. The tow fish was towed 100-200 m above the seafloor. The theoretical vertical resolution is 30 cm and the maximum penetration is 35 ms TWTT. During the 2003 cruise, 589 km of 5 kHz data were recorded.

Apart from the frequency filtering no other processing was carried out on the seismic data. Interpretation of the data was carried out with the Kingdom Suite software package.

The multi-channel GI-gun profile shown in figure 3.7. was recorded during the 2001 GHOSTDABS cruise and was made available by the Institute of Biogeochemistry and Marine Chemistry of the University of Hamburg. The profile was published before by Lüdmann et al. (2004).

3.4. Observations and results

3.4.1. Morphology

The Dnepr paleo-delta study area covers the transition zone between the continental shelf

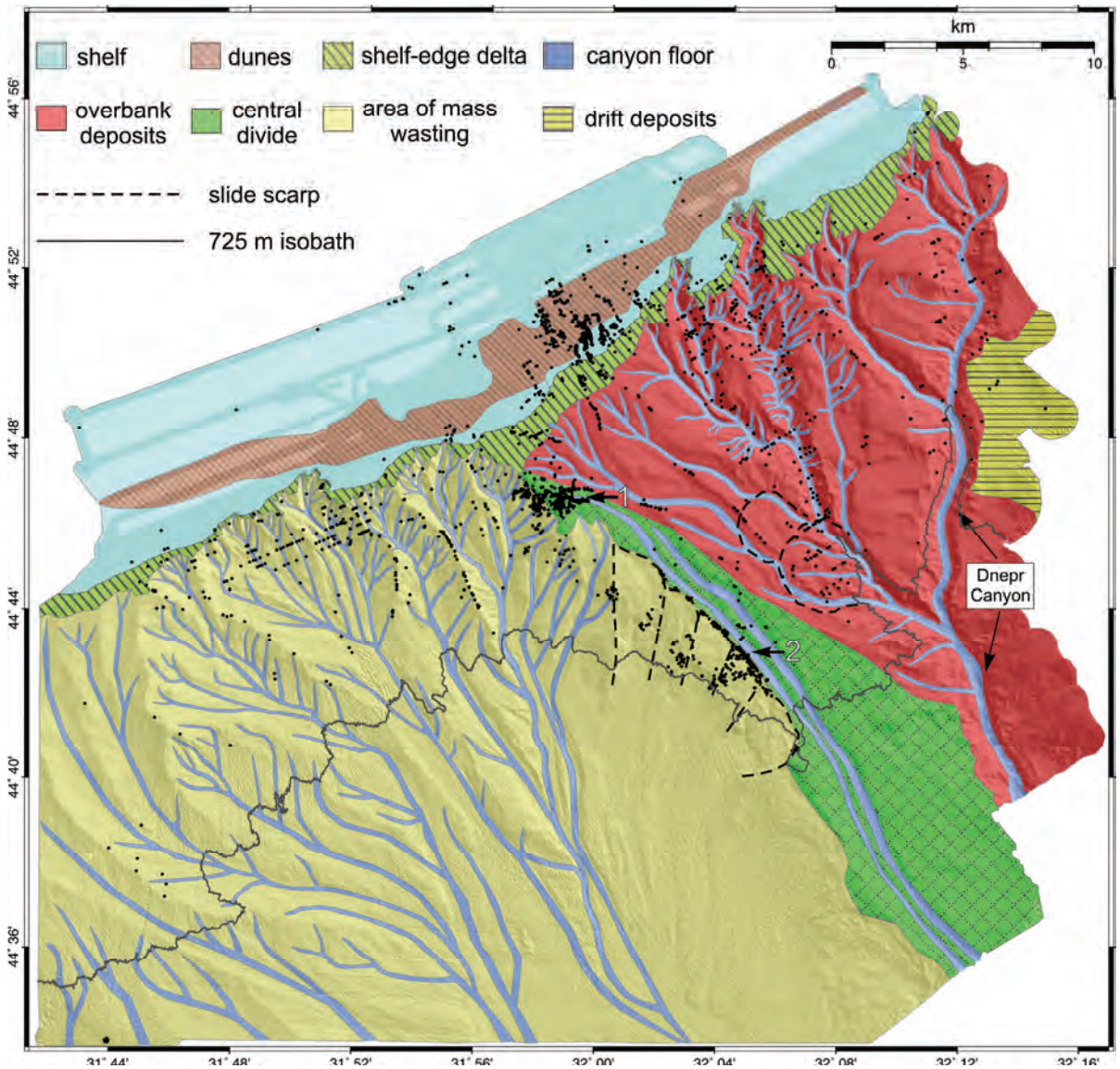

Figure 3.4. Map of the study area with indication of the major geomorphological regions and canyons. Seep locations are plotted as black dots. The scarps of the submarine landslides are emphasized by dashed lines and the position of two chimney fields is indicated by 2 horizontal arrows (1: Michaelis et al., 2002; 2: CRIMEA cruise 2004).

and the continental slope. The water depth in the study area ranges from -57 to -1248 m and the shelf break occurs at -125 m water depth (Fig. 3.2.).

3.4.1.1. Shelf

The shelf is characterized by a flat, sub-horizontal surface (Figs. 3.2., 3.4. and 3.5.) with a maximum slope of 0.5°. Close to the shelf break, this flat surface is locally interrupted by a dune field (Fig. 3.4 and 3.6). The majority of the dunes have a NW-SE orientation, a wave length of 120 m and a height of 1.5-2.5 m. Most of the dunes are symmetrical, but at the SW and NE borders of the central dune field, they are barchanoid in shape. South of the dune field, four elongated depressions occur. They have a maximum length of 500 m, a maximum width of 100 m and a maximum depth of 3 m. They appear to be an amalgamation of smaller depressions (Fig. 3.6.).

3.4.1.2. Slope

The slope can be sub-divided in two morphologically contrasting segments: a western area dominated by mass-wasting and an eastern area dominated by deposition. These two areas are separated by a clear boundary, which we will hereafter refer to as the "central divide" (Figs. 3.4., 3.5. and 3.11.).

a) Western mass-wasting dominated area

In the western area, the morphology is dominated by a canyon system with sedimentary ridges and gullied walls (Figs. 3.4. and 3.5.). Some of the canyons incise the shelf up to a water depth of 100 m and indent the shelf edge over a maximum distance of 2 km. The canyons have cauliflower-shaped heads and are bifurcated in the central part (Fig. 3.4.). The canyons at the western side of the area are more elongated and less bifurcated. At the eastern side adjacent to the central divide, canyons are absent and five submarine landslides can be identified (Figs. 3.4., 3.5. and 3.11.). The maximum size of one individual slide is 3 km by 5 km. The submarine landslides cover an area of 38 km^2 in water depths from -355 to -975 m. The head scarps have a maximum height of 45 m and form slopes of 10 to 20°. Within the slide areas, several smaller scarps are visible (Figs. 3.5.), indicating multiple failure events. Some remains of the slide deposits can be recognized, but most of the destabilized sediments have been eroded or transported out of the study area. Post-slide erosion is also evident from the smoothed morphology of the head scarps.

b) Eastern deposition-dominated area

The eastern area is dominated by deposition, with channel-levee outbuilding and deeply

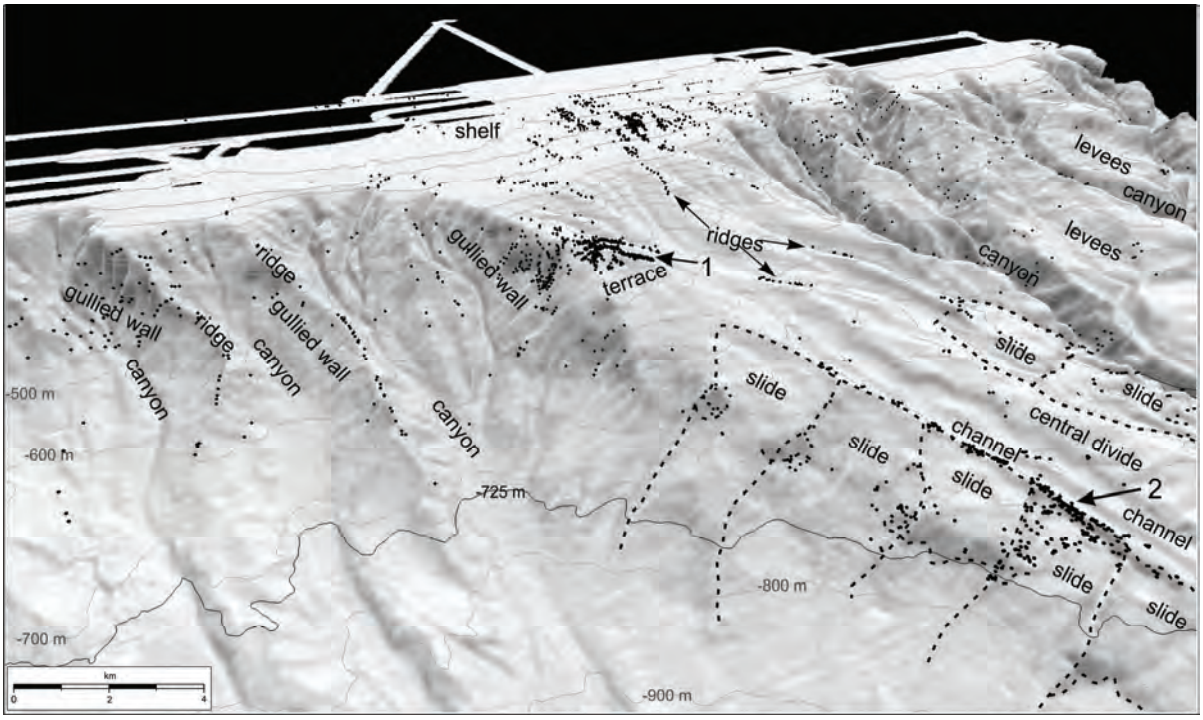

Figure 3.5. Oblique view of grey-shaded bathymetry map of the upper part of the study area with indication of different geomorphological features (see Fig. 3.2. for location). Seeps locations are plotted as black dots. The scarps of the submarine landslides are emphasized by dashed lines and the position of the 2 chimney fields is indicated by 2 arrows (1: Michaelis et al., 2002; 2: CRIMEA cruise 2004). Seep clusters are evident at the crest of sedimentary ridges, at submarine landslides, along canyons, on the shelf and at the terrace at -200 m water depth.

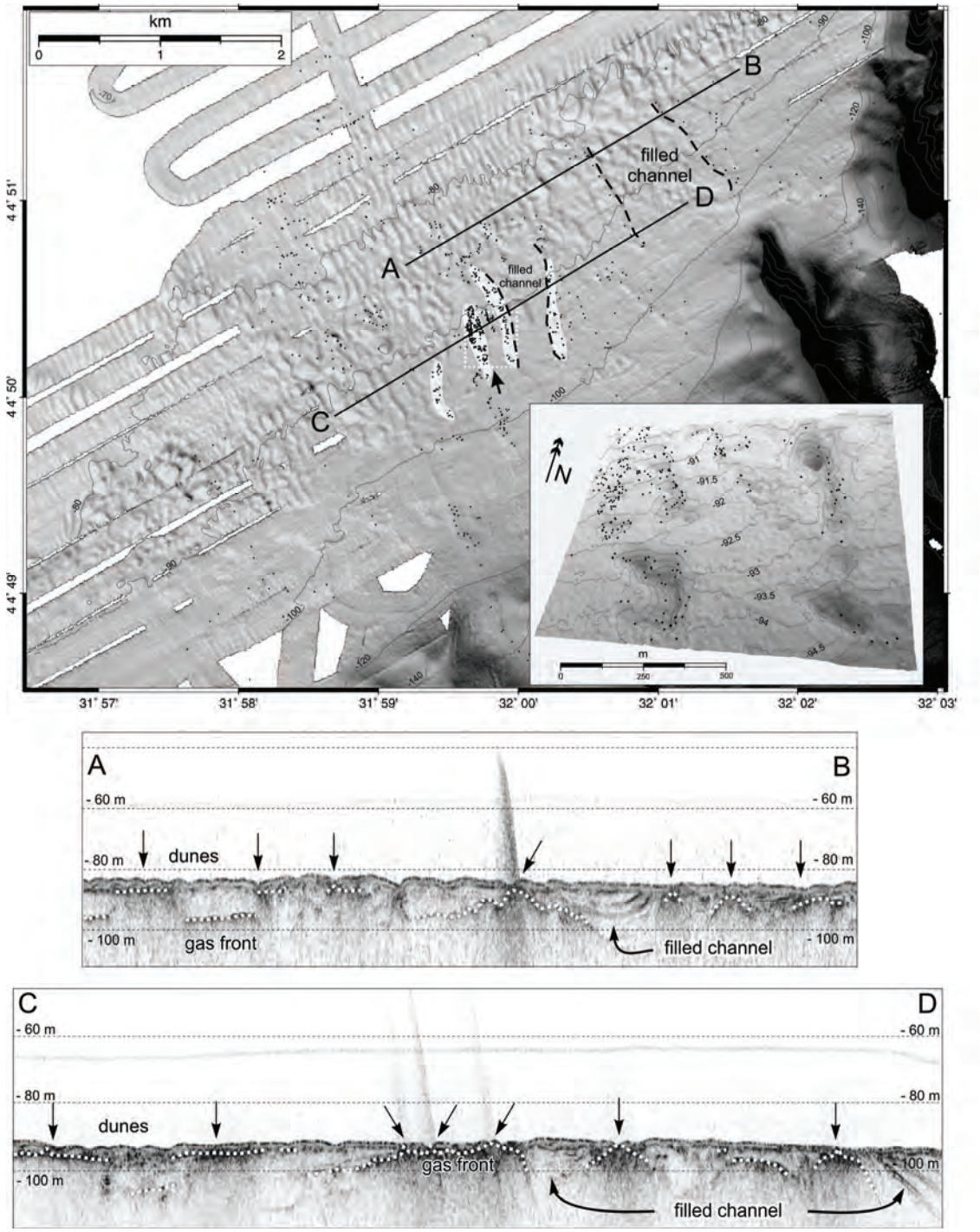

Figure 3.6. Plan view of grey-shaded bathymetry map of the shelf and the dune area (5 m grid) overlain by bathymetric contours (see Fig. 3.2. for location). The four elongated depressions are marked by a transparent white mask. The inset shows an oblique view of the intensive seep site at -92 m water depth characterized by pockmarks. Seep positions are plotted as black dots. On the 5 kHz profiles AB and CD (see Fig. 3.2.A. for location) the updoming gas front (dotted white line) underneath the seep positions (arrows) is clearly visible. Seeps are located at the margins of filled channels and not above them.

incised U-shaped canyons (Figs. 3.4. and 3.5.). The canyons have a maximum width of 2.5 km and a depth of 200 m. Similar to the erosional region in the west, the canyons incise the shelf to a water depth of 100 m, but here they indent the shelf over a maximum distance of 4 km. The

main canyon is the Dnepr Canyon (Figs. 3.4.) with all other canyons being tributaries to it and merging with the main tributary at -940 m water depth. Northwest of this confluence, opposite of the submarine landslides on the western side of the central divide, a large, double submarine landslide covers an area of 21.5 km^2 between -444 to -865 m water depth (Figs. 3.4., 3.5. and 3.11.). The crown scarp has a maximum height of 60 m. In contrast with the western submarine landslides, the slide deposits in the canyon at the base of the slide are still clearly visible in the morphology and unaffected by erosion (Fig. 3.11.).

c) Central divide

The eastern and western areas are separated by the central divide (Figs. 3.4., 3.5. and 3.11.). Within the central divide two parallel channels extend over a length of more than 24 km, with a maximum depth of 45 m and a mutual width of 1.5 km. Apart from these two parallel depressions, there are no other major channels incising the divide. Upslope, the central divide ends at a terrace-like feature at -180 to -230 m water depth, which forms the transition to the shelf.

Figure 3.7. indicates that the rather unusual morphology of the central divide has been inherited from a series of underlying, buried channel-levee systems. The two parallel channels within the central divide are formed probably due to differential compaction of the underlying channel sediments, which resulted in the two channels with central ridge morphology.

3.4.2. Seep locations

Up to 2778 methane seeps were hydro-acoustically detected in an area of 1540 km^2, in water depths ranging from -66 to -825 m. Of all detected seeps, 99.5 % are located in water depths shallower than -725 m (Figs. 3.2. and 3.4.) where they are clustered in certain morphological locations (Fig. 3.5.).

Seeps on the shelf are concentrated in the

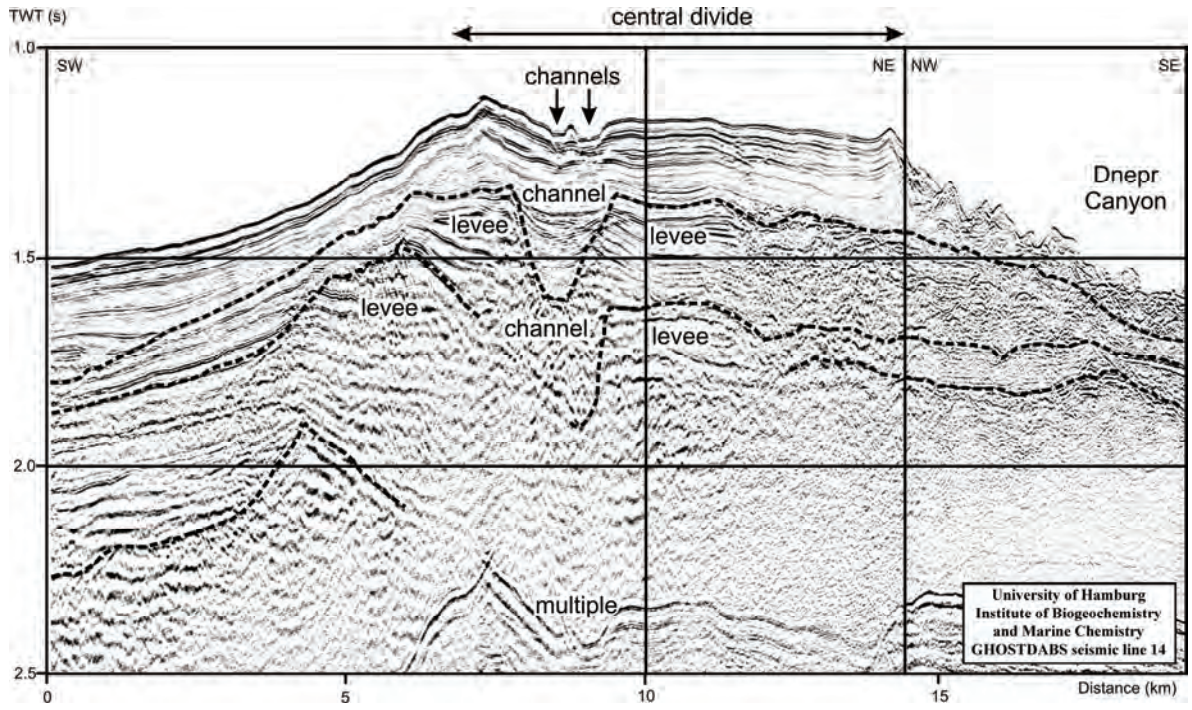

Figure 3.7. A multi-channel GI-gun profile (see Figs. 3.2. for location) from the GHOSTDABS project (Lüdmann et al., 2004) clearly indicates that the rather unusual morphology of the central divide has been inherited from a series of underlying, buried channel-levee systems. The two parallel channels within the central divide are formed probably due to differential compaction of the underlying channel sediments, which resulted in the two channels with central ridge morphology. Also notice the presence of the Dnepr Canyon.

dune field and are especially abundant in the elongated depressions to the south of the dune field. Because of the clear relationship between the seeps and the elongated depression, we interpret these depressions as pockmarks (Hovland and Judd, 1988). On the shelf, the seeps appear to be following a general NW-SE trend (Fig. 3.6.). This orientation is perpendicular to the majority of the ship tracks (Fig. 3.2.B.), which indicates that it is natural and does not originate from data acquisition.

On the slope there are several places and structures which are bound to seepage.

In the mass-wasting dominated region, the majority of the seeps occur on crests of sedimentary ridges, on gullied canyon walls or on the scarps of submarine landslides (Figs. 3.2., 3.4. and 3.5.). On one of the scarps a new carbonate chimney field was discovered during the 2004 CRIMEA cruise by visual observations and dredge sampling in about -600 m water depth (Figs. 3.4. and 3.5.).

In the deposition-dominated area, seeps are linked to canyons: either on the bottom, or on the flanks or margins. Some seeps are located on the crests of sedimentary ridges (Figs. 3.5.). The scarps of the submarine landslides in this area are not characterized by seep occurrences like in the western area, but seeps are present within the double submarine landslide (Figs. 3.4. and 3.5.).

On the central divide, seeps are in general rather scarce (Fig. 3.4.). In contrast, they are abundant on the terrace at -180 to -230 m water depth (Fig. 3.5.). The terrace actually consists of three radially spread ridges within the lobed morphology of the terrace (Fig. 3.2.). The carbonate chimney field, described earlier by Michaelis et al. (2002), is located on the crest of one of these ridges (Figs. 3.4. and 3.5.).

3.4.3. Gas hydrate and free gas occurrences

As mentioned above, the vast majority of the gas seeps occur in water depths from -66 to -725 m, and only a dozen seeps were detected below -725 m water depth (Figs. 3.2. and 3.4.). Some of these 'deep-water' seeps are located at -825 m water depth, above a subsurface mud-volcano-like structure described by Kruglyakova et al. (2004). The other 'deep-water' seeps are located close to the -725 m contour line. The almost complete absence of seeps below -725 m water depth strongly suggests that no free gas is present, at the seafloor, below this depth.

The stability limit of pure methane hydrates occurs at -725 m water depth (Sloan, 1998), when calculated using a present-day bottom-water temperature of 8.9°C (CRIMEA cruises) and a presumed average open-ocean pore-water salinity in the sedimentary column of 35 ppt. The presence of gas hydrates in the area had already been indicated by the observation of a BSR and confirmed by direct sampling (Kruglyakova et al., 2004; Lüdmann et al., 2004; Popescu and De Batist, 2004; Zillmer et al., 2005). Zillmer et al. (2005) determined for the study area, that there is 38 ± 10 % hydrate in the pore space at BSR depth, where the porosity is 57 %. Our GI-gun data also demonstrate a BSR-like event that is located at the calculated subbottom depth of the BGHSZ (Fig. 3.8.). It displays a number of characteristics of a typical BSR (i.e. low amplitudes above, enhanced reflections below, cross-cutting the stratigraphy), but instead of appearing as a distinct, single reflection, the BGHSZ on our data is expressed as a transition from high-amplitude (gas-enhanced) reflections below and low-amplitude (blanked) reflections above (Fig. 3.8.). Such seismic response is attributed to the relatively high frequency of the seismic signal and to the acquisition lay-out with relatively short offsets (Vanneste et al., 2001).

The BGHSZ reflection approaches the seafloor close to -725 m water depth. From that point on, bubbles are detected in the water column (Fig. 3.8., graph). Low reflection amplitudes within the GHSZ are often attributed to the presence of gas hydrates in the sediment pore spaces (Lee and Dillon, 2001), although this could not be confirmed in e.g. the Blake Ridge hydrate area (Holbrook, 2001). The presence of free gas below the hydrate-cemented strata is indicated by enhanced reflections below the low-amplitude zone. Since the enhanced reflections are present on our seismic records both in the "hydrate zone" and in the "no-hydrate zone", we interpret the top of the enhanced reflections as the "gas front", i.e. the

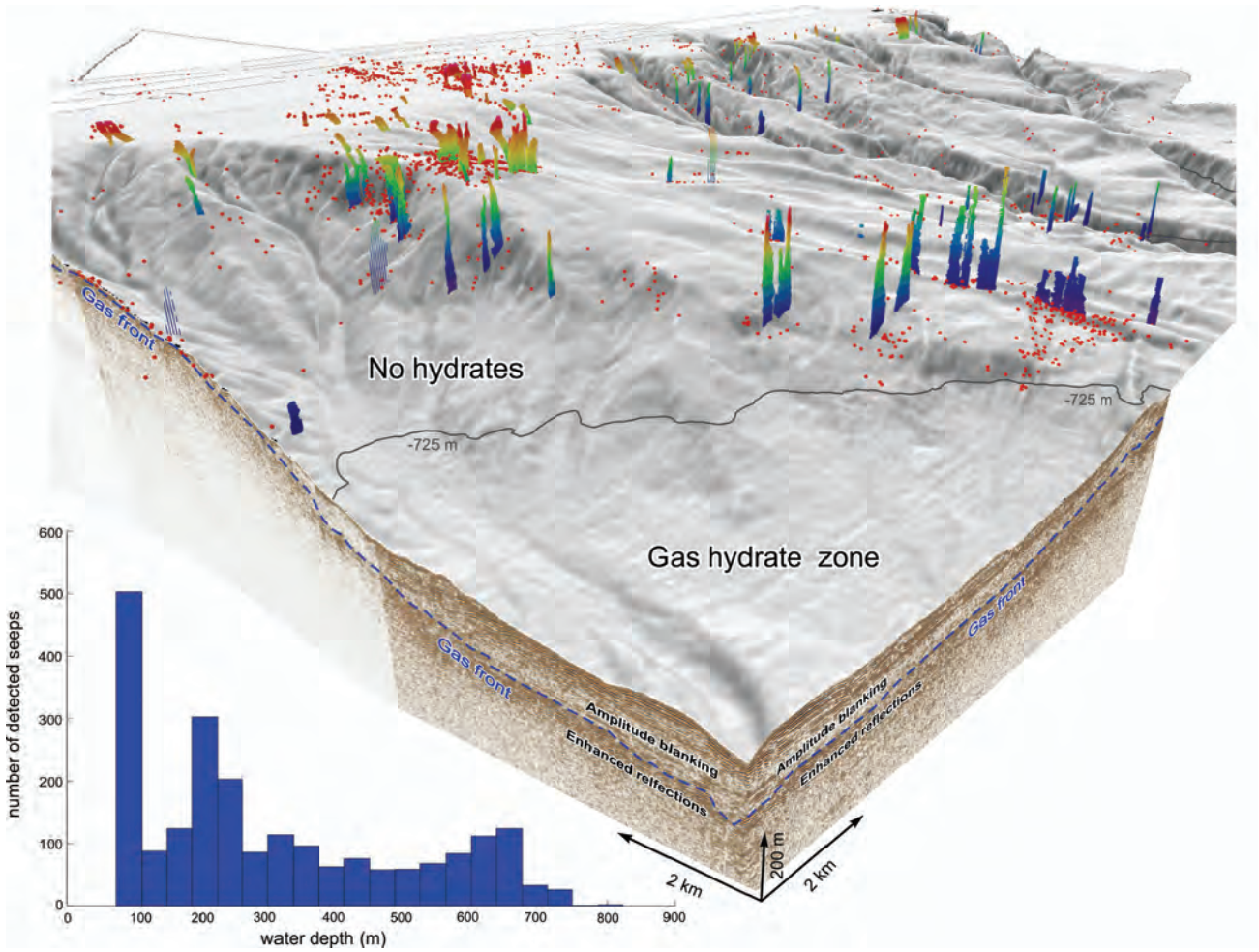

Figure 3.8. Oblique view of grey-shaded bathymetry map (see Fig. 3.2.A for location), seep locations plotted as red dots and some seeps are shown as 3D flares. Seeps are abundant upslope of the GHSZ, delineated by the -725 m contour line. The two crossing GI-gun profiles clearly show that the gas front, i.e. the top of the free gas in the subsurface as indicated by the enhanced reflections, domes up to the surface outside the GHSZ, where gas bubbles were detected in the water column. The graph in the lower left corner shows the seep distribution versus depth with clear seep clusters at -92, -200 and at -650 m water depth, just outside the GHSZ.

upper boundary of the sediment package containing free gas (Fig. 3.8.). However, it has to be taken into consideration that the physical processes controlling the depth of the free gas in both areas are different, but also that the acoustic expression of the top of the free-gas section as gas front is dependent on a.o. the frequency of the seismic signal.

Free gas can easily be identified on seismic recordings (e.g. acoustic turbidity, enhanced reflections, acoustic blanking, etc.) because of its influence on the sediment's bulk properties (Anderson and Hampton, 1980; Judd and Hovland, 1992). The exact response to the presence of free gas depends on the frequency of the seismic source (Richardson and Davis, 1998). The 5 kHz subbottom data provide the best coverage in the study area (Fig. 3.2.A.) and are best suited for mapping the gas front because of the stronger attenuation of the higher frequencies. On these data the gas front is expressed as the upper termination of a series of enhanced reflections or as a high-amplitude reflection that cross-cuts the normal stratigraphy and that completely masks all reflections below (Figs. 3.6., 3.10., 3.11. and 3.12.). Based on these criteria, the depth of the top of the free gas zone in the sediment can be mapped throughout the area.

The 5 kHz seismic data show that the depth of the gas front is variable and locally domes up to the seafloor (Figs. 3.6., 3.10., 3.11. and 3.12.). The areas of gas-front updoming coincide with seep locations as observed by hydro-acoustics. By combining the gas-front surface with the seafloor surface, a "depth-to-gas-front" map was produced (Fig. 3.9.), which illustrates the strong "gas front - versus - seep" relationship that was already observed on the seismic profiles. The majority of the seeps occur where the gas front approaches the seafloor within < 25 m, and in most cases even within < 10 m (Fig. 3.9.).

3.4.4. Seep relation to morphology and subsurface structure

3.4.4.1. Continental shelf

The highest concentrations of seeps on the shelf are found within the elongated depressions/pockmarks below which the updoming gas front approaches the seafloor within < 1 m (Fig. 3.6., profile CD). There are more seeps in the shallow pockmarks than in the deeper ones.

The distribution of the seeps and the general NW-SE trend of the elongated depressions and of the seeps on the shelf (Figs. 3.6. and 3.9.B.) appears to be related to the underlying geology. On the 5 kHz seismic profiles, seeps occur along the margins of filled channels and in association with cut-and-fill delta deposits, while no seeps have been detected above the central part of the filled channels (Fig. 3.6.). Unfortunately, due to the attenuation of the acoustic signal, it is impossible to adequately map subsurface geological features below the gas front.

The seeps within the dune area are also linked to an updoming gas front, but they are more randomly spread and not really linked to the particular dune morphology.

3.4.4.2. Continental slope

Within the western mass-wasting dominated environment, the seeps are preferentially located along crests of sedimentary ridges (Fig. 3.5.). This alignment is striking and suggests a direct genetic relationship. The seismic data provide no evidence for the existence of faults which could act as conduits for upward fluid migration. However, the 5 kHz subbottom data reveal a clear updoming of the gas front below the crests (Fig. 3.10.). Also, the upper limit of the gas front is determined by a parallel-stratified sedimentary cover, which gets thinner and pinches out towards the crests of the ridges (Fig. 3.10.).

High seep concentrations also occur within the canyons and particularly on the gullied canyon walls (Figs. 3.5. and 3.12.). These canyon walls are strongly affected by mass wasting. Seeps are predominant on the steep, freshly scarred gullied walls, but not on older smoothed canyon walls. The subsurface data shows that mass wasting at the gullied walls breaches the sedimentary cover and creates fresh scars that cut off the underlying stratigraphy. At these locations an updoming gas front is visible and gas bubbles were detected in the water column (Fig. 3.12., profile CD). No faults were observed

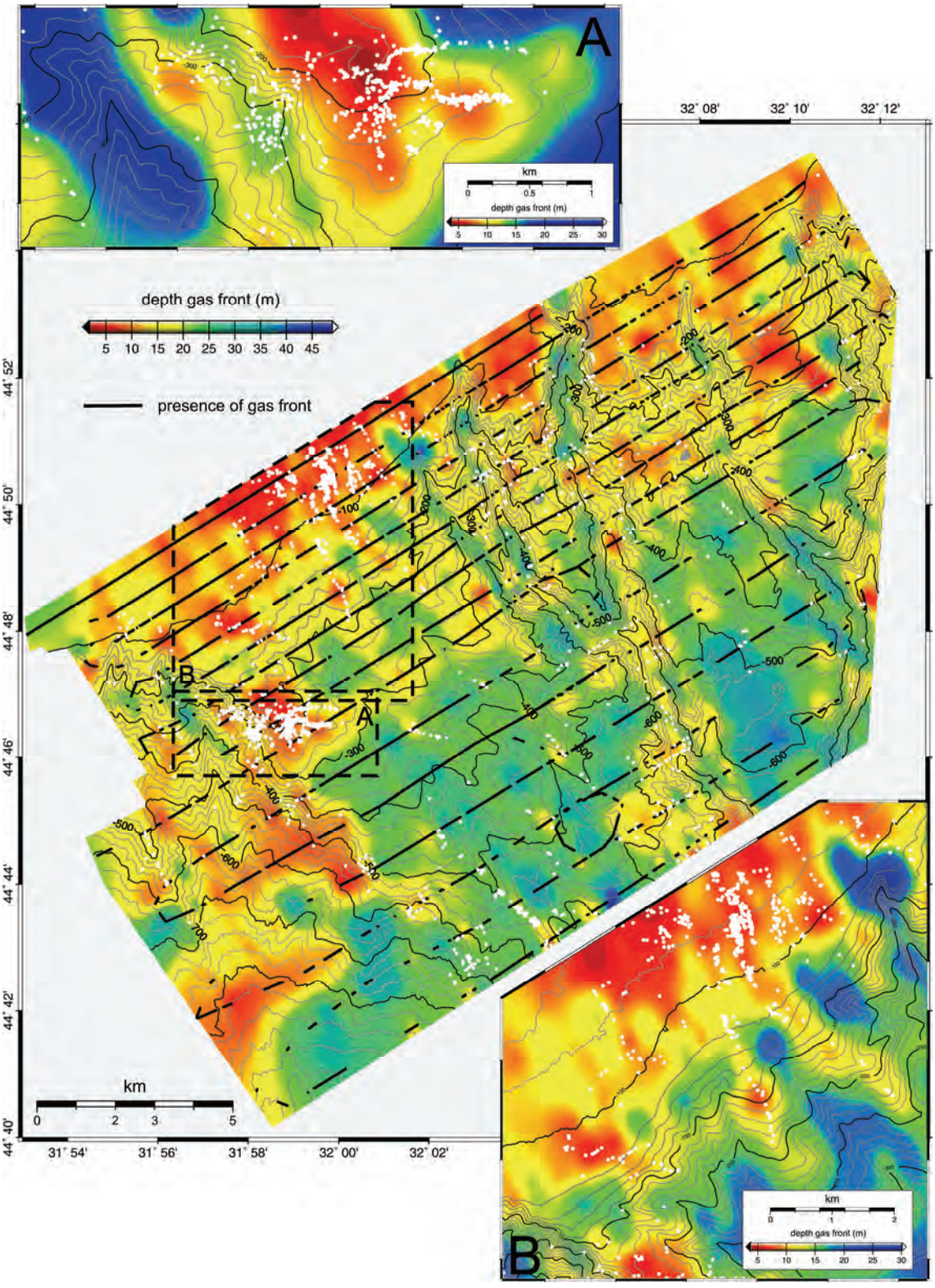

Figure 3.9. Map showing the depth of the gas front beneath the seafloor (see Fig. 3.2. for location), as mapped on 5 kHz profiles, overlain by bathymetric contours. The map emphasizes that gas seeps (white dots) are present where the gas front approaches the seafloor. Bubbles were detected where the gas front comes within 25 m of the surface. For the abundant seeps sites at the terrace (inset A) and the shelf (inset B) this is < 10 m.

below these seep locations.

A third important seep environment is formed by the scarps of the submarine landslides on the border with the central divide (Figs. 3.5. and 3.11.). The water-column, bathymetric and subsurface data show similar features as mentioned for the gullied canyon walls: scars breaching through the sediment cover and exposing underlying stratigraphy, updoming gas front and higher seep densities at fresh scars (Fig. 3.11., profile AB). In contrast, the scale of the submarine landslides is much bigger and the seep distribution and the scarps are lineated and not random as at the gullied walls. The seismic records do not show the presence of faults beneath these seeps locations, but this could also be due to acoustic attenuation. On other places where small sedimentary faults are present, these faults don't reach the surface and no bubbles were detected in the water column. GI-gun data (Fig. 3.8.) show that the gas front comes up to the surface in front of the submarine landslides at -725 m water depth (Figs. 3.5. and 3.11.), suggesting that the mass-wasting process might have been related to gas-hydrate destabilization.

To the east, in the deposition-dominated area, the same crest-seep relationship exists: i.e. no faults below seep locations, updoming gas front below the crests, parallel-stratified cover that thins out towards the crests (Figs. 3.10., 3.11. and 3.12.). One exception is that the ridges are not characterized by deeply incised canyons at the sides (Fig. 3.10.). Also for the canyon walls we observe the same relationship between the seeps and morphological and subsurface features: i.e. incised canyon walls, scars breaching trough sediment cover and cutting off original stratigraphy, updoming gas front and higher seep densities at fresh scars and at steeper canyon walls. The seismic data also reveal that the margins of the canyons are commonly covered by parallel-stratified deposits which thin out to the side of the canyons where seeps are also commonly located. Again, no major faults are observed within or near the canyons, except for a fault in the Dnepr Canyon. Our data hereby contradict those of Lüdmann et al. (2004), who observed several faults to the sides of the main canyons by using deeper-penetrating multi-channel seismic data (Fig. 3.1.). Because of the higher frequency of our data, we were able to observe small sedimentary faults affecting the overbank deposits, but no seeps were detected above these faults.

For the submarine landslide (Fig. 3.11.), we observed similarities with the submarine landslides in the mass-wasting dominated area: i.e. borders the central high, GHSZ at the base of the submarine landslide, no clear faults, updoming gas front below seep locations. However, in contrast to the submarine landslides to the west of the central divide, no seeps are present on the head scarp, which is also more circular than the linear scarps of the other landslides. Figure 3.11. clearly demonstrates that the submarine landslide has moved into the canyon in front. The subsurface data display that seeps occur within the submarine landslide in front of detached sediment ridges (Laberg and Vorren, 2000) originated from the mass movement.

3.5. Discussion

3.5.1. Pockmarks

Since we detected hundreds of seeps in the elongated depressions on the shelf (Fig. 3.6.), we interpret these as pockmarks, as defined by Hovland and Judd (1988). Pockmarks are crater-like structures that are formed by fluid expulsions, and occur worldwide on continental margins, generally in muddy sea beds. They are often associated with gas hydrates, slides and slumps (Hovland et al., 2002). Our bathymetric data show that the observed pockmarks appear to be an amalgamation of several smaller pockmarks (Fig. 3.6.). Single, smaller pockmarks are about 100 m wide and 3 m deep (Fig. 3.6.). The shallowness of the pockmarks is probably due to the relatively hard seafloor on the shelf, which consists of clayey sediments mixed with shells and shell debris. The high seep activity in the pockmarks is remarkable, as active -i.e. bubbling- pockmarks are thought to be very scarce (Hovland et al., 2002). Less active pockmarks are deeper and better developed

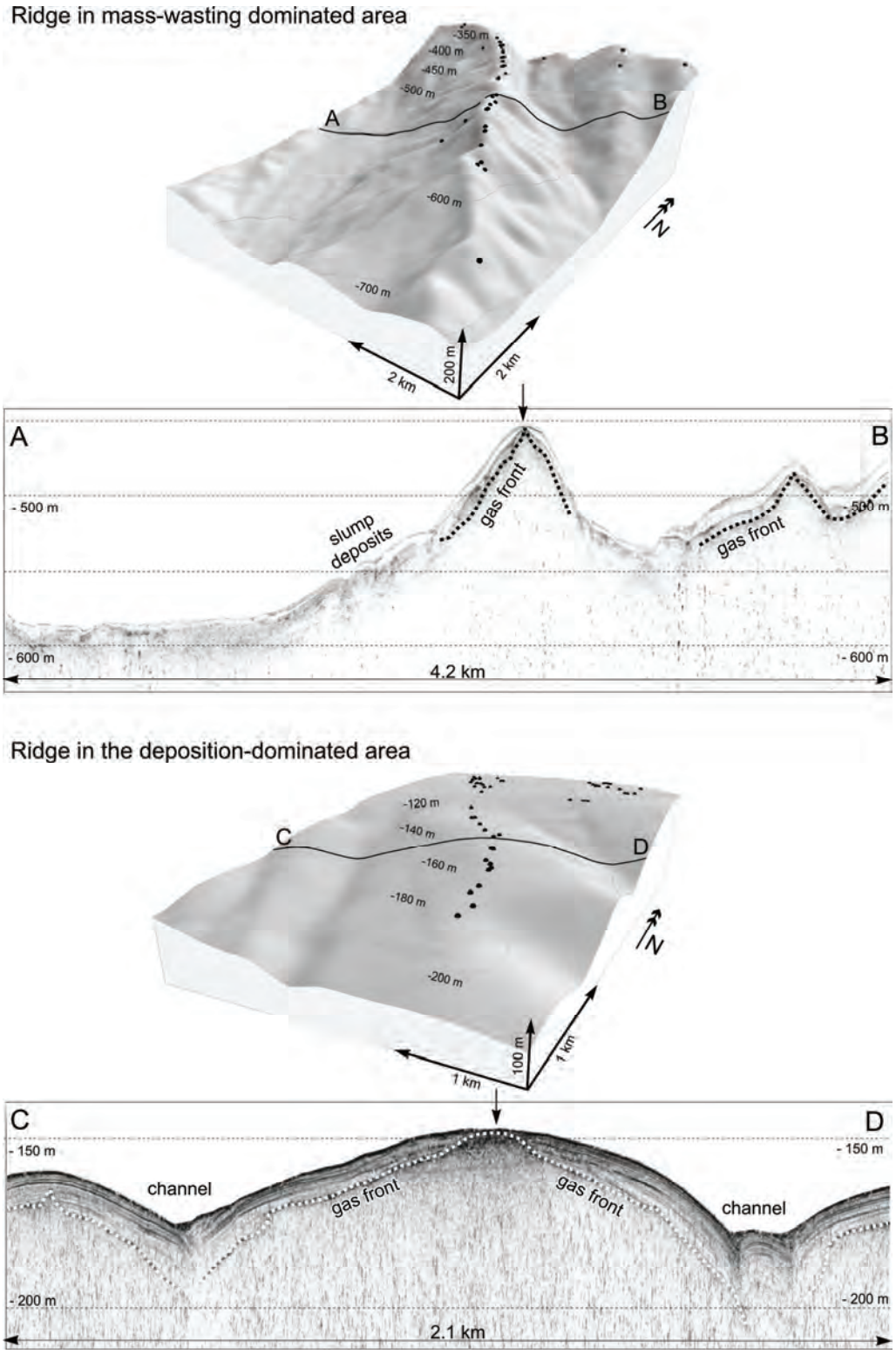

Figure 3.10. Oblique view of grey-shaded bathymetry map of a sediment ridge in the mass-wasting dominated area and of a sediment ridge in the deposition-dominated area overlain by bathymetric contours (see Fig. 3.2. for location). Both ridges are characterized by seeps (black dots) along their crests. The 5 kHz profiles (see Fig. 3.2.A. for location) crossing the ridges show that at both ridges the gas front domes up to the crest of the ridges where seeps (arrows) were detected and that the sediment cover thins out towards the crest. The gas front (dotted lines) follows the base of the sediment cover.

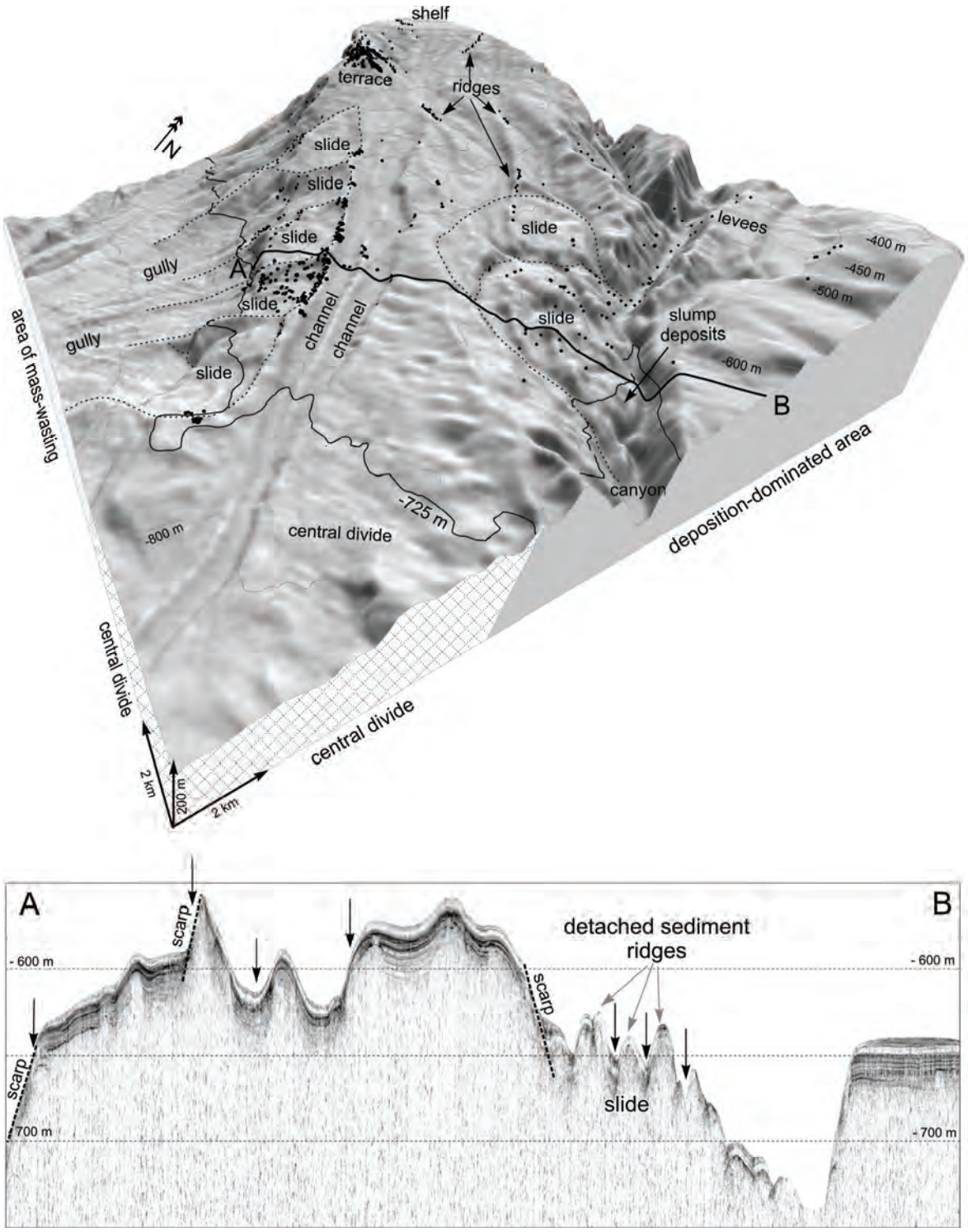

Figure 3.11. Oblique view of grey-shaded bathymetry map of the area affected by submarine landslides (see Fig. 3.2. for location) with indication for the major geomorphological regions, overlain by bathymetric contours. The 5 kHz profile (see Fig. 3.2.A. for location) and the 3D image show the difference in location of seeps (black dots or arrows) on scarps of the submarine landslides in the western mass-wasting area and seeps within the submarine landslides in front of detached sediment ridges in the eastern deposition-dominated area. The -725 m water depth contour line, marking the border of the GHSZ, is located at the base of both submarine landslide areas.

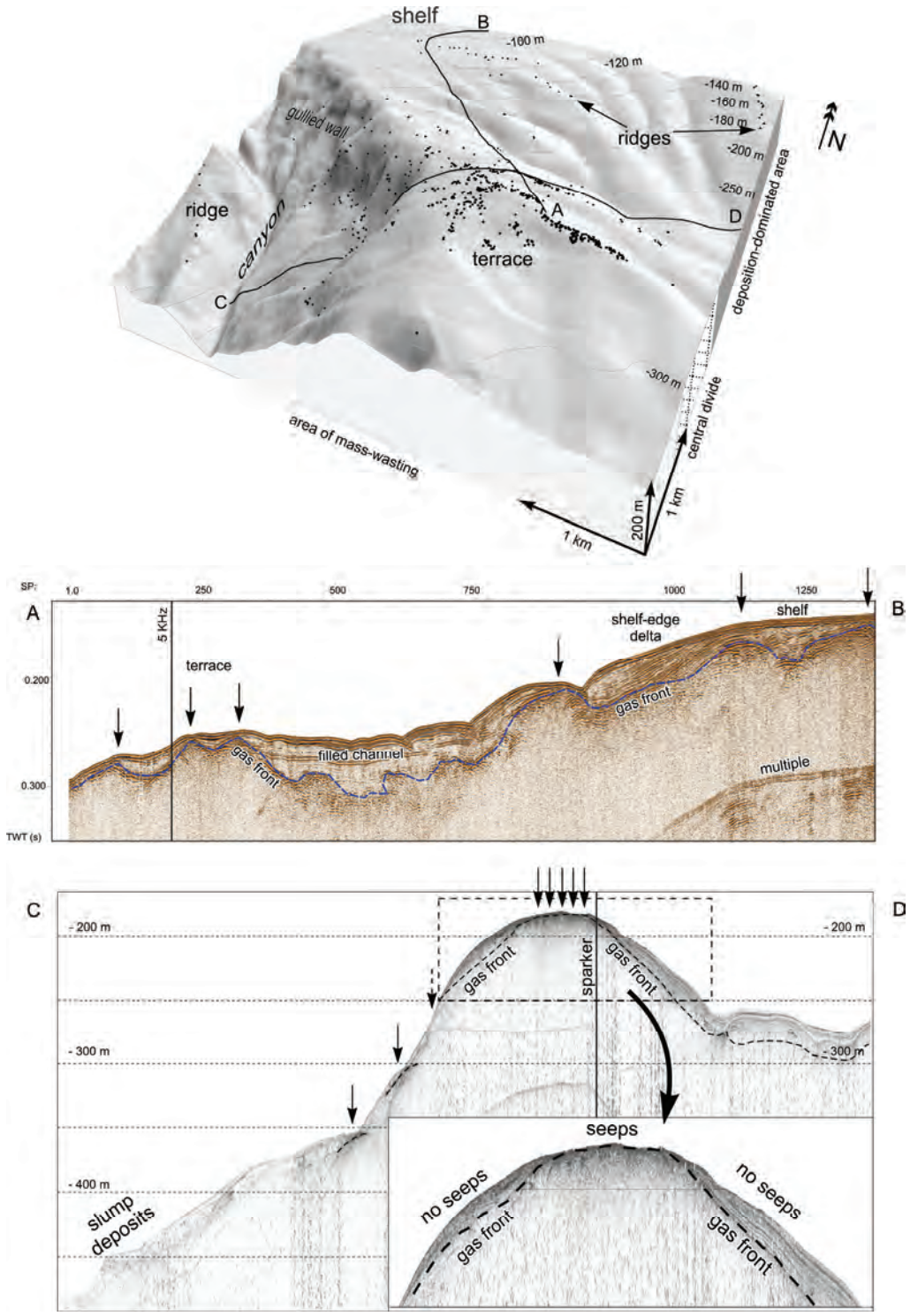

Figure 3.12. Oblique view of grey-shaded bathymetry map of the terrace seep site (see Fig. 3.2. for location), with indication the major geomorphological regions, overlain by bathymetric contours. The sparker profile AB (see Fig. 3.2.A. for location) shows that seeps (black dots or arrows) are detected where the gas front domes up to the seafloor and that no gas seeps are detected above a filled channel. The perpendicular 5 kHz (see Fig. 3.2.A. for location) profile shows the same gas front-seep relation. The inset clearly shows that the gas front can only dome up to the surface where the sediment cover diminishes or is breached by mass-wasting at the flanks. During the 2004 METROL cruise this 5 kHz profile was used as a base for coring. Sand was cored at the seep sites and clay or fine sediments were retrieved outside the seep sites from the parallel-stratified sediment cover.

than the presently active ones. This could be a result of the self-sealing nature of seeps due to carbonate cementation as postulated by Hovland (2002). Except for the updoming gas front at the margins of the filled channels, there appear to be no other subsurface structures which could be identified as potential factors controlling the pockmark and seep locations. The overall NW-SE trend of seeps and pockmarks reflect the course of the underlying filled channels (Fig. 3.6.).

3.5.2. Crests of sedimentary ridges

The alignment of the seeps on the crests of the sedimentary ridges, the general morphology of the crests (upslope-downslope trend) (Figs. 3.5. and 3.10.) and the absence of faults suggest that the ridges are formed purely by differential erosion. More erosion-resistant sediments will stand out in relief after periods of erosion and result in the typical shape of the ridges. Because of the obvious seep-crest relationship and the subsurface features below the crests (updoming gas front, parallel stratified cover that thins out towards the crest, gas front that stays below this cover) (Fig. 3.10.), we postulate that the alignment of seeps on the crest of the ridges is probably linked to a process described by Hovland (1990) and Hovland (1992). He proposed that the gas permeating from gas-bearing sediments below into a relatively thick unit of plastic clay, covering the gas-bearing sediments, causes those sediments to be buoyed up so that they form elongated ridges on the surface. This process could have breached the cover of fine sediments that acted as a stratigraphic seal permitting and also focusing seepage at the crests of the ridges. Since the ridges in our study area are sometimes up to 100 m high, the proposed process can only account for the alignment of the seeps at the crests and probably not for the formation of the ridges as a whole.

Since seepage is commonly associated with precipitation of methane-derived authigenic carbonates (Boetius et al., 2000; Michaelis et al., 2002), seeps probably have also contributed to the formation of more erosion-resistant sediment on the crests of these ridges.

3.5.3. Canyons

The floors and walls of most canyons in our study area are strongly affected by mass wasting (Figs. 3.10., 3.11. and 3.12.). Mass-wasting on canyon floors and walls creates fresh scars and breaches the fine-grained sediment cover that effectively functions as a stratigraphic seal. As a result, possible gas-bearing layers get exposed and facilitate gas seepage at these scarred steep canyon walls. That seepage commonly occurs on steep, recently eroded seafloor was also observed in Monterey Bay (Paull et al., 2005). If the fine-grained cover is not affected by mass-wasting, fluids tend to be focused upslope to the margins of the canyon where the cover diminishes and seepage can occur (Fig. 3.12.). These inferred fluid migration patterns are in agreement with the observed behavior of the gas front. Migration of fluids can also be focused by faults, but on our data, no faults affect the upper 250 m of the sediment column in the vicinity of canyons and below seeps. Therefore, we rule out faults as the main conduits for fluid migration close to the seafloor. This does not exclude that deeper faults, such as e.g. those observed by Lüdmann et al. (2004), might have influenced the position of the existing canyons and cause a pre-focusing of deeper derived fluids.

3.5.4. Submarine landslides

Differences exist in seep distribution associated with submarine landslides in the erosion-dominated area and in the deposition-dominated area. In the mass-wasting dominated area, the linear alignment of the scarps and the seeps suggest a structural control that determines the seep locations and the morphology of the submarine landslides. Helium analyses of water samples from this area sustain this suggestion by showing anomalous high ^{3}He values which point to an input from deep-derived fluids (Holzner et al., 2005). A potential link between subsurface structures and mass wasting was already suggested by several authors for other areas (Orange and Breen, 1992; Eichhubl et al., 2000; Kuscu et al., 2005).

Mass-wasting may be triggered by upward migration of fluids along faults resulting in a reduction in slope stability (Orange et al., 1997). The close relation of seepage and scarps can be explained by steepened pore-pressure gradients adjacent to scarps due to sudden erosion associated with slumping and the resulting focusing of fluid towards these scarps (Orange et al., 1997). Seepage is commonly observed at recently eroded seafloor. The different morphological expression and different distribution of seeps in relation to the submarine landslide in the deposition-dominated area suggest a different mechanism for sediment mass movement and associated seepage (Fig. 3.11.). At the double submarine landslide we do not observe seepage at the scarps, but only in front of detached sediment ridges originated from the mass movement (Fig. 3.11.). The landslide morphology and seep distribution can be the result of high water and gas contents of the sediments, which, together with the relatively steep slope, caused sediment destabilization and the observed mass movement. The seepage itself is probably a consequence of higher sediment compaction and steepened pore-pressure gradients in front of the detached sediment ridges. Since the BGHSZ is outcropping at the base of both landslide areas we have to take into account that the sediment failure could have been facilitated by gas-hydrate destabilization due to temperature and pressure changes associated with climatically-driven sealevel fluctuations, as has also been proposed for e.g. Storegga slide (Bouriak et al., 2000; Bünz et al., 2005; Poort et al., 2005). We do not observe any seepage through the GHSZ in the vicinity of these landslides that could result from overpressure and steeper pore-pressure gradients due to extra sedimentary loading or erosion at the base of the submarine landslides.

3.5.5. Terrace

As the terrace on the central divide consists of three radially spread seeping ridges, we suggest the same mechanism for the seep-crest relation as is proposed for the other sedimentary ridges on the slope. However, judging from the shape, the size and the position of the terrace, the ridges here are not common upslope-downslope ridges, like the other seep-marked ridges on the slope. The lobed morphology of the terrace with the central ridges is reminiscent of a lobed delta front with tributaries (Prior and Bornhold, 1990). We therefore propose that the terrace originated from an old delta front in which coarse sediments were deposited during a period of sealevel lowstand and that these coarser sediments currently act as highly permeable stratigraphic horizons that facilitate fluid migration and seepage at the seafloor. This is also indicated by coring (2004 METROL cruise) (Borowski et al., 2005). Since the terrace is located in a paleo-delta environment this hypothesis can indeed be valid, were it not that the water level would have had to be 180 m below current water level. This is 30 m lower than the lowest value proposed in literature for the last lowstand in the Black Sea (Winguth et al., 2000). Peckmann et al. (2001) have dated carbonates from the terrace with an age of 19 ka BP. This indicates that seepage at the terrace was already active during the last lowstand 20 ka ago (Aksu et al., 2002) and that the terrace thus represents a remnant from the last or from a previous lowstand.

3.5.6. Controls on seep distribution

The most important control on seep distribution, or rather on the absence of seeps in the study area, is the presence of gas hydrates (Figs. 3.8. and 3.13.), which have often been inferred to have the capacity to act as a buffer for upward migrating gas (Kvenvolden, 1998). Gas hydrates are theoretically stable and have directly and indirectly been observed in 585 km^2 of the 1540 km^2 covered study area. However, only 0.5 % of the 2778 detected seeps are located in the GHSZ, even though the presence of subsurface gas is indicated (i.e. by enhanced reflections below the BSR) (Figs. 3.8. and 3.13.).

Outside the GHSZ, based on the absence of faults below almost all studied seep sites, we propose that seepage in our study area is determined mainly by stratigraphic and sedimentary controls (Fig. 3.13.). A thick impermeable sedimentary cover focuses the

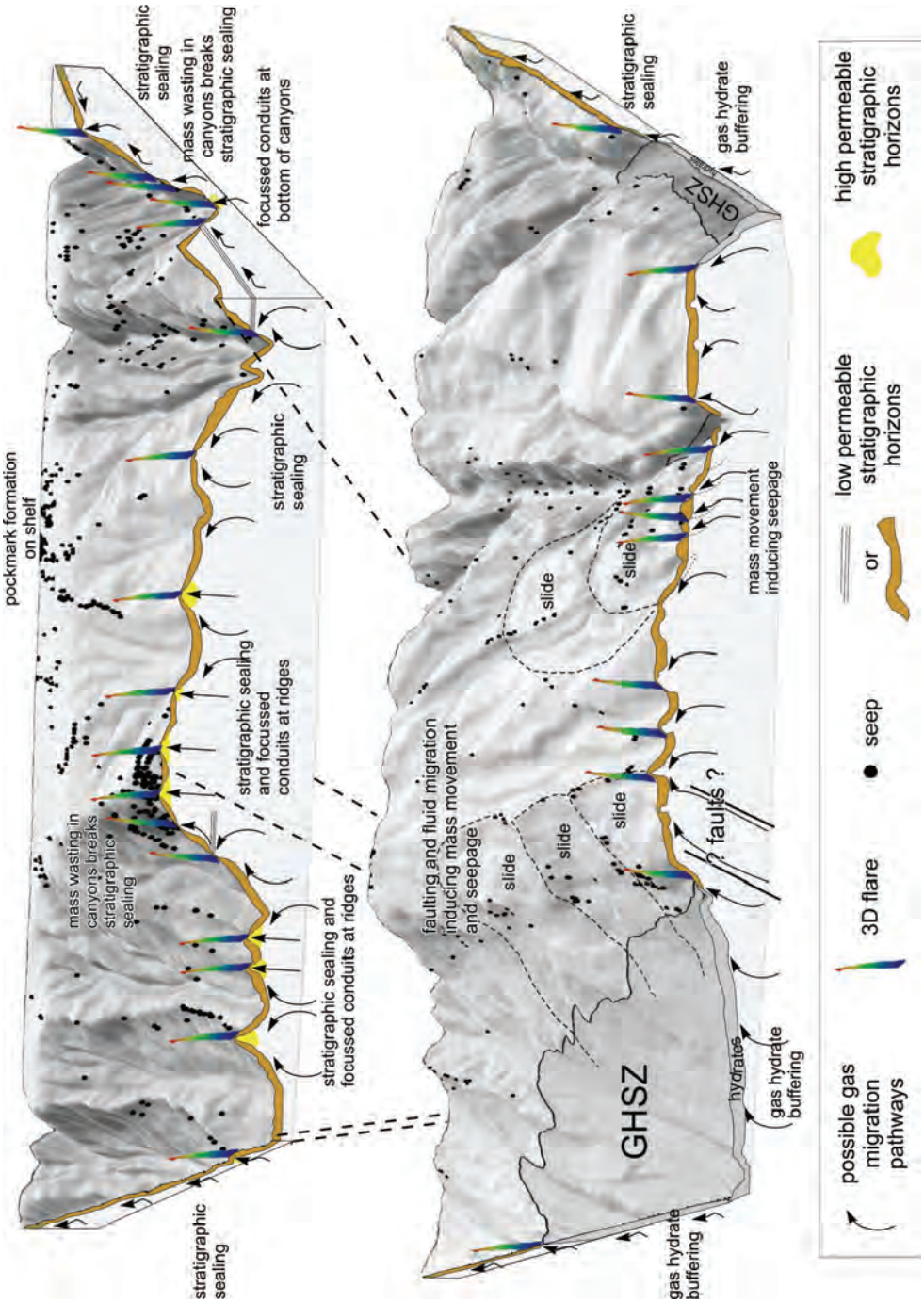

Figure 3.13. Combining model of the supposed fluid migration in the subsurface and its expression at the seafloor surface. The 3D block diagram based on the bathymetric data, seep positions and subsurface data presenting a model for the seep distribution in the Dnepr paleo-delta for the shallow-water seep sites (top) and the deep-water seep sites, with submarine landslides and gas hydrates (bottom).

migration of fluids to nearby morphological highs, where this impermeable sedimentary cover of fine-grained sediments is breached by the process proposed by Hovland (1990; 1992) (Fig. 3.13.). The almost complete absence of seeps above the finer-grained levee and overbank deposits confirm the sealing capacity of the sedimentary cover (Fig. 3.13.). It is only where this seal is destroyed by mass wasting or erosion that seepage occurs (Fig. 3.13.). The subbottom depth distribution of the gas front confirms the sealing capacity of gas hydrates and of the fine-grained sedimentary cover in our study area.

A possible structural control on seepage can only be suggested for the seeps located on the scarps of the submarine landslide in the mass-wasting dominated area. However the influence of possible gas-hydrate destabilization at the foot of the submarine landslides and the associated gas seeps can't be neglected (Fig. 3.13.).

3.6. Conclusions

Based on 5621 km of echosounder tracks we were able to detect 2778 active seeps within the 1540 km^2 of the studied Dnepr paleo-delta area. The integration of the geophysical datasets clearly indicates that methane seeps are not randomly distributed in this area, but are concentrated in specific locations. The depth limit for 99.5 % of the detected seeps coincides with the phase boundary of pure methane hydrate at -725 m water depth. This suggests that gas hydrates act as an effective seal and prevent upward migrating methane gas to be released as bubbles into the water column. Elsewhere, seeps generally occur in association with pockmarks on the continental shelf, along crests of sedimentary ridges, at bottoms, flanks and margins of canyons and near submarine landslides on the continental slope. Except for one, all these areas are characterized by the absence of faults. This does not support the hypothesis by Kruglyakova et al. (2004) that seepage is primarily associated with tectonically driven flows through regional faults in the Dnepr paleo-delta area. Our data, on the contrary, are in agreement with observations in Monterey Bay where seepage appears to be primarily associated with morphologically or stratigraphically controlled flow (Yun et al., 1999; Paull et al, 2005), and this can probably be extended to other continental margins worldwide. The stratigraphic and sedimentary control on the distribution of methane seeps is demonstrated by the absence of seeps above parallel-stratified fine-grained deposits (low-permeability stratigraphic horizons). The sealing capacity of gas hydrates and fine-grained sediment covers gets emphasized by the regional behavior of a distinct subbottom gas front that domes up to the seafloor in areas where bubbles were detected in the water column and where the abovementioned seals are locally absent or negligible. Finally, we can conclude that in the studied Dnepr paleo-delta, seep locations are mainly determined by sedimentary characteristics close to the seafloor and that seepage-producing subsurface features and fluid migration can influence the seafloor morphology by forming pockmarks and causing sediment instabilities.

Acknowledgements

We thank the captain and the crew of the 58th and 60th cruise of RV Professor Vodyanitskiy for their hard work and their hospitality and L-3 communications ELAC Nautik for their superior and fast support. This study was carried out in the framework of the CRIMEA project (EC project EVK2-2002-00162; http://www.CRIMEA-info.org). Extra data were contributed by the METROL project (EC project EVK3-2002-00080) and GHOSTDABS project (German Federal Ministry of Education and Research project 03G0559A). We also like to thank SMT (Kingdom Suite) and IVS (Fledermaus) for the academic licenses. Finally we thank Martin Hovland and Maarten Vanneste for their constructive reviews which helped improve this manuscript.

Additional information

Lieven Naudts processed and interpreted the datasets, wrote the manuscript and made all figures. Lieven Naudts also assisted with the data acquisition during the 12 weeks of expedition on RV Vodyanitskiy in 2003 and 2004.

Co-authors helped by reviewing the manuscript and/or by providing the datasets. For the processing of the multibeam data assistance was given by Jens Greinert. For processing of the seismic data assistance was given by Peter Staelens.

References

Aksu, A.E., Hiscott, R.N., Yasar, D., Isler, F.I., Marsh, S., 2002. Seismic stratigraphy of Late Quaternary deposits from the southwestern Black Sea shelf: evidence for non-catastrophic variations in sea-level during the last ~10 000 yr. Mar. Geol. 190, 61-94.

Amouroux, D., Roberts, G., Rapsomanikis, S., Andreae, M.O., 2002. Biogenic Gas (CH4, N2O, DMS) Emission to the Atmosphere from Near-shore and Shelf Waters of the North-western Black Sea. Estuarine, Coastal Shelf Sci. 54, 575-587.

Anderson, A.L., Hampton, L.D., 1980. Acoustics of Gas-Bearing Sediments .2. Measurements and Models. J. Acoust. Soc. Am. 67, 1890-1903.

Boetius, A., Ravenschlag, K., Schubert, C.J., Rickert, D., Widdel, F., Gieseke, A., Amann, R., Jorgensen, B.B., Witte, U., Pfannkuche, O., 2000. A marine microbial consortium apparently mediating anaerobic oxidation of methane. Nature 407, 623-626.

Borowski, C., Joergensen, B.B., The Poseidon 317/3 Shipboard party, . 2005. Gas-charged sediments, methane seeps and carbonate-precipitating microbial mats on the NW Black Sea Shelf-preliminary results of research project METROL from a cruise using the manned submersible JAGO. Geophys. Res. Abstr. 7, 09603.

Bouriak, S., Vanneste, M., Saoutkine, A., 2000. Inferred gas hydrates and clay diapirs near the Storegga Slide on the southern edge of the Voring Plateau, offshore Norway. Mar. Geol. 163, 125-148.

Bünz, S., Mienert, J., Bryn, P., Berg, K., 2005. Fluid flow impact on slope failure from 3D seismic data: a case study in the Storegga Slide. Basin Res. 17, 109-122.

Campbell, K.A., Farmer, J.D., Des Marais, D., 2002. Ancient hydrocarbon seeps from the Mesozoic convergent margin of California: carbonate geochemistry, fluids and palaeoenvironments. Geofluids 2, 63-94.

Egorov, V., Luth, U., Luth, C., Gulin, M.B., 1998. Gas seeps in the submarine Dnieper Canyon, Black Sea: acoustic, video and trawl data. In: U. Luth, C. Luth and H. Thiel (Editors), MEGASEEPS Gas Explorations in the Black Sea, Project Report. Zentrum für Meres- und Klimaforschung der Universität Hamburg, Hamburg, pp. 11-21.

Eichhubl, P., Greene, H.G., Naehr, T., Maher, N., 2000. Structural control of fluid flow: offshore fluid seepage in the Santa Barbara Basin, California. J. Geochem. Explor. 69, 545-549.

Finetti, I., Bricchi, G., Del Ben, A., Pipan, M., Xuan, Z., 1988. Geophysical study of the Black Sea. Boll. Geofis. Teor. Appl. 30, 197-324.

Garcia-Gil, S., Vilas, F., Garcia-Garcia, A., 2002. Shallow gas features in incised-valley fills (Ria de Vigo, NW Spain): a case study. Cont. Shelf Res. 22, 2303-2315.

Greinert, J., Bohrmann, G., Suess, E., 2001. Gas hydrate-associated carbonates and methane-venting at Hydrate Ridge: Classification, distribution, and origin of authigenic lithologies. In: C.K. Paull and W.P. Dillon (Editors), Natural Gas Hydrates: Occurrence, Distribution, and Detection, Geophysical Monograph. American Geophysical Union, pp. 99-113.

Greinert, J., Bollwerk, S.M., Derkachev, A., Bohrmann, G., Suess, E., 2002. Massive barite deposits and carbonate mineralization in the Derugin Basin, Sea of Okhotsk: precipitation processes at cold seep sites. Earth Planet. Sci. Lett. 203, 165-180.

Holbrook, W.S., 2001. Seismic studies of the Blake Ridge: implications for hydrate distribution, methane expulsion and free gas dynamics. In: C.K. Paull and W.P. Dillon (Editors), Natural Gas Hydrates: Occurrence, Distribution and Detection. Geophysical Monographs. American Geophysical Union, pp. 235-256.

Holzner, C.P., Amaral, H., Brennwald, M.S., Hofer, M., Klump, S., Kipfer, R., 2005. Methane bubble streams in the Black Sea traced by dissolved noble gases. Geophys. Res. Abstr. 7, 03846.

Hornafius, J.S., Quigley, D., Luyendyk, B.P., 1999. The world's most spectacular marine hydrocarbon seeps (Coal Oil Point, Santa Barbara Channel, California): Quantification of emissions. J. Geophys. Res., Oceans 104, 20703-20711.

Hovland, M., 1990. Suspected Gas-Associated Clay Diapirism on the Seabed Off Mid Norway. Mar. Pet. Geol. 7, 267-276.

Hovland, M., 1992. Hydrocarbon seeps in northern marine waters; their occurrence and effects. Palaios 7, 376-382.

Hovland, M., Curzi, P.V., 1989. Gas Seepage and Assumed Mud Diapirism in the Italian Central Adriatic Sea. Mar. Pet. Geol. 6, 161-169.

Hovland, M., Gardner, J.V., Judd, A.G., 2002. The significance of pockmarks to understanding fluid flow processes and geohazards. Geofluids, 127-136.

Hovland, M., Judd, A.G., 1988. Seabed Pockmarks and Seepages. Graham and Trotman, London. 293 pp.

Hovland, M., Talbot, M., Olaussen, S., Aasberg, L., 1985. Recently formed methane-derived carbonates from the North Sea floor. In: B.M. Thomas (Editor), Petroleum Geochemistry in Exploration of the Norwegian Shelf. Norwegian Petroleum Society. Graham and Trotman, pp. 263-266.

Johnson, J.E., Goldfinger, C., Suess, E., 2003. Geophysical constraints on the surface distribution of authigenic carbonates across the Hydrate Ridge region, Cascadia margin. Mar. Geol. 202, 79-120.

Jorgensen, B.B., Boettcher, M.E., Lueschen, H., Neretin, L.N., Volkov, I.I., 2004. Anaerobic methane oxidation and a deep H2S sink generate isotopically heavy sulfides in Black Sea sediments. Geochim. Cosmochim. Acta, 2095-2118.

Judd, A., Davies, G., Wilson, J., Holmes, R., Baron, G., Bryden, I., 1997. Contributions to atmospheric methane by natural seepages on the U.K. continental shelf. Mar. Geol. 140, 427-455.

Judd, A.G., 2003. The global importance and context of methane escape from the seabed. Geo-Mar. Lett. 23, 147-154.

Judd, A.G., Hovland, M., 1992. The Evidence of Shallow Gas in Marine-Sediments. Cont. Shelf Res. 12, 1081-1095.

Judd, A.G., Hovland, M., Dimitrov, L.I., Garcia Gil, S., Jukes, V., 2002. The geological methane budget at Continental Margins and its influence on climate change. Geofluids 2, 109-126.

Krastel, S., Spiess, V., Ivanov, M., Weinrebe, W., Bohrmann, G., Shashkin, P., Heidersdorf, F., 2003. Acoustic investigations of mud volcanoes in the Sorokin Trough, Black Sea. Geo-Mar. Lett. V23, 230-238.

Kruglyakova, R.P., Byakov, Y.A., Kruglyakova, M.V., Chalenko, L.A., Shevtsova, N.T., 2004. Natural oil and gas seeps on the Black Sea floor. Geo-Mar. Lett. V24, 150-162.

Kuscu, I., Okamura, M., Matsuoka, H., Gokasan, E., Awata, Y., Tur, H., Simsek, M., Kecer, M., 2005. Seafloor gas seeps and sediment failures triggered by the August 17, 1999 earthquake in the Eastern part of the Gulf of Izmit, Sea of Marmara, NW Turkey. Mar. Geol. 215, 193-214.

Kvenvolden, K.A., 1993. Gas hydrates as a potential energy resource-a review of their methane content. In: D.G. Howell (Editor), The Future of Energy Gases-U.S. Geological Survey Professional Paper. United States Government Printing Office, Washington, pp. 555- 561.

Kvenvolden, K.A., 1998. A primer on the geological occurrence of gas hydrate. In: J.P. Henriet and J. Mienert (Editors), Gas Hydrates: Relevance to World Margin Stability and Climate Change. Geological Society Special Publication, 137. Geological Society, London, pp. 9-30.

Laberg, J.S., Vorren, T.O., 2000. The Trænadjupet Slide, offshore Norway-morphology, evacuation and triggering mechanisms. Mar. Geol. 171, 95- 114.

Lee, M.W., Dillon, W.P., 2001. Amplitude blanking related to the pore-filling of gas hydrate in sediments. Mar. Geophys. Res. 22, 101-109.

Lüdmann, T., Wong, H.K., Konerding, P., Zillmer, M., Petersen, J., Flüh, E., 2004. Heat flow and quantity of methane deduced from a gas hydrate field in the vicinity of the Dnieper Canyon, northwestern Black Sea. Geo-Mar. Lett. V24, 182-193.

Luth, C., Luth, U., Gebruk, A.V., Thiel, H., 1999. Methane gas Seeps Along the Oxic/Anoxic Gradient in the Black Sea: Manifestations, Biogenic Sediment Compounds and Preliminary Results on Benthic Ecology. Mar. Ecol. 20, 221-249.

Michaelis, W., Seifert, R., Nauhaus, K., Treude, T., Thiel, V., Blumenberg, M., Knittel, K., Gieseke, A., Peterknecht, K., Pape, T., Boetius, A., Amann, R., Jorgensen, B.B., Widdel, F., Peckmann, J., Pimenov, N.V., Gulin, M.B., 2002. Microbial Reefs in the Black Sea Fueled by Anaerobic Oxidation of Methane. Science 297, 1013-1015.

Moore, J.C., Brown, K.M., Horath, F., Cochrane, G., MacKay, M., Moore, G., 1991. Plumbing accretionary prisms. In: J. Tarney, K.T. Pickering, R.J. Knipe and J.F. Dewey (Editors), The Behavior and Influence of Fluids in Subduction Zones. The Royal Society, London, pp. 49-62.

Nikishin, A.M., Korotaev, M.V., Ershov, A.V., Brunet, M.-F., 2003. The Black Sea basin: tectonic history and Neogene-Quaternary rapid subsidence modeling. Sediment. Geol. 156, 149- 168.

Orange, D.L., Anderson, R.S., Breen, N.A., 1994. Regular canyon spacing in the submarine environment: the link between hydrology and geomorphology. Geol. Soc. Am. Bull. 4, 29-39.

Orange, D.L., Breen, N.A., 1992. The Effects of Fluid Escape on Accretionary Wedges. 2. Seepage Force, Slope Failure, Headless Submarine Canyons, and Vents. J. Geophys. Res. Solid Earth 97, 9277-9295.

Orange, D.L., McAdoo, B.G., Moore, J.C., Tobin, H., Screaton, E., Chezar, H., Lee, H., Reid, M., Vail, R., 1997. Headless submarine canyons and fluid flow on the toe of the Cascadia accretionary complex. Basin Res. 9, 303-312.

Orange, D.L., Yun, J., Maher, N., Barry, J., Greene, G., 2002. Tracking California seafloor seeps with bathymetry, backscatter and ROVs. Cont. Shelf Res. 22, 2273-2290.

Paull, C.K., Ussler, W., Greene, H.G., Barry, J., Keaten, R., 2005. Bioerosion by chemosynthetic biological communities on Holocene submarine slide scars. Geo-Mar. Lett. V25, 11-19.

Peckmann, J., Reimer, A., Luth, U., Luth, C., Hansen, B.T., Heinicke, C., Hoefs, J., Reitner, J., 2001. Methane-derived carbonates and authigenic pyrite from the northwestern Black Sea. Mar. Geol. 177, 129-150.

Polikarpov, G.G., Egorov, V.N., Gulin, S.B., Gulin, M.B., Stokozov, N.A., 1992. Gas seeps from the bottom of the Black Sea-a new object of molismology. In: G.G. Polikarpov (Editor), Molismology of the Black Sea. Nauka, Kiev pp. 10-28.

Polikarpov, G.G., Egorov, V.N., Nezhdanonv, A.I., Gulin, S.B., Kulev, Y.D., Gulin, M.B., 1989. Methane gas seeps in the Black Sea-a new object of molismology. In: G.G. Polikarpov (Editor), Molismology of the Black Sea. Nauka, Kiev pp. 10-20.

Poort, J., Vassilev, A., Dimitrov, L., 2005. Did postglacial catastrophic flooding trigger massive changes in the Black Sea gas hydrate reservoir? Terra Nova 17, 135-140.

Popescu, I., De Batist, M., 2004. Gas and hydrates in the Black Sea, EUROCEAN 2004 "European Conference Marine Science and Ocean Technology", Galway (Ireland),10-13 May 2004.

Popescu, I., Lericolais, G., Panin, N., Normand, A., Dinu, C., Le Drezen, E., 2004. The Danube submarine canyon (Black Sea): morphology and sedimentary processes. Mar. Geol. 206, 249-265.

Popescu, I., Lericolais, G., Panin, N., Wong, H.K., Droz, L., 2001. Late Quaternary channel avulsions on the Danube deep-sea fan, Black Sea. Mar. Geol. 179, 25-37.

Prior, D.B., Bornhold, B.D., 1990. The underwater development of Holocene fan deltas. In: A. Colella and D.B. Prior (Editors), Coarse-grained Deltas. Special Publication of the International Association of Sedimentologists, 10. Blackwell Scientific Publications, pp. 75- 90.

Reeburgh, W.S., Whalen, S.C., Alperin, A.J., 1993. The role of methylotrophy in the global methane budget. In: J.A. Murrel and D.P. Kelley (Editors), Microbial Growth on C-1 Compounds. Intercept, Andover, Uk, pp. 1-14.

Richardson, M.D., Davis, A.M., 1998. Modeling methane-rich sediments of Eckenförde Bay. Cont. Shelf Res. 18, 1671-1688.

Robinson, A.G., Rudat, J.H., Banks, C.J., Wiles, R.L.F., 1996. Petroleum geology of the Black Sea. Mar. Pet. Geol. 13, 195-223.

Ryan, W.B.F., Pitman, W.C., Major, C.O., Shimkus, K., Moskalenko, V., Jones, G.A., Dimitrov, P., Gorur, N., Sakinc, M., Yuce, H., 1997. An abrupt drowning of the Black Sea shelf. Mar. Geol. 138, 119-126.

Sills, G.C., Wheeler, S.J., 1992. The significance of gas for offshore operations. Cont. Shelf Res. 12, 1239-1250.

Sloan, E.D.J., 1998. Clathrate hydrates of natural gases. Marcel Dekker Inc., New York/Basel. 705 pp.

Suess, E., Torres, M.E., Bohrmann, G., Collier, R.W., Rickert, D., Goldfinger, C., Linke, P., Hauser, A., Sahling, H., Heeschen, K., Jung, C., Nakamura, K., Greinert, J., Pfannkuche, O., Trehu, A., Klinkhammer, G., Whiticar, M.J., Eisenhauer, A., Teichert, B., Elvert, M., 2001. Sea floor methane hydrates at Hydrate Ridge, Cascadia Margin. In: C.K. Paull, Dillon, W.P. (Editor), Natural Gas Hydrates: Occurrence, Distribution and Detection. Geophysical Monograph, 124. AGU, pp. 87- 98.

Thiel, V., Peckmann, J., Richnow, H.H., Luth, U., Reitner, J., Michaelis, W., 2001. Molecular signals for anaerobic methane oxidation in Black Sea seep carbonates and a microbial mat. Mar. Chem. 73, 97-112.

Van Rensbergen, P., De Batist, M., Klerkx, J., Hus, R., Poort, J., Vanneste, M., Granin, N., Khlystov, O., Krinitsky, P., 2002. Sublacustrine mud volcanoes and methane seeps caused by dissociation of gas hydrates in Lake Baikal. Geology 30, 631-634.

Vanneste, M., De Batist, M., Golmshtok, A., Kremlev, A., Versteeg, W., 2001. Multi-frequency seismic study of gas hydrate-bearing sediments in Lake Baikal, Siberia. Mar. Geol. 172, 1-21.

Wever, T.F., Abegg, F., Fiedler, H.M., Fechner, G., Stender, I.H., 1998. Shallow gas in the muddy sediments of Eckernforde Bay, Germany. Cont. Shelf Res. 18, 1715- 1739.

Winguth, C., Wong, H.K., Panin, N., Dinu, C., Georgescu, P., Ungureanu, G., Krugliakov, V.V., Podshuveit, V., 2000. Upper quaternary water level history and sedimentation in the northwestern Black Sea. Mar. Geol. 167, 127- 146.

Wong, H.K., Luedmann, T., Panin, N., Konerding, P., Dinu, C., 2002. Northwestern Black Sea: Upper Quaternary water level and sedimentation. In: F. Briand (Editor), Turbidite Systems and Deep-Sea Fans of the Mediterranean and the Black Seas. CIESM Workshop series, 17, Monaco, pp. 85-89.

Yun, J.W., Orange, D.L., Field, M.E., 1999. Subsurface gas offshore of northern California and its link to submarine geomorphology. Mar. Geol. 154, 357-368.

Zillmer, M., Flueh, E.R., Petersen, J., 2005. Seismic investigation of a bottom simulating reflector and quantification of gas hydrate in the Black Sea. Geophys. J. Int. 161, 662-678.

CHAPTER 4

Anomalous seafloor backscatter patterns in methane venting areas, Dnepr paleo-delta, NW Black Sea

Lieven Naudts, Jens Greinert, Yuriy Artemov, Stan E. Beaubien, Christian Borowski, Marc De Batist

Abstract

The relation between acoustic seafloor backscatter and seep distribution is examined by integrating multibeam backscatter data and seep locations detected by single-beam echosounder. This study is further supported by side scan sonar recordings, high-resolution 5 kHz seismic data, pore-water analysis, grain-size analysis and visual seafloor observations. The datasets were acquired during the 2003 and 2004 expeditions of the EC-funded CRIMEA project in the Dnepr paleo-delta area, northwestern Black Sea.

More than 600 active methane seeps were hydro-acoustically detected within a small (3.96 km by 3.72 km) area on the continental shelf of the Dnepr paleo-delta in water depths ranging from -72 m to -156 m. Multibeam and side scan sonar recordings show backscatter patterns that are clearly associated with seepage or with a present dune area. Seeps generally occur within medium- to high-backscatter areas which often coincide with pockmarks.

High-resolution seismic data reveal the presence of an undulating gas front, i.e. the top of the free gas in the subsurface, which domes up towards and intersects the seafloor at locations where gas seeps and medium- to high-backscatter values are detected. Pore-water analysis of 4 multi-cores, taken at different backscatter intensity sites, shows a clear correlation between backscatter intensity and dissolved methane fluxes. All analyzed chemical species indicate increasing anaerobic oxidation of methane (AOM) from medium- to high-backscatter locations. This is confirmed by visual seafloor observations, showing bacterial mats and authigenic carbonates formed by AOM. Grain-size analysis of the 4 multi-cores only reveals negligible variations between the different backscatter sites.

Integration of all datasets leads to the conclusion that the observed backscatter patterns are the result of ongoing methane seepage and the precipitation of methane-derived authigenic carbonates (MDACs) caused by AOM. The carbonate formation also appears to lead to a gradual (self-)sealing of the seeps by cementing fluid pathways/horizons followed by a relocation of the bubble-releasing locations.

Keywords

Methane seeps; acoustic seafloor backscatter; anaerobic oxidation of methane; bacterial mats; pockmarks; methane-derived authigenic carbonates

4.1. Introduction

In recent years, considerable research efforts have been invested to gain a better understanding of how methane emissions from natural marine gas seeps contribute to the global atmospheric methane budget (Hovland et al., 1993; Hornafius et al., 1999; Dimitrov, 2002; Etiope and Klusman, 2002; Etiope, 2004; Judd, 2004; Kvenvolden and Rogers, 2005; Luyendyk et al., 2005). Given that methane is a potent greenhouse gas, with 21-23 times the global warming potential as the same mass of carbon dioxide (Lelieveld et al., 1998; IPCC, 2001b), a correct assessment of all natural sources is essential to better evaluate the human impact on global atmospheric methane concentrations and consequently on global climate change (IPCC, 2001a).

The amount of methane released by natural gas seeps from the seafloor, into the water column and possibly into the atmosphere, is highly variable and remains -despite several attempts at quantification- largely unknown, even for small well-studied areas (Hovland et al., 1993; Hornafius et al., 1999; Dimitrov, 2002; Etiope and Klusman, 2002; Etiope, 2004; Judd, 2004; Kvenvolden and Rogers, 2005; Luyendyk et al., 2005; Bange, 2006; Kessler et al., 2006). Current estimates of global methane fluxes from the seabed to the atmosphere vary between 0.4 and 48 Tg yr^{-1} (Judd, 2004), i.e. over two orders of magnitude. The main problems in establishing reliable estimates of regional and global fluxes are the uncertainties regarding i) the total area involved in active seepage, and ii) the temporal variability in seep intensity and activity.

Recent studies have shown that methane transfer from marine and lacustrine seeps to the atmosphere is only effective when methane is transported by bubbles released in relatively shallow water (< 100 m water depth) (Leifer and Patro, 2002; MacDonald et al., 2002; Schmale et al., 2005; McGinnis et al., 2006). In most cases, even if a bubble reaches the surface with a significant size, most of the methane is dissolved into the water column and replaced by other stripped gases, particularly oxygen (in oxic conditions) and nitrogen. Therefore, only a massive release of large amounts of bubbles may create a bubble plume and enable significant volumes of methane to be transferred to the atmosphere from deeper-water seeps (> 100 m water depth) (Judd, 2004; McGinnis et al., 2006; Judd and Hovland, 2007).

The increased scientific interest in marine gas seeps goes hand in hand with the discovery of new seep sites around the world. The identification and delineation of seep sites on the ocean floor often arises from the detection of anomalously high acoustic backscatter on side scan sonar or multibeam echosounder recordings (Hovland, 1991; Hovland, 1992; Orange et al., 2002; Van Rensbergen et al., 2002; Johnson et al., 2003; Sager et al., 2003; Shoji et al., 2005; Gay et al., 2006; Klaucke et al., 2006; Rollet et al., 2006). High-acoustic backscatter is caused by the enhanced acoustic impedance or roughness contrast between certain regions of the seafloor and their surroundings (Blondel and Murton, 1997). At methane seeps, this contrast is primarily caused by the presence of methane-derived authigenic carbonates (MDACs), chemosynthetic “cold seep” communities (clams, tube worms), bubbles or gas hydrates in the sediment (Hovland et al., 1985; Ritger et al., 1987; Paull et al., 1992; von Rad et al., 1996; Greinert et al., 2001; Peckmann et al., 2001; Fonseca et al., 2002; Greinert et al., 2002b; Orange et al., 2002; Johnson et al., 2003; Niemann et al., 2005; Holland et al., 2006; Ivanov et al., 2007). Multibeam and side scan sonar surveys also detect changes in the seafloor morphology, which can mark the location of gas seeps (e.g. pockmarks, mud volcanoes) (Judd and Hovland, 1992; Judd and Hovland, 2007). Furthermore, seeps can be inferred from shallow seismic signatures indicative of free gas in the subsurface (e.g. shallow gas fronts, enhanced reflections, acoustic blanking) or potential gas or fluid conduits (e.g. faults, diapirs) (Judd and Hovland, 1992; Orange and Breen, 1992; Yun et al., 1999; Garcia-Gil et al., 2002; Van Rensbergen et al., 2002; Krastel et al., 2003; Naudts et al., 2006; Judd and Hovland, 2007). Direct localization of seeps, i.e. locations of bubble release, is performed by echosounders that detect gas bubbles in the water column due to the acoustic impedance contrast between water and the free gas in the bubbles (Egorov et al., 1998; Artemov, 2006; Naudts et al., 2006; Rollet

et al., 2006).

In this paper, we examine the cause of anomalously high acoustic backscatter and its relation -in space and time, and through which processes- with gas venting on the shelf of the Dnepr paleo-delta, NW Black Sea. We use multibeam backscatter and bathymetry data, as well as side scan sonar images, very-high-resolution seismic data, sediment cores, visual observations and single-beam seep detection. Our data and results confirm that acoustic seafloor backscatter analysis can be used as a proxy for seep distribution and seep activity (Greinert et al., 2010).

4.2. Study area

The paleo-delta of the Dnepr River is located on the outer shelf and upper continental slope of the northwestern Black Sea, west of the Crimea Peninsula (Fig. 4.1.A.). The region is well-known for abundant gas seeps, carbonate buildups and shallow gas (Polikarpov et al., 1989; Polikarpov et al., 1992; Egorov et al., 1998; Luth et al., 1999; Peckmann et al., 2001; Thiel et al., 2001; Amouroux et al., 2002; Michaelis et al., 2002; Kruglyakova et al., 2004; Kutas et al., 2004; Popescu et al., 2004; Pape et al., 2005; Pimenov and Ivanova, 2005; Reitner et al., 2005; Schmale et al., 2005; Treude et al., 2005; McGinnis et al., 2006; Naudts et al., 2006). During the 58th (May-June 2003) and 60th (May-June 2004) cruise of R.V. Vodyanitskiy, conducted during the EC (European Community)-funded CRIMEA project, almost 3000 active seeps (i.e. bubble-releasing locations) were detected with an EK-500 split-beam echosounder within the 1540 km^2 of the studied area (Fig. 4.1.A.) (Naudts et al., 2006). The distribution of these seeps is not random, but is controlled by morphology, by underlying stratigraphy and sediment properties, and by the presence of gas hydrates acting as a seal and preventing upward migrating gas to be released as bubbles in the water column (Naudts et al., 2006).

This study focuses on a small (3.96 km by 3.72 km) part of the continental shelf, centered on a dense seep and pockmark site at -92 m water depth (Figs. 4.1.B. and 4.1.C.). The area is characterized by a slightly undulating seafloor that dips gently at 0.55° to the SE until it intersects the shelf break at -105 m water depth. Within this area, 605 actively bubbling methane seeps were detected in water depths ranging from -72 m to -156 m (Fig. 4.1.B.). The seeps commonly occur in association with up to 3 m deep, large, elongated pockmarks, which are up to 100 m wide and 500 m long (Fig. 4.1.C.) (Naudts et al., 2006). These elongated pockmarks and related seep sites show a preferential NW-SE orientation, as their location is controlled by underlying, filled channels incised in the outer shelf (Naudts et al., 2006). Apart from the pockmarks, the shelf morphology is characterized by the presence of sediment dunes. These have a maximum height of 2.5 m and a maximum wave length of 120 m (Fig. 4.1.B.). The observed seeps and dunes appear to be unrelated (Naudts et al., 2006).

Only a small part of the study area lies within the oxygen-rich euphotic zone (above -80 m, in this part of the Black Sea). Most of it falls within the oxycline, between -80 m and -115 m, in which the oxygen concentration decreases from 285 to 10 µM at the top of the suboxic layer (Oguz, 2002). Oxygen concentration drops to zero at around -145 m.

Sea-air methane flux calculations show that methane emission from the study area (i.e., 0.96-2.32 nmol m^{-2} s^{-1}) is 3 times higher than from the surrounding shelf (0.32–0.77 nmol m^{-2} s^{-1}) and 5 times higher than from open water in the Black Sea (0.19-0.47 nmol m^{-2} s^{-1}) (Schmale et al., 2005). During dives with the submersible JAGO in October 2004 (as part of the EC-funded METROL project) gas bubbles at -92 m seep site were collected directly at the seafloor. The initial gas composition of the bubbles was almost pure methane (80 to 90 %) of presumed microbial origin as indicated by the isotopic composition (-62 to -68 ^{13}C‰ PDB) (McGinnis et al., 2006). Peckmann et al. (2001) assumes that the methane originates from organic-rich lacustrine sediments deposited during the Black Sea's fresh-water phase.

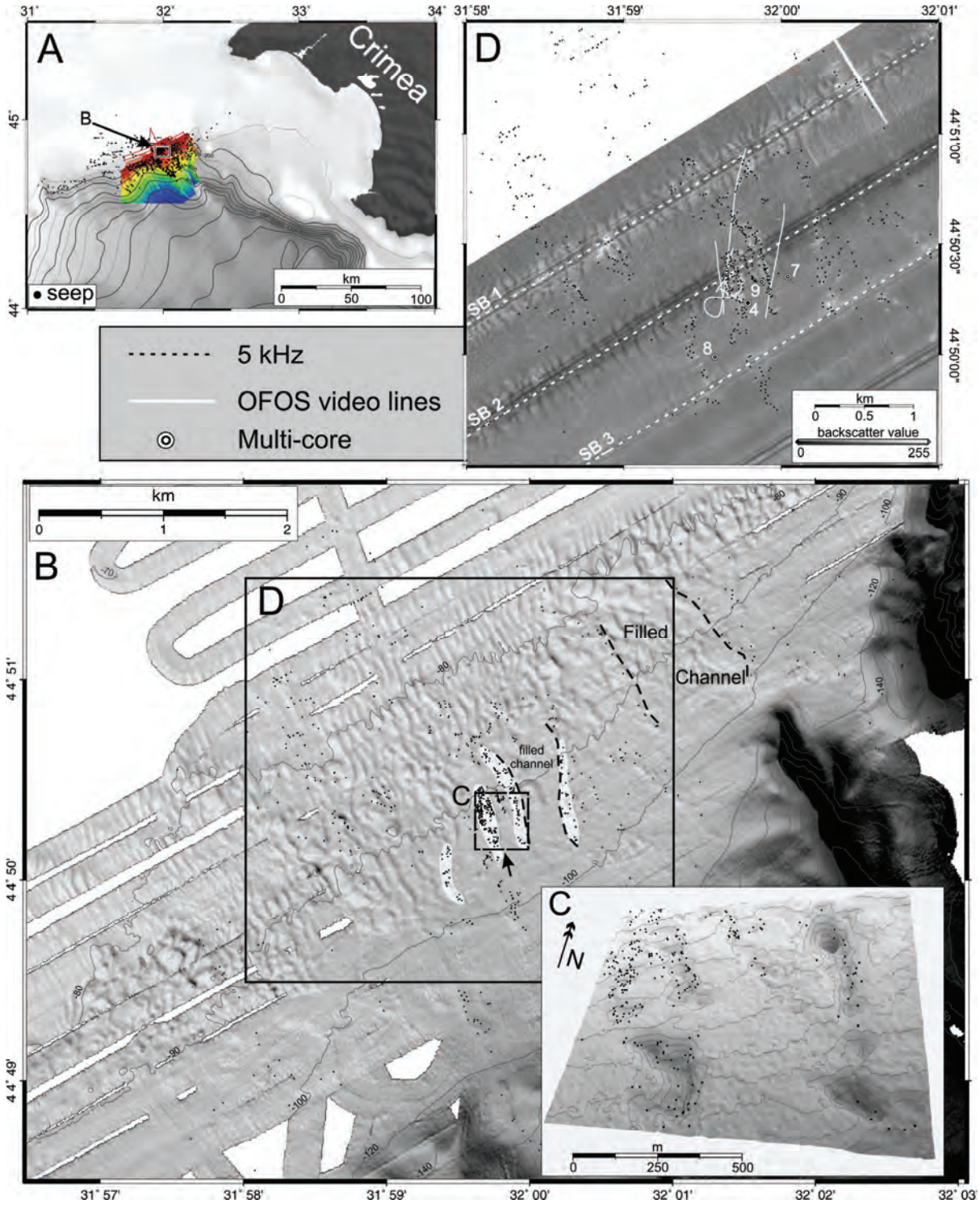

Figure 4.1. A. The location of the study area in the NW Black Sea with seeps (black dots) and acquired multibeam data (Egorov et al., 1998; Naudts et al., 2006). **B.** The multibeam bathymetry of the shelf with dunes, pockmarks (transparent white masks) and seeps (see Fig. 4.1.A. for location). **C.** Oblique view on the multibeam bathymetry of the high-intensity seep and pockmark site at -92 m water depth (after Naudts et al., 2006) (see Fig. 4.1.B. for location). **D.** Side scan sonar mosaic of the studied area with indication for the multi-cores (MC: 4, 7, 8, 9), 5 kHz seismic lines (SB 1-3: dashed white lines) and video lines (white lines) and seeps (see Fig. 4.1.B. for location).

4.3. Methods and data

4.3.1. Single-beam echosounding and seep detection

Single-beam seep detection was performed with a hull-mounted SIMRAD EK-500 dual-frequency (38 and 120 kHz) split-beam echosounder installed onboard of the R.V. Professor Vodyanitskiy. This system operates with a total beam width of 7°. The hydro-acoustic water-column data was continuously digitally recorded during both cruises and was afterwards processed with the WaveLens software package (Artemov, 2006; Artemov et al., 2007). This software traces and locates the origin of bubble streams at the seafloor based on the real target strength analysis. During the two cruises, a total length of 5261 km echosounder tracks was recorded within the 1540 km^2 study area which resulted in the detection of 2778 active seep positions (Naudts et al., 2006). For this study we only focus on a small area on the shelf where 605 active seeps were detected based on 767 km of echosounder tracks (Fig. 4.1.A.-D.).

4.3.2. Multibeam mapping

Bathymetric and acoustic backscatter mapping was performed with a mobile 50 kHz SeaBeam 1050 multibeam echosounder, simultaneously with the single-beam seep detection. The multibeam system was operated with 120° swath, transmitting and receiving 108 beams of 3° by 3° beam angle. Sound-velocity profiles were acquired via CTD casts and the sound velocity at the transducers was continuously measured by an online sound-velocity probe. Data acquisition was managed with Hydrostar Online and data-processing was carried out with HDPEdit and HDPPost software from L-3 ELAC Nautik GMBH. Fine editing of the data, by deleting bad data points, was done with Fledermaus (6.1.2) software. During the two cruises, an area of 1540 km^2 was covered in water depths from -57 to -1248 m (Fig. 4.1.A.). In this study we focused on an area of 14.7 km^2 in water depths ranging from -72 to -156 m (Fig. 4.2.A.).

Raw backscatter data (bottom-amplitude values) were corrected with HDPPost for their grazing-angle dependency assuming a flat seafloor. Data were exported as gridded xyz data from HDPPost and spikes were removed with Fledermaus. During processing in HDPPost, backscatter values were normalized and thus do not represent 'real' dB values, but rather undefined backscatter units (BU). All maps shown in this paper are based on grids of 5 by 5 m cell size, except for Fig. 4.1.A.

4.3.3. Side scan sonar imaging and subbottom profiling

During the 2003 cruise seafloor backscatter data was also acquired with a deep-towed SONIC-3 sonar system. This system consists of a tow-fish, including a 30 kHz side scan sonar and 5 kHz subbottom profiler. The fish was towed 50 to 60 m above the seafloor resulting in 700 to 850 m wide swath. The theoretical maximum resolution of the acquired sonar image is 0.5 m. Towing speed averaged 5.6 knots and the data were gridded to a pixel size of 6.4 m, using SONIC's in-house developed processing software. 22 parallel profiles were collected with a total length of 589 km, in total covering an area of 418 km^2. Only 4 profiles are used here, covering an area of 11.8 km^2 (Fig. 4.1.D.).

Very-high-resolution seismic data was acquired with the 5 kHz profiler system. The theoretical vertical resolution is 30 cm and the maximum penetration is 35 ms two-way travel time (TWTT). Here, 3 profiles are displayed with a total length of 12.6 km (Fig. 4.1.D.). No processing has been carried out on the seismic data. Interpretation was carried out with the Kingdom Suite Software package.

4.3.4. Pore-water and grain-size analysis

Sediment coring was undertaken with a TV-guided multi-core system allowing real-time selection of the coring site via the

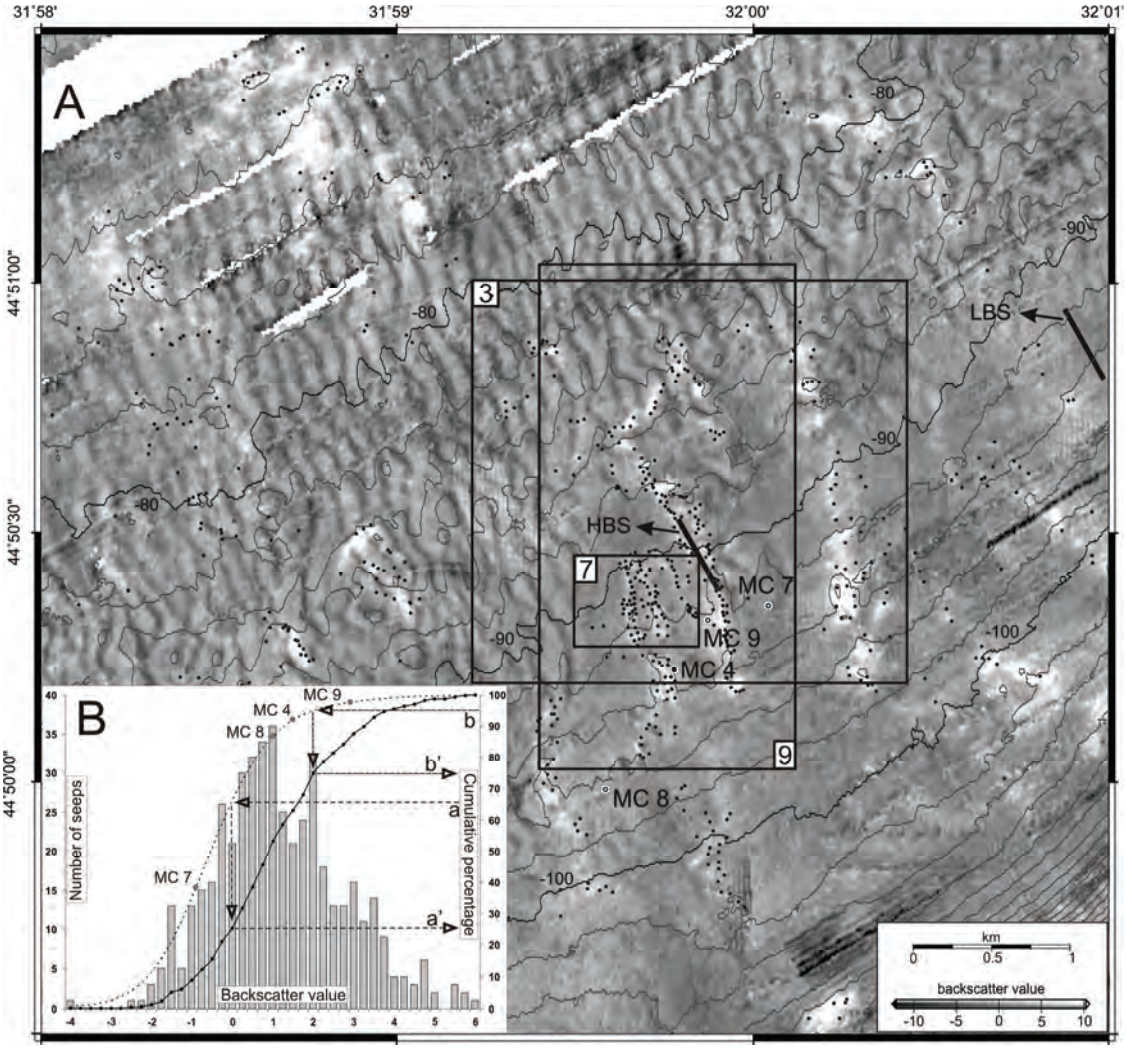

Figure 4.2. A. Multibeam-derived backscatter map overlain with bathymetric contours, detected seep locations (black dots), positions of multi-core stations and outlines for Figs. 4.3., 4.7. and 4.9. (see Fig. 4.1.B. for location). Furthermore the positions of the high-backscatter (HBS) and low-backscatter (LBS) swaths used in Figure 4.10. are indicated by the solid bold lines. **B.** Graph showing the distribution of the number of seeps with respect to their backscatter values, both, as a histogram and cumulative percentage curve (full line). The second cumulative percentage curve (dashed line) shows the distribution of all backscatter values recorded in the shown study area. Arrows a-a' show that 74 % of all seeps occur in the high-backscatter areas above 0 BU, thus within only 33 % of the studied area. Arrows b-b' show that 75 % of all seeps with the lowest backscatter values occur below 2 BU.

video connection. The multi-corer accommodates 4 plastic liners with a diameter of 10 cm which are able to sample sediment layers up to ca. 40 cm. Three sediment cores were taken from areas with different backscatter intensities (MC7, MC8 and MC9) and one directly at an actively bubbling bacterial mat (MC4) (Figs. 4.1.D. and 4.2.A.). Pore water was immediately extracted from the cores at a 0.5 cm interval with cut-off 5 ml plastic syringes and analyzed on board for total alkalinity, hydrogen sulfide, and ammonia, following the methods of Grasshoff et al. (1999). Methane content was determined with the headspace method, following the procedure used by ODP (Pimmel and Claypool, 2001). 5 ml of sediment were filled in 20 ml headspace vials and heated in an oven at 70°C over 30 minutes. The headspace was analyzed as volume ppm and the final concentrations in mol/l pore water were

calculated by weighing the water content and by converting to volume percent, using 2.5 g/cm^3 as an assumed sediment-grain density. On-shore ion chromatography analyses were used to measure sulfate concentrations; Ca was analyzed by ICP-OES.

After extraction of the pore waters, five sediment samples representing each centimeter of the uppermost 5 cm of each core were used for grain-size analysis. Samples were sieved wet on a 50 µm sieve and dried. The dried coarse fractions were dry sieved on 600, 500, 425, 355, 300, 250, 180, 150, 125, 106 and 90 µm sieves. Since the sediment samples were rich in shells and shell debris, carbonate and organic matter were not chemically removed, to ensure that their possible contribution to generating backscatter was not omitted.

4.3.5. Visual seafloor observations

Visual seafloor observations were carried out with the OFOS (Ocean Floor Observation System) video sled and with the submersible JAGO to get a better insight on the distribution of possible seep-related seafloor features (e.g. seeps, bacterial mats, etc.).

OFOS carries a downward-looking online black/white video camera, two Xenon lights, a color still camera with flash, a stand-alone memory CTD and an extra color digital camera. The system was towed at about 2 m above the seafloor. No underwater positioning system was used with OFOS; instead the position was calculated relative to the ship's GPS antenna by taking cable length, course and ship speed into account, resulting in a maximum offset of 50 m. Corrections for the offset between OFOS and the ship's GPS position were made for every video line separately (Fig. 4.1.D.). The made offsets were confirmed by comparing the seep distribution visible on video footage and the seeps traced by single-beam detection.

One dive with the submersible JAGO (JAGO 852) enabled us to perform additional direct seafloor observations in the area previously surveyed with OFOS. This dive took place in October 2004 as part of the R.V. Poseidon 317/3 cruise, which was conducted in the framework of the EC-funded METROL project. Video recording was done using a digital camera from inside the submersible through the large front porthole. The area covered by JAGO is shown as outline 7 in Figure 4.2. During the JAGO dive ultra-short-base-line underwater positioning was used.

4.4. Observations and results

4.4.1. Backscatter anomalies, seafloor morphology and seep distribution

The multibeam-derived seafloor backscatter map reveals three distinct features (Fig. 4.2.A.): a wave-like pattern, irregular patches with high-backscatter and acquisition artifacts with low-backscatter values.

Based on the number of backscatter values, three backscatter classes with equal number of backscatter values were created: areas with low-backscatter (LBS: BU < -1.06), areas with medium-backscatter (MBS: -1.06 < BU < 0) and areas with high-backscatter (HBS: BU > 0) (Fig. 4.2.B.). Since each backscatter value corresponds to a grid cell, a surface of 25 m^2, each backscatter class also corresponds to one third of the studied surface. Areas with the lowest 5 % of backscatter values are regarded as very-low-backscatter areas (BU < -2.5). Areas with the highest 5 % of backscatter values are regarded as very-high-backscatter areas (VHBS: BU > 2).

The wave-like pattern consists of low- to high-backscatter values that vary between -2.4 and 1.9 BU and corresponds to the field of sediment dunes (Fig. 4.1.B.), which generally display the higher backscatter values on their ENE-orientated flanks (Fig. 4.3.). There is no obvious correlation between seep distribution and the backscatter pattern related to the sediment dunes.

When comparing the cumulative percentage curve of the backscatter values of the entire area (dashed line Fig. 4.2.B.) with the percentage curve and histogram of the amount of seeps falling in specific backscatter value ranges (full line Fig. 4.2B), it can be noticed that 74 % of all seeps occur in the high-backscatter

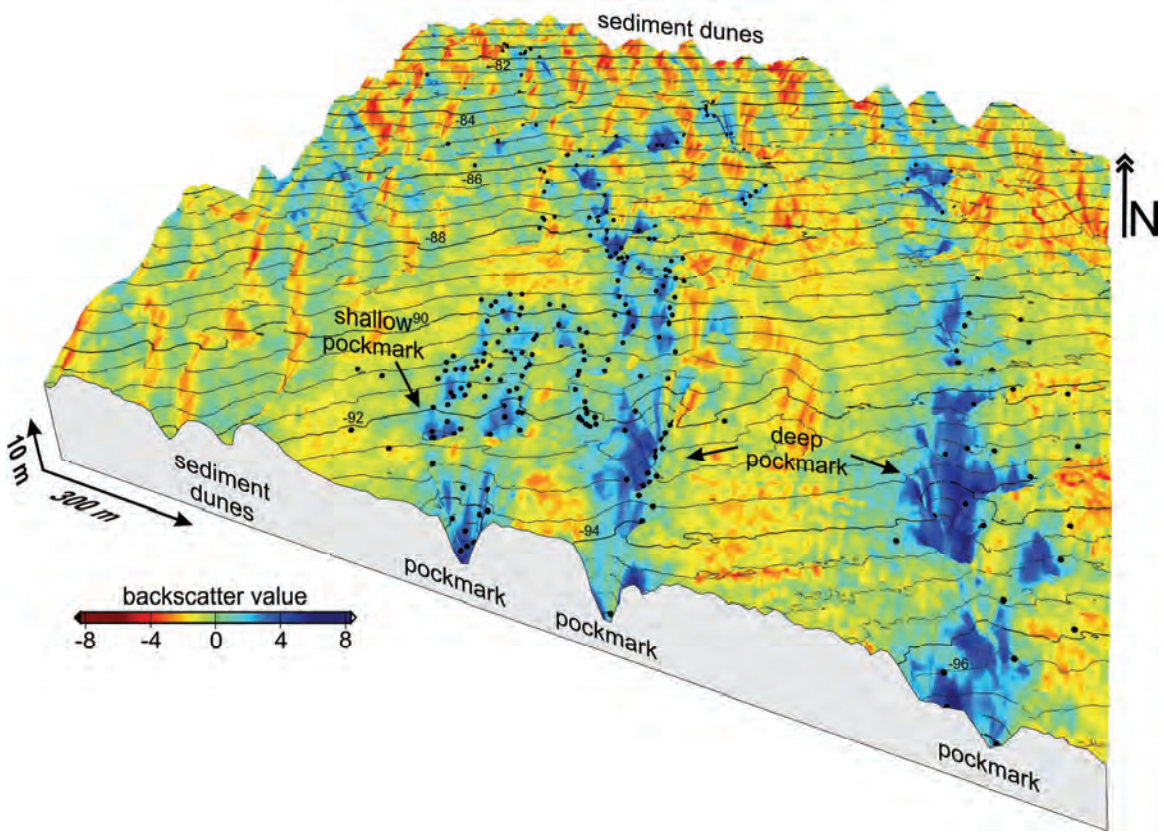

Figure 4.3. 3D view of the multibeam bathymetry overlain with the color-coded backscatter data, bathymetric contours and seep locations (black dots) (for location, see Fig. 4.2.A.). Pockmarks are characterized by high- to very-high-backscatter values with seeps located on their margins. The sediment dunes have higher backscatter values on the ENE flanks.

areas above 0 BU, thus within only 33 % of the studied area (Fig. 4.2.B. a-a'). However 75 % of all seeps, with the lowest backscatter values, occur below 2 BU (Fig. 4.2.B. b-b'). This indicates that most seeps don't occur in the very-high-backscatter areas.

The pockmarks are characterized by a specific backscatter pattern (Fig. 4.3.); deeper pockmarks are characterized by higher backscatter values and lower seep densities, whereas shallower pockmarks have relatively lower backscatter values and often show much higher seep densities.

The same relations between backscatter intensity, morphology and seep locations are observed in the side scan sonar data (Figs. 4.1.D. and 4.4.).

4.4.2. Seismic observations

The seismic data show the presence of a distinct "gas front", which marks the top of the free gas zone in the sediments (Figs. 4.4.C., 4.4.F. and 4.4.I.) (Naudts et al., 2006; Judd and Hovland, 2007). The gas front is expressed as a high-amplitude reflection that cross-cuts the normal stratigraphy and completely masks all reflections below (Figs. 4.4.C., 4.4.F. and 4.4.I.). Naudts et al. (2006) already observed that the depth of the gas front in the study area is strongly variable and controlled by the presence of filled channels, and that seeps preferentially occur where the gas front approaches the seafloor within 10 m (Figs. 4.4.C., 4.4.F. and 4.4.I.). At the same time a correlation exists between the depth of the gas front and the acoustic seafloor backscatter (Fig. 4.4.). Shallow gas fronts correspond to high- and medium-backscatter areas with seeps, whereas deep gas

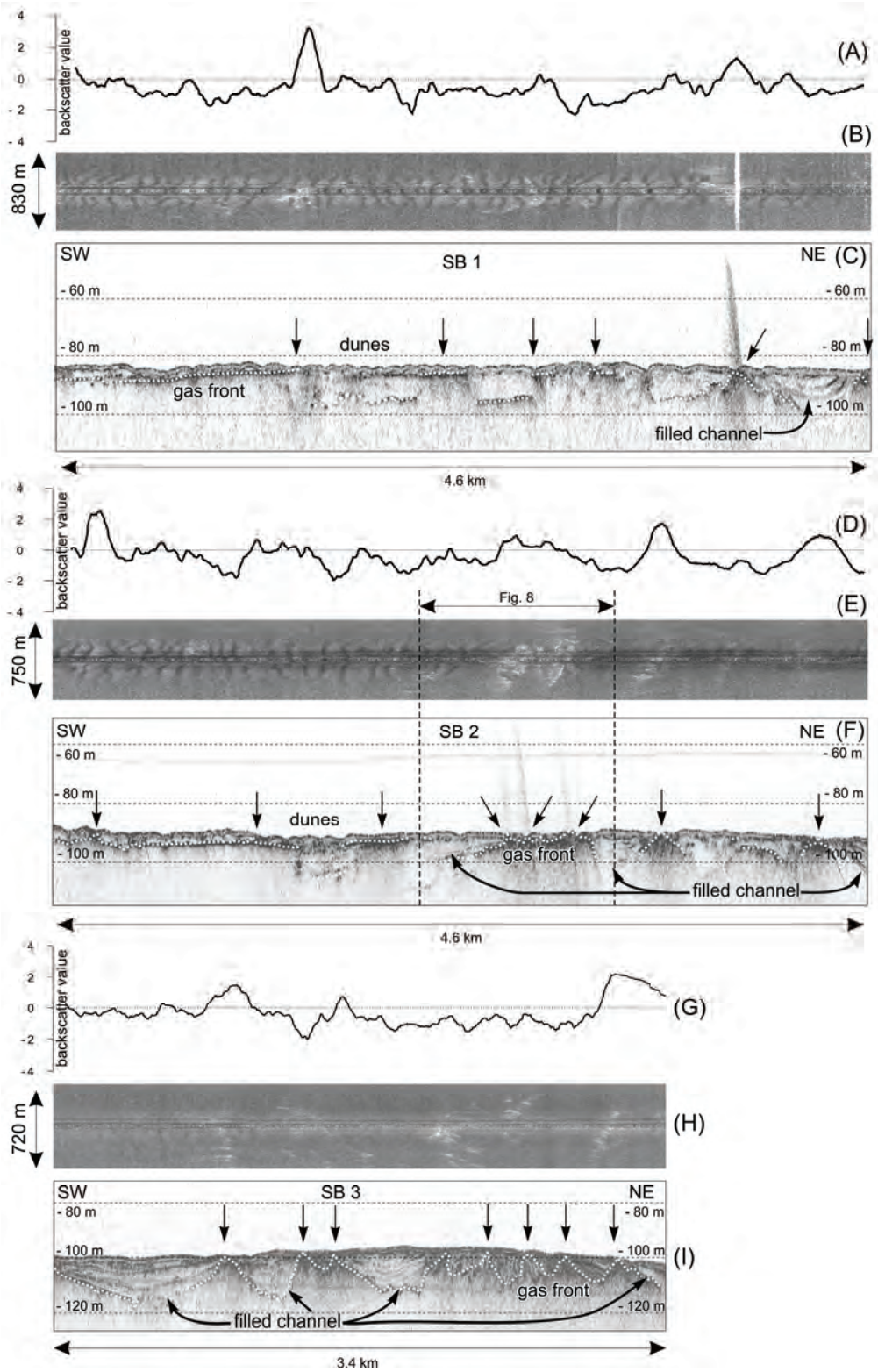

Figure 4.4. Three 5 kHz subbottom profiles SB1, SB2 and SB3 (**C**, **F** and **I**) with their respective multibeam-derived backscatter profiles (**A**, **D** and **G**) and side scan sonar images (**B**, **E** and **H**) (for location see Fig. 4.1.D.). Shallow gas fronts (dashed white line) occur at medium- and high-backscatter areas associated with seeps (arrows), whereas deep gas fronts occur at low-backscatter areas without seeps. Bubbles recorded as noise in the water column on the subbottom data (SB 1 & 2) sometimes blank out the side scan sonar recordings (see NE of SB1) (Fig. 4.4.B.).The extent of SB2 shown in Figure 4.8. is indicated.

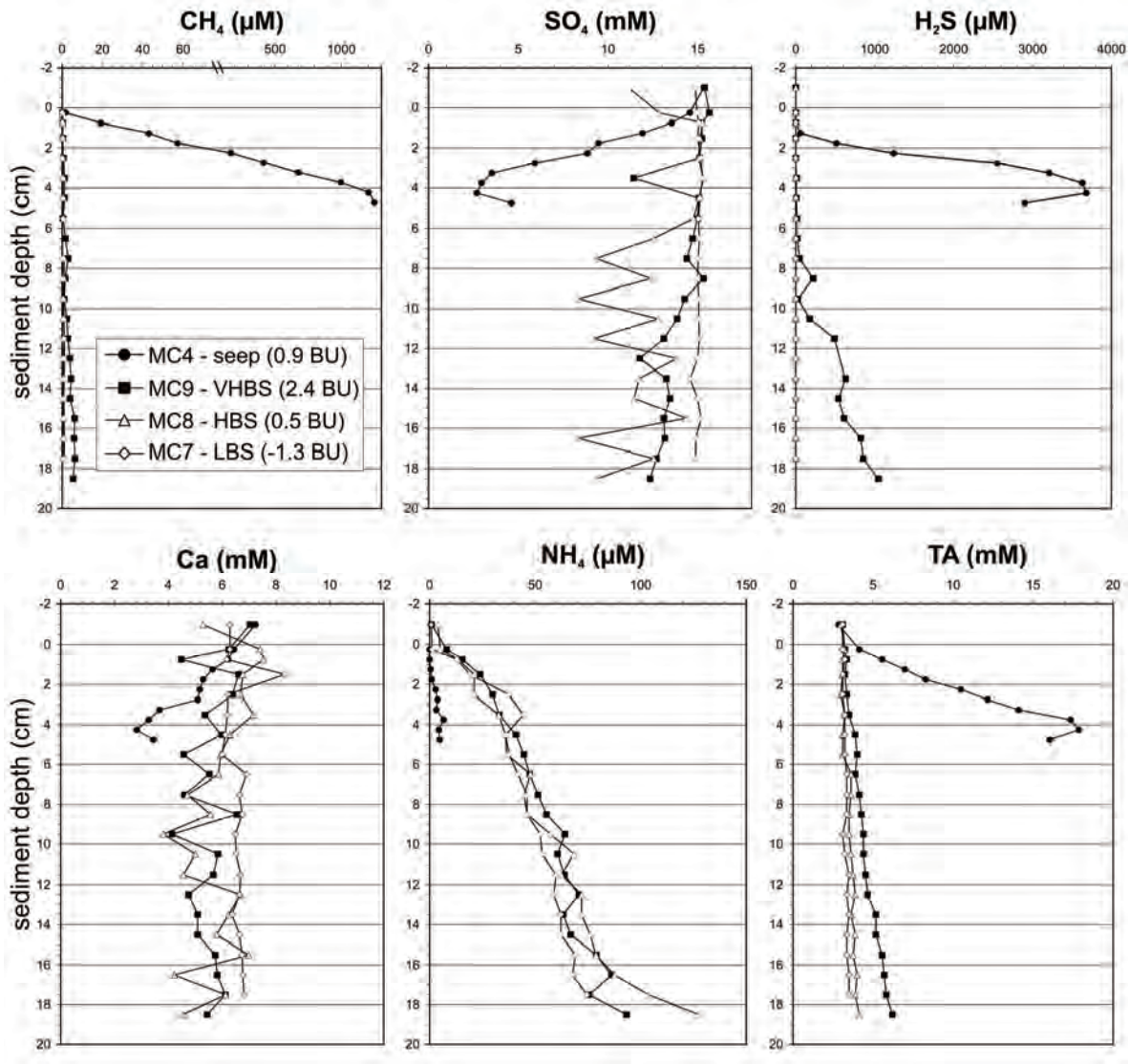

Figure 4.5. Pore-water data from multi-cores taken at different backscatter intensity sites. MC 4 was taken at an actively bubbling high-backscatter site. MC 7-9 are taken from areas with backscatter values ranging from low- to very-high-backscatter values. Values at -1 cm depth are water samples taken from the core liner above the sediment surface (for locations see Figs. 4.1.D. and 4.2.).

fronts correspond to low-backscatter areas without seeps. This observation is valid for both the multibeam-derived backscatter profiles (Figs. 4.4.A., 4.4.D. and 4.4.G.) and the side scan sonar images (Figs. 4.4.B., 4.4.E. and 4.4.H.).

4.4.3. Pore-water and grain-size analysis

The pore-water analyses of the 4 multi-cores, taken at sites of different backscatter intensity, show significant differences (Fig. 4.5.). Core MC4 was taken directly at a bacterial mat with bubble release inside a high-backscatter area (0.9 BU), whereas MC7, MC8 and MC9 were taken in non-seeping low- to very-high-backscatter sites (-1.3 BU, 0.5 BU and 2.4 BU, respectively) (Fig. 4.1.D. and Fig. 4.2.). It has to be stated that a core only represent a small subsample (0.0314 m^2) of the area over which the backscatter value was measured (25 m^2).

Core MC4 had limited penetration, with only 5 cm compared to at least 17 cm for the other three cores. Methane concentrations increase with depth in all four cores: very slightly in MC7

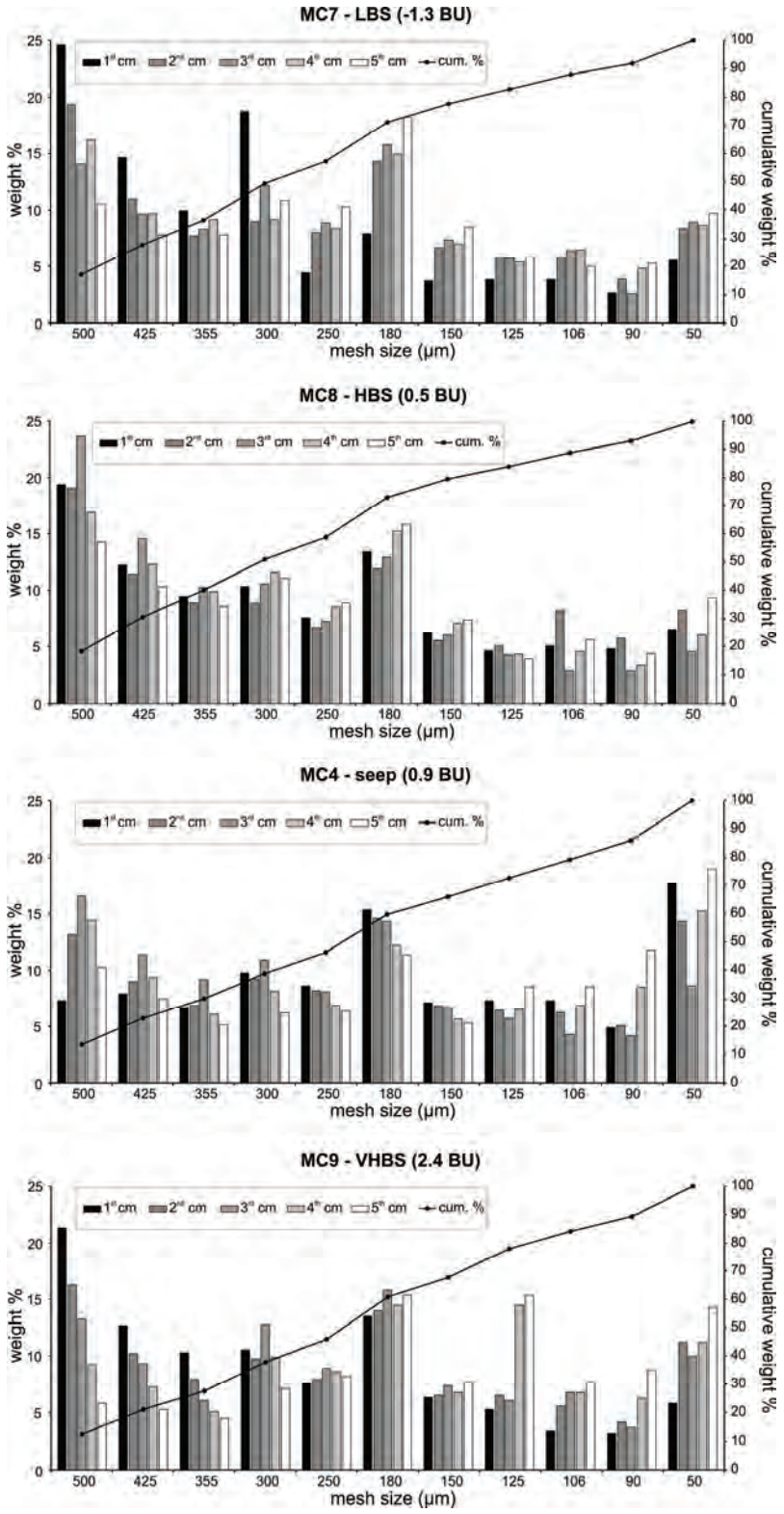

Figure 4.6. Grain-size data from multi-cores taken at different backscatter intensity sites shown as histograms and cumulative percentage curves for each centimeter of the uppermost 5 cm. MC 4 was taken at an actively bubbling high-backscatter site. MC 7-9 are taken from areas with backscatter values ranging from low- to very-high-backscatter values (for locations see Figs. 1D and 2).

and MC8, more in MC9 and very strongly in MC4 (Fig. 4.5.). Equivalent trends can be seen for the increase of sulfide and total alkalinity (TA) and the decrease of sulfate with depth (Fig. 4.5.). Ammonium shows a constant increase with depth for MC7, MC8 and MC9; whereas the concentrations for MC4 are generally much lower with only a slight increase with depth (Fig.

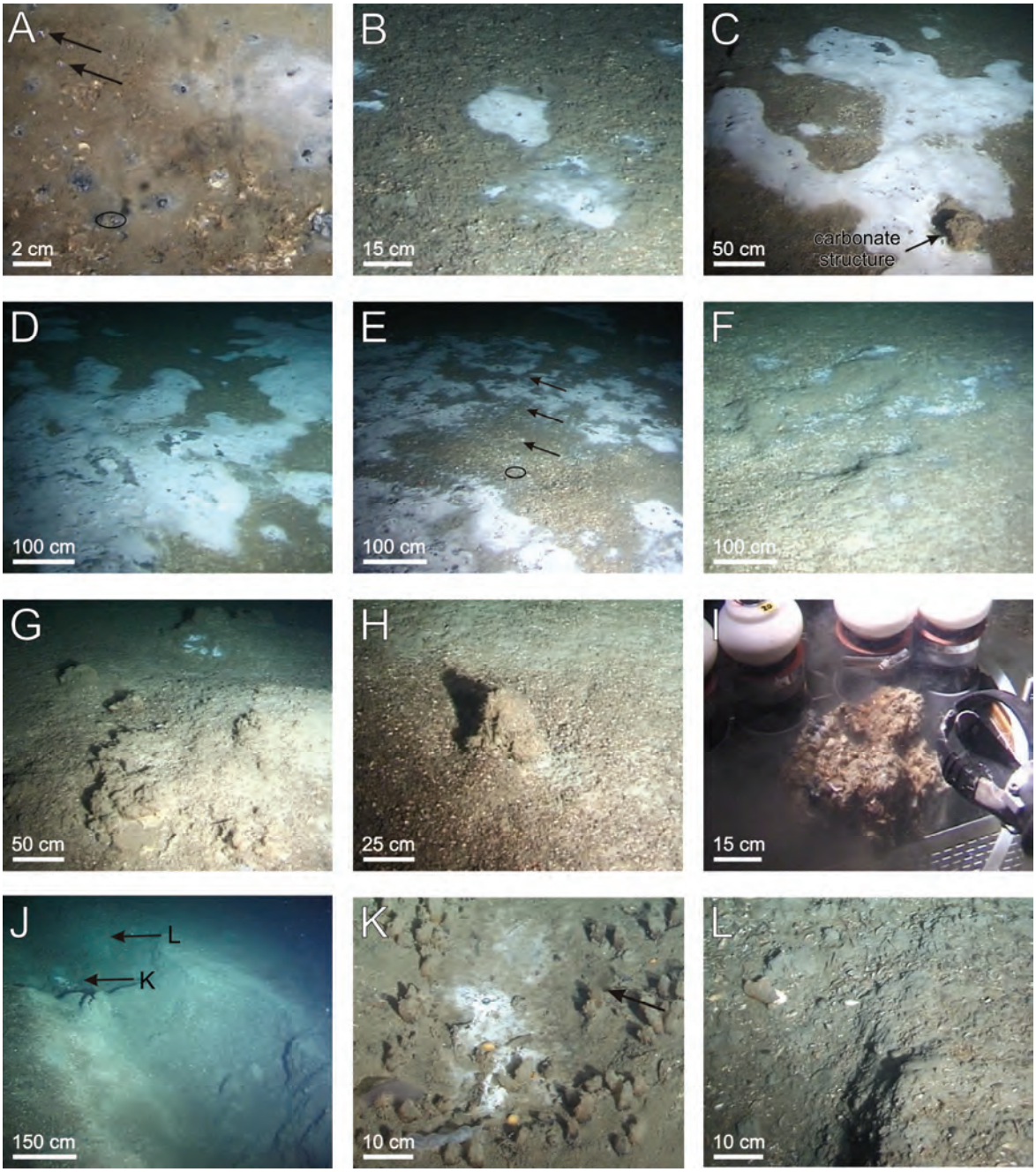

Figure 4.7. Screenshots captured from the JAGO dive 852 video (for outline of dive area see Fig. 4.2A) **A-E**: Bacterial mats of different sizes surrounding black venting holes all or not associated with bubble release (arrows) or carbonate structures. **G-I**: Semi-buried to fully-exposed carbonate structures, all or not associated with bacterial mats. **J-L**: Seafloor depression (pockmark) with rough, probably carbonate-cemented, edges and with a small bacterial mat on the bottom surrounded by Tunicates. Bubble release was observed on the right of the bacterial mat (arrow).

4.5.). Calcium concentrations are relatively constant; only in MC4 a distinct decrease with depth is observed (Fig. 4.5.). In addition, water samples were taken from the core liner above the sediment surface. Cores MC4, MC8 and MC9 show changes between the pore-water and bottom-water data, whereas core MC7 almost shows no changes with respect to the bottom-water concentrations (Fig. 4.5.).

The grain-size analysis of the 4 multi-cores reveals very limited differences in grain-size distribution for the uppermost 5 cm of the different cores. The fraction coarser than 50 µm only consists of shell fragments (*Modiolus phaseolinus)*, up to centimeter scale, with rare carbonate-cemented sediments (shell fragments and fine-grained sediments). All cores are characterized by a polymodal grain-size distribution for the fraction between 600 and 50 µm (Fig. 4.6.).

4.4.4. Visual seafloor observations

Visual observations generally show a rather flat, featureless seafloor with a micro-relief of a few centimeters. In decimeter scale very little relief is present, except for a small depression/pockmark observed during the JAGO dive (Figs. 4.7. J.-L.). The sediment surface is typically composed of shells and shell fragments in a fine-grained matrix, as confirmed by the grain-size analyses (Figs. 4.7.A.-L. and Fig. 4.8.A.). Seeps are generally characterized by bubbles escaping from small black venting holes, which may or may not be surrounded by bacterial mats (possibly *Beggiatoa sp.*) (Fig. 4.7.A.). Bubbles are released either from within bacterial mats (Fig. 4.7.A.), from their edges (Fig. 4.7.K.) or from between bacterial mats if the mats occur in larger clusters (Fig. 4.7.E.). The bright white bacterial mats occur as irregularly shaped single patches or in clusters with sizes ranging from a couple of square centimeters to several square meters (Figs. 4.7.A.-F. and Figs. 4.8.B.-E.). JAGO's sampling claw revealed that quite often the sediment below bacterial mats is hard. The sediment usually gets softer within a few centimeters away from the mat. Digging underneath bacterial mats frequently exposed solid carbonate crusts or simply failed because the sediment was too hard. The distribution of the bacterial mats corresponds very well with the high-to very-high-backscatter areas and with shallow gas fronts (Fig. 4.9., for the extent of SB2 in Fig. 4.9. see Fig. 4.4.). Almost no bacterial mats occur within the low-backscatter areas. Generally, during the visual observations no bubbles were observed being released from the bacterial mats, which is in agreement with the absence of single-beam-detected seeps at the bacterial-mat locations (Fig. 4.9.).

Bacterial mats were also observed in association with carbonates that form positive elevations on the seafloor. Some only form a moderate relief of a couple of centimeters (Fig. 4.7.F. and Figs. 4.8.D. and F.), whereas other fully-exposed carbonate structures are irregularly shaped and tens of centimeters high and wide (Figs. 4.7.G.-I.). Areas around carbonates often show up as rougher surfaces resembling erosion features (Figs. 4.7.F.-G., Fig. 4.7.L. and Figs. 4.8.G.-I.), which correspond well with the high to very-high-backscatter areas.

4.5. Discussion

4.5.1. Bacterial mats, carbonates and their relation to seep distribution

Based on the visual observations and analysis of the core data, different stages of bacterial-mat growth and authigenic carbonate formation can be determined. This process appears to lead to a gradual (self-)sealing of the seeps by carbonate clogging, followed by a relocation of the bubble-releasing locations. Our observations confirm the three-stage self-sealing process of seeps, proposed by Hovland (2002).

The self-sealing process starts with gas bubbles, generated from methane-supersaturated pore waters (Boudreau et al., 2001), being released into the water column from small holes in the sea bed (Fig. 4.7.A.). The venting holes generally have a dark color indicating the precipitation of sulfide minerals like pyrite (Peckmann et al., 2001) and are often surrounded by bacterial mats of different sizes (Figs. 4.7.A.-E.). These bacterial mats are formed by sulfide-oxidizing bacteria (e.g. *Beggiatoa sp.*),

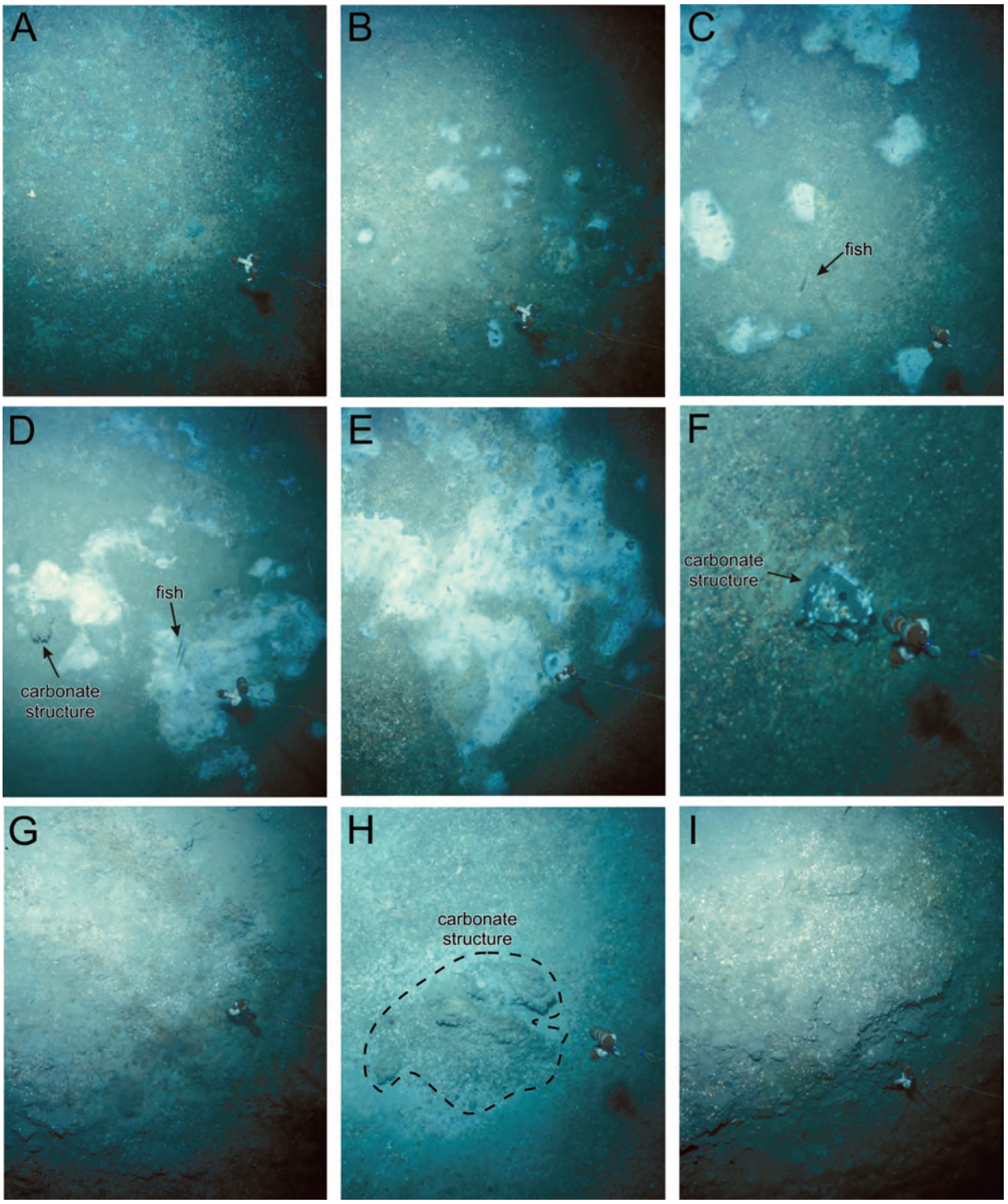

Figure 4.8. Screenshots taken during the OFOS video lines shown in Figure 4.9., characterizing the study-area seafloor (for scale see the 10 by 10 cm shackles). **A**: Usual flat, shell-covered, seafloor. **B-E**: Bacterial mats of different sizes. **F-I**: Carbonate formations showing up as solitary buildups with small bacterial mats or as rough, carbonate-cemented, seafloor.

which profit from the high fluxes of sulfide generated by the anaerobic oxidation of methane (AOM) (Boetius et al., 2000; Boetius and Suess, 2004; Sommer et al., 2006).

The pore-water analysis of MC4 shows typical profiles and concentrations indicative of AOM near the sediment surface, with strong gradients of increasing alkalinity, sulfide and methane concentrations (Fig. 4.5.). Decreasing sulfate and very low ammonium concentrations indicate

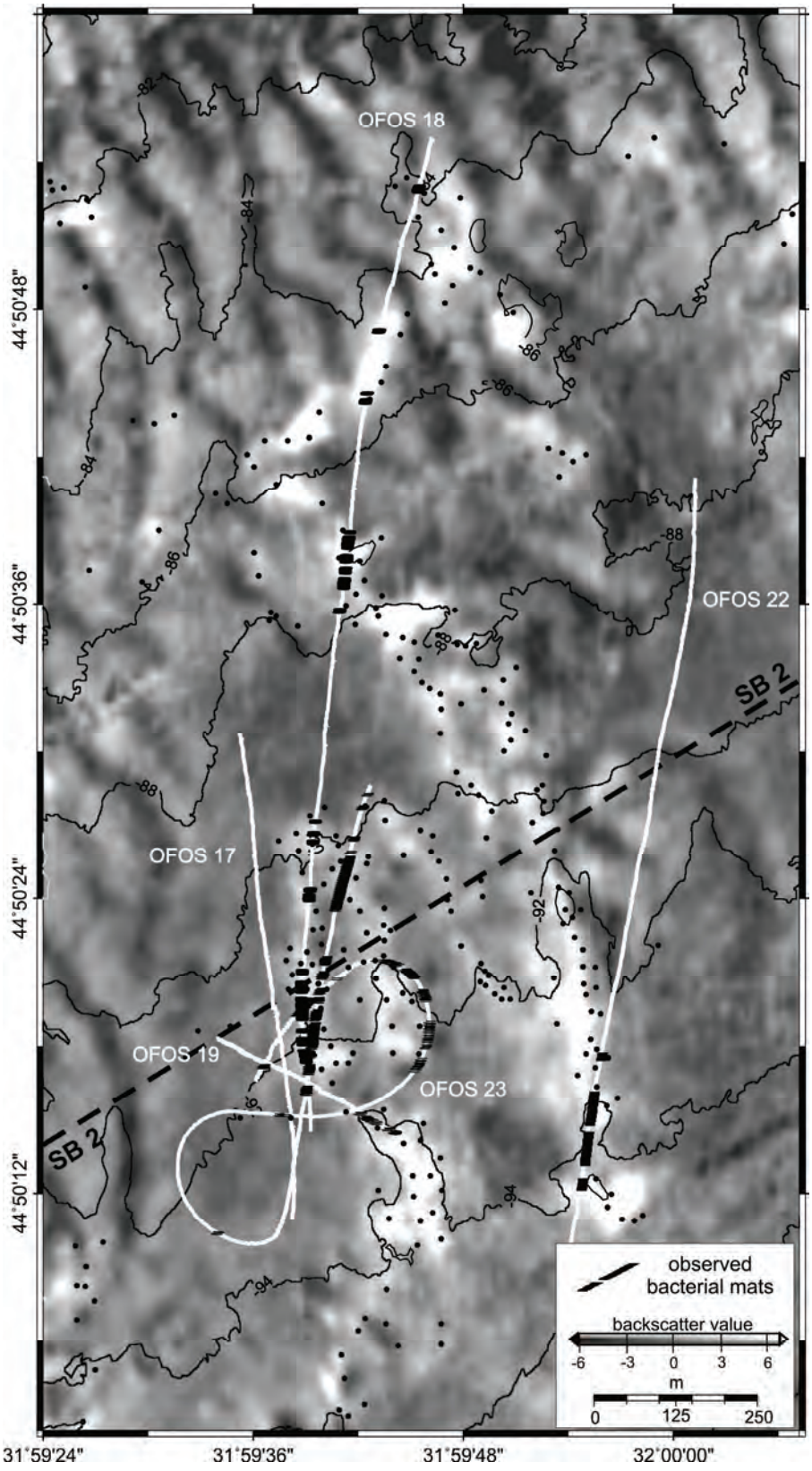

Figure 4.9. Multibeam backscatter map overlain with bathymetric contours (for location see Fig. 4.2.A.), seep locations (black dots) and the outline of seismic profile SB2 (see Fig. 4.1.D. and Fig. 4.4.). Visually observed bacterial mats are indicated by black markers along the offset-corrected OFOS video lines (white lines). Bacterial mats occur solely at high to very-high-backscatter areas.

that AOM is the only sulfate-consuming process. From the other cores, only MC9 shows evidence of AOM, with changes in sulfate, sulfide and methane below 6 cm sediment depth. The sulfate decrease is 2.4 higher than the sulfide increase, pointing to precipitation of sulfides such as troilite or pyrite.

The bacterial mats may cover several square meters by capturing dissolved and free gas at venting locations (Figs. 4.7.A.-E. and Figs. 4.8.B.-E.). This enhances AOM in the sediments beneath the mats which facilitates their lateral growth (Boetius and Suess, 2004; Sommer et al., 2006).

AOM is typically associated with the formation of methane-derived authigenic carbonates (MDACs) (Hovland et al., 1985; Paull et al., 1992; Peckmann et al., 2001; Greinert et al., 2002a; Orange et al., 2002; Johnson et al., 2003; Mazzini et al., 2006; Judd and Hovland, 2007). Therefore, locations with increased methane-rich fluid fluxes causing AOM and bacterial-mat development, are often linked with MDAC formation, as was shown by JAGO sampling and visual observations (Figs. 4.7.C., 4.7.F.-G. and 4.7.J.-K., Figs. 4.8.D. and 4.8.F.). This also explains the limited penetration of MC4 and the decreasing calcium concentrations within this core, pointing to a calcium-rich carbonate formation. XRD analyses of recovered carbonate pieces from MC4 show aragonite as the dominant cementing carbonate phase. The carbonate-cementation of the seafloor sediments increases their resistance to erosion, thus enhancing seafloor roughness and resulting in exposed carbonate-cemented structures (Figs. 4.7.C., 4.7.F.-J. and 4.7.L., Figs. 4.8.D. and 4.8.F.-I.).

Once MDAC formation has started, ongoing precipitation may result in clogging fluid pathways and also blocking the migration of free gas through the sediments, thus forcing bubbles to migrate laterally towards the edge of the carbonate crust or carbonate-cemented sediments. Therefore bubbles are often released at the edge of large bacterial mats (Figs. 4.7.E. and 4.7.K.). Eventually, carbonate precipitation will lead to the self-sealing of the entire seep, leaving behind a carbonated-cemented seafloor with exposed and buried carbonates (Hovland, 2002), associated with only small or no bacterial mats, and no seeps (Figs. 4.7.F.-L. and Figs. 4.8.F.-I.).

4.5.2. Controls on acoustic seafloor backscatter

The high to very-high-backscatter areas in our study area often coincide with pockmarks, therefore the angle of incidence and the morphology of the seafloor could be a prime factor causing the high-backscatter return (Blondel and Murton, 1997). However, for the pockmarks as well as for the dunes, the differences in backscatter do not seem to be related to the morphology of these features. First of all, the backscatter data is acquired when sailing in all possible directions. If differences in backscatter response are caused by differences in morphology, this would give differences in backscatter response for different acquisition orientation. But this is not the case. Furthermore when comparing the backscatter data from low- and high-backscatter areas (Figs. 4.2.A. and 4.10.). The similar morphology of the seafloor together with the similar incidence angles along the swath for high- and low-backscatter swaths clearly indicates that the observed difference in seafloor amplitude and the resulting normalized-backscatter strength between both swaths is morphology-independent (Fig. 4.10.). Finally, the high-backscatter patches associated with seeps were also observed outside pockmarks on a flat seafloor (Fig. 4.2.A.). These observations indicate that the high to very-high-backscatter anomalies observed in our study area are not caused by morphological effects, but by differences in sediment properties, such as roughness, acoustic impedance or grain size at and around the seep sites (Blondel and Murton, 1997). For the dunes, the backscatter differences are most likely related to sediment-property differences between the sediments covering the western and eastern flanks of the dunes; e.g. difference in grain-size distribution induced by prevailing currents (Todd, 2005).

Since the medium- to high-backscatter areas seem to be related to shallow gas fronts, (Figs. 4.4. and 4.9.), gas bubbles captured close to the seafloor might increase the backscattering

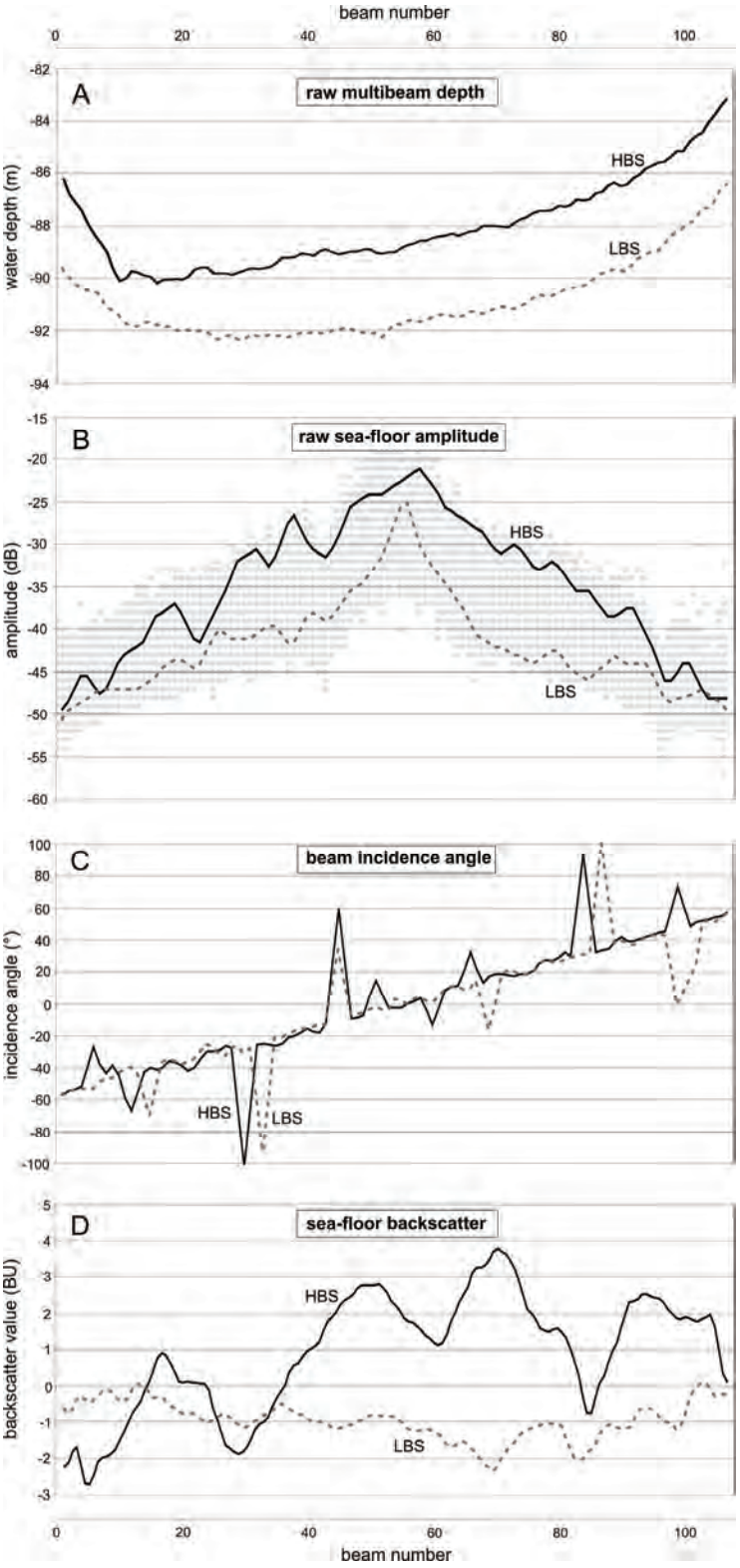

Figure 4.10. Comparison of two multibeam swaths from one multibeam line, one recorded in a high-backscatter area (full line) and one from a low- to medium-backscatter area (dotted line). **A**. The raw depth for both swaths (see Fig. 4.2.A. for location). **B**. The raw amplitude for both swaths within a cloud representing all amplitudes recorded during the particular multibeam line. **C**. The incidence angle for each beam of both swaths. **D**. Normalized backscatter values for both swaths.

because of the increased acoustic impedance affecting both the interface and volume backscattering (Fonseca, 2001; Fonseca et al., 2002). Fonseca et al. (2002) postulated, however, that in shallow water (< 100 m water depth) the interface backscatter is severely reduced due to the decrease in sediment sound speed. The gain in volume backscatter due to the presence of methane bubbles is insufficient to compensate for the loss in interface backscatter, resulting in a net decrease in the total backscatter response. Since the water depth in our study area is generally less than 100 m, free gas present in the seafloor sediments can probably be discarded as the main factor for backscatter enhancement. This assumption is further sustained by our raw backscatter measurements, with differences up to 18 dB between low- and high-backscatter areas (Fig. 4.10.). Fonseca (2001) observed that sub-surface gas, even in -785 m water depth, only leads to a 4 dB and a 7 dB gain in backscatter strength for a 95 kHz and a 30 kHz multibeam system respectively.

Grain-size or shell-fragment distribution as well as bioturbation can determine the acoustic backscatter response of the seafloor (Pouliquen and Lyons, 2002; Collier and Brown, 2005; Lyons, 2005). Since no signs of bioturbation were observed, bioturbation can be ruled out as a cause for the observed backscatter patterns. Grain-size and shell fragment distribution could be of importance since the fraction > 50 µm consist solely of shell fragments. However, the difference in grain-size distribution between the cores is too small to cause the observed differences in backscatter response.

Authigenic carbonates are known to be major contributors to seafloor roughness and acoustic impedance contrast in seep areas, and thus also to acoustic backscatter intensity (Orange et al., 2002; Johnson et al., 2003; Holland et al., 2006). Holland et al. (2006) shows that authigenic carbonate structures lead to a backscatter increase of 10-15 dB above background measurements. This is very similar to our raw backscatter measurements, with differences of up to 18 dB between low- and high-backscatter areas (Fig. 4.10.). This suggests, together with the lack of other backscatter enhancers, that for our study area the observed authigenic carbonates are probably the main reason for the high to very-high-backscatter patches.

4.5.3. Backscatter, seep distribution and sub-surface integrative model

When disregarding the backscatter pattern caused by the sediment dunes and the acquisition artifacts, we can conclude from our data, that the remaining backscatter anomalies are mainly caused by the presence of authigenic carbonates. Since ongoing carbonate formation causes a self-sealing of seep sites and a subsequent relocation of fluid pathways/seeps we conclude that the observed seafloor backscatter and seep distribution in our study area can be explained by the degree of authigenic carbonate formation (Fig. 4.11.).

Considering the formation of MDACs beneath bacterial mats and the non-seeping of most of these observed bacterial mats it can be concluded that the very-high-backscatter patches correspond to areas where intense/long-lived methane seepage has favored MDAC formation, which in turn has led to the self-sealing of these seep areas (Figs. 4.9. and 4.11.). Based on this, the high- and medium-backscatter distribution can be interpreted as representing different stages of carbonate cementation (Fig. 4.11.). Locations with active methane seepage and ongoing carbonate precipitation show up as medium- to high-backscatter areas, whereas those with advanced, massive carbonate cementation -and due to the self-sealing possibly lower seep activity- are characterized by very high and maximum backscatter values. These very-high-backscatter areas are the result of long-lived and/or intensive seepage which resulted in the precipitation of massive MDACs and sometimes in the formation of pockmarks, due to fine-grained sediment remobilization.

On a larger scale, the filled delta channels that control shallow gas migration and seep occurrence (Naudts et al., 2006) also determine the distribution of the seep-related backscatter anomalies; areas with deep sub-surface gas fronts and the absence of active seepage, correspond to low-backscatter areas (Figs. 4.4. and 4.11.). The medium- to high-backscatter

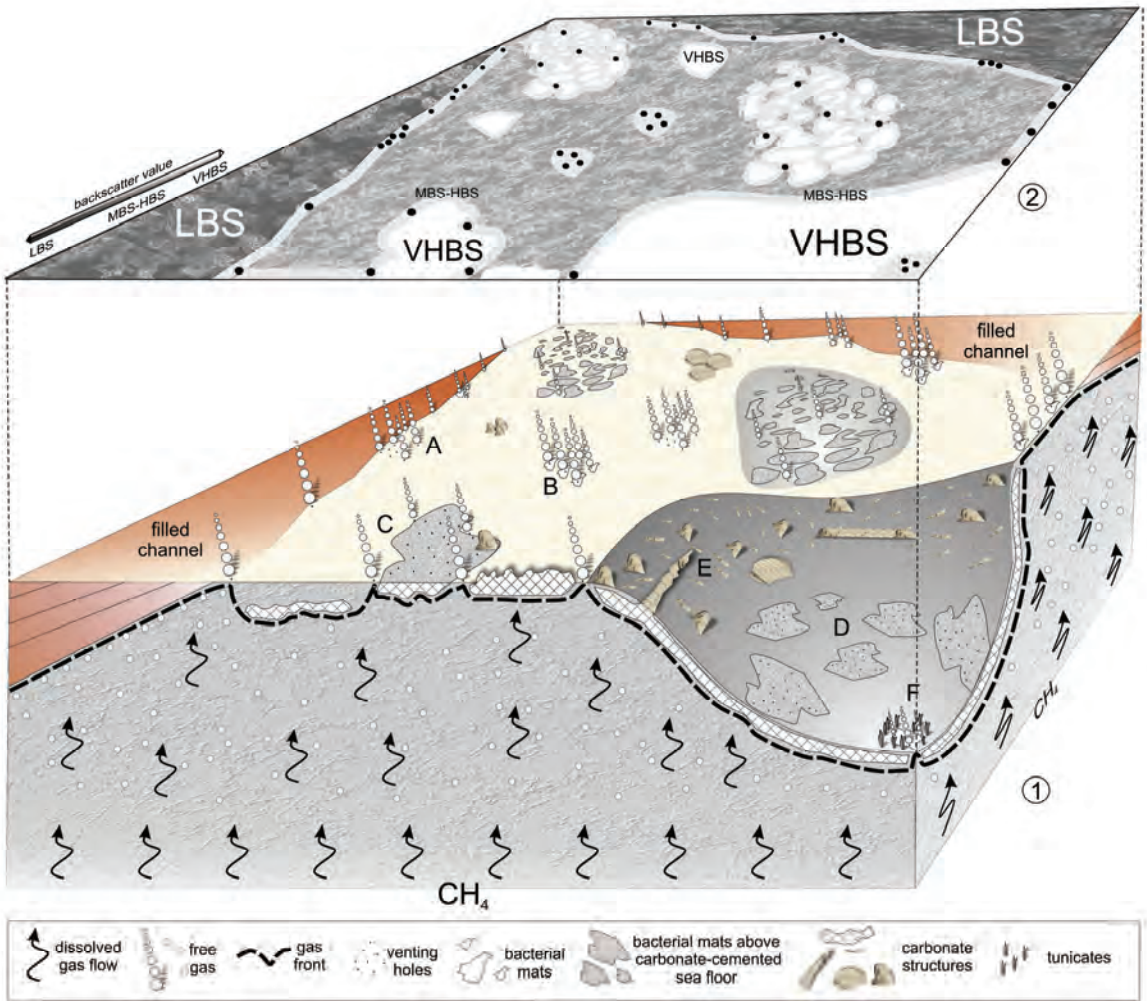

Figure 4.11. Overview model of the supposed fluid migration in the subsurface, carbonate formation with seep relocation and the acoustic seafloor backscatter expression. ① A. Gas-bubble release from black venting holes. B. Bacterial-mat formation around the black venting holes. C-D. Precipitation of methane-derived authigenic carbonates underneath bacterial mats with subsequent relocation or termination of seepage. E. Semi-buried to fully exposed methane-derived authigenic carbonate structures. F. Bacterial mats with limited gas-bubble release and associated with chemosynthetic communities (e.g. Tunicates). All mentioned features can occur in association with or without pockmark formation. ② Acoustic seafloor backscatter expression resulting from the seep distribution and associated features. Filled channels, blocking fluid migration, are characterized by low backscatter values (LBS) and the absence of seeps. Locations with active seepage and ongoing authigenic carbonate precipitation show up as medium- to high-backscatter areas (MBS), whereas those with advanced, massive carbonate precipitation and at present less or no seep activity show up as very high to maximum backscatter areas (VHBS).

areas only occur in between the channels, where the sub-surface gas front reaches the sediment-water interface and where active seepage takes place, accompanied by bacterial-mat growth and authigenic carbonate formation, as a result of the higher methane fluxes and the associated AOM (Fig. 4.11.).

4.6. Conclusions

The 600 active methane bubble-releasing seeps that were detected in an area of 14.73km^2 on the continental shelf of the Dnepr paleo delta occur systematically in areas that are characterized by a higher-than-average acoustic backscatter response on side scan sonar and/or multibeam echosounder recordings. Detailed

spatial analysis shows that the seeps occur preferentially in areas with medium- to high-backscatter strength, but not in areas with very high and maximum backscatter strength.

Visual observations made with the JAGO submersible and OFOS video sled showed that the high-backscatter areas are characterized by the occurrence of bacterial mats and methane-derived authigenic carbonates (MDACs) in the seafloor sediments, both indicative of AOM. This was confirmed by pore-water analyses, which showed increasing methane, total alkalinity and sulfide concentrations in correspondence with decreasing sulfate concentrations and no increase in ammonium.

Complete integration of all available data excluded morphology, grain-size distribution and the presence of free gas bubbles in the shallow subsurface as possible causes for the observed high backscatter associated with the active seeps. Instead we conclude that the high-backscatter values in areas with active methane bubble release are caused by the presence of methane-derived authigenic carbonates in the sediment. The absence of active seeps in areas with the highest backscatter values supports the model proposed by Hovland (2002), in which AOM-induced carbonate formation may lead to (self-)sealing of fluid pathways by carbonate clogging, followed by a relocation of the fluid/gas pathways around the cemented, impermeable areas. As a final point, our analysis shows that acoustic backscatter of the seafloor can indeed be used as a proxy –and as a rapid mapping tool– for detecting seep provinces that are very likely actively seeping. Furthermore, areas with the highest backscatter values should be excluded from backscatter-based estimations of the total area involved in active seepage.

Acknowledgements

We thank the captain and the crew of the 58th and 60th cruise of RV Professor Vodyanitskiy for their hard work and their hospitality and L-3 ELAC Nautik GMBH for their superior and fast support. We like to thank Matthias Haeckel for his help with the pore-water analysis. This study was carried out in the framework of the CRIMEA project (EC project EVK-2-CT-2002-00162; http://www.CRIMEA-info.org) and of a Bilateral Flanders-Russian Federation Project (Gas hydrate accumulations associated with active fluid seeps: a combined thermal and acoustic approach). JAGO dive 852 was carried out in the framework of the METROL project (EC project EVK3-CT-2002-00080). We also like to thank SMT (Kingdom Suite) and IVS (Fledermaus) for the academic licenses. Finally we thank Martin Hovland, David Piper and two anonymous reviewers for their constructive reviews which helped improve this manuscript.

Additional information

Lieven Naudts processed and interpreted most of the datasets, wrote the manuscript and made most figures. The pore-water data and figure was provided by Jens Greinert and Stan E. Beaubien. Lieven Naudts also assisted with the data acquisition during the 12 weeks of expedition on RV Vodyanitskiy in 2003 and 2004. Co-authors helped by reviewing the manuscript and/or by providing the datasets. For the processing of the multibeam data assistance was given by Jens Greinert. For processing of the seismic data assistance was given by Peter Staelens.

References

Amouroux, D., Roberts, G., Rapsomanikis, S., Andreae, M.O., 2002. Biogenic Gas (CH4, N2O, DMS) Emission to the Atmosphere from Near-shore and Shelf Waters of the North-western Black Sea. Estuarine, Coastal Shelf Sci. 54, 575-587.

Artemov, Y.G., 2006. Software support for investigation of natural methane seeps by hydroacoustic method. Mar. Ecol. J., 57-71.

Artemov, Y.G., Egorov, V., Polikarpov, N., Gulin, S.B., 2007. Methane emission to the hydro- and atmosphere by gas bubble streams in the Dnieper paleo-delta, the Black Sea. Reports of the Natl. Acad. of Sci. of Ukraine 5, 110-116.

Bange, H.W., 2006. Nitrous oxide and methane in European coastal waters. Estuarine, Coastal Shelf Sci. 70, 361-374.

Blondel, P., Murton, B.J., 1997. Handbook of Seafloor Sonar Imagery. Wiley-Praxis Series in Remote Sensing. John Wiley and Sons Ltd. in association with Praxis Publishing Ltd., Chichester. 314 pp.

Boetius, A., Ravenschlag, K., Schubert, C.J., Rickert, D., Widdel, F., Gieseke, A., Amann, R., Jorgensen, B.B., Witte, U., Pfannkuche, O., 2000. A marine microbial consortium apparently mediating anaerobic oxidation of methane. Nature 407, 623-626.

Boetius, A., Suess, E., 2004. Hydrate Ridge: a natural laboratory for the study of microbial life fueled by methane from near-surface gas hydrates. Chem. Geol. 205, 291-310.

Boudreau, B.P., Gardiner, B.S., Johnson, B.D., 2001. Rate of growth of isolated bubbles in sediments with a diagenetic source of methane. Limnol. Oceanogr. 46, 616-622.

Collier, J.S., Brown, C.J., 2005. Correlation of sidescan backscatter with grain size distribution of surficial seabed sediments. Mar. Geol. 214, 431-449.

Dimitrov, L., 2002. Contribution to atmospheric methane by natural seepages on the Bulgarian continental shelf. Cont. Shelf Res. 22, 2429-2442.

Egorov, V., Luth, U., Luth, C., Gulin, M.B., 1998. Gas seeps in the submarine Dnieper Canyon, Black Sea: acoustic, video and trawl data. In: U. Luth, C. Luth and H. Thiel (Editors), MEGASEEPS Gas Explorations in the Black Sea, Project Report. Zentrum für Meres- und Klimaforschung der Universität Hamburg, Hamburg, pp. 11-21.

Etiope, G., 2004. New Directions: GEM--Geologic Emissions of Methane, the missing source in the atmospheric methane budget. Atmos. Environ. 38, 3099-3100.

Etiope, G., Klusman, R.W., 2002. Geologic emissions of methane to the atmosphere. Chemosphere 49, 777-789.

Fonseca, L., 2001. A model for backscattering angular response of gassy sediments: Applications to petroleum exploration and development programs. Ph.D. Thesis, University of New Hampshire, 126 pp.

Fonseca, L., Mayer, L., Orange, D., Driscoll, N., 2002. The high-frequency backscattering angular response of gassy sediments: Model/data comparison from the Eel River Margin, California. J. Acoust. Soc. Am. 111, 2621-2631.

Garcia-Gil, S., Vilas, F., Garcia-Garcia, A., 2002. Shallow gas features in incised-valley fills (Ria de Vigo, NW Spain): a case study. Cont. Shelf Res. 22, 2303-2315.

Gay, A., Lopez, M., Ondreas, H., Charlou, J.L., Sermondadaz, G., Cochonat, P., 2006. Seafloor facies related to upward methane flux within a Giant Pockmark of the Lower Congo Basin. Mar. Geol. 226, 81-95.

Grasshoff, K., Ehrhardt, M., Kremling, K., 1999. Methods of seawater analysis. Verlag Chemie, Weinheim.

Greinert, J., Bohrmann, G., Elvert, M., 2002a. Stromatolitic fabric of authigenic carbonate crusts: result of anaerobic methane oxidation at cold seeps in 4,850 m water depth. Int. J. Earth Sci. 91, 698-711.

Greinert, J., Bohrmann, G., Suess, E., 2001. Gas hydrate-associated carbonates and methane-venting at Hydrate Ridge: Classification, distribution, and origin of authigenic lithologies. In: C.K. Paull and W.P. Dillon (Editors), Natural Gas Hydrates: Occurrence, Distribution, and Detection, Geophysical Monograph. American Geophysical Union, pp. 99-113.

Greinert, J., Bollwerk, S.M., Derkachev, A., Bohrmann, G., Suess, E., 2002b. Massive barite deposits and carbonate mineralization in the Derugin Basin, Sea of Okhotsk: precipitation processes at cold seep sites. Earth Planet. Sci. Lett. 203, 165-180.

Greinert, J., McGinnis, D.F., Naudts, L., Linke, P., De Batist, M., 2010. Atmospheric methane flux from bubbling seeps: Spatially extrapolated quantification from a Black Sea shelf area. J. Geophys. Res. 115, 1-18.

Holland, C.W., Weber, T.C., Etiope, G., 2006. Acoustic scattering from mud volcanoes and carbonate mounds. J. Acoust. Soc. Am. 120, 3553-3565.

Hornafius, J.S., Quigley, D., Luyendyk, B.P., 1999. The world's most spectacular marine hydrocarbon seeps (Coal Oil Point, Santa Barbara Channel, California): Quantification of emissions. J. Geophys. Res., Oceans 104, 20703-20711.

Hovland, M., 1991. Large Pockmarks, Gas-Charged Sediments and Possible Clay Diapirs in the Skagerrak. Mar. Pet. Geol. 8, 311-316.

Hovland, M., 1992. Hydrocarbon seeps in northern marine waters; their occurrence and effects. Palaios 7, 376-382.

Hovland, M., 2002. On the self-sealing nature of marine seeps. Cont. Shelf Res. 22, 2387-2394.

Hovland, M., Judd, A.G., Burke, R.A., 1993. The Global Flux of Methane from Shallow Submarine Sediments. Chemosphere 26, 559-578.

Hovland, M., Talbot, M., Olaussen, S., Aasberg, L., 1985. Recently formed methane-derived carbonates from the North Sea floor. In: B.M. Thomas (Editor), Petroleum Geochemistry in Exploration of the Norwegian Shelf. Norwegian Petroleum Society. Graham and Trotman, pp. 263-266.

IPCC, 2001a. Climate Change 2001: Synthesis Report. A Contribution of Working Groups I, II, and III to the Third Assessment Report of the Intergovernmental Panel on Climate Change. Cambridge University Press, Cambridge, United Kingdom and New York, NY, USA. 398 pp.

IPCC, 2001b. Climate Change 2001: The Scientific Basis. Contribution of Working Group I to the Third Assessment. Cambridge University Press, Cambridge, United Kingdom and New York, NY, USA. 881 pp.

Ivanov, M., Blinova, V., Kozlova, E., Westbrook, G.K., Mazzini, A., Minshull, T.A., Nouzé, H., 2007. First Sampling of Gas Hydrate From the Vøring Plateau. Eos Trans. Am. Geophys. Union 88, 209.

Johnson, J.E., Goldfinger, C., Suess, E., 2003. Geophysical constraints on the surface distribution of authigenic carbonates across the Hydrate Ridge region, Cascadia margin. Mar. Geol. 202, 79-120.

Judd, A., Hovland, M., 2007. Seabed fluid flow: the impact on geology, biology and the marine environment. Cambridge University Press, Cambridge. 475 pp.

Judd, A.G., 2004. Natural seabed gas seeps as sources of atmospheric methane. Environ. Geol. (Berlin) 46, 988-996.

Judd, A.G., Hovland, M., 1992. The Evidence of Shallow Gas in Marine-Sediments. Cont. Shelf Res. 12, 1081-1095.

Kessler, J.D., Reeburgh, W.S., Southon, J., Seifert, R., Michaelis, W., Tyler, S.C., 2006. Basin-wide estimates of the input of methane from seeps and clathrates to the Black Sea. Earth Planet. Sci. Lett. 243, 366-375.

Klaucke, I., Sahling, H., Weinrebe, W., Blinova, V., Burk, D., Lursmanashvili, N., Bohrmann, G., 2006. Acoustic investigation of cold seeps offshore Georgia, eastern Black Sea. Mar. Geol. 231, 51-67.

Krastel, S., Spiess, V., Ivanov, M., Weinrebe, W., Bohrmann, G., Shashkin, P., Heidersdorf, F., 2003. Acoustic investigations of mud volcanoes in the Sorokin Trough, Black Sea. Geo-Mar. Lett. V23, 230-238.

Kruglyakova, R.P., Byakov, Y.A., Kruglyakova, M.V., Chalenko, L.A., Shevtsova, N.T., 2004. Natural oil and gas seeps on the Black Sea floor. Geo-Mar. Lett. V24, 150-162.

Kutas, R.I., Paliy, S.I., Rusakov, O.M., 2004. Deep faults, heat flow and gas leakage in the northern Black Sea. Geo-Mar. Lett. V24, 163-168.

Kvenvolden, K.A., Rogers, B.W., 2005. Gaia's breath--global methane exhalations. Mar. Pet. Geol. 22, 579-590.

Leifer, I., Patro, R.K., 2002. The bubble mechanism for methane transport from the shallow sea bed to the surface: A review and sensitivity study. Cont. Shelf Res. 22, 2409-2428.

Lelieveld, J., Crutzen, P.J., Dentener, F.J., 1998. Changing concentration, lifetime and climate forcing of atmospheric methane. Tellus, Ser. B. 50, 128-150.

Luth, C., Luth, U., Gebruk, A.V., Thiel, H., 1999. Methane gas Seeps Along the Oxic/Anoxic Gradient in the Black Sea: Manifestations, Biogenic Sediment Compounds and Preliminary Results on Benthic Ecology. Mar. Ecol. 20, 221-249.

Luyendyk, B., Kennett, J., Clark, J.F., 2005. Hypothesis for increased atmospheric methane input from hydrocarbon seeps on exposed continental shelves during glacial low sea level. Mar. Pet. Geol. 22, 591-596.

Lyons, A.P., 2005. The potential impact of shell fragment distributions on high-frequency seafloor backscatter. IEEE J. Oceanic Eng. 30, 843-851.

MacDonald, I.R., Leifer, I., Sassen, R., Stine, P., Mitchell, R., Guinasso, N., 2002. Transfer of hydrocarbons from natural seeps to the water column and atmosphere. Geofluids 2, 95-107.

Mazzini, A., Svensen, H., Hovland, M., Planke, S., 2006. Comparison and implications from strikingly different authigenic carbonates in a Nyegga complex pockmark, G11, Norwegian Sea. Mar. Geol. 231, 89-102.

McGinnis, D.F., Greinert, J., Artemov, Y., Beaubien, S.E., Wuest, A., 2006. Fate of rising methane bubbles in stratified waters: How much methane reaches the atmosphere? J. Geophys. Res., Oceans 111.

Michaelis, W., Seifert, R., Nauhaus, K., Treude, T., Thiel, V., Blumenberg, M., Knittel, K., Gieseke, A., Peterknecht, K., Pape, T., Boetius, A., Amann, R., Jorgensen, B.B., Widdel, F., Peckmann, J., Pimenov, N.V., Gulin, M.B., 2002. Microbial Reefs in the Black Sea Fueled by Anaerobic Oxidation of Methane. Science 297, 1013-1015.

Naudts, L., Greinert, J., Artemov, Y., Staelens, P., Poort, J., Van Rensbergen, P., De Batist, M., 2006. Geological and morphological setting of 2778 methane seeps in the Dnepr paleo-delta, northwestern Black Sea. Mar. Geol. 227, 177-199.

Niemann, H., Elvert, M., Hovland, M., Orcutt, B., Judd, A., Suck, I., Gutt, J., Joye, S., Damm, E., Finster, K., Boetius, A., 2005. Methane emission and consumption at a North Sea gas seep (Tommeliten area). Biogeosciences 2, 335-351.

Oguz, T., 2002. Role of physical processes controlling oxycline and suboxic layer structures in the Black Sea. Global Biogeochem. Cycles 16.

Orange, D.L., Breen, N.A., 1992. The Effects of Fluid Escape on Accretionary Wedges. 2. Seepage Force, Slope Failure, Headless Submarine Canyons, and Vents. J. Geophys. Res. Solid Earth 97, 9277-9295.

Orange, D.L., Yun, J., Maher, N., Barry, J., Greene, G., 2002. Tracking California seafloor seeps with bathymetry, backscatter and ROVs. Cont. Shelf Res. 22, 2273-2290.

Pape, T., Blumenberg, M., Seifert, R., Egorov, V.N., Gulin, S.B., Michaelis, W., 2005. Lipid geochemistry of methane-seep-related Black Sea carbonates. Palaeogeogr. Palaeoclimatol. Palaeoecol. 227, 31-47.

Paull, C.K., Chanton, J.P., Neumann, A.C., Coston, J.A., Martens, C.S., Showers, W., 1992. Indicators of methane-derived carbonates and chemosynthetic organic carbon deposits; examples from the Florida Escarpment. Palaios 7, 361-375.

Peckmann, J., Reimer, A., Luth, U., Luth, C., Hansen, B.T., Heinicke, C., Hoefs, J., Reitner, J., 2001. Methane-derived carbonates and authigenic pyrite from the northwestern Black Sea. Mar. Geol. 177, 129-150.

Pimenov, N.V., Ivanova, A.E., 2005. Anaerobic Methane Oxidation and Sulfate Reduction in Bacterial Mats on Coral-Like Carbonate Structures in the Black Sea. Microbiology 74, 362-370.

Pimmel, A., Claypool, G., 2001. Introduction to shipboard organic geochemistry on the JOIDES Resolution, Texas A&M University.

Polikarpov, G.G., Egorov, V.N., Gulin, S.B., Gulin, M.B., Stokozov, N.A., 1992. Gas seeps from the bottom of the Black Sea-a new object of molismology. In: G.G. Polikarpov (Editor), Molismology of the Black Sea. Nauka, Kiev pp. 10-28.

Polikarpov, G.G., Egorov, V.N., Nezhdanonv, A.I., Gulin, S.B., Kulev, Y.D., Gulin, M.B., 1989. Methane gas seeps in the Black Sea-a new object of molismology. In: G.G. Polikarpov (Editor), Molismology of the Black Sea. Nauka, Kiev pp. 10-20.

Popescu, I., Lericolais, G., Panin, N., Normand, A., Dinu, C., Le Drezen, E., 2004. The Danube submarine canyon (Black Sea): morphology and sedimentary processes. Mar. Geol. 206, 249-265.

Pouliquen, E., Lyons, A.P., 2002. Backscattering from bioturbated sediments at very high frequency. IEEE J. Oceanic Eng. 27, 388-402.

Reitner, J., Peckmann, J., Blumenberg, M., Michaelis, W., Reimer, A., Thiel, V., 2005. Concretionary methane-seep carbonates and associated microbial communities in Black Sea sediments. Palaeogeogr. Palaeoclimatol. Palaeoecol. 227, 18-30.

Ritger, S., Carson, B., Suess, E., 1987. Methane-Derived Authigenic Carbonates Formed by Subduction Induced Pore-Water Expulsion Along the Oregon Washington Margin. Geol. Soc. Am. Bull. 98, 147-156.

Rollet, N., Logan, G.A., Kennard, J.M., O'Brien, P.E., Jones, A.T., Sexton, M., 2006. Characterisation and correlation of active hydrocarbon seepage using geophysical data sets: An example from the tropical, carbonate Yampi Shelf, Northwest Australia. Mar. Pet. Geol. 23, 145-164.

Sager, W.W., MacDonald, I.R., Hou, R., 2003. Geophysical signatures of mud mounds at hydrocarbon seeps on the Louisiana continental slope, northern Gulf of Mexico. Mar. Geol. 198, 97-132.

Schmale, O., Greinert, J., Rehder, G., 2005. Methane emission from high-intensity marine gas seeps in the Black Sea into the atmosphere. Geophys. Res. Lett. 32.

Shoji, H., Soloviev, V., Matveeva, T., Mazurenko, L., Minami, H., Hachikubo, A., Sakagami, H., Hyakutake, K., Kaulio, V., Gladysch, V., Logvina, E., Obzhirov, A., Baranov, B., Khlystov, O., Biebow, N., Poort, J., Jin, Y.K., Kim, Y., 2005. Hydrate-Bearing Structures in the Sea of Okhotsk. Eos Trans. Am. Geophys. Union 86, 13-18.

Sommer, S., Pfannkuche, O., Linke, P., Luff, R., Greinert, J., Drews, M., Gubsch, S., Pieper, M., Poser, M., Viergutz, T., 2006. Efficiency of the benthic filter: Biological control of the emission of dissolved methane from sediments containing shallow gas hydrates at Hydrate Ridge. Global Biogeochem. Cycles 20.

Thiel, V., Peckmann, J., Richnow, H.H., Luth, U., Reitner, J., Michaelis, W., 2001. Molecular signals for anaerobic methane oxidation in Black Sea seep carbonates and a microbial mat. Mar. Chem. 73, 97-112.

Todd, B.J., 2005. Morphology and composition of submarine barchan dunes on the Scotian Shelf, Canadian Atlantic margin. Geomorphology 67, 487-500.

Treude, T., Knittel, K., Blumenberg, M., Seifert, R., Boetius, A., 2005. Subsurface Microbial Methanotrophic Mats in the Black Sea. Appl Environ Microbiol 71, 6375-6378.

Van Rensbergen, P., De Batist, M., Klerkx, J., Hus, R., Poort, J., Vanneste, M., Granin, N., Khlystov, O., Krinitsky, P., 2002. Sublacustrine mud volcanoes and methane seeps caused by dissociation of gas hydrates in Lake Baikal. Geology 30, 631-634.

von Rad, U., Rosch, H., Berner, U., Geyh, M., Marchig, V., Schulz, H., 1996. Authigenic carbonates derived from oxidized methane vented from the Makran accretionary prism off Pakistan. Mar. Geol. 136, 55-77.

Yun, J.W., Orange, D.L., Field, M.E., 1999. Subsurface gas offshore of northern California and its link to submarine geomorphology. Mar. Geol. 154, 357-368.

CHAPTER 5

Active venting sites on the gas-hydrate-bearing Hikurangi Margin, Off New Zealand: Diffusive- versus bubble-released methane

Lieven Naudts, Jens Greinert, Jeffrey Poort, Joke Belza, Elke Vangampelaere, Dries Boone, Peter Linke, Jean-Pierre Henriet, Marc De Batist

Abstract

During the 'New Vents' SO191 cruise in 2007, the activity and distribution of seep sites on the gas-hydrate-bearing Hikurangi Margin, off northeastern New Zealand, were subjected to a highly detailed interdisciplinary study. Here we report on the visual observations and in situ measurements of physical properties performed with a ROV (remotely operated vehicle) and other video-guided platforms at two seep sites in the Rock Garden area; Faure Site and LM-3. The ROV allowed first ever visual observations of bubble-releasing methane seeps at the Hikurangi Margin. At Faure Site, bubble release was monitored during 4 dives, up to periods of 20 minutes. During the first dive, this resulted in the observation of six violent outbursts, each lasting one minute over a three minute interval. These outbursts were accompanied by the displacement and resuspension of sediment grains, and the formation of small depressions, with a maximum diameter of 50 cm and depth of 15 cm, showing what is possibly an initial stage of pockmark formation. During subsequent dives at this bubble site, bubble release rates were rather constant and the previously observed outbursts could no longer be witnessed. At LM-3, the strongest manifestation of seep activity was a large platform (100 m^2), consisting of fresh authigenic carbonates, which was covered by seep fauna (live *Bathymodiolus* sp. mussels, *Calyptogena* sp. shells and live *Lamellibrachia* sp. tubeworms). Bubble activity near this platform was less prominent than at Faure Site. Our observations suggest that the two seep environments result from different types of methane release; mainly by bubble release at Faure Site and rather diffusive at LM-3. We propose a conceptual model where the different ways of methane release and seep environments may be explained by the depth of underlying hydrate occurrences and different tectonic histories of both seep sites.

Keywords

Methane seeps; ROV, Hikurangi Margin; seafloor observations; temperature measurements; bubble-release activity

5.1. Introduction

Gas seeps, i.e. locations of bubble release at the seafloor, are widespread on continental margins (Judd, 2003; Judd and Hovland, 2007). Their presence is commonly indicated by anomalies that are visible on different types of acoustic data, such as seismics, single-beam or multibeam echosounder or side-scan sonar. (Greinert et al., 2006; Klaucke et al., 2006; Naudts et al., 2006; Gay et al., 2007; Judd and Hovland, 2007; Schneider von Deimling et al., 2007; Greinert, 2008; Naudts et al., 2008). While acoustic data are very useful to identify areas in which seeps occur, they usually fail to pinpoint the exact location of bubble release at the seafloor on meter or sub-meter scale. Seeps are often associated with distinct ecosystems with chemosynthetic fauna (bacterial mats, clams, tubeworms etc.) (Boetius and Suess, 2004; Judd and Hovland, 2007). Furthermore, seeps are often characterized by the presence of authigenic carbonates, which are easy to identify during near-bottom investigations, even without bubble release during the observations (Hovland et al., 1985; Paull et al., 1992; Peckmann et al., 2001; Greinert et al., 2002a; Orange et al., 2002; Judd and Hovland, 2007; Naudts et al., 2008). A very good method to observe and study seeps, their activity and the associated ecosystems is by detailed, visual, seafloor observations in possible seep areas indicated by acoustic investigations.

Visual seafloor observations can be made with a towed video sled, a manned submersible or a remotely operated vehicle (ROV). Towed video sleds make it possible to gain a regional overview of the seafloor features by criss-crossing a target area (Greinert et al., 2002b; Naudts et al., 2008; Sahling et al., 2008). However, with video sleds it is not possible to stay on position, to move within small areas, to take samples or to perform measurements at a certain position over longer time. Manned submersibles have the disadvantage that they are commonly very large and require a large ship and specialized crew. By contrast, ROVs are more adapted and have been used extensively in the last decade to study seep areas (Fujikura et al., 1999; Coleman and Ballard, 2001; Hovland, 2002; Orange et al., 2002; Ondréas et al., 2005; Paull et al., 2005; Gay et al., 2006; Sauter et al., 2006; Jerosch et al., 2007; Judd et al., 2007; Olu-Le Roy et al., 2007; Paull et al., 2007; Nikolovska et al., 2008).

In this paper, we present the first ever visual observations of bubble-releasing seeps at the Hikurangi Margin. In 2007, ROV and video-guided deployments enabled us to precisely locate the active methane seeps on the margin, and to perform detailed seafloor observations, measurements and sampling at and around the seeps. Moreover, the use of ROV 'GENESIS' allowed us to investigate short-term temporal variations in seep activity, alternating from almost complete inactivity to violent outbursts, and to estimate bubble-release rates and methane flow rates.

5.2. Study area

The Hikurangi Margin, on the east side of New Zealand's North Island, is an accretionary margin related to the oblique subduction of the Pacific Plate underneath the Australian Plate (Lewis et al., 1998; Barnes et al., 2010) (Fig. 5.1.). Several areas with methane seeps and with bottom-simulating reflections (BSRs) visible on seismic recordings, possibly indicating the presence of gas hydrates, have already been described along this margin (Katz, 1982; Townend, 1997; Henrys et al., 2003; Pecher et al., 2004; Pecher et al., 2005; Faure et al., 2006; Crutchley et al., 2010; Greinert et al., 2010a).

Here, we focus on Rock Garden, which is the southern termination of Ritchie Ridge, as our study area on the Hikurangi Margin, (Figs. 5.1. and 5.2.). Rock Garden is an informal name, given by local fishermen, and refers to its rocky seafloor (Faure et al., 2006). The origin of Rock Garden's flat-topped relief and its uplift is still under debate. The uplift may be related to the subduction of a seamount or to major subduction-related thrust faults, perhaps in relation to gas hydrate dissociation (Pecher et al., 2004; Barnes et al., 2010; Ellis et al., 2010). Gas hydrates are suspected to be present at Rock Garden, even at shallow subsurface depths. This is based on several BSR

observations and a calculated hydrate stability zone (HSZ) for pure methane hydrates, starting at water depths between 630 and 710 m (Pecher et al., 2004; Pecher et al., 2005; Faure et al., 2006; Crutchley et al., 2010; Ellis et al., 2010). However, they have never been sampled in Rock Garden, partially due to its rocky seafloor which makes gravity coring highly difficult. Since the water depth at Rock Garden ranges from -579 to -1100 m, pure methane hydrates are theoretically not stable in the shallowest areas, as is also indicated by BSR pinch outs towards the ridge crest (Pecher et al., 2005; Crutchley et al., 2010). Seismic data indicate the presence of shallow free gas above the base of the gas-hydrate stability zone (BGHSZ) (Fig. 5.2.) (Crutchley et al., 2010). Two such shallow gas occurrences in Rock Garden are associated with the observation on echograms of vertical acoustic anomalies rising from the seafloor into the water column (Crutchley et al., 2010). These anomalies are caused by rising gas bubbles and are hereafter referred to as "flares". These two seep sites, here called "Faure Site" and "LM-3", are the main targets of this study (Lewis and Marshall, 1996; Faure et al., 2006; Crutchley et al., 2010) (Fig. 5.2.).

LM-3, referring to "seep site 3" as described by Lewis and Marshall (1996), is located in the northern part of Rock Garden (Fig. 5.2.). In 1994, fishermen observed a flare on a fish-finder echosounder there and retrieved live bivalves (*Bathymodiolus* sp.) and a small piece

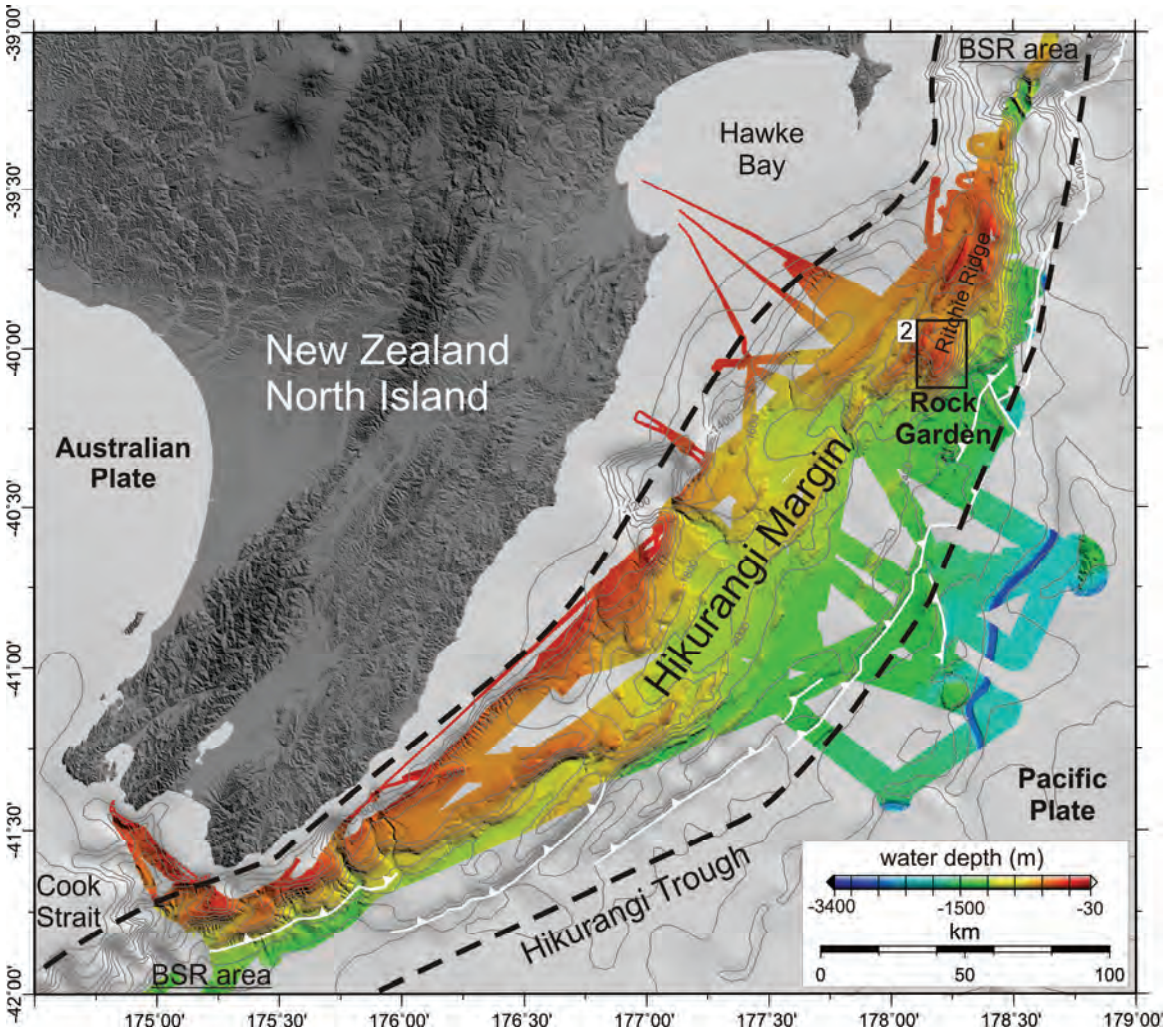

Figure 5.1. Location map of the Hikurangi Margin, east of New Zealand's North Island, with acquired multibeam data (Greinert et al., 2010a) and indication of the area with observed BSRs (black dashed line) and major tectonic features with the white lines indicating the deformation front (Lewis et al., 1998; Henrys et al., 2003; Barnes et al., 2010). Outline for Fig. 5.2. is also given. Land topography is derived from Shuttle Radar Topography Mission (SRTM) data. The bathymetry data is courtesy of NIWA.

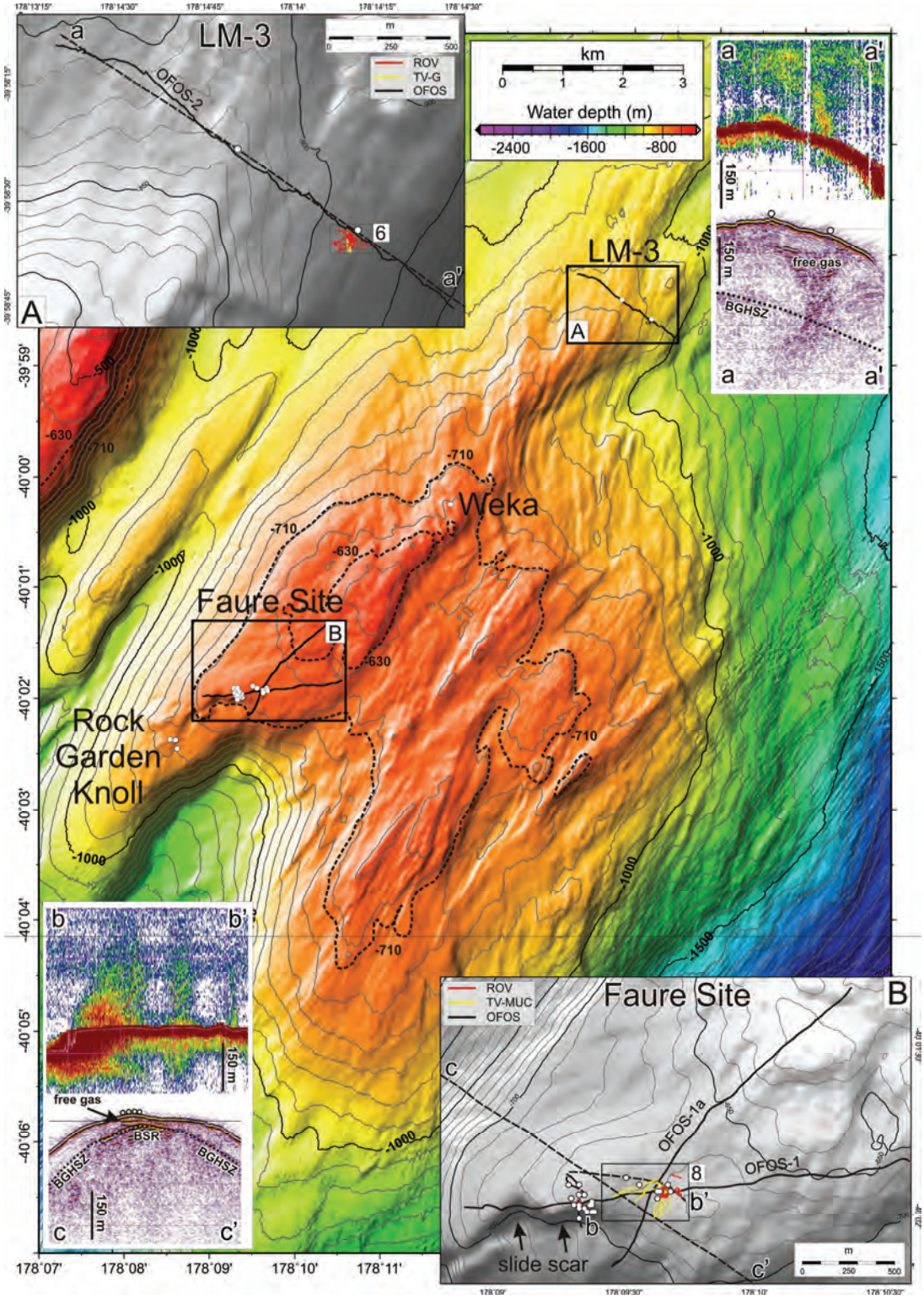

Figure 5.2. Multibeam bathymetry of Rock Garden (30 m grid) with indications of the known seep sites, video tracks (black lines) and acoustic flare locations (white dots) (see Fig. 5.1. for location) (Greinert et al., 2010a). The possible depth limit for the GHSZ is indicated by the -630 m and -710 m isobaths (Faure et al., 2006). **A.** Multibeam bathymetry map of the LM-3 area with indications of ROV (red), TV-G (yellow) and OFOS tracks (black), flares (white dots) and the track line of the echosounder and seismic recordings (**a-a'**) (black dashed line). Outline for Fig. 5.6. is also indicated. **B.** Multibeam bathymetry map of the area around Faure Site with indications of ROV (red), TV-MUC (yellow) and OFOS video tracks (black), flares (white dots) and the track lines of the echosounder (**b-b'**) and seismic recording (**c-c'**) (black dashed lines). Outline for Fig. 5.8. is also indicated.

of carbonate chimney. Subsequent sampling resulted in the retrieval of chemosynthetic fauna (empty vestimentiferan tubes, *Calyptogena* sp. and *Bathymodiolus* sp. valves) as well as the observation of an acoustic flare, rising 250 m above the seafloor (Lewis and Marshall, 1996).

Faure Site, referring to the seep site discovered by Faure et al. (2006), is located in the western part of Rock Garden (Fig. 5.2.). During the 2004 TAN0411 survey, an acoustic flare and a localized geochemical methane anomaly in the water column were observed at this site, near the scarp of a submarine landslide (Pecher et al., 2005; Faure et al., 2006). Pecher et al. (2005) proposed that the submarine landslide is caused by gas-hydrate-induced 'frost heave', driven by fluctuations of bottom-water temperatures and pressures.

In 2006 during the subsequent TAN0607 survey, seismic and single-beam recordings, as well as water sampling confirmed LM-3 and Faure site as active seep sites (Fig. 5.2.) (Crutchley et al., 2010; Faure et al., 2010).

5.3. Methods and data

5.3.1. Single-beam seep detection

Due to the high impedance contrast between water and free gas, gas bubbles rising in the water column can be acoustically detected by means of single-beam echosounder recordings. They show up as "acoustic flares" on echograms (Greinert et al., 2006; Naudts et al., 2006; Artemov et al., 2007). The seep locations in this study, were determined from single-beam echosounder records acquired during two cruises with RV TANGAROA (TAN0607 and TAN0616) in 2006 (Fig. 5.2.). For further information see Greinert et al. (2010).

5.3.2. Multibeam mapping

The multibeam bathymetry and backscatter data were acquired during the SO191 expedition with RV SONNE in January-March 2007 (SIMRAD EM120; 20 kHz) and during two surveys with RV TANGAROA (TAN0607 and TAN0616) in 2006 (SIMRAD EM300; 30 kHz) (Fig. 5.2.). Depending on the size of the displayed area, the grid sizes vary between 150 m to 10 m. Backscatter data processing was done with the FMGeocoder software from IVS3D. For further information about the multibeam mapping see Greinert et al. (2010).

5.3.3. Visual observations

ROV 'GENESIS'

During the SO191-3 expedition seven dives with ROV 'GENESIS' were carried out to localize, to observe, to map and to perform measurements at methane seeps on the Hikurangi Margin. ROV 'GENESIS' is owned and operated by RCMG-UGENT (Renard Centre of Marine Geology - Ghent University). The main focus was Rock Garden, with two dives at LM-3 (Lewis and Marshall, 1996) and four dives in the vicinity of Faure Site (Faure et al., 2006). The ROV is a sub-Atlantic CHEROKEE ROV that was operated in TMS (Tether Management System) mode. The TMS is a metal frame that contains the ROV during the descent to the ocean floor and a cable of 200 m (tether). The ROV was equipped with a forward-looking color video camera, a black-and-white video camera and one backward-looking black-and-white video camera. For object detection (e.g. bubbles) a forward-looking 'Super Seeking Sonar System' (325 or 675 kHz) was used. Accurate positioning and navigation of the ROV was achieved through the use of an USBL (ultra-short baseline) positioning system, consisting of a ship-mounted IXSEA GAPS and a ROV-mounted IXSEA transponder. The OFOP (Ocean Floor Observation Protocol) software package was used to navigate the ROV, store ROV parameters and make preliminary seafloor characterization in real time (Huetten and Greinert, 2008). OFOP was also used for post-cruise navigation processing, video replay and seafloor characterization. At Faure Site, 1385 m of ROV video tracks were recorded during 4h18' of effective survey time. At LM-3, 2213 m of ROV video tracks were recorded in 3h23'.

OFOS, TV-MUC and TV-G

In addition to the video records from the ROV, visual seafloor observations also were acquired with an OFOS (Ocean Floor Observation System) video sled, a TV-MUC (TV-guided multi-corer) and a TV-G (TV-guided grab). The OFOS was equipped with downward-looking color and monochrome CCD (charge-coupled device) video cameras, a 4 megapixel stills camera and a memory CTD (conductivity-temperature-depth sensor). The scale of the images, as well as the height of OFOS above the seafloor, was visually indicated by an array of three red lasers. The distance between the two outer lasers is 20 cm. The TV-MUC and TV-G are sediment sampling devices that both use a camera for real-time selection of sampling sites. Positioning and navigation of OFOS, TV-MUC and TV-G was done by either a SIMRAD DHT 163 system, or one of the two IXSEA systems (POSIDONIA or a GAPS), depending on availability during the cruise. The OFOP software package was used in a similar way as for the ROV dives. Mosaics of video sequences were made with IFREMER's ADELIE software package.

5.3.4. Measurements of physical properties

The ROV also was equipped with a stand-alone memory FSI CTD, a NKE THP (THermoProbe) temperature sensor and two Niskin bottles. The CTD was mounted on the ROV at ca. 50 cm from the base of the ROV, while the THP temperature sensor was operated using the manipulator arm in order to allow penetration within the sediments. The temperatures measured with the CTD and the THP sensors have accuracies of 0.002°C and 0.007°C, respectively. Water samples from the Niskin bottles were used to obtain dissolved methane concentrations and $\delta^{13}C_{CH_4}$ values (Faure et al., 2010).

5.4. Observations and results

5.4.1. Regional seafloor observations

5.4.1.1. Northern Rock Garden: LM-3

During OFOS-2 video survey, the northern extent of Rock Garden was surveyed in NW-SE direction, hereby crossing the LM-3 site (Figs. 5.2.A. and 5.3.). The seafloor is generally hard and covered by a thin drape of bioturbated hemipelagic sediments, alternating with soft-sediment areas, boulders and rocky outcrops (Figs. 5.3. and 5.4.). The seafloor on the western flank of the NE-SW trending ridge is often covered by deep-water coral rubble (Figs. 5.2. and 5.4.C.). Trawl marks are visible as linear features in areas shallower than -900 m water depth (Fig. 5.3.). LM-3, located on the east side of the ridge, is a very small area consisting of a platform-like structure, composed of authigenic carbonate rocks, within an area of softer sediments covered by shell fragments (*Calyptogena* sp.) (Figs. 5.3. and 5.4.A.-B.) (Campbell et al., 2010). The area around the platform-like structure is the only area in which dense fields of shell fragments (*Calyptogena* sp.) were observed, sometimes in association with scattered dead bivalves (*Bathymodiolus* sp.) and/or vestimentiferan tubeworms (*Lamellibrachia* sp.) (Fig. 5.3.). Live *Bathymodiolus* sp. bivalves were only observed on top of the platform (Figs. 5.3.C. and 5.4.A.). No bubble-releasing seeps were observed during OFOS-2 survey.

5.4.1.2. Western Rock Garden: Faure Site

During OFOS-1 and OFOS-1a video surveys, the western extent of Rock Garden was surveyed in W-E and NE-SW directions respectively, thereby crossing Faure Site (Figs. 5.2.B. and 5.5.). The seafloor generally consists of bioturbated soft sediments alternating with small buildup, platform-like features or outcrops (Figs. 5.4D-F and 5.5.). The elevated areas are rockier with boulders and rocky outcrops, often in association with coral rubble (Figs. 5.4.F.-H. and 5.5.). *Calyptogena* sp. shell fragments are widespread, but no live clams or mussels were observed. At Faure Site, the seafloor morphology is relatively uniform with large platform-like structures in the western part of the investigated area. These structures are associated with vestimentiferan tubeworms

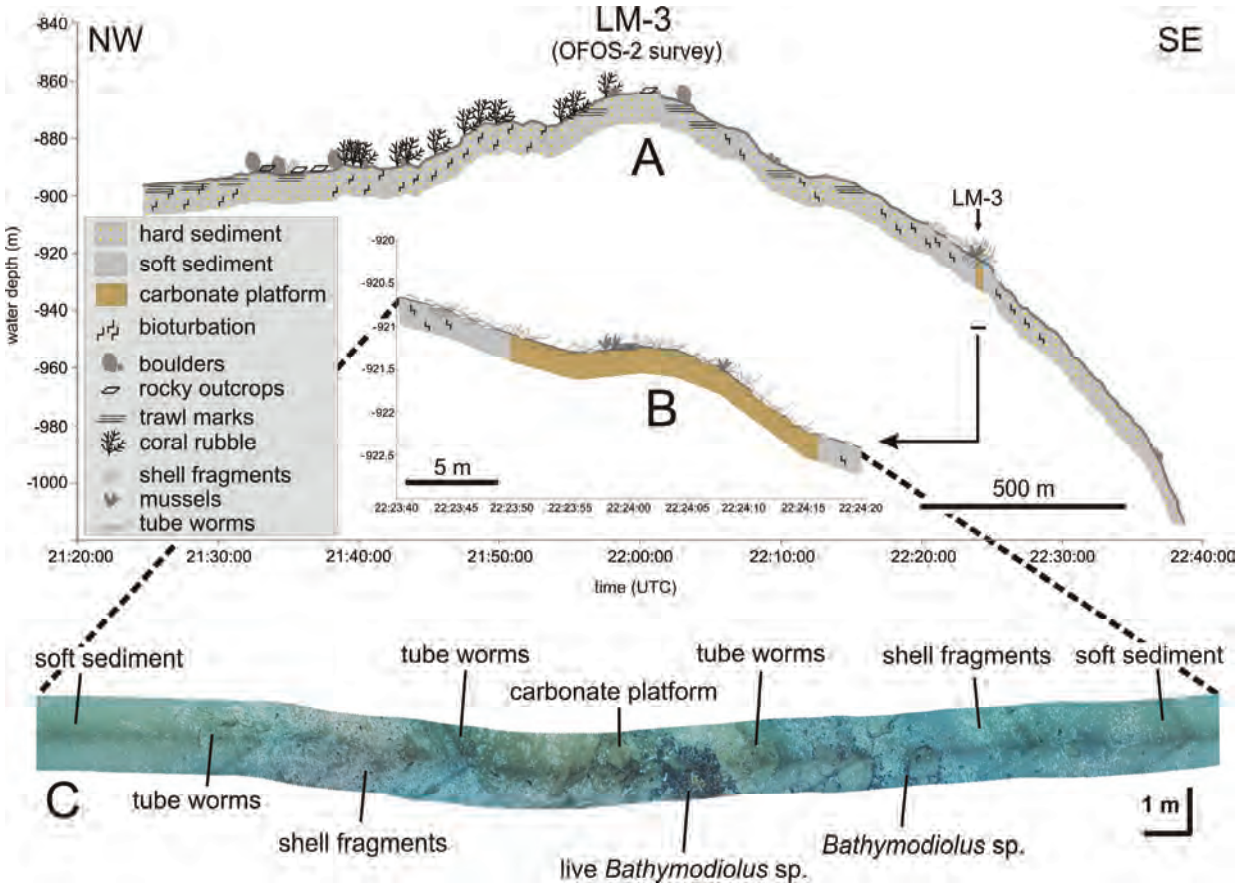

Figure 5.3. A. Seafloor observations along NW-SE orientated OFOS-2 track over the northern part of Rock Garden, crossing the LM-3 site (for location see Fig. 5.2.). **B.** Zoom of the OFOS-2 track over the LM-3 site. **C.** Video mosaic created with ADELIE software from the OFOS-2 video sequence over the LM-3 site. Video mosaic shown in C corresponds to the track shown in B.

(*Lamellibrachia sp*.) and sometimes with great amounts of shell fragments (*Calyptogena sp.*) (Figs. 5.4.E. and 5.5.A.). This area forms the transition to a slide scarp, with rocky outcrops and occurrences of coral rubble and shell fragments (Figs. 5.2., 5.4.H. and 5.5.A.). No bubbling seeps were observed during OFOS-1 and OFOS-1a surveys.

5.4.2. Local seafloor observations

5.4.2.1. LM-3

Based on the regional reconnaissance during OFOS-2 survey, an area was selected for local seafloor observations during ROV-4 and ROV-5 dives, and subsequent sampling during TV-G-17 survey at LM-3 (Figs. 5.2. and 5.6.). The 10,000 m^2 area surveyed with the ROV generally consists of bioturbated sandy sediments covered by shell fragments (*Calyptogena* sp.) surrounding the platform-like structure (Figs. 5.6. and 5.7.). The platform has an extent of 100 m^2 and consists of large blocks, which form a pavement-like structure with a distinct positive relief (Figs. 5.6.B. and 5.7.A.-C.). The cracks in between the large blocks are filled with live *Bathymodiolus* sp. mussels, live *Lamellibrachia* sp. tubeworms and some *Calyptogena* sp. shells. The live *Bathymodiolus* sp. mussels only occur on top of the platform, whereas *Calyptogena* sp. shell hashes occur in the depressions surrounding the platform (Figs. 5.6.C.-E. and 5.7.A.-C. and 5.7.E.). Small sponges and soft-tissue corals also cover the top of the platform (Figs. 5.6.F. and 5.7.A.-C.). The multibeam bathymetry shows that the platform occurs on the transition from a flat (ca. 1 %) to a steeper (ca. 10 %) sloping seafloor (Fig. 5.6.A.). This

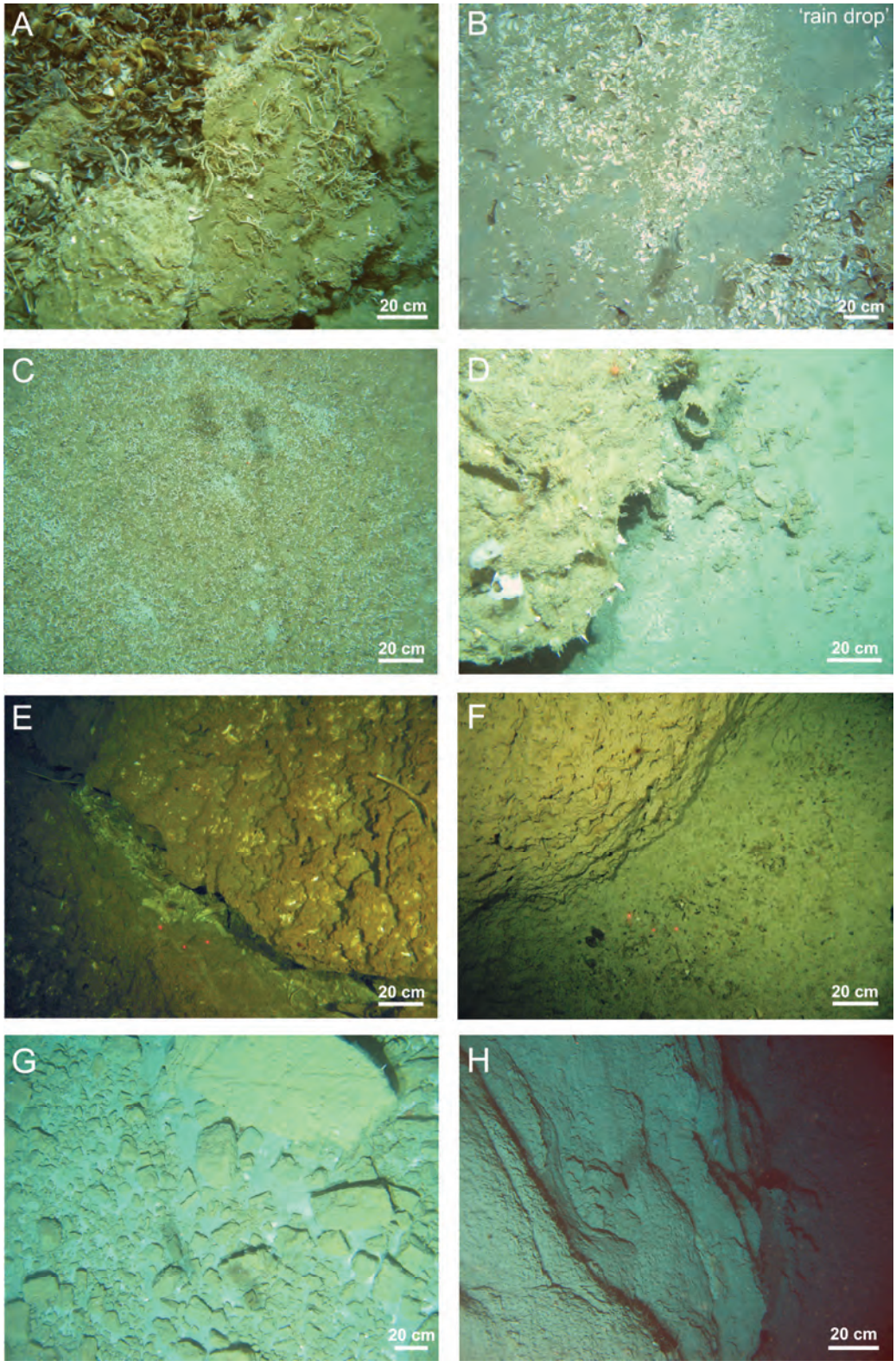

Figure 5.4. Stills taken during the OFOS video tracks shown in Figs. 5.2., 5.3. and 5.5. as a characterization of the seafloor in Rock Garden. **A.** Authigenic carbonate platform with live *Bathymodiolus* sp. mussels at LM-3. **B.** *Calyptogena* sp. shell hash with some *Bathymodiolus* sp. mussels at the LM-3 site. The darker patch referred to as 'rain drop site' is an area with ampheretid polychaetes (Sommer et al., 2010). **C.** Coral rubble. **D.** Chemoherm and bioturbated soft sediments. **E.** Presumed carbonate platform with *Calyptogena* sp. shells and a tubeworm from the area west of the Faure Site. **F.** Semi-indurated outcrops at the Faure Site. **G.** Boulders **H.** Rocky outcrop from the slide scarp west of the Faure Site.

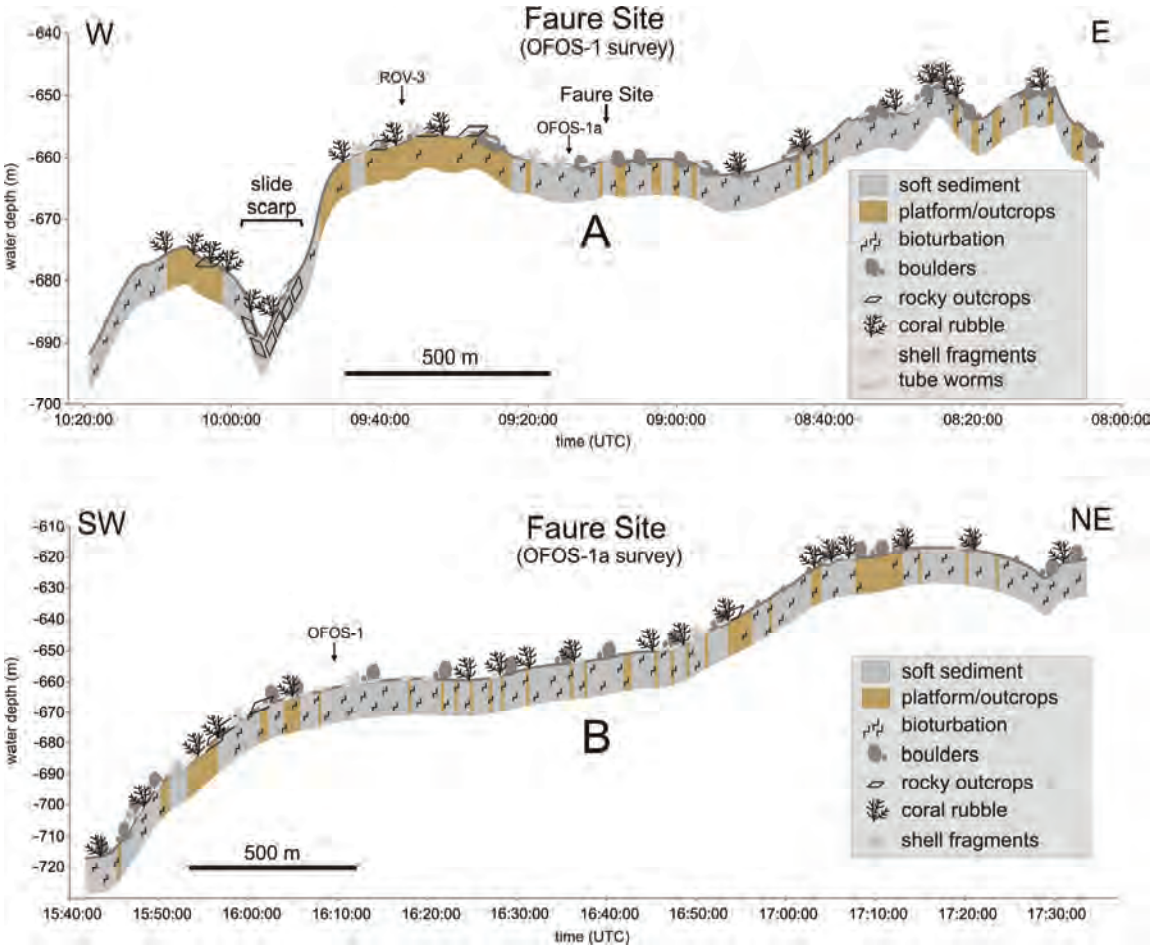

Figure 5.5. A. Seafloor observations along W-E orientated OFOS-1 track over the western part of Rock Garden, crossing Faure Site (for location see Fig. 5.2.). **B.** Seafloor observations along NE-SW orientated OFOS-1a track over the western part of Rock Garden, crossing Faure Site (for location see Fig. 5.2.). The crossing point of the two tracks is indicated in A and B.

transition is associated with one of the major thrust faults in Rock Garden (Fig. 5.2.) (Barnes et al., 2010). The platform location also corresponds to a patch of high-backscatter seen in the multibeam-backscatter data (Figs. 5.6.B.-F.). During ROV-4 and TV-G-17 surveys bubble release was observed at two sites south of this platform, just at the border of the high-backscatter area (Figs. 5.6.B.-F. and 5.7.E.-F.). Between these two active seep sites and close to a *Calyptogena* sp. shell hash, a peculiar spotted micromorphology is present, referred to as 'rain drop site' (Figs. 5.4.B. and 5.6.C.-F.). The name 'rain drop site' refers to the characteristic seafloor appearance of a polychaete bed (Sommer et al., 2010). Sampling shows that the seafloor sediments from this area are densely populated by ampheretid polychaetes which form small, crater-like depressions in the seafloor. The bubble-releasing seep site observed during ROV-4 dive is located closest to the platform, in between *Calyptogena* sp. shell hashes, and consists of a single bubble-releasing outlet (Figs. 5.6. and 5.7.E.). The seep site observed during TV-G-17 survey is located further away from the platform and consists of 5 different bubble-releasing outlets. Here bubbles are released from sandy sediments covered by a small amount of shell fragments (Figs. 5.6. and 5.7.F.). These observations agree with the general perception that the seafloor further away from the platform is covered with smaller amounts of shell fragments (*Calyptogena* sp.). At about 100 m from the platform, the seafloor also changes from soft and sandy to hard and sediment-starved. Within the soft sandy area,

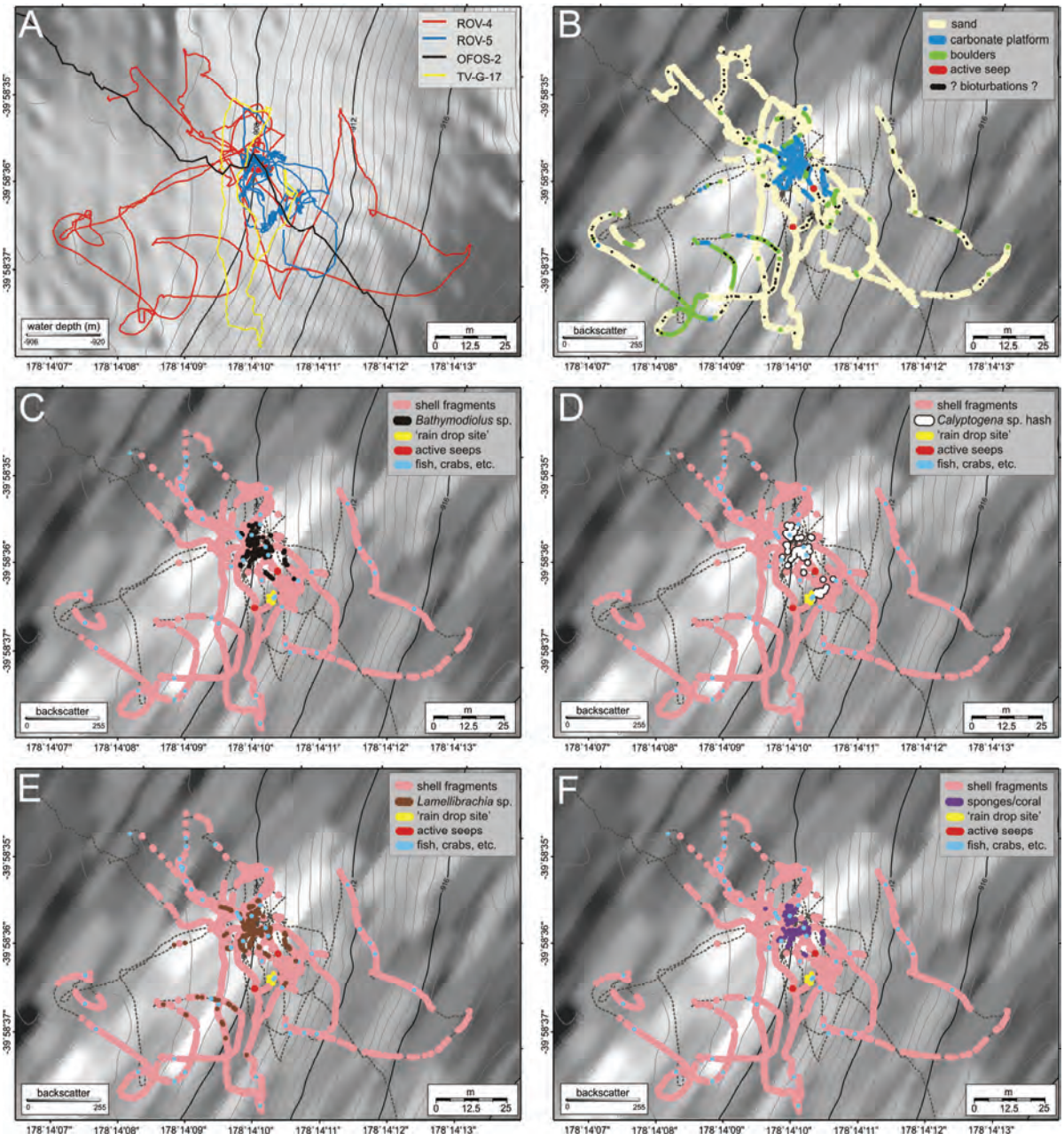

Figure 5.6. Seafloor observation maps at the LM-3 site. **A.** Multibeam bathymetry map with the ROV, OFOS and TV-G tracks. **B.** Sediment-type distribution. **C.** *Bathymodiolus* sp. distribution within the fauna distribution **D.** *Calyptogena* sp. shell hash distribution within the fauna distribution. **E.** *Lamellibrachia* sp. distribution within the fauna distribution. **F.** Distribution of sponges and soft tissue corals within the fauna distribution. B-F have multibeam backscatter as background.

several large depressions occur (dm-scale), which clearly differ from the small holes (cm-scale) generally attributed to bioturbation (see difference between Figs. 5.4.D. and 5.7.D.). These large depressions are often accompanied by small hills, giving a hummocky appearance to the seafloor. No bubble release was observed from these depressions at LM-3.

5.4.2.2. Faure Site

Based on Faure et al. (2006) and the single-beam seep detection performed during the TAN0607 cruise in 2006, the Faure Site was studied during the ROV-2, ROV-3, ROV-6 and ROV-7 dives. The first dive (ROV-2) resulted in the first ever visual observation of bubble-releasing seeps at the Hikurangi Margin and in

the subsequent ROV, TV-MUC and lander deployments (Figs. 5.8. and 5.9.). The 20,000 m^2 area surveyed with the ROV generally consists of bioturbated sandy sediments alternating with strongly eroded outcrops (Figs. 5.8.B. and 5.9.A.-C.). These outcrops stand a couple of decimeters in relief and are semi-indurated, which made it impossible to sample them with the ROV's claw, and to determine their nature (Figs. 5.9.A.-B.). Shallow subsurface presence of the rock formations was confirmed by the observations made during ROV-6, which showed that the

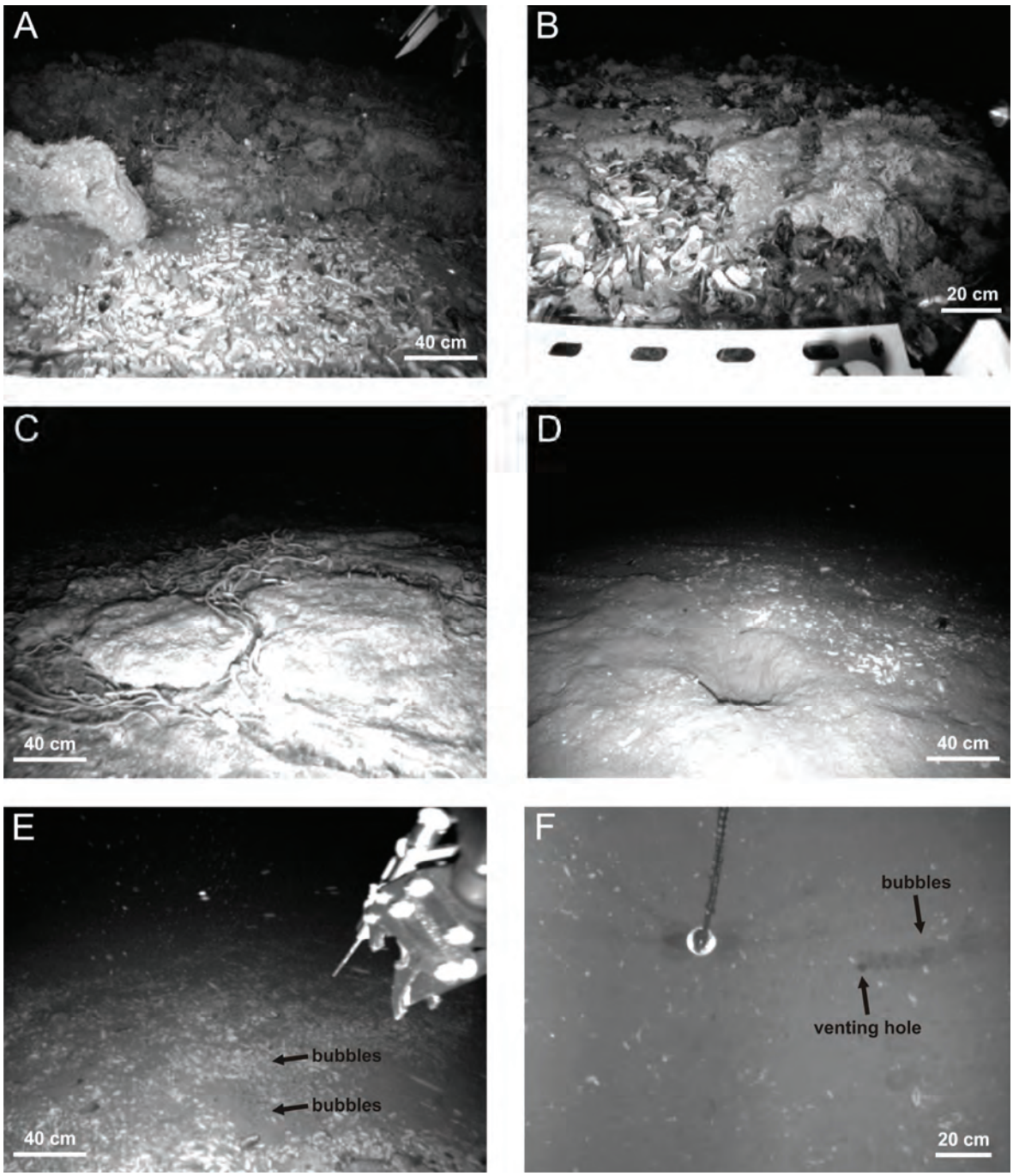

Figure 5.7. Stills taken from ROV-4, ROV-5 and TV-G-17 deployments at LM-3. **A.** Side view of the authigenic carbonate platform surrounded by a *Calyptogena* sp. hash. **B.** Top of the carbonate platform with live *Bathymodiolus* sp. mussels. **C.** Side view of the carbonate platform with abundant *Lamellibrachia* sp. tubeworms. **D.** One of the multiple depressions/bioturbations observed at LM-3. **E.** Bubbling seep observed in-between shell hashes during ROV-4. **F.** Bubbling seep observed during TV-G-17.

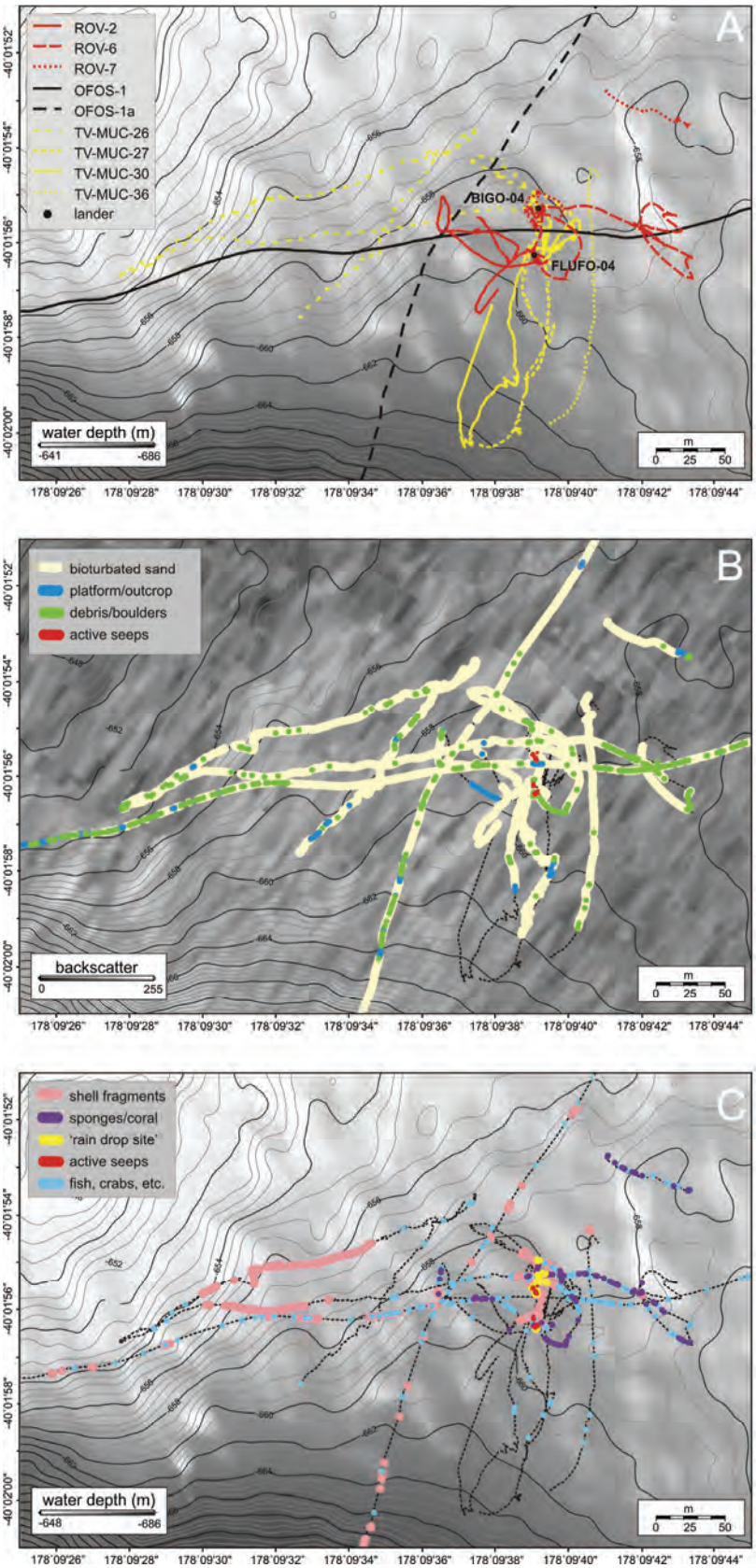

Figure 5.8. Seafloor observation maps at Faure Site with multibeam bathymetry (A and C) or backscatter (B) as background. **A.** Overview of the BIGO-04 and FLUFO-04 lander positions and ROV, OFOS and TV-MUC tracks. **B.** Sediment-type distribution**. C.** Fauna distribution.

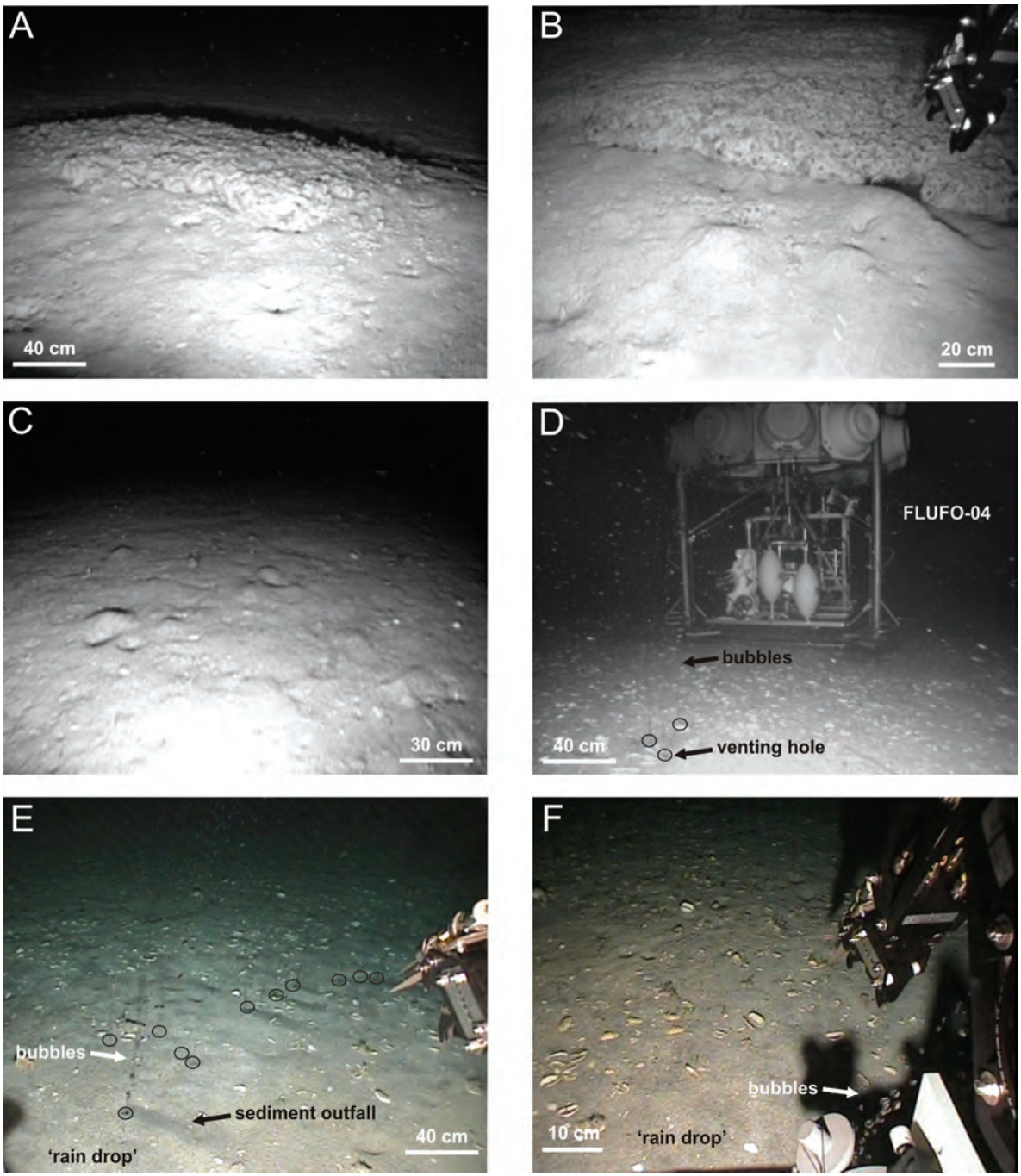

Figure 5.9. Stills taken from ROV deployments at Faure Site. **A.** Side view of a strongly eroded outcrop. **B.** Close-up of the transition between the bioturbated sandy sediments and the outcrop shown in Fig. 5.9A. **C.** Bioturbated sandy sediments with depression-hill morphology. **D.** BIGO-04 lander visited during ROV-6 dive with in front bubble-releasing seeps. **E.** Alignment of bubble-releasing outlets at a 'rain drop site'. **F.** Bottom-water sampling at one of the active seeps seen in Fig. 5.9.E.

sediment chambers from both landers were only able to penetrate 11 cm into the sediment causing both landers to be tilted (Fig. 5.9.D.) (Linke et al., 2010). But again no rock samples could be taken for analysis. The depression-and-hill morphology, as seen at LM-3, is also very common at Faure Site (Figs. 5.9.A.-C.). Shell fragments (*Calyptogena* sp.) are not widespread but are abundant around the active seep sites (red dots in Fig. 5.8.) and in the area west of this site (Fig. 5.8.C.). Sessile fauna (corals, sponges) are abundant just east of the seep sites, at

locations with boulders or rock debris. During all three ROV dives, bubble-releasing seeps were observed at Faure Site. The two main seep areas, ca. 20 m apart, were characterized by the occurrence of ampheretid polychaetes ('rain drop sites') and *Calyptogena* sp. shell fragments (Figs. 5.8.C. and 5.9.D.-F.). Bubble release occurs from differently sized depressions which are often aligned in NW-SE direction; the largest depression observed, was 50 cm in diameter and 15 cm deep (Figs. 5.10.C.-D.). Observations made during ROV-2 and ROV-7 clearly show that these depressions are formed by the often violent release of bubbles. These bubbles entrain sediment particles, which then get carried away by the water currents, creating the depressions and a sediment outfall away from the venting holes (Figs. 5.9.E. and 5.10.C.-D.). No active seeps were observed during the ROV-3 dive within the area near the top of the slide scarp where abundant flares were observed on echosounder recordings obtained during the TAN0616 cruise in 2006 (Fig. 5.2.B.). Nevertheless, the seafloor in this area is characterized by the widespread occurrence of platform-like structures or outcrops of presumably carbonate rocks, which are sometimes covered by *Calyptogena* sp. shell fragments and *Lamellibrachia* sp. tubeworms (Fig. 5.4.E.).

5.4.2.3. Methane bubble-release rates

Based on ROV video observations, we estimate the amount of methane released by bubbles at the different seep sites. At LM-3, the observation time was too short to approximate the size and the amount of the released bubbles. At Faure Site, 39 different bubbling seeps/outlets could be observed in detail for up to 20 minutes per observation. These seeps are arranged in three main seep clusters located in two seep areas 20 m apart (red dots in Figs. 5.8.B.-C. and 5.10.E.). During ROV-2 dive, bubble release was observed from 13 outlets in five depressions over a period of 20'39" (Fig. 5.10.). During this period, bubble-release rates and bubble sizes were highly variable over time and space, with periods of low activity (i.e. 16 bubbles per second for bubbles of 6 mm diameter), alternating with periods of violent outburst (i.e. up to 190 bubbles per second for bubbles of 9 mm diameter) (Fig. 5.10.). In total, six outbursts were observed, each starting violently and diminishing after 43 to 89 seconds (Fig. 5.10.). Periods between the outbursts varied from 125 to 159 seconds. During one of the outbursts seen in the ROV-2 dive (lasting 43 seconds with bubbles of 9 mm diameter), an in situ flow rate of 2.424 liter per minute was estimated, corresponding to a mole flow rate of 7.019 mol of methane per minute, for in situ conditions of 7°C and 67.45 bar (Fig. 5.10.). During the following period of low activity (6 mm bubble), the flow rate was 0.163 liter per minute, corresponding to 0.473 mol of methane per minute. During the ROV-6 dive, the latter seep cluster at Faure Site was revisited, i.e. southern seep area near FLUFO-4 (Figs. 5.8. and 5.9.). However, no outbursts were observed during this dive, only changes in bubble-release rates and patterns over a period of 16'54" (Figs. 5.10. ROV-6B and ROV-6B'). Within this period, bubble rates were constant for at least 9'26" at ca. 5 Hz (two outlets), changing to ca. 22 Hz for 6'14" (three outlets), before returning to 5 Hz (one outlet). Within the southern seep area a new seep cluster, consisting of three outlets, was found 5 m north of the previous cluster which was bubbling constantly during the 22'57" of observation (Figs. 5.8., 5.9.D. and 5.10. ROV-6A). During ROV-7, more than 23 bubbling seeps were observed in one seep cluster, which constituted a new seep area 20 m to the north of the seep area observed during ROV-2 and ROV-6 (Fig. 5.10.E.). During a THP sediment-temperature measurement at a 'rain drop site', no bubbles were observed during 5'24". Hereafter bubble release started and intensified from one outlet to over 23 outlets with increasing bubble rates and sizes (Figs. 5.9.E.-F., Figs. 5.10. ROV-7A and ROV-7A'). Overall bubble release from single outlets displayed a variety of patterns, from constant single-bubble trains over dual or triple bubble release, to multiple bubble release during outbursts. The bubble patterns not only changed during the period of observation, but could be different for two outlets in the same cluster, even if the outlets were only a few centimeters apart.

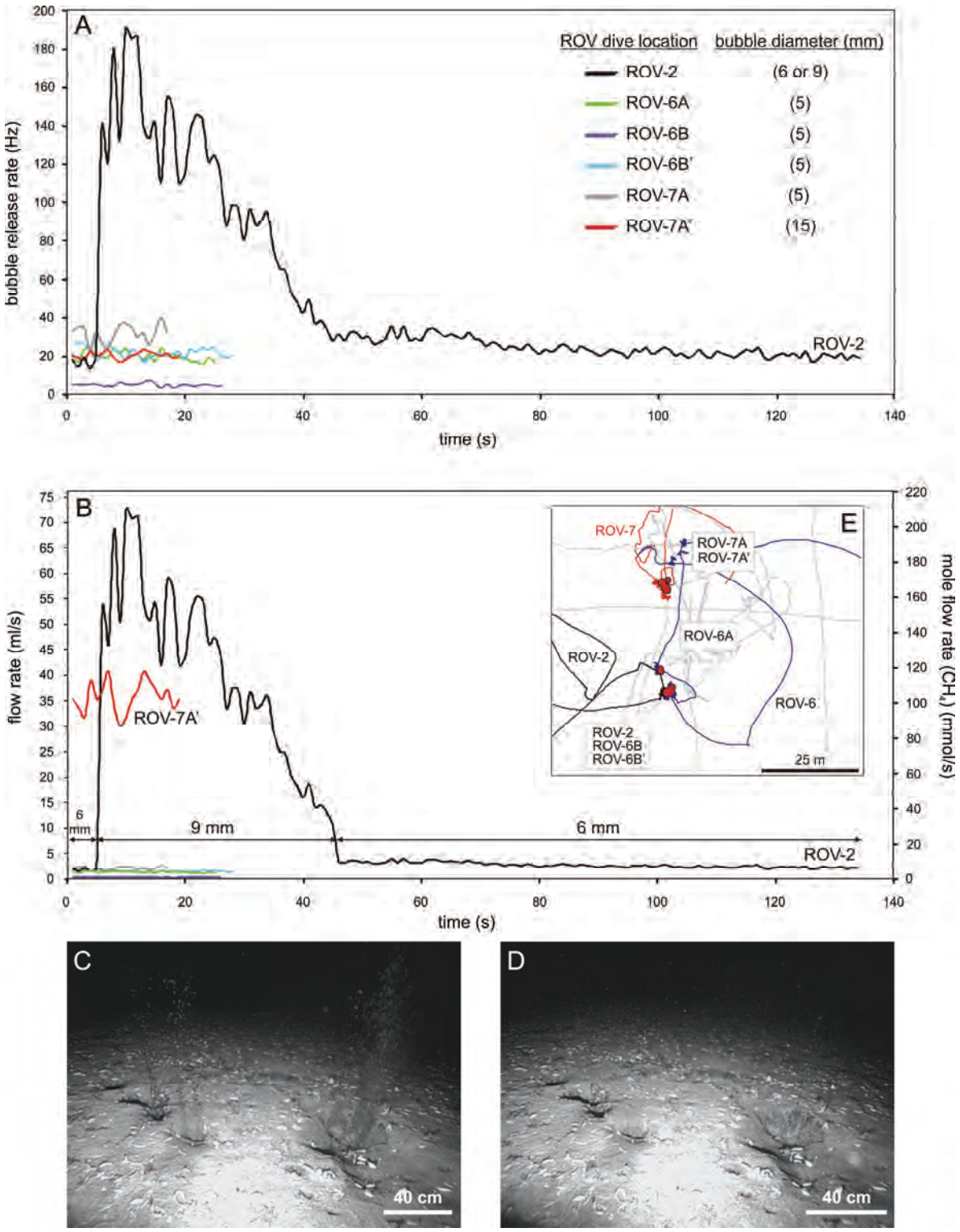

Figure 5.10. A. Bubble-release rates at Faure Site observed during the different ROV dives. The assumed bubble size is also indicated between brackets. **B.** Flow rates and mole flow rates estimated for methane bubbles and based on bubble sizes and release rates given in Fig. 5.10A. Flow rate and mole flow rate (for methane) based on the bubble sizes and release rates given in A. During ROV-2 dive, bubbles sizes were ca. 9 mm and 6 mm, during the outbursts and the regular periods respectively. **C.** Still from ROV-2 during an outburst. **D.** Still from ROV-2 during a regular period. **E.** Schematic map showing the dive tracks, seep locations (red dots) and the locations of seep observation.

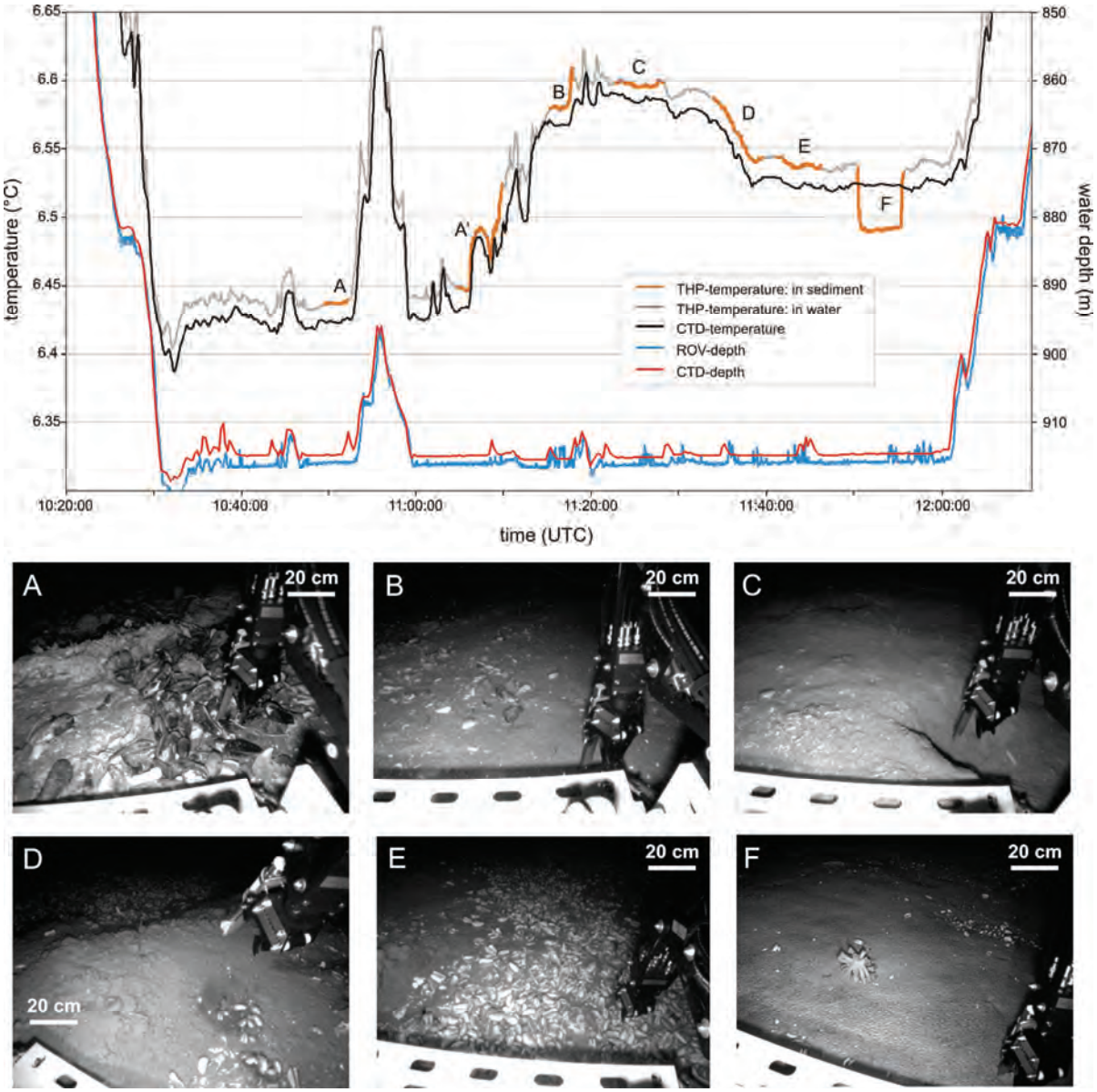

Figure 5.11. Bottom-water and sediment temperature measured during ROV-5 at LM-3. Stills A to F show the different locations where sediment temperatures were measured with the ROV-mounted THP sensor. **A-A'.** Top of the platform, in a live *Bathymodiolus* sp. bed. **B.** Sandy seafloor with *Calyptogena* sp. shell fragments. **C.** Depression with a depth of ca. 20 cm. **D.** Dark reduced sediment on a hill feature. **E.** *Calyptogena* sp. shell hash **F.** A 'Rain drop site' with ampheretid polychaetes (Sommer et al., 2010). This location was characterized by a negative sediment-temperature anomaly (see graph Fig. 5.11.).

5.4.3. Thermal measurements

Bottom-water and sediment temperature measurements were performed with a ROV-mounted CTD and THP sensor during the ROV-5, ROV-6 and ROV-7 dives. At Faure Site, during ROV-6 and ROV-7, temperatures at the seafloor fluctuated between 6.814°C and 6.909°C and between 7.170°C and 7.120°C, respectively, for water depths of ca. -663 m (ROV depth at the seafloor). At LM-3, temperatures ranged from 6.437°C to 6.598°C at ca. -915 m water depth (ROV depth at the seafloor). These temperature fluctuations were long-term (i.e. 0.5-1.5 hour) and appeared to be unrelated to the location and/or movement of the ROV (Fig. 5.11.). Moreover, there was little or no difference between the bottom-water temperatures measured with the CTD and the sediment

temperatures measured with the THP sensor (Fig. 5.11.). It was only during ROV-5 dive, at a 'rain drop site' at LM-3, that a negative sediment-temperature anomaly of ca. 0.05°C was measured in comparison with near-bottom water temperature recorded with the CTD (Fig. 5.11.). This difference in temperature is much larger than the CTD's and THP's accuracies, 0.002°C and 0.007°C respectively.

5.5. Discussion

5.5.1. Differences in seep environment: diffusive versus bubble-released methane

Based on our visual observations, Faure Site and LM-3 seem to portray different seep environments and distinct past/current seep activity; nevertheless they also bear some resemblances. Both seep areas are local features, where bubble release occurs in bioturbated sandy sediments covered by dead *Calyptogena* sp. shells, and both are associated with ampheretid polychaetes near the bubble-releasing locations (Sommer et al., 2010) (Figs. 5.3.-5.11.). The seafloor at the LM-3 strongly differs from the rocky environment generally observed in the Northern Rock Garden area, whereas Faure Site rather blends in with the Western Rock Garden surroundings (Figs. 5.3. and 5.5.).

The major differences between both seep environments are:

- the presence of a relatively large (100 m^2) platform-like structure composed of methane-derived carbonate (Campbell et al., 2010) associated with live methane-related megafauna (*Bathymodiolus* sp. mussels and *Lamellibrachia* sp. tubeworms) and seemingly marginal bubble release at LM-3 (Figs. 5.3., 5.6. and 5.7.);
- a very prominent bubble release, the absence of live methane-related megafauna and the presence of semi-indurated and strongly bioturbated/eroded outcrops at Faure Site (Figs. 5.5., 5.8. and 5.9.).

Based on these observations, we suggest that the differences observed between the two seep environments result from different methane release mechanisms: diffusive at LM-3 and mainly by bubble release at Faure Site.

The strong diffusive methane supply at LM-3 is clear from the presence of *Bathymodiolus* sp. mussels and *Lamellibrachia* sp. tubeworms, which are symbiont-bearing megafauna that strongly depend on a supply of dissolved methane or related sulfide (Brooks et al., 1987; Cary et al., 1988; Van Dover et al., 2003; Olu-Le Roy et al., 2004; Gay et al., 2006; Thurber et al., 2010). As this megafauna is located on a platform-like structure of methane-derived carbonate, which results from anaerobic oxidation of dissolved methane (AOM) (Campbell et al., 2010), a long-term, strong, diffusive input of methane into the seafloor sediments at LM-3 can be inferred (Hovland et al., 1985; Paull et al., 1992; Peckmann et al., 2001; Greinert et al., 2002a; Orange et al., 2002; Johnson et al., 2003; Pape et al., 2005; Mazzini et al., 2006; Judd and Hovland, 2007). This inference is sustained by the very high methane concentrations of 16542 nM, measured in water samples collected by the ROV ca. 50 cm above a field of live *Bathymodiolus* sp. mussels at the top of the carbonate platform (Faure et al., 2010). The concentric arrangement of the different habitats in this seep site, with high methane concentration and methane-depending megafauna surrounded by sulfide-depending megafauna, is very similar to seep areas observed in e.g. the Lower Congo Basin (Fig. 5.6) (Gay et al., 2006).

At Faure Site, visual observations have shown that bubble release is the dominant, albeit highly variable, methane-releasing process. The absence of fresh authigenic carbonate structures with live, methane-related megafauna also points to a bubble-release-controlled fluid system with very limited diffusive methane venting. The dominance of the bubble-transport mechanism is further sustained by high dissolved methane concentrations (up to 3500 nM) taken at ca. 10 m above the seafloor (Faure et al., 2010). These are the highest concentrations for all water samples taken from CTD casts at the Hikurangi Margin. These high methane concentrations so

high in the water column can only be achieved through methane bubble release, as dissolved methane would most likely be consumed very effectively in the shallow seafloor sediments and bottom waters by anaerobic and aerobic oxidation (Boetius et al., 2000; Boetius and Suess, 2004; Sommer et al., 2006).

The presence of such a 'benthic filter' for the transfer of dissolved methane from the sediments and bottom waters to the water column is very clear at LM-3. It explains the discrepancy between the very high methane concentrations of 16542 nM, obtained from water samples collected by the ROV just above the seafloor and the 'low' methane concentration of maximum 90 nM, measured in water samples taken during CTD casts only a few meters above the seafloor (Faure et al., 2010). This pattern again indicates that methane release at LM-3 is mainly diffusive and release of methane by bubbles is rather insignificant.

The discussed difference in type of methane release between LM-3 and Faure Site, diffusive- versus bubble-released methane respectively, does not seem to influence the presence of ampheretid polychaetes ('rain drop sites') and suberitid sponges, which are live, seep-related fauna found at both seep sites (Campbell et al., 2010; Sommer et al., 2010; Thurber et al., 2010). The heterotrophic polychaetes mainly depend on aerobic oxidation of methane (AeOM) and do not seem to depend on strong AOM. The ampheretid polychaete beds together with the suberitid sponges seem to act as ecosystem engineers, which facilitate the transition from a soft sediment environment with mainly bubble release to a hard substrate seep environment with associated fauna where AOM and diffusive methane transport prevail (Sommer et al., 2010; Thurber et al., 2010).

The transport by large amounts of deep-derived fluids seems negligible at both sites since the sediment temperatures measurements were always comparable with the near-bottom water temperatures. At one 'rain drop site' at LM-3, a negative sediment temperature anomaly was measured. Colder sediment temperature in comparison with the near-bottom water temperature is opposite to what is expected at seepage sites. The negative temperature anomaly can be explained as a remnant of cold water infiltration induced by earlier gas bubble release through a process of recharge, as discussed by Poort et al. (2007). This could be plausible, since near-bottom water temperatures were indeed similar or colder in comparison to the anomalous sediment temperature measurements, ca. 40 minutes before the anomalous measurement (Fig. 5.11.). The fact that this temperature anomaly was observed at a 'rain drop site' (and not in nearby measurements) suggests a relation with this specific habitat (Fig. 5.11.) (Sommer et al., 2010). However, no temperature anomalies were observed at other 'rain drop sites' at Faure Site during ROV-6 and ROV-7. It is unclear whether the absence of such a negative sediment-temperature anomaly at the 'rain drop sites' at Faure Site could be related to differences in bubble-release rates in comparison with LM-3.

5.5.2. Temporal variations in bubble-release activity

Previous studies of bubble-release activity in seep areas have shown that bubble release is highly variable, both in space and in time (Table 5.1) (Torres et al., 2002; Leifer and MacDonald, 2003; Greinert et al., 2006; Sauter et al., 2006; Nikolovska et al., 2008; Greinert et al., 2010b). Our ROV observations at the Hikurangi Margin confirm this general observation. During the three ROV dives at Faure Site, bubble release from three seep clusters was visually monitored over a total time of 80'31". Estimated bubble rates from single outlets ranged from 5 to 190 bubbles per second with bubble sizes ranging from 5 mm to over 15 mm. This results in average flow rates of 0.018 to 2.424 liter of methane per minute, which corresponds to mole flow rates of 0.053 to 7.019 mol per minute at in situ conditions of 7°C and 67.45 bar (Table 5.1.). These values are comparable to published data from other seeps around the world (Table 5.1.), although our bubble-size estimations were only based on ROV video footage. Compared to these other sites, the vent site monitored during ROV-2, ROV-6B and ROV-6B' dives at Faure Site can be regarded

Location	Seep cluster	Bubble-release rate (Hz)	Bubble size (mm)	Flow rate per outlet (l/minute)	Mole flow rate per outlet (mol/minute)	Outlets
Pacific Ocean Rock Garden Faure Site	ROV-2	24	6	0.163	0.473	7
Pacific Ocean Rock Garden Faure Site	ROV-2	106	9	2.424	7.019	13
Pacific Ocean Rock Garden Faure Site	ROV-6A	20	5	0.078	0.227	3
Pacific Ocean Rock Garden Faure Site	ROV-6B	5	5	0.018	0.053	1
Pacific Ocean Rock Garden Faure Site	ROV-6B'	22	5	0.084	0.242	2
Pacific Ocean Rock Garden Faure Site	ROV-7A	32	5	0.125	0.361	>23
Pacific Ocean Rock Garden Faure Site	ROV-7A'	20	15	2.152	6.232	>23
Black Sea, Dnepr paleo delta (Greinert et al., 2010b)	shelf	36	2-16	0.033-0.0864	0.03	2709
Black Sea, Kobuleti Ridge (Nikolovska et al., 2008)	Batumi seep	Not stated	2-5	0.01-5.5	0.037-20.5	10
Gulf of Mexico (Leifer and MacDonald, 2003)	Bush Hill	Not stated	1-20	0.213-1.32	0.453-3.192	2
Atlantic Ocean Håkon Mosby Mud Volcano (Sauter et al., 2006)	north of center	(558)	1-10	(0.64-2.85)	4.8-21.6	3
Pacific Ocean Hydrate Ridge (Torres et al., 2002)	northern summit	Not stated	Not stated	1-5	(2.616 - 13.079)	10

Table 5.1.
Overview of average bubble-release rates, flow rates and mole flow rates (CH_4) of seeps observed at Rock Garden (this study) in comparison with published data from seeps around the world. Values in between brackets are calculated based on provided data and where needed, the SiBu-GUI was used to calculate (mole) flow rates (Greinert and McGinnis, 2009).

as the most variable one, portraying fluxes that differ up to two orders of magnitude. The differences in seep activity for seep sites elsewhere, as shown in Table 1, are related to observations of several seep clusters/sites or are estimation boundaries. The changing bubble-release activity seen during ROV-2 dive can be attributed to different controls over different time scales, from seconds to days. We suggest, that the long-term changes in bubble-release activity, i.e. from periods without outburst (e.g. ROV-6B and ROV-6B') to periods with outbursts (ROV-2 dive), are probably related to external pressure changes (e.g. tides and changes in current directions) (Boles et al., 2001; Torres et al., 2002; Newman et al., 2008; Linke et al., 2010). Linke et al. (2010) confirms the correlation between flare observations and tides at the Hikurangi Margin. For the short-term changes (e.g. alternation between outburst and low activity as seen during the ROV-2 dive) we suggest an relationship to internal pressure changes during the filling of a shallow subsurface reservoir that creates an overpressure situation leading to the observed outbursts (Leifer et al., 2004). The outbursts depressurize the seep system, so the pressure/reservoir can build/fill up again. The regularity of the outbursts/bubble release indicates that over a certain time the seep system (internal configuration, external pressure and gas supply) does not change. Changes in bubble-release rates (ROV-6B to ROV-6B') and bubble sizes (ROV-7A to ROV-7A') are probably

caused by changes in gas supply, rather than pressure changes (Leifer et al., 2004). Based on our observations, we could not substantiate whether the three seep clusters observed at Faure Site belong to one gas reservoir or are two or three separated systems. Changes in the outlet geometry, like the observed pockmark formation, could also affect bubble sizes and release rates, but this could not be confirmed or disproved by our observations. Whether the depression-and-hill morphology, as seen at both Faure Site and LM-3, results in all cases from bubble release is doubtful (Figs. 5.7.D. and 5.9.C.). In most cases, they are probably burrows made by crabs or fish (Gerino et al., 1995).

5.5.3. An integrative seep model

The different aspects of Faure Site and LM-3 probably results from different methane release mechanisms; bubbles versus diffusive fluid flow respectively (see 5.5.1.). To explain what causes these differences in gas release, we propose an integrative model, taking into account the water depth, the depth of the BGHSZ and the observed seafloor features (morphology, fauna, authigenic carbonates, bubble release, etc.) (Fig. 5.12.).

The strong bubble release and the observed seep environment at Faure Site is a result of water depth (-659 m) and the related shallow subsurface depth of the BGHSZ/BSR (<35 m) (Fig. 5.2.c-c'). High gas concentrations present below the shallow BGHSZ allow gas (free and dissolved) to migrate towards the seafloor surface rather easily, resulting in the observed gas venting (Fig. 5.2.c-c' and 5.12.). Crutchley et al. (2010) suggests that gas migrates along relatively permeable sedimentary layers (Fig. 5.12.). Free gas is assumed to be able to migrate in the GHSZ along gas-hydrate-coated veins that prevent additional hydrate formation due to limitation of water availability (Pecher et al., 2010). The migration of warmer or saline fluids will also favor free gas transport within the GHSZ (Ginsburg and Soloviev, 1997; Wood et al., 2002; Liu and Flemings, 2006). However, our observations and measurements (CTD and THP) do not point to migration of warmer or saline fluids to the seafloor. Furthermore, salt layers in the subsurface of Rock Garden are unlikely.

LM-3 is located at a greater depth of -908 m. Together with the prevailing temperature, this situation results in a deeper subsurface depth of the BGHSZ/BSR of ca. 300 m (Fig. 5.2. a-a' and 5.12.) (Crutchley et al., 2010). Therefore a seemingly direct supply of free gas from beneath the BGHSZ towards the seafloor, as suggested for Faure Site, is significantly less likely. The free gas close to the seafloor was seismically detected in the GHSZ and is imaged as being 'spread out' . This pattern points to a lesser and not so intense focusing of the gas-charged fluids, and thus results in a more diffusive methane release at the seabed associated with authigenic carbonates, seep-related fauna and modest bubble release at LM-3. The modest bubble release at LM-3 does not counter this proposed model. The enhanced precipitation of methane-derived carbonates associated with AOM leads to both self-sealing of the LM-3 seep site and to methane accumulation underneath. When gas concentrations increase and reach supersaturation, bubbles can form and be released into the water column (Boudreau et al., 2001). The methane-driven carbonate cementation at the seafloor causes relocation of the actual bubble-releasing sites (Hovland, 2002; Naudts et al., 2008). This is indicated by the observed locations of the bubble release from sandy sediments away from the carbonate platform, just at the border of the high-backscatter area (Fig. 5.6.). The self-sealing process is not complete, since a live methane-related megafauna is still present on the carbonate platform, and high methane concentrations were measured just above this site. Nevertheless, the self-sealing is already at an advanced stage, explaining the absence of live *Calyptogena* sp. The large amount of disarticulated *Calyptogena* sp. shells and the formation of the extensive carbonate platform (100 m^2), however, do indicate that dissolved methane supply was high in the past and AOM was important during an early stage of the self-sealing process. We conclude that the seep site at LM-3, which is mainly diffusive at present, is relatively old in comparison with the seep site at Faure Site.

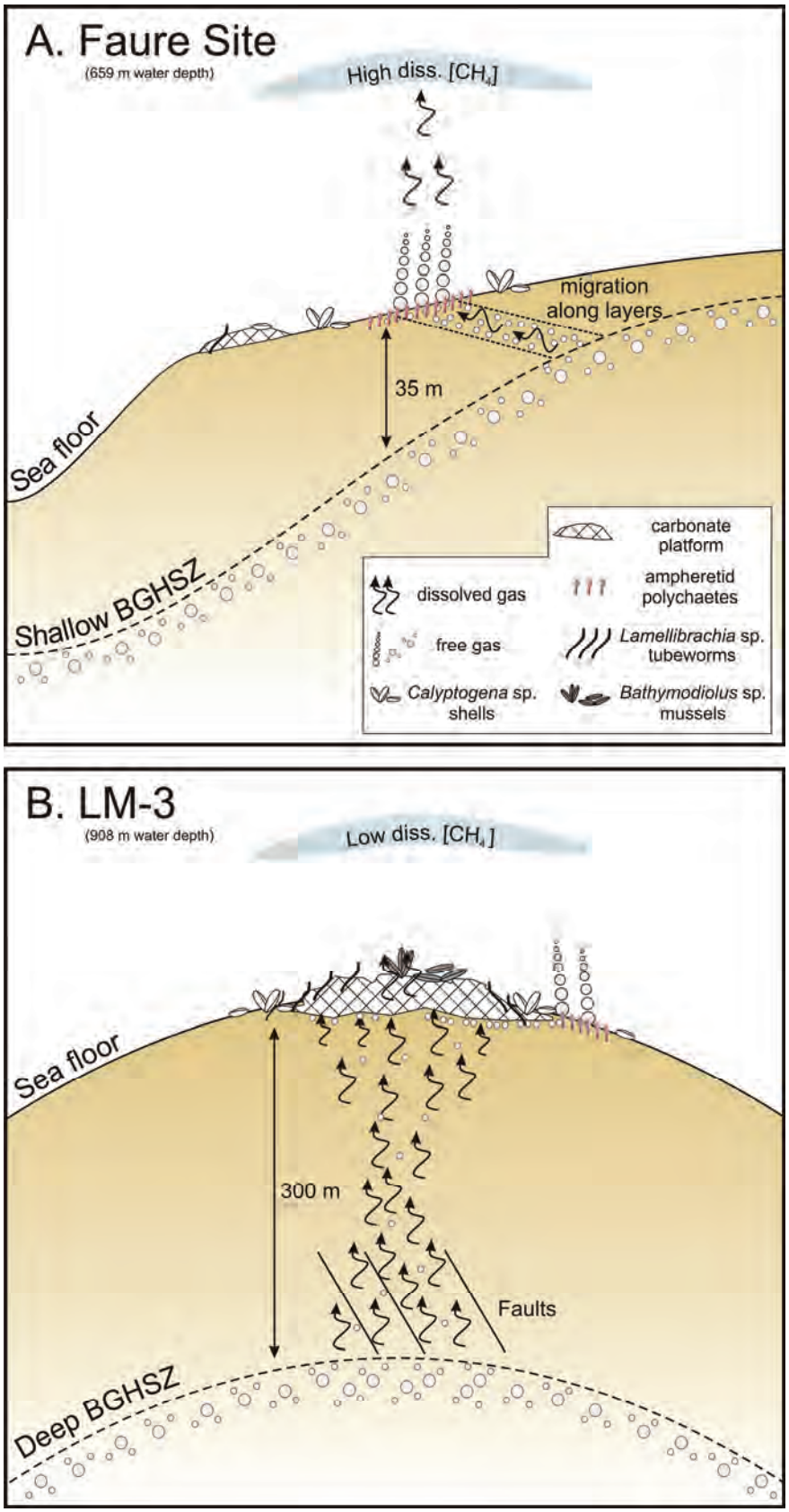

Figure 5.12. Proposed seep model for Faure Site and LM-3 to explain the differences in methane-releasing mechanism (bubble versus diffusive) and resulting seep environments based on difference in depth, subsurface depth of the BGHSZ/BSR and observed seafloor features.

The "evolution" of Faure Site seems to be more complicated and therefore implies more speculation in our interpretation. At present, bubble release is certainly the main, but probably a relatively recent, methane-releasing mechanism (see 5.5.1). The presence of disarticulated *Calyptogena* sp. shells indicates that diffusive methane supply was more important in the past. This is also indicated by the presence of possible methane-derived carbonates and dead seep fauna in the area west of Faure Site, near the scarp of the submarine landslide (Figs. 5.2., 5.4.E. and 5.5.A.). We speculate that this change in methane-release mechanism can be explained in the context of the tectonic uplift of Rock Garden as the result of a subducting seamount (Pecher et al., 2005; Barnes et al., 2010; Ellis et al., 2010). The uplift of Rock Garden modified the depth of the GHSZ resulting in 1) a shallower BGHSZ and 2) more focused methane fluxes and 3) enhanced seafloor destabilization (Ellis et al., 2010). The latter is reflected in the large submarine landslide near Faure Site (Fig. 5.2.) (Pecher et al., 2005; Faure et al., 2006). The associated occurrence of submarine landslides, shallow gas and seeps, whether or not in relation with gas hydrates, is a common feature at continental margins worldwide (Orange and Breen, 1992; Orange et al., 1997; Bouriak et al., 2000; Eichhubl et al., 2000; Bünz et al., 2005; Naudts et al., 2006). The close relation between seeps and scarps of submarine landslides can be explained by steepened pore-pressure gradients adjacent to scarps due to sudden erosion associated with slumping, and the resulting focusing of fluids towards the scarp areas (Orange et al., 1997; Naudts et al., 2006). The combination of tectonic uplift implying a shallower BGHSZ with a submarine landslide might have caused the change in methane release mechanism at Faure Site, from more diffusive in the past to bubble-release dominated at present.

5.6. Conclusions

ROV observations at Rock Garden allowed the first ever visual observation of bubble-releasing seeps at the Hikurangi Margin, and this at two sites; Faure Site and LM-3. The two seep areas portray different seep environments resulting from different types of methane release; mainly by bubble release at Faure Site and by diffusive release at LM-3. At Faure Site, bubble sizes (5-15 mm) and bubble-release rates (5-190 Hz) varied within minutes to hours, leading to variations in average mole flow rates per outlet of 0.018-7.019 mol of methane per minute. This is comparable with published data from bubble-releasing seeps around the world. Ampheretid polychaetes and suberitid sponges were the only live methane-related fauna observed at Faure Site. These organisms are ecosystem engineers facilitating the transition from a soft sediment environment with mainly bubble release to a hard substrate seep environment with associated fauna where AOM and diffusive methane transport prevail (Sommer et al., 2010; Thurber et al., 2010).

At LM-3, seep activity was confirmed by the occurrence of a large methane-derived carbonate platform (100 m^2) covered with live seep-related mega fauna (*Bathymodiolus* sp. mussels and *Lamellibrachia* sp. tubeworms). Bubble release at LM-3 was rather modest, but was also associated with similar ecosystem-engineering fauna as observed at Faure Site. Based on the integration of all observations, a conceptual seep model is proposed that explains the differences in methane-releasing mechanisms and resulting seep environments based on differences in the depth of the BGHSZ and the different tectonic histories of the seep areas.

Acknowledgements

We like to thank the captain and the crew of RV SONNE for their work during the third leg of the SO191 cruise. Jeroen Vercruysse and Wim Versteeg are gratefully thanked to get ROV "Genesis" aka "Suzee" installed and working on RV SONNE. Jens Greinert thanks the EU for financial support and the possibility to work at GNS Science and RCMG via a Marie Curie Grant (MOIF-CT-2005-007436). Jeffrey Poort was supported by the Flemish Fund for Scientific Research (FWO-Flanders). Purchase of the ROV was possible thanks to an Impulsfinanciering of the Special Research Fund of Universiteit Gent.

Participation to the expedition was co-financed by FWO-Flanders. This is publication Geotech-1228. Cruise SO191 was part of the COMET project in the framework of the R&D program GEOTECHNOLOGIEN, both funded by the German Ministry of Education and Research (Grant No: 03G0600D and 03G0191A). Finally we thank Kathleen Campbell, Stéphanie Dupré and Keith Lewis for their constructive reviews which helped improve this manuscript.

Additional information

Lieven Naudts processed and interpreted most of the datasets, wrote the manuscript and made all figures. Lieven Naudts also assisted with the data acquisition during the 4 weeks of expedition on RV Sonne. Co-authors helped by reviewing the manuscript, by helping during the data acquisition and/or by providing the datasets. The processing of the multibeam data was mainly done by Jens Greinert. For the interpretation of the seafloor observations assistance was given by Joke Belza and Elke Vangampelaere. Temperature data was interpreted with assistance of Jeffrey Poort.

References

Artemov, Y.G., Egorov, V.N., Polikarpov, G.G., Gulin, S.B., 2007. Methane emission to the hydro - and atmosphere by gas bubble streams in the Dnieper paleo-delta, the Black Sea. Mar. Ecol. J., 5-26.

Barnes, P.M., Lamarche, G., Bialas, J., Henrys, S., Pecher, I., Netzeband, G.L., Greinert, J., Mountjoy, J.J., Pedley, K., Crutchley, G., 2010. Tectonic and geological framework for gas hydrates and cold seeps on the Hikurangi subduction margin, New Zealand. Mar. Geol. 272, 26-48.

Boetius, A., Ravenschlag, K., Schubert, C.J., Rickert, D., Widdel, F., Gieseke, A., Amann, R., Jorgensen, B.B., Witte, U., Pfannkuche, O., 2000. A marine microbial consortium apparently mediating anaerobic oxidation of methane. Nature 407, 623-626.

Boetius, A., Suess, E., 2004. Hydrate Ridge: a natural laboratory for the study of microbial life fueled by methane from near-surface gas hydrates. Chem. Geol. 205, 291-310.

Boles, J.R., Clark, J.F., Leifer, I., Washburn, L., 2001. Temporal variation in natural methane seep rate due to tides, Coal Oil Point area, California. Journal of Geophysical Research-Oceans 106, 27077-27086.

Boudreau, B.P., Gardiner, B.S., Johnson, B.D., 2001. Rate of growth of isolated bubbles in sediments with a diagenetic source of methane. Limnol. Oceanogr. 46, 616-622.

Bouriak, S., Vanneste, M., Saoutkine, A., 2000. Inferred gas hydrates and clay diapirs near the Storegga Slide on the southern edge of the Voring Plateau, offshore Norway. Mar. Geol. 163, 125-148.

Brooks, J.M., Kennicutt, M.C., Fisher, C.R., Macko, S.A., Cole, K., Childress, J.J., Bidigare, R.R., Vetter, R.D., 1987. Deep-sea hydrocarbon seep communities - evidence for energy and nutritional carbon-sources. Science 238, 1138-1142.

Bünz, S., Mienert, J., Bryn, P., Berg, K., 2005. Fluid flow impact on slope failure from 3D seismic data: a case study in the Storegga Slide. Basin Res. 17, 109-122.

Campbell, K.A., Nelson, C.S., Alfaro, A.C., Boyd, S., Greinert, J., Nyman, S., Grosjean, E., Logan, G.A., Gregory, M.R., Cooke, S., Linke, P., Milloy, S., Wallis, I., 2010. Geological imprint of methane seepage on the seabed and biota of the convergent Hikurangi Margin, New Zealand: survey of core and grab carbonates. Mar. Geol. 272, 285-306.

Cary, S.C., Fisher, C.R., Felbeck, H., 1988. Mussel growth supported by methane as sole carbon and energy-source. Science 240, 78-80.

Coleman, D., Ballard, R., 2001. A highly concentrated region of cold hydrocarbon seeps in the southeastern Mediterranean Sea. Geo-Mar. Lett. 21, 162-167.

Crutchley, G.J., Pecher, I.A., Gorman, A.R., Henrys, S.A., Greinert, J., 2010. Seismic imaging of gas conduits beneath seafloor seep sites in a shallow marine gas hydrate province, Hikurangi Margin, New Zealand. Mar. Geol. 272, 114-126.

Eichhubl, P., Greene, H.G., Naehr, T., Maher, N., 2000. Structural control of fluid flow: offshore fluid seepage in the Santa Barbara Basin, California. J. Geochem. Explor. 69, 545-549.

Ellis, S., Pecher, I., Kukowski, N., Xu, W., Henrys, S., Greinert, J., 2010. Testing proposed mechanisms for seafloor weakening at the top of gas hydrate stability on an uplifted submarine ridge (Rock Garden), New Zealand. Mar. Geol. 272, 127-140.

Faure, K., Greinert, J., Pecher, I.A., Graham, I.J., Massoth, G.J., De Ronde, C.E.J., Wright, I.C., Baker, E.T., Olson, E.J., 2006. Methane seepage and its relation to slumping and gas hydrate at the Hikurangi margin, New Zealand. N. Z. J. Geol. Geophys. 49, 503-516.

Faure, K., Greinert, J., von Deimling, J.S., McGinnis, D.F., Kipfer, R., Linke, P., 2010. Methane seepage along the Hikurangi Margin of New Zealand: Geochemical and physical data from the water column, sea surface and atmosphere. Mar. Geol. 272, 170-188.

Fujikura, K., Kojima, S., Tamaki, K., Maki, Y., Hunt, J., Okutani, T., 1999. The deepest chemosynthesis-based community yet discovered from the hadal zone, 7326 m deep, in the Japan Trench. Mar. Ecol.-Prog. Ser. 190, 17-26.

Gay, A., Lopez, M., Berndt, C., Seranne, M., 2007. Geological controls on focused fluid flow associated with seafloor seeps in the Lower Congo Basin. Mar. Geol. 244, 68-92.

Gay, A., Lopez, M., Ondreas, H., Charlou, J.L., Sermondadaz, G., Cochonat, P., 2006. Seafloor facies related to upward methane flux within a Giant Pockmark of the Lower Congo Basin. Mar. Geol. 226, 81-95.

Gerino, M., Stora, G., Poydenot, F., Bourcier, M., 1995. Benthic fauna and bioturbation on the Mediterranean continental slope:Toulon Canyon. Cont. Shelf Res. 15, 1483-1496.

Ginsburg, G.D., Soloviev, V.A., 1997. Methane migration within the submarine gas-hydrate stability zone under deep-water conditions. Mar. Geol. 137, 49-57.

Greinert, J., 2008. Monitoring temporal variability of bubble release at seeps: The hydroacoustic swath system GasQuant. Journal of Geophysical Research-Oceans 113, 20.

Greinert, J., Artemov, Y., Egorov, V., De Batist, M., McGinnis, D., 2006. 1300-m-high rising bubbles from mud volcanoes at 2080m in the Black Sea: Hydroacoustic characteristics and temporal variability. Earth Planet. Sci. Lett. 244, 1-15.

Greinert, J., Bohrmann, G., Elvert, M., 2002a. Stromatolitic fabric of authigenic carbonate crusts: result of anaerobic methane oxidation at cold seeps in 4,850 m water depth. Int. J. Earth Sci. 91, 698-711.

Greinert, J., Bollwerk, S.M., Derkachev, A., Bohrmann, G., Suess, E., 2002b. Massive barite deposits and carbonate mineralization in the Derugin Basin, Sea of Okhotsk: precipitation processes at cold seep sites. Earth Planet. Sci. Lett. 203, 165-180.

Greinert, J., Lewis, K.B., Bialas, J., Pecher, I.A., Rowden, A., Bowden, D.A., De Batist, M., Linke, P., 2010a. Methane seepage along the Hikurangi Margin, New Zealand: Overview of studies in 2006 and 2007 and new evidence from visual, bathymetric and hydroacoustic investigations. Mar. Geol. 272, 6-25.

Greinert, J., McGinnis, D.F., 2009. Single bubble dissolution model - The graphical user interface SiBu-GUI. Environmental Modelling & Software 24, 1012-1013.

Greinert, J., McGinnis, D.F., Naudts, L., Linke, P., De Batist, M., 2010b. Atmospheric methane flux from bubbling seeps: Spatially extrapolated quantification from a Black Sea shelf area. J. Geophys. Res. 115, 1-18.

Henrys, S.A., Ellis, S., Uruski, C., 2003. Conductive heat flow variations from bottom-simulating reflectors on the Hikurangi margin, New Zealand. Geophys. Res. Lett. 30, 1065–1068.

Hovland, M., 2002. On the self-sealing nature of marine seeps. Cont. Shelf Res. 22, 2387-2394.

Hovland, M., Talbot, M., Olaussen, S., Aasberg, L., 1985. Recently formed methane-derived carbonates from the North Sea floor. In: B.M. Thomas (Editor), Petroleum Geochemistry in Exploration of the Norwegian Shelf. Norwegian Petroleum Society. Graham and Trotman, pp. 263-266.

Huetten, E., Greinert, J., 2008. Software controlled guidance, recording and post-processing of seafloor observations by ROV and other towed devices: The software package OFOP. Geoph. Res. Abstr. 10, 03088.

Jerosch, K., Schluter, M., Foucher, J.-P., Allais, A.-G., Klages, M., Edy, C., 2007. Spatial distribution of mud flows, chemoautotrophic communities, and biogeochemical habitats at Hakon Mosby Mud Volcano. Mar. Geol. 243, 1-17.

Johnson, J.E., Goldfinger, C., Suess, E., 2003. Geophysical constraints on the surface distribution of authigenic carbonates across the Hydrate Ridge region, Cascadia margin. Mar. Geol. 202, 79-120.

Judd, A., Croker, P., Tizzard, L., Voisey, C., 2007. Extensive methane-derived authigenic carbonates in the Irish Sea. Geo-Mar. Lett. 27, 259-267.

Judd, A., Hovland, M., 2007. Seabed fluid flow: the impact on geology, biology and the marine environment. Cambridge University Press, Cambridge. 475 pp.

Judd, A.G., 2003. The global importance and context of methane escape from the seabed. Geo-Mar. Lett. 23, 147-154.

Katz, H.R., 1982. Evidence of gas hydrates beneath the continental-slope, East Coast, North Island, New Zealand. N. Z. J. Geol. Geophys. 25, 193-199.

Klaucke, I., Sahling, H., Weinrebe, W., Blinova, V., Burk, D., Lursmanashvili, N., Bohrmann, G., 2006. Acoustic investigation of cold seeps offshore Georgia, eastern Black Sea. Mar. Geol. 231, 51-67.

Leifer, I., Boles, J.R., Luyendyk, B.P., Clark, J.F., 2004. Transient discharges from marine hydrocarbon seeps: spatial and temporal variability. Environ. Geol. (Berlin) 46, 1038-1052.

Leifer, I., MacDonald, I., 2003. Dynamics of the gas flux from shallow gas hydrate deposits: interaction between oily hydrate bubbles and the oceanic environment. Earth Planet. Sci. Lett. 210, 411-424.

Lewis, K.B., Collot, J.-Y., Lallem, S.E., 1998. The dammed Hikurangi Trough: a channel-fed trench blocked by subducting seamounts and their wake avalanches (New Zealand-France GeodyNZ Project). Basin Res. 10, 441-468.

Lewis, K.B., Marshall, B.A., 1996. Seep faunas and other indicators of methane-rich dewatering on New Zealand convergent margins. N. Z. J. Geol. Geophys. 39, 181-200.

Linke, P., Sommer, S., Rovelli, L., McGinnis, D.F., 2010. Physical limitations of dissolved methane fluxes: The role of bottom-boundary layer processes. Mar. Geol. 272, 209-222.

Liu, X.L., Flemings, P.B., 2006. Passing gas through the hydrate stability zone at southern Hydrate Ridge, offshore Oregon. Earth Planet. Sci. Lett. 241, 211-226.

Mazzini, A., Svensen, H., Hovland, M., Planke, S., 2006. Comparison and implications from strikingly different authigenic carbonates in a Nyegga complex pockmark, G11, Norwegian Sea. Mar. Geol. 231, 89-102.

Naudts, L., Greinert, J., Artemov, Y., Beaubien, S.E., Borowski, C., De Batist, M., 2008. Anomalous sea-floor backscatter patterns in methane venting areas, Dnepr paleo-delta, NW Black Sea. Mar. Geol. 251, 253-267.

Naudts, L., Greinert, J., Artemov, Y., Staelens, P., Poort, J., Van Rensbergen, P., De Batist, M., 2006. Geological and morphological setting of 2778 methane seeps in the Dnepr paleo-delta, northwestern Black Sea. Mar. Geol. 227, 177-199.

Newman, K.R., Cormier, M.-H., Weissel, J.K., Driscoll, N.W., Kastner, M., Solomon, E.A., Robertson, G., Hill, J.C., Singh, H., Camilli, R., Eustice, R., 2008. Active methane venting observed at giant pockmarks along the U.S. mid-Atlantic shelf break. Earth Planet. Sci. Lett. 267, 341-352.

Nikolovska, A., Sahling, H., Bohrmann, G., 2008. Hydroacoustic methodology for detection, localization, and quantification of gas bubbles rising from the seafloor at gas seeps from the eastern Black Sea. Geochem. Geophys. Geosyst. 9.

Olu-Le Roy, K., Caprais, J.C., Fifis, A., Fabri, M.C., Galeron, J., Budzinsky, H., Le Menach, K., Khripounoff, A., Ondreas, H., Sibuet, M., 2007. Cold-seep assemblages on a giant pockmark off West Africa: spatial patterns and environmental control. Mar. Ecol. 28, 115-130.

Olu-Le Roy, K., Sibuet, M., Fiala-Médioni, A., Gofas, S., Salas, C., Mariotti, A., Foucher, J.-P., Woodside, J., 2004. Cold seep communities in the deep eastern Mediterranean Sea: composition, symbiosis and spatial distribution on mud volcanoes. Deep Sea Research Part I: Oceanographic Research Papers 51, 1915-1936.

Ondréas, H., Olu, K., Fouquet, Y., Charlou, J.L., Gay, A., Dennielou, B., Donval, J.P., Fifis, A., Nadalig, T., Cochonat, P., Cauquil, E., Bourillet, J.F., Moigne, M.L., Sibuet, M., 2005. ROV study of a giant pockmark on the Gabon continental margin. Geo-Mar. Lett. V25, 281-292.

Orange, D.L., Breen, N.A., 1992. The Effects of Fluid Escape on Accretionary Wedges. 2. Seepage Force, Slope Failure, Headless Submarine Canyons, and Vents. J. Geophys. Res. Solid Earth 97, 9277-9295.

Orange, D.L., McAdoo, B.G., Moore, J.C., Tobin, H., Screaton, E., Chezar, H., Lee, H., Reid, M., Vail, R., 1997. Headless submarine canyons and fluid flow on the toe of the Cascadia accretionary complex. Basin Res. 9, 303-312.

Orange, D.L., Yun, J., Maher, N., Barry, J., Greene, G., 2002. Tracking California seafloor seeps with bathymetry, backscatter and ROVs. Cont. Shelf Res. 22, 2273-2290.

Pape, T., Blumenberg, M., Seifert, R., Egorov, V.N., Gulin, S.B., Michaelis, W., 2005. Lipid geochemistry of methane-seep-related Black Sea carbonates. Palaeogeogr. Palaeoclimatol. Palaeoecol. 227, 31-47.

Paull, C.K., Chanton, J.P., Neumann, A.C., Coston, J.A., Martens, C.S., Showers, W., 1992. Indicators of methane-derived carbonates and chemosynthetic organic carbon deposits; examples from the Florida Escarpment. Palaios 7, 361-375.

Paull, C.K., Ussler Iii, W., Peltzer, E.T., Brewer, P.G., Keaten, R., Mitts, P.J., Nealon, J.W., Greinert, J., Herguera, J.-C., Elena Perez, M., 2007. Authigenic carbon entombed in methane-soaked sediments from the northeastern transform margin of the Guaymas Basin, Gulf of California. Deep Sea Research Part II: Topical Studies in Oceanography 54, 1240-1267.

Paull, C.K., Ussler, W., Greene, H.G., Barry, J., Keaten, R., 2005. Bioerosion by chemosynthetic biological communities on Holocene submarine slide scars. Geo-Mar. Lett. V25, 11-19.

Pecher, I.A., Henrys, S.A., Ellis, S., Chiswell, S.M., Kukowski, N., 2005. Erosion of the seafloor at the top of the gas hydrate stability zone on the Hikurangi Margin, New Zealand. Geophys. Res. Lett. 32.

Pecher, I.A., Henrys, S.A., Wood, W.T., Kukowski, N., Crutchley, G.J., Fohrmann, M., Kilner, J., Senger, K., Gorman, A.R., Coffin, R.B., Greinert, J., Faure, K., 2010. Focussed fluid flow on the Hikurangi Margin, New Zealand -- Evidence from possible local upwarping of the base of gas hydrate stability. Mar. Geol. 272, 99-113.

Pecher, I.A., Henrys, S.A., Zhu, H., 2004. Seismic images of gas conduits beneath vents and gas hydrates on Ritchie Ridge, Hikurangi margin, New Zealand. N. Z. J. Geol. Geophys. 47, 275-279.

Peckmann, J., Reimer, A., Luth, U., Luth, C., Hansen, B.T., Heinicke, C., Hoefs, J., Reitner, J., 2001. Methane-derived carbonates and authigenic pyrite from the northwestern Black Sea. Mar. Geol. 177, 129-150.

Sahling, H., Masson, D.G., Ranero, C.R., Huhnerbach, V., Weinrebe, W., Klaucke, I., Burk, D., Bruckmann, W., Suess, E., 2008. Fluid seepage at the continental margin offshore Costa Rica and southern Nicaragua. Geochemistry Geophysics Geosystems 9, 22.

Sauter, E.J., Muyakshin, S.I., Charlou, J.-L., Schluter, M., Boetius, A., Jerosch, K., Damm, E., Foucher, J.-P., Klages, M., 2006. Methane discharge from a deep-sea submarine mud volcano into the

upper water column by gas hydrate-coated methane bubbles. Earth Planet. Sci. Lett. 243, 354-365.

Schneider von Deimling, J.S., Brockhoff, J., Greinert, J., 2007. Flare imaging with multibeam systems: Data processing for bubble detection at seeps. Geochemistry Geophysics Geosystems 8.

Sommer, S., Linke, P., Pfannkuche, O., Niemann, H., Treude, T., 2010. Benthic respiration in a seep habitat dominated by dense beds of ampharetid polychaetes at the Hikurangi Margin (New Zealand). Mar. Geol. 272, 223-232.

Sommer, S., Pfannkuche, O., Linke, P., Luff, R., Greinert, J., Drews, M., Gubsch, S., Pieper, M., Poser, M., Viergutz, T., 2006. Efficiency of the benthic filter: Biological control of the emission of dissolved methane from sediments containing shallow gas hydrates at Hydrate Ridge. Global Biogeochem. Cycles 20.

Thurber, A.R., Kröger, K., Neira, C., Wiklund, H., Levin, L.A., 2010. Stable isotope signatures and methane use by New Zealand cold seep benthos Mar. Geol. 272, 260-269.

Torres, M.E., McManus, J., Hammond, D.E., de Angelis, M.A., Heeschen, K.U., Colbert, S.L., Tryon, M.D., Brown, K.M., Suess, E., 2002. Fluid and chemical fluxes in and out of sediments hosting methane hydrate deposits on Hydrate Ridge, OR, I: Hydrological provinces. Earth Planet. Sci. Lett. 201, 525-540.

Townend, J., 1997. Estimates of conductive heat flow through bottom-simulating reflectors on the Hikurangi and southwest Fiordland continental margins, New Zealand. Mar. Geol. 141, 209-220.

Van Dover, C.L., Aharon, P., Bernhard, J.M., Caylor, E., Doerries, M., Flickinger, W., Gilhooly, W., Goffredi, S.K., Knick, K.E., Macko, S.A., Rapoport, S., Raulfs, E.C., Ruppel, C., Salerno, J.L., Seitz, R.D., Sen Gupta, B.K., Shank, T., Turnipseed, M., Vrijenhoek, R., 2003. Blake Ridge methane seeps: characterization of a soft-sediment, chemo synthetically based ecosystem. Deep-Sea Res. Part I-Oceanogr. Res. Pap. 50, 281-300.

Wood, W.T., Gettrust, J.F., Chapman, N.R., Spence, G.D., Hyndman, R.D., 2002. Decreased stability of methane hydrates in marine sediments owing to phase-boundary roughness. Nature 420, 656-660.

CHAPTER 6

Stratigraphic and structural controls on the location of active methane seeps on Posolsky Bank, Lake Baikal

Lieven Naudts, Oleg Khlystov, Nick Granin, Alexander Chensky, Jeffrey Poort, Marc De Batist

Abstract

The distribution and origin of shallow gas seeps occurring at the crest of the Posolsky Bank in Lake Baikal have been studied based on the integration of detailed seismic, multibeam and hydro-acoustic water-column investigations. In total 65 acoustic flares, indicating gas-bubble release at the lake floor (seepage), have been detected within the 630 km^2 area of the Posolsky Bank. All seeps are located on the Posolsky Fault scarp near the crest of the Posolsky Bank or on similar locations in water depths of -43 m to -332 m. Lake Baikal is the only fresh-water basin in the world where gas hydrates have been inferred from BSRs on seismic data and have been sampled. Our seismic data also portray BSRs occurring up to water depths of -300 m, which is much shallower than the previously reported -500 m water depth. Calculations for hydrate stability, heat flow and topographic effect based on the BSR occurrence and multibeam bathymetry allowed the determination of a methane-ethane gas mixture and heat-flow values wherefore gas hydrates could be stable in the lake sediments at the given ambient conditions. None of the seeps associated with the Posolsky Bank have been detected within this newly established gas-hydrate stability zone. Our observations and data integration suggest that the seeps at the crest of Posolsky Bank occur where gas-bearing strata are cut off by the Posolsky Fault. These gas-bearing layers could be traced down the Posolsky Bank to below the base of the gas-hydrate stability zone (BGHSZ), suggesting that the detected seeps on the crest of the Posolsky Bank are mainly fed by gas coming from below the BGHSZ.

Keywords

Methane seeps; flares; seismic reflection data; multibeam; gas-hydrate stability; Posolsky Bank; Lake Baikal

6.1. Introduction

Active methane seeps occur worldwide in the marine environment especially at continental margins, and often in association with gas hydrates (Judd, 2003; Judd and Hovland, 2007). Scientific interest in the relationship between gas hydrates and methane seeps is mostly motivated by the understanding that gas hydrates can act either as: i) buffers, sealing off the upward migration of methane and preventing gas-bubble release in the water column (Naudts et al., 2006; Haacke et al., 2007); ii) sources for methane fluid flow within the sediment and seepage into the water column (Suess et al., 1999; Reeburgh et al., 2006) and iii) sinks for methane present in the gas-hydrate stability zone (GHSZ) (Henriet and Mienert, 1998). While gas hydrates are widespread in the marine environment, their presence has up to now been demonstrated in only one fresh-water lacustrine setting, i.e. Lake Baikal (Golmshtok et al., 2000). In this tectonically active rift lake, gas hydrates are present in the deeper subsurface and as near-bottom accumulations in mud-volcano-like structures (Klerkx et al., 2006). The gas hydrates in the deeper subsurface have been proposed as the main source of the methane that is being released at the mud volcano structures and that crosses the GHSZ along active faults (De Batist et al., 2002; Van Rensbergen et al., 2002; Vanneste et al., 2002). Apart from the methane release at the mud volcanoes in the deep parts of Lake Baikal (i.e. within the GHSZ), seepage also occurs outside of the GHSZ (Granin and Granina, 2002; Granin et al., in press). The sources and controls on these shallow seeps are, however, still poorly understood. This study focuses on one of these shallow seepage areas outside the GHSZ (i.e. on the Posolsky Bank) and tries to explain the source and distribution of shallow methane-bubble release.

6.2. Study area

Lake Baikal, located in South-Central Siberia, is the deepest lake in the world (1637 m) (Galaziy, 1993; Naudts et al., submitted) (Fig. 6.1.). It contains 20% of the worlds fresh liquid surface water (23000 km^3) (Galaziy, 1993). The lake occupies 3 basins within the Baikal Rift Zone (BRZ): the North Baikal Basin (NBB), the Central Baikal Basin (CBB) and the South Baikal Basin (SBB) (Fig. 6.1.). These three basins are separated by two structural highs: the Academician Ridge Accommodation Zone (ARAZ), between the NBB and the CBB, and the Selenga Delta Accommodation Zone (SDAZ) between the CBB and the SBB. Up to now, Lake Baikal is the only fresh-water basin in the world in which gas hydrates have been both inferred and sampled. Hydrates are present both as “deep hydrates” which occur in the subsurface at relatively large sediments depths, and as “shallow hydrates”, which occur near the lake floor. The presence of the deep hydrates was inferred based on the observation of distinct bottom-simulating reflections (BSRs) on multi-channel reflection seismic recordings (Hutchinson et al., 1991; Golmshtok et al., 1997) (Fig. 6.1.). BSRs have been observed in an area that exceeds 4000 km^2 covering the slope of the Selenga River Delta and adjacent CBB and SBB lake floors in water depths exceeding -500 m (Fig. 6.1.) (Golmshtok et al., 2000; Vanneste et al., 2001; De Batist et al., 2002). In the SBB, hydrates were retrieved at -121 and -161 m subbottom depth during the Baikal Drilling Project (BDP-97) (Williams et al., 2001) (Fig. 6.1.). Geochemical analyses showed that the gas hydrates consist of microbial methane ($\delta^{13}C_{CH_4}$ between -58 and -68 ‰) (Kuzmin et al., 1998; Kuzmin et al., 2000). Since 2000, shallow gas hydrates have been retrieved from several mud volcanoes in the SBB and CBB (Klerkx et al., 2003; Matveeva et al., 2003; Kalmychkov et al., 2006; Khlystov, 2006; Kida et al., 2006; Klerkx et al., 2006; Krylov et al., 2008a; Krylov et al., 2008b; Hachikubo et al., 2009; Poort et al., submitted) (Fig. 6.1.). The discovery of these gas-hydrate-bearing mud volcanoes was based on the observations of anomalous shallow BSRs which dome up towards the lake floor, instead of simulating the lake bottom (Vanneste et al., 2001; De Batist et al., 2002; Van Rensbergen et al., 2002; Vanneste et al., 2002). The mud volcanoes and shallow BSRs have been attributed to the destabilization of gas hydrates at the base of the gas hydrate stability zone

(BGHSZ) by tectonically driven geothermal fluid pulses near large faults (De Batist et al., 2002; Van Rensbergen et al., 2002; Vanneste et al., 2002; Klerkx et al., 2006). The shallow seeps, outside the GHSZ, occur typically in coastal areas and in the vicinity of river deltas and canyons. These shallow seeps were already described in historical records reporting on areas with absent ice cover in winter ('ice streamthroughs'), abundant dead fish and observation of bubbles at the lake surface (Granin and Granina, 2002). The two most prolific seep areas are offshore the town of Babushkhin on the southeastern shore of the SBB and around the crest of the

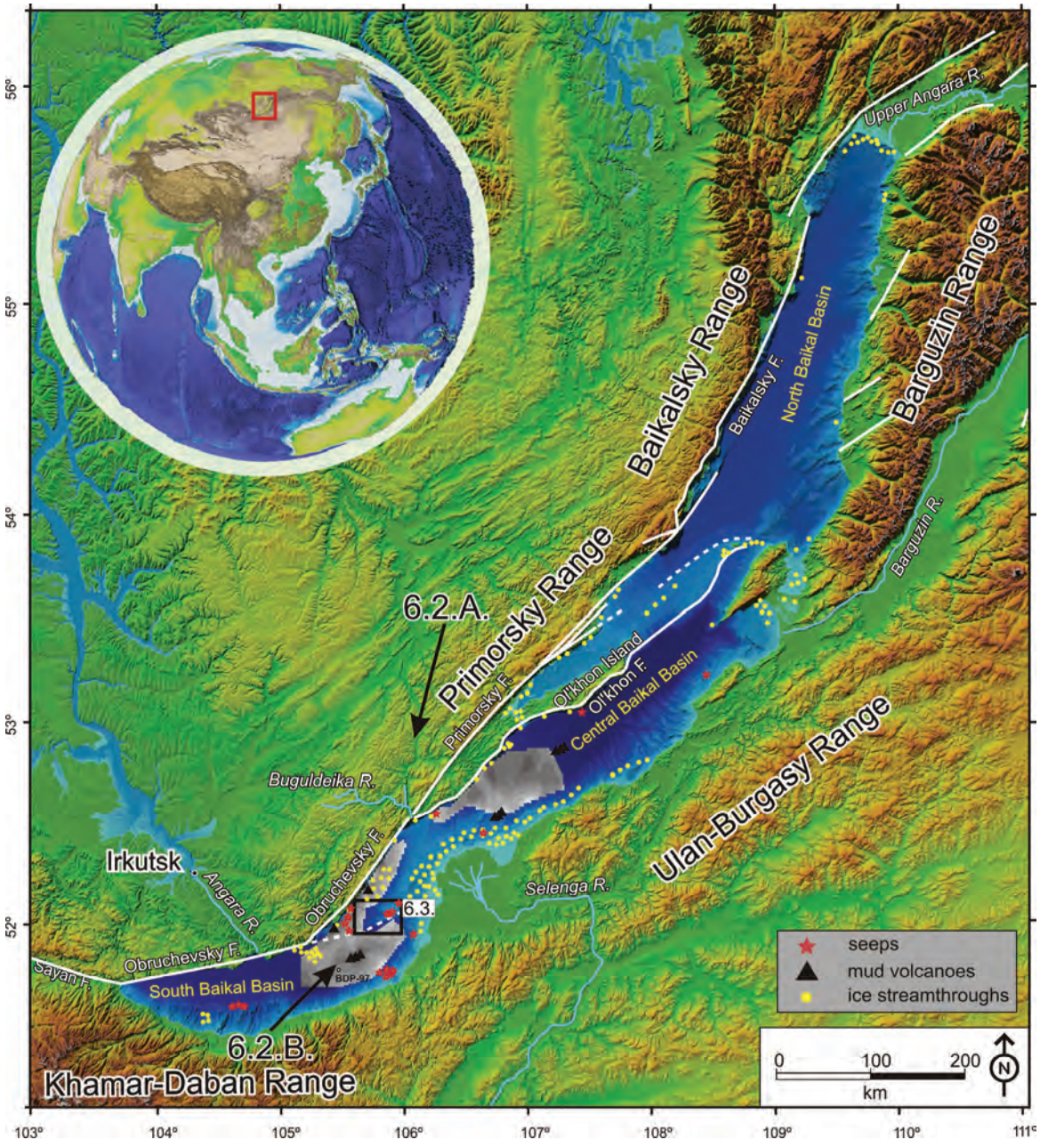

Figure 6.1. Location map of the study area in Lake Baikal with indications for regional faults, Baikal Basins, mountain ranges, rivers and area with observed bottom-simulating reflections (BSRs) (Golmshtok et al., 2000). The location of seeps (red stars), mud volcanoes (black triangles), ice streamthroughs (yellow dots) and the BDP-97 drill hole is also indicated (Granin and Granina, 2002; Klerkx et al., 2006; Schmid et al., 2007). The location on Planet Earth, the view directions for Figs. 6.2.A. & 6.2.B. and outline for Fig. 6.3. are also indicated. The map is constructed by compiling SRTM-derived topography data with bathymetry data from Lake Baikal (INTAS Project 99-1669 Team, 2002) and multibeam bathymetry data (Naudts et al., submitted).

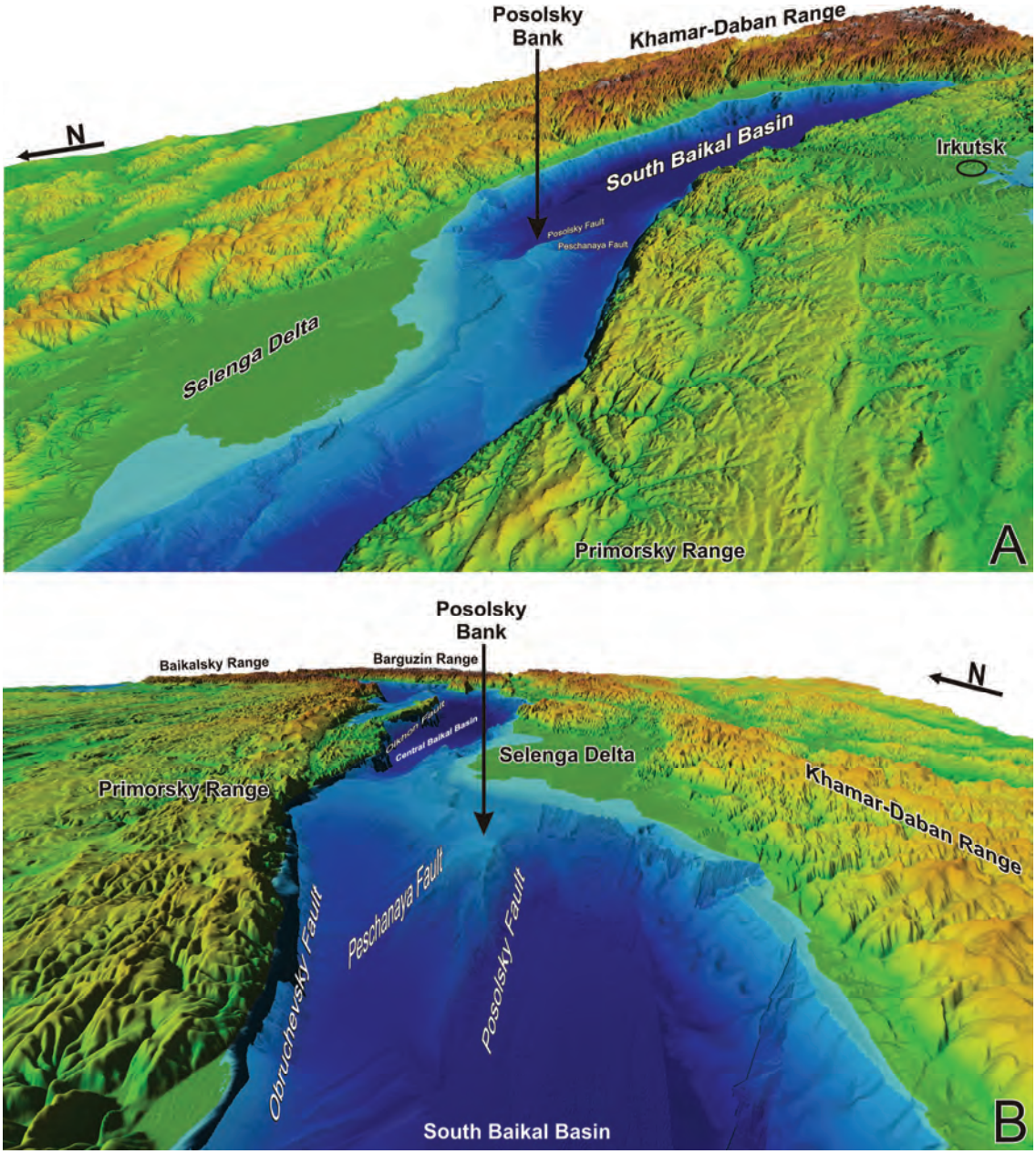

Figure 6.2. 3D views of Lake Baikal and Posolsky Bank with indication for the most prominent features. The view directions (A and B) are indicated on Fig. 6.1. The images are constructed by compiling SRTM-derived topography data with bathymetry data from Lake Baikal (INTAS Project 99-1669 Team, 2002) and multibeam bathymetry data (Naudts et al., submitted).

Posolsky Bank in the northeastern part of the SBB (Granin et al., in press). The distribution and source of the seeps on the crest of the Posolsky Bank are the focus of this paper. The Posolsky Bank is a tilted fault block within the Selenga Delta within the Selenga Delta Accommodation Zone (Figs. 6.1. and 6.2.) (Scholz and Hutchinson, 2000; Bezrukova et al., 2005; Charlet et al., 2005). The crest of the Posolsky Bank reaches water depths of less than -50 m (Naudts et al., submitted). The southern slope is very steep and coincides with the Posolsky border fault, i.e. the northern boundary fault of the SBB, while the northern slope is more gradually dipping (Figs. 6.2. and 6.3.). The sedimentary build-up of the Posolsky Bank mainly consists of fine hemipelagic sediments and spread sand lenses and laminae as shown by BDP-99 (Bezrukova et al., 2005).

6.3. Methods and data

6.3.1. Single-beam echosounding and seep detection

Due to the high impedance contrast between water and free gas, gas bubbles rising in the water column (seeps) can be acoustically detected by means of single-beam echosounder recordings. Rising bubbles show up as “acoustic flares” on echograms (Fig. 6.4.) (Greinert et al., 2006; Naudts et al., 2006; Artemov et al., 2007). Single-beam seep detection was performed from 2004 to 2008 with a FURUNO-1000 or a FURUNO-1100 echosounders (28 kHz) installed on R.V. Vereshchagin or R.V. Titov. The hydro-acoustic water-column data was continuously digitally recorded using a digitizing system developed in-house by the Limnological Institute in Irkutsk (LIN) (Granin et al., in press). During theses cruises, a total length of 666 km of echosounder tracks was recorded within the 630 km^2 Posolsky Bank area, which resulted in the detection of 65 active flare locations (Figs. 6.3., 6.4. and 6.5.). Since a flare can comprise one single bubble stream or can be a conjugation of different bubble streams or seeps within the footprint of the echosounder, the real amount of seeps, i.e. bubble-releasing locations on the lake floor is unknown.

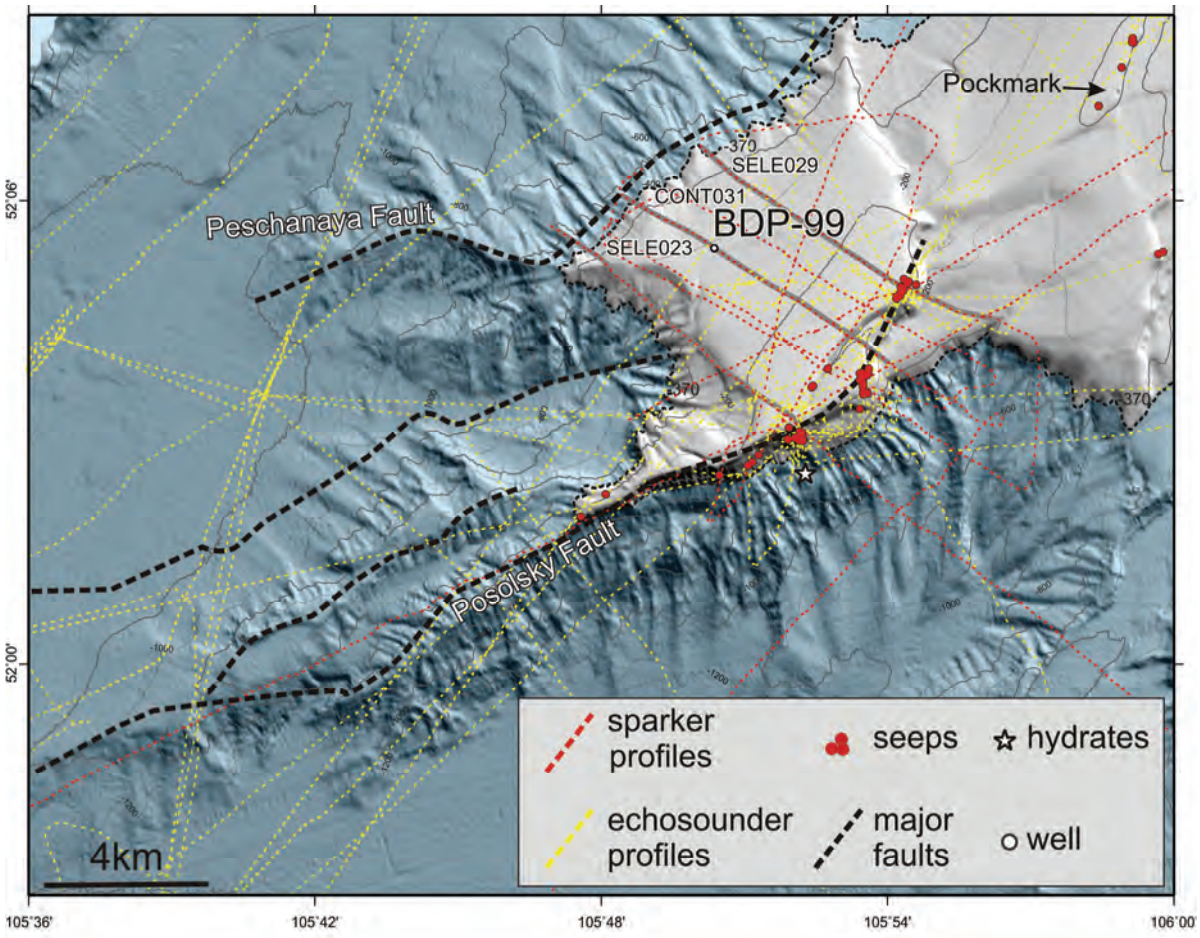

Figure 6.3. Multibeam bathymetry map of the Posolsky Bank overlain by bathymetric contours, detected seep locations (red dots), acquired sparker and echosounder profiles (respectively red and yellow dashed lines) and main faults (black dashed lines) (see Fig. 6.1. for location). Location of BDP-99 drill hole is also indicated together with depth contour of -370 m which forms the theoretical boundary of the GHSZ for pure methane hydrate (blue area) (Sloan, 1998).

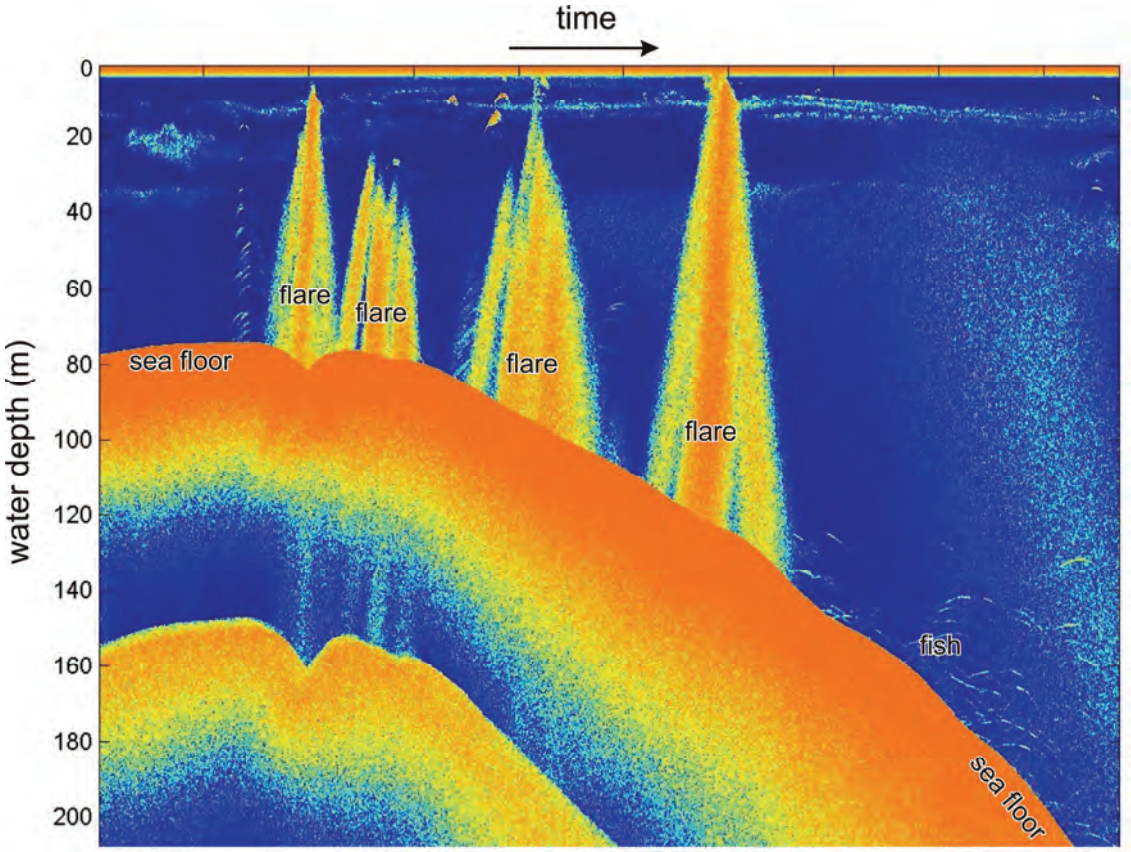

Figure 6.4. Echogram from the central seep area on the scarp of the Posolsky Bank (for location see Fig. 6.8.) where rising bubbles are hydro-acoustically detected as „flares". The other backscatter signals in the water column probably correspond to fish.

6.3.2. Multibeam bathymetry

Multibeam swath bathymetry was acquired in the summer of 2009 with RCMG's mobile 50 kHz SeaBeam 1050 multibeam system during a two-month-long survey with R.V. Titov (Naudts et al., submitted). In total 12600 km of multibeam echosounder tracks were sailed covering 15000 km^2, including the Posolsky Bank area (Figs. 6.1.-6.3.). The system was operated with 120° swath, transmitting and receiving 108 beams of 3° by 3° beam angle and was motion-compensatend by an IXSEA OCTANS 3000 sensor from IFM-GEOMAR. Sound-velocity profiles were acquired via CTD casts and the sound velocity at the transducers was continuously measured by an online sound-velocity probe. Data acquisition was managed with Hydrostar Online and data-processing was carried out with HDPEdit and HDPPost software from L-3 ELAC Nautik GMBH. All grids shown in this paper have a cell size of 30 m.

6.3.3. Seismic subbottom data

The high-resolution seismic data were collected with RCMG's multi-electrode CENTIPEDE-sparker as a source (energy: 500 J) and a SIG single-channel streamer with 10 hydrophones as a receiver. The analog signal was bandpass-filtered (200-2000 Hz) and recorded on a Triton Elics Delph-2 system. The theoretical vertical resolution is 1 m and the maximum penetration is 200-300 ms two-way travel time (TWTT). Apart from the frequency filtering no other processing was carried out on the seismic data. Interpretation of the data was carried out with the Kingdom Suite software

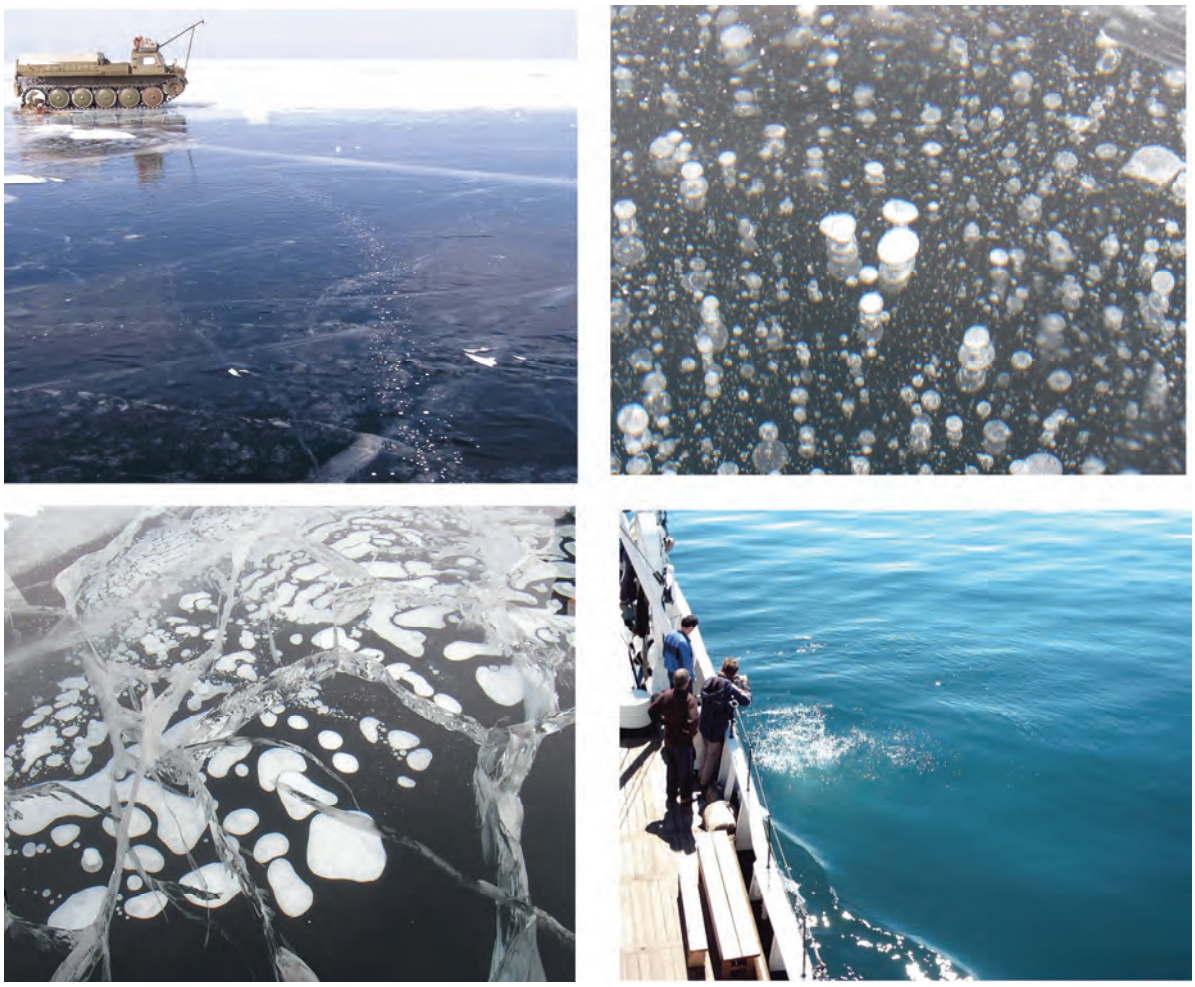

Figure 6.5. Pictures of gas bubbles being trapped underneath and within the frozen lake surface above seep sites at Posolsky Bank (pictures courtesy of N. Granin). The lower-right picture shows gas bubbles reaching the lake surface at a seep site close to the Selenga Delta (picture courtesy of V. Kapitanov).

package from SMT. During the 1997 (SELE-profiles) and 2000 (CONT-profiles) cruises, 175 km of sparker data were recorded in the Posolsky Bank area (Fig. 6.3.).

6.4. Observations and results

6.4.1. Lake-floor morphology

The Posolsky Bank, an uplifted basement block that is covered by a reduced sedimentary cover, can morphologically be seen as the southern extent of the Selenga Delta into the SBB (Figs. 6.1. and 6.2.). The Posolsky Bank is bounded by two major faults, the Peschanaya Fault in the north and the Posolsky Fault in the south, which strongly affect the lake-floor morphology (Figs. 6.2., 6.3. and 6.5.) (Scholz and Hutchinson, 2000). The top of the Posolsky Bank is flat and slopes gently to the NW (ca. 1° - 2°) from a minimum water depth of -36 m. At ca. -370 m water depth there is a strong change in slope to ca. 5°-15°; below this depth the lake bed is strongly incised. The incised morphology with ridges and gullies defining several canyon systems can also be seen on the steep western and southern slopes to water depths of -1100 to -1200 m (Figs. 6.3. and 6.5.). These incised flanks are often associated with scarps of small sublacustrine landslides (Fig. 6.3.). The northeastern side of the Posolsky Bank is not incised and forms, via a fault scarp, the transition to the Selenga Delta (Fig. 6.2. and 6.3.).

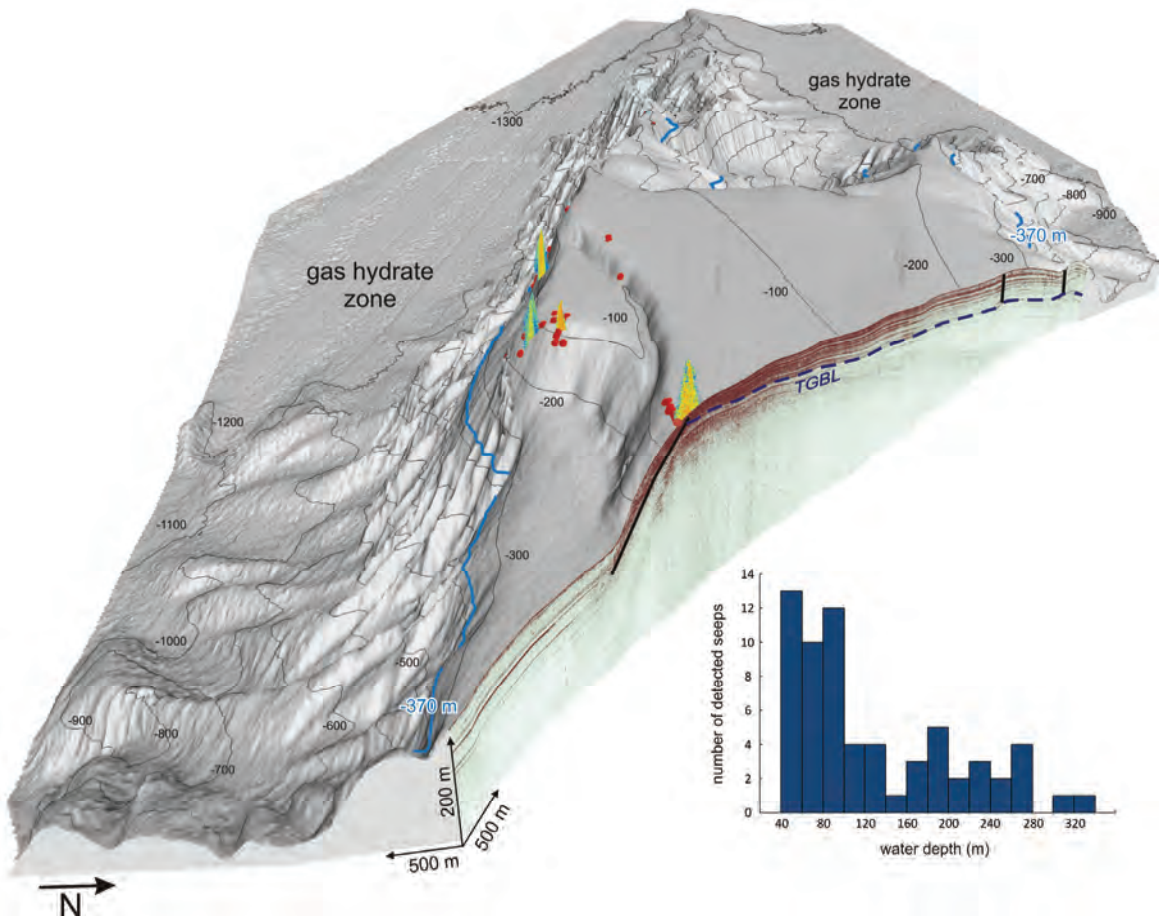

Figure 6.6. 3D view of multibeam bathymetry overlain by bathymetric contours and seep locations, plotted as red dots or shown as 3D flares in combination with sparker profile SELE029 (for location see Fig. 6.3.). Seeps occur at the crest of the Posolsky Bank upslope of the GHSZ, delineated by the -370 m blue contour line. No seeps have been detected near the Posolsky Bank within the GHSZ. On the seismic profile, strong acoustic attenuation in combination with dispersed enhanced reflections can be seen along one reflection. This reflection is interpreted as the TGBL. Seeps occur where the TGBL is cut off by the Posolsky Fault. The graph in the lower right corner shows the seep distribution versus depth with a clear seep cluster at -40 to -100 m water depth and no seeps in water depths greater than -340 m.

6.4.2. Stratigraphic framework

The sedimentary cover of the Posolsky Bank is well-stratified with a bedding that is generally parallel to the lake-floor morphology, except in the vicinity of faults (Figs. 6.6. and 6.7.) (Charlet et al., 2005). Seismic profiles SELE029 and CONT031 clearly show the presence of a well-stratified sediment package that thickens away from the crest of the Posolsky Bank towards the NW under the influence of the activity of the Posolsky Fault System. This set of continuous parallel high-amplitude reflections can be found throughout the Selenga area and represents the deposition of fine-grained hemipelagic muds which reaches a maximum thickness of ca. 100 m and represents 650 ka (Fig. 6.6. and 6.7.) (Colman et al., 2003; Bezrukova et al., 2005). Below this package with high-amplitude reflections, almost no reflections can be observed on SELE029 and CONT031. This sharp transition corresponds to a radical change in sedimentation environment with coarser sediments deposited during the glacial period preceding the quiet hemipelagic sedimentation of the last 650 ka (Colman et al., 2003; Bezrukova et al., 2005). This boundary and change in sedimentation environment corresponds to the start of increased subsidence in the SBB and Selenga area (Scholz and Hutchinson, 2000; Colman et al., 2003).

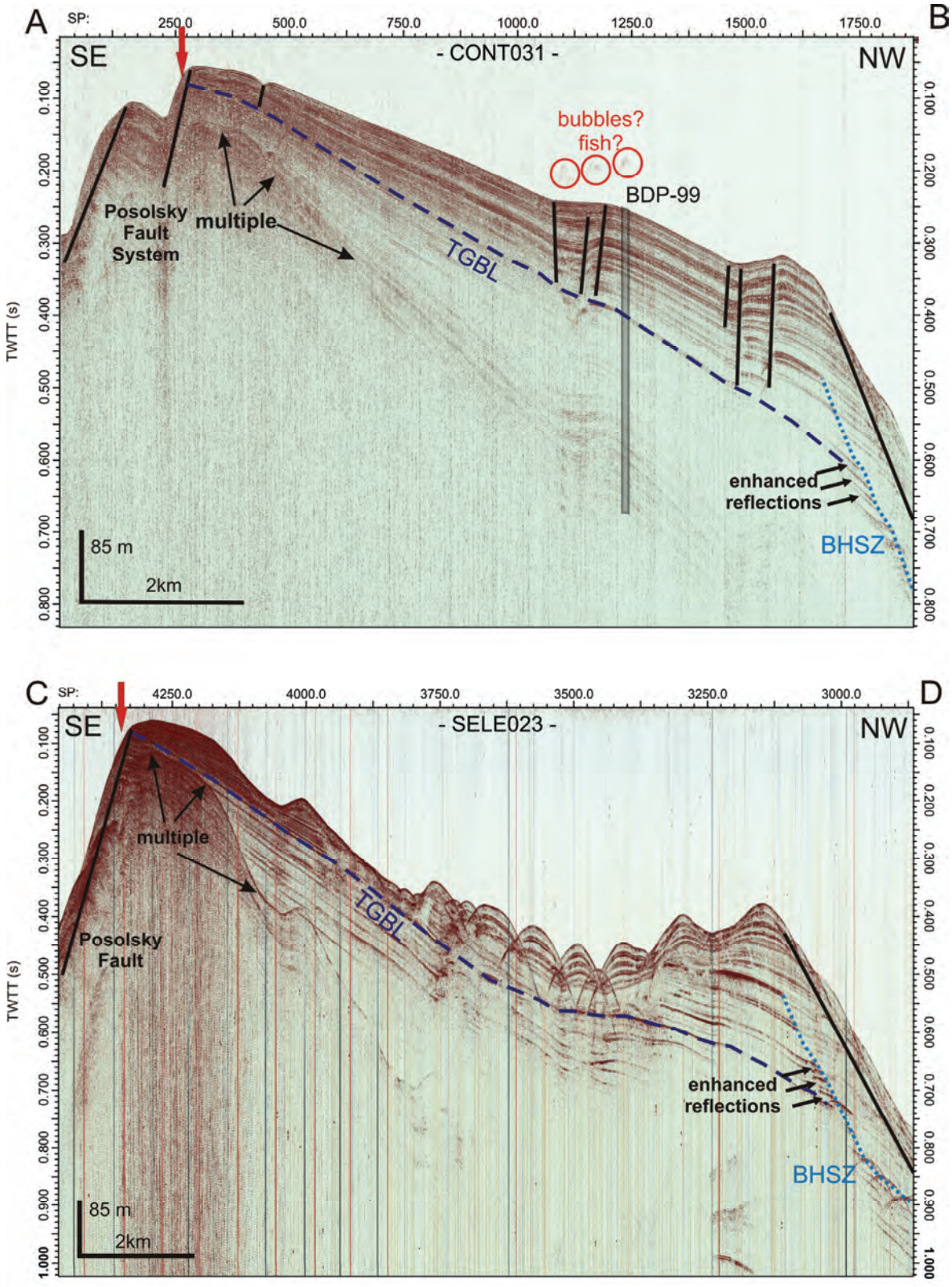

Figure 6.7. Seismic sparker profiles CONT031 (AB) and SELE023 (CD) where the TGBL can be traced from the seeps at the crest of the Posolsky Bank to below the BGHSZ. The BGHSZ shows up as a series of enhanced reflections. The location of BDP-99 well is also indicated. For locations of both profiles see Fig. 6.3.

6.4.3. Gas seep distribution

Up to 65 flares, each possibly consisting of several individual seeps, were hydro-acoustically detected within the 630 km^2 area around the Posolsky Bank in the NE part of the SBB. The seeps occur at -43 to -332 m water depth, with 54 % at water depths shallower than -100 m and 97 % at water depths shallower than -265 m (Fig. 6.6.). In many cases flares, visible on echograms, reached the lake surface; this was confirmed by the observations of bubbles at the lake surface (Figs. 6.4. and 6.5.). Integration of seep locations, multibeam bathymetry and seismic profiles shows that the majority of the seeps occur at the fault scarp in front of the crest of the Posolsky Bank where the sedimentary strata are cut off by the Posolsky Fault (Figs. 6.3., 6.6. and 6.7.). The seeps in the northeastern part of the study area are not directly related to the Posolsky Bank; they do, however, occur at similar locations, i.e. near a crest and at a fault scarp (Fig. 6.3.). Apart from the flares, an almost perfect circular pockmark, with a diameter of 160 m and a depth of 14 m can be observed in this area at -100 m water depth (Fig. 6.3.). The pockmark, indicative for fluid release at the lake floor, occurs at the conjunction of two fault scarps.

6.4.4. Indications for shallow gas and gas-hydrate occurrence

Apart from the release of free gas into the water column, as indicated by the hydro-acoustically detected flares, the presence of shallow gas and fluid-flow structures in the subsurface can also be inferred from seismic reflection data. Shallow gas strongly influences the mechanical and acoustic properties of the sediment (increased sound attenuation, acoustic energy scattering, affecting sound velocity, etc.). Therefore geo-acoustic methods, like reflection profiling, are significantly affected by the presence of shallow gas and are thus very well suited for the detection of free gas in the sediments. Even small concentrations of free gas present in the sediment pore space (0.5% gas by volume) already generate a variety of shallow-gas signatures (e.g. enhanced reflections, acoustic turbidity and acoustic blanking, etc) (Judd and Hovland, 2007; Naudts et al., 2009). Our sparker data demonstrate several types of enhanced and blanked reflections, which could or could not be indicative for the presence of shallow gas. Distinct alternations of high- and low-amplitude reflections in the upper well-stratified package are manifested on all profiles (Fig. 6.6. and 6.7.). This seismic response is, however, most likely not related to shallow gas but rather to temporal changes in the sedimentation environment and to variations in the physical properties of the associated sediments (Charlet et al., 2005). Possible gas-enhanced high-amplitude reflections associated with acoustic blanking occur near the crest of the Posolsky Bank and at the northwestern edge of the Posolsky Bank (Figs. 6.6. and 6.7.). At the crest of the Posolsky Bank, these enhanced reflections occur exclusively beneath the seep locations, indicating a clear relation with shallow gas. The enhanced reflections at the northwestern part of the Posolsky Bank generally occur over a short distance and are overlain by low-amplitude (blanked) reflections (Fig. 6.7.). This kind of seismic signature is well-known from a similar sparker dataset acquired in the deep part of the SBB. The transition line between both acoustic responses cross-cuts the stratigraphy and mimics the lake floor morphology and therefore is interpreted as a BSR (Vanneste et al., 2001; De Batist et al., 2002; Vanneste et al., 2002). This BSR is not a local feature but is present on all seismic profiles recorded at northwestern edge of the Posolsky Bank in water depths exceeding -290 m and at a subsurface depth of ca. 60 m (Fig. 6.7. and 6.8.). Generally it is assumed that the characteristic seismic signatures of BSRs are the result of relative dense hydrate-bearing layers with higher acoustic velocity overlying gassy sediments with low acoustic velocity. The presence of gas hydrates within the Posolsky Bank sediments is not only indirectly indicated by the geophysical data, hydrates have also been sampled at the lake floor at -500 m water depth, during a dive with the MIR-2 submersible at the Posolsky Fault scarp in the summer of 2009 (Oleg Khlystov, personal communication). Gas hydrates were retrieved at a small slide

scarp 250 m below one of the major seep sites on the crest of the Posolsky Bank (Fig. 6.3.). The location with hydrates was also characterized by the presence of big bacterial mats indicating active fluid flow.

6.5. Discussion

6.5.1. Gas-hydrate stability, heat flow and topographic effect

The occurrence of BSRs from -290 m water depth at a subsurface depth of 60 m discussed in previous section does not correspond to earlier BSR observations in Lake Baikal starting at water depths of -500 to -580 m and at 50-100 m beneath the lake floor (Golmshtok et al., 2000; Vanneste et al., 2001).In most cases, the BSR corresponds to the lower, P-T controlled boundary of the GHSZ, also known as the BGHSZ. The stability limit for pure methane hydrates in Lake Baikal occurs at -370 m water depth (Sloan, 1998), when calculated using a present-day bottom water temperature of 3.5°C and a salinity of 0.76 ‰ (Golmshtok et al., 2000). So the newly observed BSRs occur well outside of the GHSZ for pure methane hydrate and occur in shallower water than the previously observed BSRs. This indicates that the inferred hydrates, assuming that the observed BSRs are indeed associated with hydrates, can only be stable if the local hydrate gas composition consist of a mixture of methane

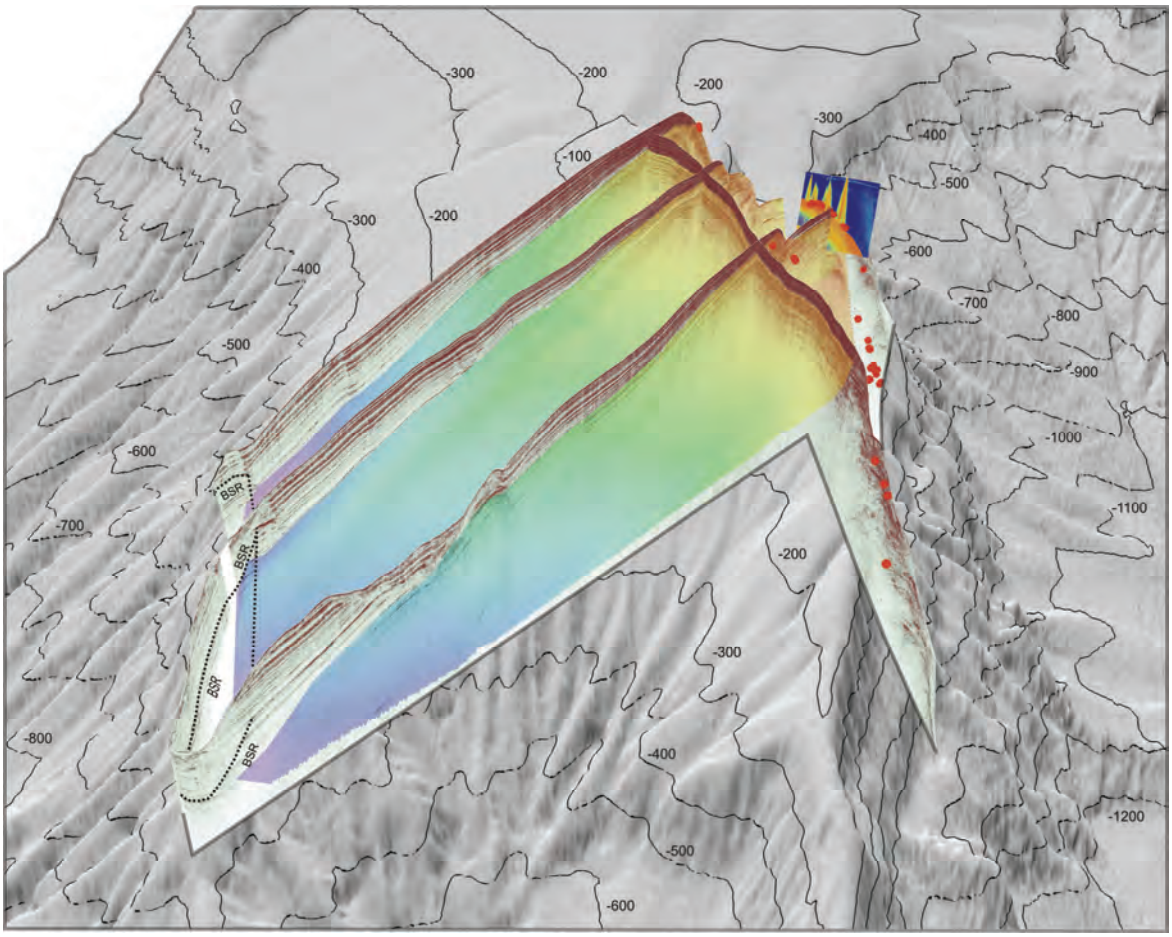

Figure 6.8. 3D view of multibeam bathymetry overlain with bathymetric contours and with seep locations plotted as red dots or shown on an echogram in combination with three sparker profiles. The top of the gas-bearing layer (TGBL) is shown as depth color-coded surface. This surface starts from or above the seeps positions at the scarp of the Posolsky Bank and can be traced down the Posolsky Bank to below the BSR or BGHSZ.

and higher hydrocarbons. Furthermore, the large subsurface depth of the observed BSRs at the limit of the GHSZ indicates that the local thermal conditions also strongly differ from the regional background values.

Based on hydrate stability calculations, a gas mixture of ca. 96 % methane and 4 % ethane would allow to shift the limit of the GHSZ to a water depth of -290 m (Sloan, 1998). There are several indications that such gas mixture indeed does occur at the Posolsky Bank. First of all, higher ethane concentrations have been measured in gas bubbles sampled from the Posolsky Bank gas seeps and at other gas seeps in Lake Baikal (Kalmychkov et al., 2006). Furthermore, the sharp depth limit of the seep distribution indicates that gas hydrates are probably present at the Posolsky Bank and that these hydrates act as a buffer preventing seepage in the GHSZ as was observed in other regions (Naudts et al., 2006; Westbrook et al., 2009). The depth limit for the majority of the seeps (97%) is -265 m water depth. When using the -265 m water depth as the limit of the GHSZ, a gas mixture of 94-95% methane and 5-6% ethane is needed to allow hydrates to be stable for the given ambient conditions. The latter is of course only an indirect indication that higher ethane concentrations probably do occur at the Posolsky Bank.

BSRs have never been observed to intersect the lake floor/seafloor at the limit of the GHSZ. This is partially related to the local geothermal gradient and associated heat flow. This is also the case for the BSRs observed at the Posolsky Bank, which occur at a subsurface depth of 60 m

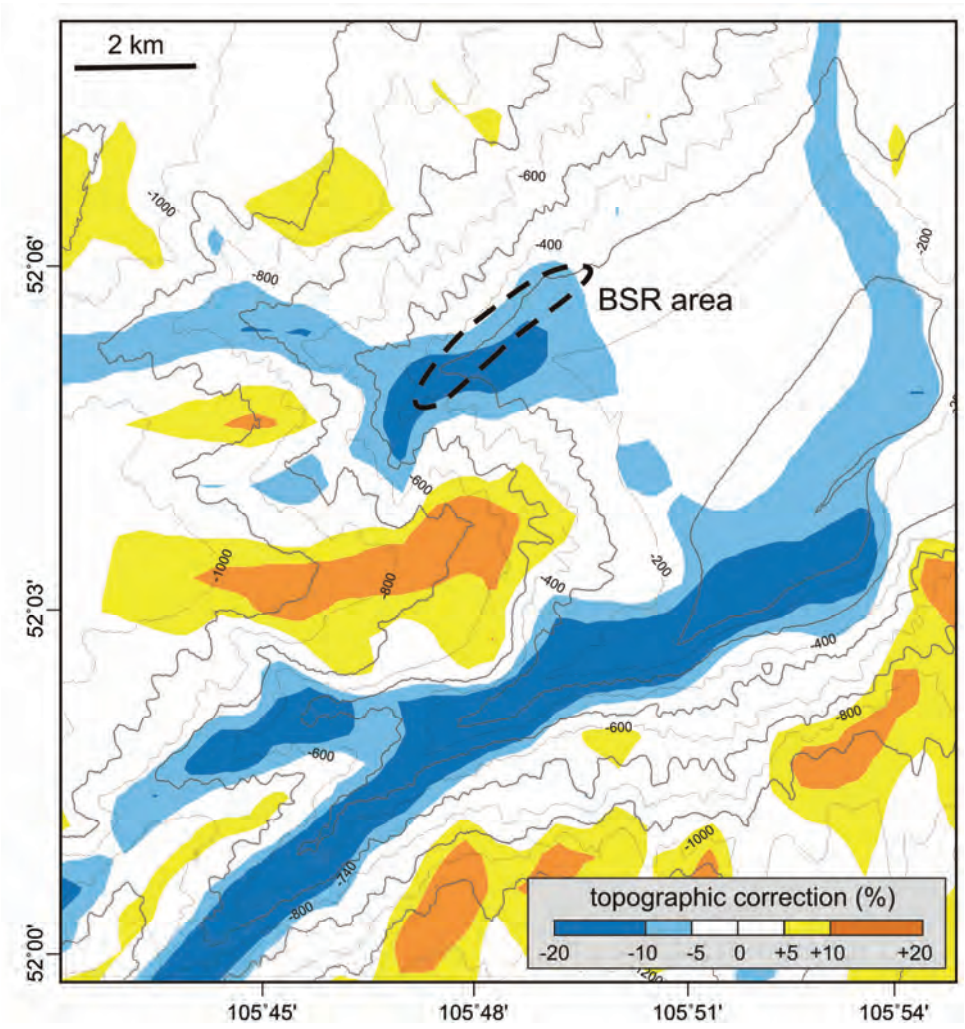

Figure 6.9. Bathymetric contour map of the Posolsky Bank area, showing the modeled topographic correction on background regional heat flow caused by the relief of the Posolsky Bank.

at the limit of the GHSZ (Figs. 6.7. and 6.8.). To obtain such a subsurface depth of the BSRs and thus the BGHSZ at the limit of the GHSZ, a local heat-flow value of 32-34 mW/m² is required. Heat-flow measurements for the Posolsky Bank are absent, but measured heat-flow values in Lake Baikal vary between 40 ± 6 and 195 ± 25 mW/m^2, with a mean value of 71 ± 21 mW/m^2 (Golubev et al., 1993; Vanneste et al., 2002; Poort and Klerkx, 2004). These heat flow values are clearly too high to allow a subsurface depth of 60 m for the observed BSRs at the limit of the GHSZ. However, local topographic variations can lead to changes in the conductive background heat flow (Poort et al., 2007). Topographic relief will attenuate heat flow in topographic highs and enhance it topographic lows. Therefore, the influence of the Posolsky Bank relief on the regional heat flow has been modeled using the procedure and code for topographic correction described in Balling et al (1981) and adjusted for digital terrain models by F. Lucazeau (personal communication). The model uses a background thermal gradient of 50 mKm^{-1} and a uniform thermal conductivity of 1.11 $Wm^{-1}K^{-1}$. For the upper meters of sediments, this model predicts a thermal gradient that differs up to 20 % in comparison with the background thermal gradient as a result of the topography of the Posolsky Bank (see Fig. 6.9.). When assuming a feasible background thermal gradient of 40 mKm^{-1} and considering the modeling results, the pronounced topographic relief of the Posolsky Bank can lead to a reduction of the local heat flow to the needed heat flow values of 32-34 mW/m².

These results indicate that the observed BSR probably does correspond to the BGHZS and that hydrates possibly do occur at the observed 60 m subbottom depth at -290 m water depth.

6.5.2. Fluid flow and seep distribution model

The observations and results discussed in the previous sections show that gas is being released at the Posolsky Fault scarp near the crest of the Posolsky Bank and that gas hydrates and shallow free gas are present in the subsurface of the NW edge of the Posolsky Bank (Figs. 6.6., 6.7. and 6.8.). In addition gas hydrates have been sampled at the fault scarp at a depth of -500 m (Oleg Khlystov, personal communication). The occurrence of seeps on the Posolsky Fault scarp could indicate that the fault system acts as a fluid conduit resulting in seepage. On the other hand, seismic data show that there is a stratigraphic connection between the seep locations and the free gas trapped underneath the BSRs indicating that fluid flow occurs along the tilted strata of the Posolsky Bank (Figs. 6.6. and 6.7.). Another alternative could be that the released gas comes from a shallow and local source near the seep locations. But this option is rather unlikely because of the presence of higher hydrocarbons in the released gas indicating at least an admixture of fluids from a deep source (Kalmychkov et al., 2006).

The first option with the fault acting as a fluid conduit for the seeps on the Posolsky Bank is also rather unlikely. Most compelling evidence is provided by the distribution of the gas seeps. The seeps occur only at the upper part of the Posolsky Fault scarp; the deepest seep is observed at -332 m water depth, whereas 97 % of the seeps occur in water depths shallower than -265 m and even 54 % of the seeps occur in water depths shallower than -100 m (Fig. 6.6.). Since the Posolsky Fault system is a combination of several faults forming a combined fault scarp of over 600 m, it is rather unlike that such an open system is able to act as a conduit for fluids that only allows the majority of the methane to be released at less than -100 m water depth (Figs. 6.6. and 6.7.). If the Posolsky Fault did act as a conduit, the seep distribution would have been completely different with seepage being more widespread over the fault scarp at all water depths. One could argue that gas hydrates act as a buffer and prevent gas release in the GHSZ as was already postulated in this study and by others (Naudts et al., 2006; Westbrook et al., 2009). But in this case, most of the methane migrating along the fault would be either trapped within the present gas hydrates or would be released just outside of the GHSZ, as was observed for the seeps in West Spitsbergen (Westbrook et al., 2009). In the case of the Posolsky Bank this would lead to a seep distribution with mainly seeps occurring at

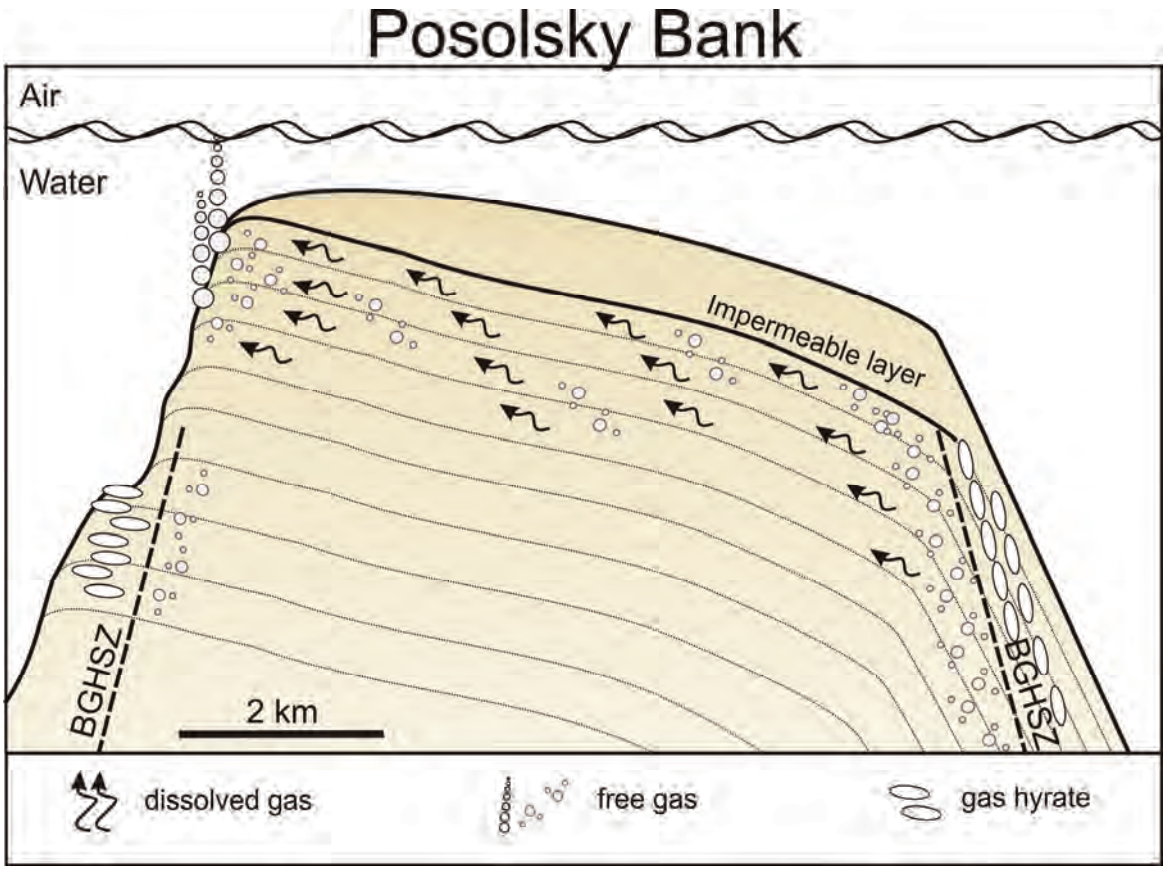

Figure 6.10. Proposed seep model for the Posolsky Bank gas seeps.

water depths of ca. 300-350 m, depending on the present gas composition and ambient conditions affecting gas-hydrate stability. However the observed seep distribution shown in figure 6.6. demonstrates the opposite with mainly seeps being released in water depths shallower than -100 m. So we can safely postulate that the fault system probably doesn't act as a fluid conduit for the seeps detected within the study area.

The second option wherein the seeps on the Posolsky Fault scarp are fed by fluid migration along the tilted strata of the Posolsky Bank can only be valid if the stratigraphic and sedimentary buildup of the Posolsky Bank allows such a migration pathway. The seismic data does indeed indicate the presence of such a possible migration pathway which connects the seeps at the scarp with the free gas present below the BSRs (Figs. 6.6., 6.7. and 6.8.). On the seismic data the top this possible gas-bearing layer (TGBL) shows up as the transition from the upper seismic unit consisting of continuous parallel high-amplitude reflections to the lower seismic unit with an almost transparent seismic facies (Figs. 6.6., 6.7. and 6.8.). Based on the eight sparker profiles available on the Posolsky Bank, the TGBL could be mapped as an almost continuous surface throughout the subsurface of the Posolsky Bank (Figs. 6.8.). The transition represented by the TGBL corresponds to a change in sedimentary characteristics with hemipelagic fine grained sediments overlaying coarser sediments (Colman et al., 2003; Bezrukova et al., 2005). The core data from the BDP-99 drill core provides some extra indication that the sediment layer underneath the TGBL is indeed suitable as a fluid conduit (BDP-99 locations is indicated on Figs. 6.3. and 6.7.) (Bezrukova et al., 2005). The core data shows that below the TGBL at a depth interval between 94-109 m there are much coarser sediments than in the overlying and underlying sediments as indicated by the clay and silt percentages and the gamma log (Bezrukova et al., 2005). This interval is also characterized by the widespread occurrence of granules and pebbles. The upper meter of this interval even consist of more than

50 % sand (Bezrukova et al., 2005). The grain size distribution in the sediment package below the TGBL, together with its confinement in between much fine finer sedimentary units, makes the sediment package below the TGBL extremely well-suited as a fluid migration pathway. This is also the first sedimentary unit in the BDP-99 core, starting from top, with plant and wood fragments indicating that this layer possibly also contributes as a source for the released methane (Bezrukova et al., 2005).

Based on the seismic stratigraphy and the BDP-99 well data we postulate that the seeps on the Posolsky Fault scarp near the crest of the Posolsky Bank are supplied by gas that migrated along relatively permeable sedimentary strata which are cut off by the Posolsky Fault system (Fig. 6.10.). This gas is partially sourced by the free gas present underneath the BSRs/BGHSZ at the NW edge of the Posolsky Bank. The seismic data show that the free gas present below the BGHSZ is not completely trapped by the gas hydrates; the geometry and permeability of the sedimentary build up of the Posolsky Bank enables the gas to migrate upwards along the sedimentary strata (Figs. 6.7., 6.8. and 6.10.).
Even the gas hydrates and seeps present at larger depths along the Posolsky Fault scarp are probably supplied by gas migration through the tilted sediment layers that make up the Posolsky Bank.

6.6. Conclusions

Integration of the seep distribution, the seismic stratigraphy, well data and gas-hydrate stability analysis suggest that the shallow gas seeps near the crest of the Posolsky Bank are partially supplied by gas from below the base of the gas-hydrate stability zone. Gas-hydrate-cemented strata act as a seal and together with the geometry and stratigraphy of the Posolsky Bank, gas is focused upwards via permeable stratigraphic pathways. Gas is eventually released in the water column, where these pathways are cut off by faults. This setting differs from the deep-water Baikal seeps and mud volcanoes, which are believed to be related to destabilizing gas hydrates under the influence of a tectonically-controlled geothermal fluid pulse along adjacent faults.

Acknowledgements

We like to thank the captains and the crews of R/V Vereshchagin and R/V Titov for their craftsmanship and all scientists and students who have contributed to the several studies on Lake Baikal. This research was supported by the Federal Office for Scientific, Technical and Cultural Affairs (OSTC) (Project BL/02/R11 phase 2 and IN/RU/005) and INTAS project (INTAS-2001-2309). The multibeam mapping survey was conducted in the framework of SBRAS project 17.8 and FWO Flanders project 1.5.198.09. We specially like to thank Boris Schulze (L-3 ELAC Nautik GMBH) Jens Greinert, Jeroen Vercruysse and Wim Versteeg for getting us prepared for the multibeam survey. Joerg Bialas and Wili Weinrebe (IFM-GEOMAR) are thanked for the use of the OCTANS motions sensor. We also would like to thank Andrey Habuev, Igor Seminsky, Robbert, Casier Myriam Cuylaerts, Joris Synaeve, Nele Vlamynck, Pavel Generalchenko, Oleg Belousov, Ruslan Gnatovsky, Mikhail Makarov and Konstantin Kucher for their much appreciate help during the multibeam expedition. We also thank Dr. Francis Lucazeau for kindly providing us his adopted version of the code for topographic corrections on heat-flow data. Finally we thank IVS 3D (Fledermaus) and SMT (Kingdom Suite) for providing us with academic licenses.

Additional information

Lieven Naudts processed and interpreted most of the datasets, wrote the manuscript and made all figures. Lieven Naudts was chief scientist during the 9 weeks of the multibeam expedition on RV Titov and provided funds for this expedition via an FWO grant. Co-authors helped by reviewing the manuscript, by helping during the data acquisition and/or by providing the datasets. Corrections for topographic effect were made by Jeffrey Poort; who also assisted with the heatflow and gas-hydrate stability calculations.

References

Artemov, Y.G., Egorov, V.N., Polikarpov, G.G., Gulin, S.B., 2007. Methane emission to the hydro - and atmosphere by gas bubble streams in the Dnieper paleo-delta, the Black Sea. Mar. Ecol. J., 5-26.

Bezrukova, E., Bukharov, A., Bychinsky, V., Fedenya, S., Gelety, V., Goreglyad, A., Gorokhov, I., Gvozdkov, A., Ivanov, E., Kalmychkov, G., Kawai, T., Kerber, E., Khakhaev, B., Khomutova, M., Khursevich, G., Kochukov, V., Krainov, V., Kravchinsky, V., Kudryashov, N., Kulagina, N., Kuzmin, M., Letunova, P., Levina, O., Ochiai, S., Pevzner, L., Prokopenko, A., Solotchin, P., Tanaka, A., Tkachenko, L., Williams, D., Yamaguchi, J., 2005. A new Quaternary record of regional tectonic, sedimentation and paleoclimate changes from drill core BDP-99 at Posolskaya Bank, Lake Baikal. Quat. Int. 136, 105-121.

Charlet, F., Fagel, N., De Batist, M., Hauregard, F., Minnebo, B., Meischner, D., Sonic Team, 2005. Sedimentary dynamics on isolated highs in Lake Baikal: evidence from detailed high-resolution geophysical data and sediment cores. Global Planet. Change 46, 125-144.

Colman, S.M., Karabanov, E.B., Nelson, C.H., 2003. Quaternary sedimentation and subsidence history of Lake Baikal, Siberia, based on seismic stratigraphy and coring. J. Sediment. Res. 73, 941-956.

De Batist, M., Klerkx, J., Van Rensbergen, P., Vanneste, M., Poort, J., Golmshtok, A.Y., Kremlev, A.A., Khlystov, O.M., Krinitsky, P., 2002. Active hydrate destabilization in Lake Baikal, Siberia? Terra Nova 14, 436-442.

Galaziy, G.I., 1993. Baikal Atlas (in Russian). Federal Agency for Geodesy and Cartography, Moscow. 160 pp.

Golmshtok, A.Y., Duchkov, A.D., Hutchinson, D.R., Khanukaev, S.B., 2000. Heat flow and gas hydrates of the Baikal Rift Zone. Int. J. Earth Sci. 89, 193-211.

Golmshtok, A.Y., Duchkov, A.D., Hutchinson, D.R., Khanukaev, S.B., Elnikov, A.I., 1997. Estimations of heat flow on Baikal from seismic data on the lower boundary of the gas hydrate layer. Geol. Geofiz. 38, 1677-1691.

Granin, N., Makarov, M., Kucher, K., Gnatovsky, R., in press. Gas seeps in Lake Baikal—detection, distribution, and implications for water column mixing. Geo-Mar. Lett.

Granin, N.G., Granina, L.Z., 2002. Gas hydrates and gas venting in Lake Baikal. Russian Geology and Geophysics 43, 589-597.

Greinert, J., Artemov, Y., Egorov, V., De Batist, M., McGinnis, D., 2006. 1300-m-high rising bubbles from mud volcanoes at 2080m in the Black Sea: Hydroacoustic characteristics and temporal variability. Earth Planet. Sci. Lett. 244, 1-15.

Haacke, R.R., Westbrook, G.K., Hyndman, R.D., 2007. Gas hydrate, fluid flow and free gas: formation of the bottom-simulating reflector. Earth Planet. Sci. Lett. 261, 407-420.

Hachikubo, A., Khlystov, O., Manakov, A., Kida, M., Krylov, A., Sakagami, H., Minami, H., Takahashi, N., Shoji, H., Kalmychkov, G., Poort, J., 2009. Model of formation of double structure gas hydrates in Lake Baikal based on isotopic data. Geophys. Res. Lett. 36.

Henriet, J.P., Mienert, J., 1998. Gas hydrates: Relevance to world margin stability and climate change. Special Publications. The Geological Society, London. 338 pp.

Hutchinson, D.R., Golmshtok, A.Y., Scholz, C.A., Moore, T.C., Lee, M.W., Kuz'min, M., 1991. Bottom simulating reflector in Lake Baikal. Eos Trans. Am. Geophys. Union, 307.

INTAS Project 99-1669 Team, 2002. A new bathymetric map of Lake Baikal, [cd-rom], open-file report. Renard Centre of Marine Geology (RCMG), Ghent University, Belgium.

Judd, A., Hovland, M., 2007. Seabed fluid flow: the impact on geology, biology and the marine environment. Cambridge University Press, Cambridge. 475 pp.

Judd, A.G., 2003. The global importance and context of methane escape from the seabed. Geo-Mar. Lett. 23, 147-154.

Kalmychkov, G., Egorov, A., Kuz'min, M., Khlystov, O., 2006. Genetic types of methane from Lake Baikal. Doklady Earth Sciences 411, 1462-1465.

Khlystov, O.M., 2006. New findings of gas hydrates in the Baikal bottom sediments. Russian Geology and Geophysics 47, 972-974.

Kida, M., Khlystov, O., Zemskaya, T., Takahashi, N., Minami, H., Sakagami, H., Krylov, A., Hachikubo, A., Yamashita, S., Shoji, H., Poort, J., Naudts, L., 2006. Coexistence of structure I and II gas hydrates in Lake Baikal suggesting gas sources from microbial and thermogenic origin. Geophys. Res. Lett. 33.

Klerkx, J., De Batist, M., Poort, J., Hus, R., Van Rensbergen, P., Khlystov, O., Granin, N., 2006. Tectonically controlled methane escape in Lake Baikal, Advances in the Geological Storage of Carbon Dioxide, pp. 203-219.

Klerkx, J., Zemskaya, T.I., Matveeva, T.V., Khlystov, O.M., Namsaraev, B.B., Dagurova, O.P., Golobokova, L.P., Vorob'eva, S.S., Pogodaeva, T.P., Granin, N.G., Kalmychkov, G.V., Ponomarchuk, V.A., Shoji, H., Mazurenko, L.L., Kaulio, V.V., Solov'ev, V.A., Grachev, M.A., 2003. Methane hydrates in deep bottom sediments of Lake Baikal. Doklady Earth Sciences 393A, 1342-1346.

Krylov, A., Khlystov, O., Zemskaya, T., Minami, H., Hachikubo, A., Nunokawa, Y., Kida, M., Shoji, H., Naudts, L., Poort, J., Pogodaeva, T., 2008a. First discovery and formation process of authigenic siderite from gas hydrate-bearing mud volcanoes in fresh water: Lake Baikal, Eastern Siberia. Geophys. Res. Lett. 35.

Krylov, A., Khlystov, O., Zemskaya, T., Minami, H., Hachikubo, A., Shoji, H., Kida, M., Pogodaeva, T., Naudts, L., Poort, J., 2008b. Crystallization of authigenic carbonates in mud volcanoes at Lake Baikal. Geochem. Int. 46, 985-995.

Kuzmin, M.I., Geletiy, V.F., Kalmychkov, G., Kuznetsov, F.A., Larionov, E.G., Manakov, A.Y., Mironov, Y.I., Smoljakov, B.S., Dyadin, Y.A., Duchkov, A.D., Bazin, N.M., Mahov, G.M., 2000. The first discovery of the gas hydrates in the sediments of the Lake Baikal. Gas Hydrates: Challenges for the Future 912, 112-115.

Kuzmin, M.I., Kalmychkov, G.V., Geletij, V.F., Gnilusha, V.A., Goreglyad, A.V., Khakhaev, B.N., Pevzner, L.A., Kavai, T., Ioshida, N., Duchkov, A.D., Ponomarchuk, V.A., Kontorovich, A.E., Bazhin, N.M., Mahov, G.A., Dyadin, Y.A., Kuznetsov, F.A., Larionov, E.G., Manakov, A.Y., Smolyakov, B.S., Mandelbaum, M.M., Zheleznyakov, N.K., 1998. First find of gas hydrates in sediments of Lake Baikal (in Russian). Dok Akad Nauk SSSR, 541-543.

Matveeva, T.V., Mazurenko, L.L., Soloviev, V.A., Klerkx, J., Kaulio, V.V., Prasolov, E.M., 2003. Gas hydrate accumulation in the subsurface sediments of Lake Baikal (Eastern Siberia). Geo-Mar. Lett. 23, 289-299.

Naudts, L., De Batist, M., Greinert, J., Artemov, Y., 2009. Geo- and hydro-acoustic manifestations of shallow gas and gas seeps in the Dnepr paleodelta, northwestern Black Sea. The Leading Edge 28, 1030-1040.

Naudts, L., Greinert, J., Artemov, Y., Staelens, P., Poort, J., Van Rensbergen, P., De Batist, M., 2006. Geological and morphological setting of 2778 methane seeps in the Dnepr paleo-delta, northwestern Black Sea. Mar. Geol. 227, 177-199.

Naudts, L., Khlystov, O.M., Khabuev, A.V., Seminskiy, I., Casier, R., Cuylaerts, M., General'chenko, P., Synaeve, J., Vlamynck, N., De Batist, M., Grachev, M.A., submitted. Newly collected multibeam swath bathymetry data herald a new phase in gas-hydrate research on Lake Baikal. *Eos Trans. AGU*.

Poort, J., Khlystov, O.M., Naudts, L., Duchkov, A.D., Shoji, H., Nishio, S., De Batist, M., Hachikubo, A., Kida, M., Minami, H., Manakov, A.Y., Kulikova, M.V., Krylov, A.A., submitted. Low thermal anomalies associated with double structure gas hydrates in K-2 mud volcano, Lake Baikal. Geochemistry Geophysics Geosystems.

Reeburgh, W.S., Tyler, S.C., Carroll, J., 2006. Stable carbon and hydrogen isotope measurements on Black Sea water-column methane. Deep-Sea Res., Part II 53, 1893-1900.

Schmid, M., De Batist, M., Granin, N.G., Kapitanov, V.A., McGinnis, D.F., Mizandrontsev, I.B., Obzhirov, A.I., Wuust, A., 2007. Sources and sinks of methane in Lake Baikal: A synthesis of measurements and modeling. Limnol. Oceanogr. 52, 1824-1837.

Scholz, C.A., Hutchinson, D.R., 2000. Stratigraphic and structural evolution of the Selenga Delta Accommodation Zone, Lake Baikal Rift, Siberia. Int. J. Earth Sci. 89, 212-228.

Sloan, E.D.J., 1998. Clathrate hydrates of natural gases. Marcel Dekker Inc., New York/Basel. 705 pp.

Suess, E., Torres, M.E., Bohrmann, G., Collier, R.W., Greinert, J., Linke, P., Rehder, G., Trehu, A., Wallmann, K., Winckler, G., Zuleger, E., 1999. Gas hydrate destabilization: enhanced dewatering, benthic material turnover and large methane plumes at the Cascadia convergent margin. Earth Planet. Sci. Lett. 170, 1-15.

Van Rensbergen, P., De Batist, M., Klerkx, J., Hus, R., Poort, J., Vanneste, M., Granin, N., Khlystov, O., Krinitsky, P., 2002. Sublacustrine mud volcanoes and methane seeps caused by dissociation of gas hydrates in Lake Baikal. Geology 30, 631-634.

Vanneste, M., De Batist, M., Golmshtok, A., Kremlev, A., Versteeg, W., 2001. Multi-frequency seismic study of gas hydrate-bearing sediments in Lake Baikal, Siberia. Mar. Geol. 172, 1-21.

Vanneste, M., Poort, J., De Batist, M., Klerkx, J., 2002. Atypical heat-flow near gas hydrate irregularities and cold seeps in the Baikal Rift Zone. Mar. Pet. Geol. 19, 1257-1274.

Westbrook, G.K., Thatcher, K.E., Rohling, E.J., Piotrowski, A.M., Pallike, H., Osborne, A.H., Nisbet, E.G., Minshull, T.A., Lanoiselle, M., James, R.H., Hohnerbach, V., Green, D., Fisher, R.E., Crocker, A.J., Chabert, A., Bolton, C., Beszczynska-Moller, A., Berndt, C., Aquilina, A., 2009. Escape of methane gas from the seabed along the West Spitsbergen continental margin. Geophys. Res. Lett. 36, L15608.

Williams, D.F., Kuzmin, M.I., Prokopenko, A.A., Karabanov, E.B., Khursevich, G.K., Bezrukova, E.V., 2001. The Lake Baikal drilling project in the context of a global lake drilling initiative. Quat. Int. 80-81, 3-18.

CHAPTER 7

Final discussion

The previous chapters have shown that bubble-releasing seeps occur at different oceanographic and plate-tectonic settings, at different seafloor morphologies, at different water depths, in or outside of the gas-hydrate stability zone. Furthermore, bubble-releasing seeps are often associated with various kinds of chemosynthetic communities and authigenic methane-derived carbonates. Within this chapter an integration and comparison is made of the obtained results and of published data from other seep sites around the world which occur in similar or different geological settings. The comparison and integration allows a better understanding of the controls and the manifestations associated with bubble-releasing seeps.

7.1. Global occurrence of bubble-releasing seeps

Before comparing and integrating the obtained results, an overview is given of bubble-releasing seeps around the world to better assess the similarities and differences between seep sites with regard to their locations, their geological controls and associated subsurface and seafloor manifestations (table 7.1.). Since bubble-releasing seeps form the main subject of this study, only those locations with proven bubble release are listed, be it by visual observations of gas bubbles or by observations of acoustic flares. Locations which are exclusively characterized by indicators of fluid flow or seepage activity, like bacterial mats, chemosynthetic megafauna, MDACs, shallow gas features, etc., are not added to this list. The locations with gas-bubble release are indicated on figure 7.1. The overview given in table 7.1. points out that seep locations occur worldwide in a variety of geological environments at various water depths ranging from coastal areas into the deep ocean basins, where they occur up to water depths of several kilometers. Despite this wide variety of seep locations, the amount of known sites with bubble release is relatively small. But this is probably biased by the restricted ability to find these very small locations at the seafloor. The publication years of the references given in table 7.1. are an indication of how recent and emergent our knowledge is regarding the distribution of bubble-releasing seeps, their controls, and the influence they have on the environment. It is only since the last decade that a more widespread availability of e.g. ROVs, adapted acoustical methods, etc. allows us to pinpoint bubble-release locations at the seafloor and adequately study seeps and their associated features. This study wants to better understand the geological controls that influence the seep distribution, the seep activity and their associated manifestations.

7.2. Subsurface controls on the distribution of bubble-releasing seeps

Within this section, the main subject of this study is discussed; what are the geological subsurface controls on the distribution of bubble-releasing seeps and on what scale do these controls act. The obtained results are also compared to data from other published seep sites (table 7.1.).

7.2.1. Fluid sources

The fluids released at seeps can have several sources and compositions, however methane is the most common gas released at the seafloor. Methane present in the ocean or lake sediments can have several different origins: microbial, thermogenic, geothermal-volcanic or abiogenic (Judd and Hovland, 2007).

Methane produced in the upper 1000 m below the seafloor is often referred to as shallow gas. It mainly consists of methane which is microbially formed by methanogenesis of

✓ **Location** ✓ **Tectonic setting**	**Water depth**	✓ **Fluid source** ✓ **Fluid pathway** ✓ **Fluid type**	**Features related to seepage**	**References**
		Within gas-hydrate stability zone		
✓ Batumi seep area, Black Sea ✓ passive margin	600-890 m	✓ organic-rich shales ✓ faults, diapirs ✓ microbial/thermogenic	gas bubbles, acoustic flares, sampled hydrates, seismic anomalies	(Klaucke et al., 2006; Nikolovska et al., 2008)
✓ Blake Ridge, Atlantic Ocean ✓ passive margin	>2000 m	✓ contourites, gas hydrates ✓ faults, salt diapirs ✓ microbial	gas bubbles, acoustic flares, pockmarks, sampled hydrates, seismic anomalies, chemosynthetic fauna	(Kvenvolden and Dillon, 1981; Holbrook, 2001; Van Dover et al., 2003)
✓ Congo Basin, Atlantic Ocean ✓ passive margin	3200 m	✓ turbiditic fan, gas hydrates ✓ faults, salt diapirs, erosional surfaces, buried chimneys ✓ Microbial/thermogenic	gas bubbles, pockmarks, sampled hydrates, seismic anomalies, chemosynthetic fauna	(Gay et al., 2007; Olu-Le Roy et al., 2007; Sahling et al., 2008)
✓ Dvurechenskiy Mud Volcano area, Black Sea ✓ passive margin	2055 m	✓ organic-rich shales ✓ faults, diapirs, buried chimneys ✓ microbial/thermogenic	gas bubbles, acoustic flares, sampled hydrates, enhanced heat flow, seismic anomalies	(Bohrmann et al., 2003; Greinert et al., 2006; Kutas and Poort, 2008; Feseker et al., 2009)
✓ Gulf of Mexico ✓ passive margin	300-3000 m	✓ carbonate source rocks ✓ faults, salt diapirs ✓ thermogenic/oil/brines	gas bubbles, acoustic flares, sampled hydrates, seismic anomalies, authigenic carbonates, chemosynthetic fauna	(MacDonald et al., 2002; MacDonald et al., 2003; Joye et al., 2004; Solomon et al., 2009)
✓ Håkon Mosby Mud Volcano, Barents Sea ✓ passive margin	1270 m	✓ preglacial biosiliceous oozes ✓ fault, pseudo-mud chamber ✓ microbial/thermogenic	gas bubbles, sampled hydrates, enhanced heat flow, seismic anomalies, chemosynthetic fauna	(Niemann et al., 2006; Jerosch et al., 2007; Perez-Garcia et al., 2009)
✓ Hikurangi accretionary margin, Pacific Ocean ✓ active convergent margin	640-1500 m	✓ accreted marine sediments ✓ faults, stratigraphic conduits ✓ microbial	gas bubbles, acoustic flares, sampled hydrates, enhanced heat flow, seismic anomalies, authigenic carbonate, chemosynthetic fauna	this study, (Lewis and Marshall, 1996; Greinert et al., 2010a; Naudts et al., 2010)
✓ Hydrate Ridge, accretionary margin, Pacific Ocean ✓ active convergent margin	600-840 m	✓ accreted marine sediments, gas hydrates ✓ faults ✓ microbial/thermogenic	gas bubbles, acoustic flares, sampled hydrates, seismic anomalies, authigenic carbonate, chemosynthetic fauna	(Bohrmann et al., 1998; Greinert et al., 2001; Boetius and Suess, 2004; Haeckel et al., 2004)
✓ Lake Baikal, ✓ Rift lake, mud volcanoes	500-1500 m	✓ biosiliceous oozes, gas hydrates ✓ faults, buried chimneys ✓ microbial/thermogenic/oil	gas bubbles, acoustic flares, sampled hydrates, enhanced heat flow, seismic anomalies, authigenic carbonate	(De Batist et al., 2002; Van Rensbergen et al., 2002; Kida et al., 2006; Krylov et al., 2008a)
✓ Makran accretionary margin ✓ active convergent margin	450-2500 m	✓ accreted marine turbidites ✓ faults, mud diapirs ✓ microbial/thermogenic	gas bubbles, acoustic flares, sampled hydrates, tube worms, seismic anomalies, authigenic carbonate, chemosynthetic fauna	(von Rad et al., 1996; von Rad et al., 2000; Judd and Hovland, 2007; Ghosh and Sain, 2008)
✓ Mercator and Darwin Mud Volcano, Gulf of Cadiz, Atlantic Ocean ✓ compressional setting	388-1100 m	✓ marine shales and marls ✓ faults, mud diapirs ✓ microbial/thermogenic/brines	gas, bubbles, seismic anomalies, enhanced heat flow, authigenic carbonate	(Depreiter et al., 2005; Van Rooij et al., 2005)

✓Nile deep sea fan mud volcanoes, Mediterranean Sea ✓deep sea fan	550-2100	✓deltaic sediments ✓faults, salt diapirs ✓microbial/thermogenic/oil/brines	gas bubbles, acoustic flares, sampled hydrates, tube worms, enhanced heat flow, seismic anomalies, authigenic carbonate, chemosynthetic fauna	(Dupre et al., 2007; Bayon et al., 2009; Huguen et al., 2009; Omoregie et al., 2009; Feseker et al., in press)
✓northern Cascadia margin, Pacific Ocean ✓active convergent margin, accretionary prism	1200-1400 m	✓accreted marine sediments, hydrates ✓faults ✓microbial	gas bubbles, acoustic flares, sampled hydrates, enhanced heat flow, seismic anomalies, authigenic carbonate, chemosynthetic fauna	(Judd and Hovland, 2007; Riedel et al., in press)
✓Sea of Marmara ✓inland sea, pull apart basins	600-1200 m	✓deltaic sediments ✓faults, sandy turbidites ✓microbial/thermogenic/brines	gas bubbles, acoustic flares, sampled hydrates, tube worms, seismic anomalies, authigenic carbonate, chemosynthetic fauna	(Gürgey et al., 2005; Géli et al., 2008; Zitter et al., 2008)
✓Sea of Okhotsk ✓back-arc basin	400-1000 m	✓highly organic-rich sediments ✓faults ✓microbial/thermogenic/oil	acoustic flares, sampled hydrates, seismic anomalies, authigenic carbonated, chemosynthetic fauna	(Greinert et al., 2002b; Ludmann and Wong, 2003; Sahling et al., 2003; Shoji et al., 2005)
Outside of gas-hydrate stability zone				
✓Adriatic Sea ✓foreland basin	80-250 m	✓Holocene-Pliocene sediments ✓faults, clay diapirism ✓microbial/thermogenic	acoustic flares, pockmarks seismic anomalies, authigenic carbonate	(Hovland and Curzi, 1989; Conti et al., 2002; Panieri, 2006; Geletti et al., 2008)
✓Arabian Gulf ✓rift system	5-50 m	✓leaking hydrocarbon reservoirs ✓erosional surface ✓thermogenic/oil	gas bubbles, acoustic flares, pockmarks, seismic anomalies	(Judd and Hovland, 2007)
✓Bering Sea ✓active convergent margin	<200 m	✓peaty mud ✓storm-related liquefaction, diffusion ✓microbial/thermogenic	acoustic flares, pockmarks, seismic anomalies	(Judd and Hovland, 2007)
✓Bulgarian shelf, Black Sea ✓passive margin	0-20 m	✓deltaic sediments, sapropels ✓faults ✓microbial	gas bubbles, acoustic flares, seismic anomalies	(Dimitrov, 2002)
✓Danube canyon, Black Sea ✓passive margin	70-400 m	✓deltaic sediments ✓faults ✓microbial	gas bubbles, acoustic flares, seismic anomalies	(Egorov et al., 1998; Popescu et al., 2004)
✓Dnepr paleo-delta, Don paleo-delta, Black Sea ✓passive margin	66-825 m	✓deltaic sediments ✓stratigraphic conduits in association with seals formed by fine-grained and hydrated-bearing sediments ✓microbial	gas bubbles, acoustic flares, pockmarks, seismic anomalies, authigenic carbonates, chemosynthetic fauna	this study, (Michaelis et al., 2002; Naudts et al., 2006; Naudts et al., 2008; Naudts et al., 2009)
✓Eckernförde Bay, Baltic Sea ✓inland bay	10-15 m	✓organic rich mud ✓glacial outwash sands, diffusion ✓microbial/fresh-water seepage	acoustic flares, pockmarks, seismic anomalies, chemosynthetic fauna	(Wever et al., 1998; Judd and Hovland, 2007)

✓ Eel River Basin, Pacific Ocean ✓ fore-arc basin	<550 m	✓ deltaic sediments ✓ faults, mud diapirs, structural anticlines ✓ microbial/thermogenic	gas bubbles, acoustic flares, pockmarks, seismic anomalies, authigenic carbonates, chemosynthetic	(Orange et al., 2002; Orphan et al., 2004)
✓ Gulf of Cadiz, Atlantic Ocean ✓ compressional setting	300-400 m	✓ deltaic sediments ✓ faults, stratigraphic conduits ✓ microbial	acoustic flares, pockmarks, seismic anomalies	(Baraza and Ercilla, 1996)
✓ Lake Baikal ✓ rift lake	20-340	✓ deltaic sediments, biosiliceous oozes ✓ faults, stratigraphic conduits ✓ microbial/thermogenic	gas bubbles, acoustic flares, pockmarks, seismic anomalies	this study, (Granin and Granina, 2002; Granin et al., in press; Naudts et al., submitted)
✓ Irish Sea ✓ inland sea	66-85 m	✓ coal-bearing rocks, lignites, silts ✓ faults, salt diapirs outcropping source rock ✓ microbial/thermogenic	Acoustic flares, authigenic carbonate, seismic anomalies	(Judd et al., 2007)
✓ North Sea ✓ sag margin	<100-250 m	✓ leaking hydrocarbon reservoirs ✓ salt diapirs, glacial sediments ✓ microbial/thermogenic	gas bubbles, acoustic flares, pockmarks, seismic anomalies, authigenic carbonates, chemosynthetic faun	(Niemann et al., 2005; Hovland, 2007; Judd and Hovland, 2007)
✓ Rias Baixas, Atlantic Ocean ✓ passive margin	10-55 m	✓ deltaic sediments ✓ stratigraphic conduits ✓ microbial	gas bubbles, pockmarks, seismic anomalies	(Garcia-Gil et al., 2002; Iglesias and Garcia-Gil, 2007)
✓ Santa Barbara Channel, Pacific Ocean ✓ fore-arc basin	20-70 m	✓ leaking hydrocarbon reservoirs ✓ faults, structural anticlines ✓ thermogenic/oil	gas bubbles, acoustic flares, seismic anomalies	(Clark et al., 2003; Leifer et al., 2006a)
✓ Skagerrak, Kattegat, Norwegian Sea ✓ passive margin	55-360 m, 10-12 m	✓ leaking hydrocarbon reservoirs, (post-)glacial sediments ✓ faults, clay diapirism, stratigraphic conduits ✓ microbial/thermogenic	acoustic flares, pockmarks, seismic anomalies, authigenic carbonates, chemosynthetic fauna	(Dando et al., 1994; Rise et al., 1999; Judd and Hovland, 2007)
✓ South China Sea ✓ mud volcanoes	<100 m	✓ leaking hydrocarbon reservoirs ✓ mud diapirs, buried chimneys ✓ microbial/thermogenic/oil	gas bubbles, acoustic flares, pockmarks, seismic anomalies	(Judd and Hovland, 2007)
✓ Stockholm Archipelago, Baltic Sea ✓ Inland bay	6-16 m	✓ subducted sediments ✓ faults, stratigraphic conduit ✓ microbial/ thermogenic	gas bubbles, pockmarks	(Judd and Hovland, 2007)
✓ Timor and Arafura Sea, Eastern Indian Ocean ✓ passive margin	40-500 m	✓ leaking hydrocarbon reservoirs, Holocene mud ✓ faults ✓ microbial/thermogenic/oil	acoustic flares, pockmarks, authigenic carbonate, seismic anomalies	(Rollet et al., 2006; Rollet et al., 2009; Logan et al., 2010)
✓ West Spitsbergen continental margin, Barents Sea ✓ passive margin	150-400 m	✓ partially from gas hydrates ✓ stratigraphic conduit in association with seals formed by hydrate-bearing sediments ✓ microbial	acoustic flares	(Westbrook et al., 2009)
✓ Yellow Sea ✓ Inverted extensional basin	80-100 m	✓ deltaic sediments, leaking hydrocarbon reservoirs ✓ mud diapirs, buried chimneys ✓ microbial	acoustic flares, pockmarks, seismic anomalies	(Jeong et al., 2004; Judd and Hovland, 2007)

Table 7.1.
Overview of all known bubble-releasing seep sites in the world with indication of water depth, tectonic setting and associated features.

organic material. This organic material is supplied by river runoff or by sedimentation of plankton, present in the water column. Microbial methane consists mainly of the light carbon isotope ^{12}C and has therefore very low $\delta^{13}C_{CH_4}$ values, commonly between -55‰ and -110‰ (Whiticar, 1999). Methanogenesis commonly takes places by CO_2-reduction, common in marine environments, or by acetate-fermentation, common in freshwater environments (Whiticar, 1999). When organic matter gets buried deep enough to within the oil window, e.g. from 2000 m below surface, where high pressures and temperatures prevail, thermogenic methane (dry gas) can be formed by catagenesis, often in association with crude oil (C_{15+}), condensate (C_6-C_{15}) and wet gas (C_2-C5). Thermogenic methane commonly has $\delta^{13}C_{CH_4}$ values between -25‰ and -55‰ (Whiticar, 1999). Catagenesis sources the gas and oil fields produced on many continental margins worldwide. In most cases the source rocks are different from the reservoir rocks; the escape of petroleum from source rocks is called primary migration, and the migration into the reservoirs rocks is referred to as secondary migration. As for the source rocks, the reservoir rocks are also unable to contain and seal off all hydrocarbon fluids and thus allow further fluid migration towards the seafloor (tertiary migration). In this way the methane seeping into the water column can be mixture of microbial and thermogenic methane with admixtures of higher hydrocarbons. As shown, in table 7.1. tertiary migration seems to be an important source for bubble-releasing seeps worldwide. Abiogenic methane originates from degassing of the earth's mantle, whereas geothermal-volcanic methane is formed by the thermal breakdown of organic hydrocarbons under the influence of volcanic activity (Judd and Hovland, 2007; Etiope, 2009). The importance of the two latter methane sources is still under debate.

Generally, 99% of the gas emitted at bubble-releasing seeps is methane, mainly of a microbial or a microbial-thermogenic origin with small admixtures of higher hydrocarbons (ethane, propane, etc.).

The compositions of the gases released at our study sites are in good agreement with what is observed at other bubble-releasing seeps worldwide. None of the seep sites occur above producible petroleum-bearing sediments, only in the Dnepr paleo-delta seeps occurs in a region with several nearby gas and oil fields (Fig. 2.1.).

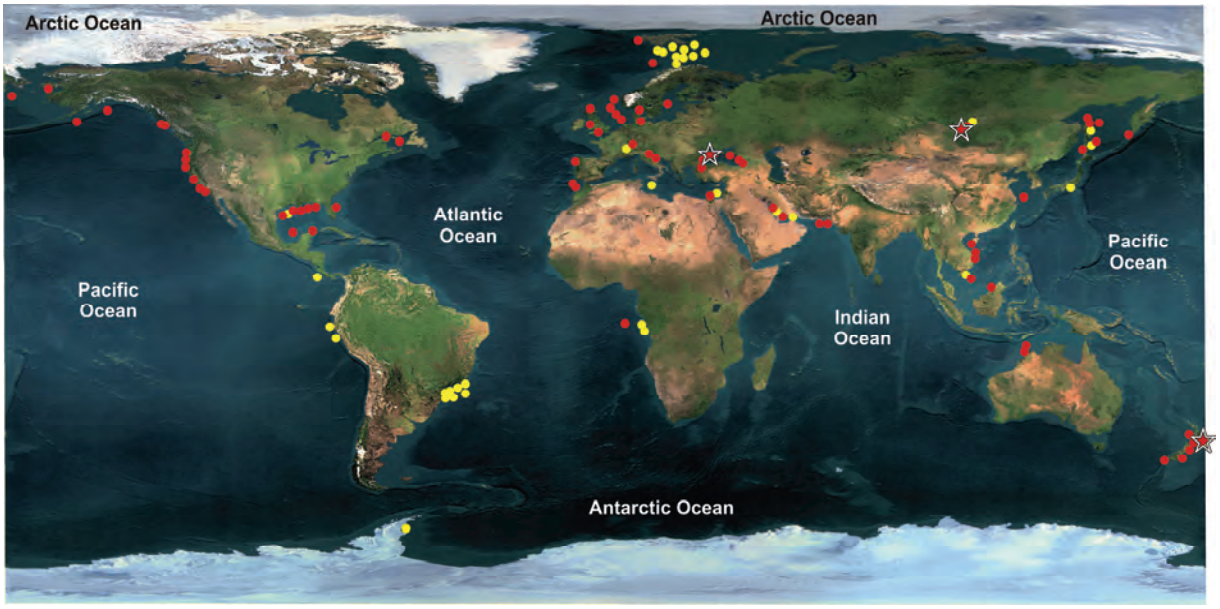

Figure 7.1. The locations of our study areas (indicated by white stars) within the worldwide distribution of bubble-releasing seeps (red dots) and gas seepage indicators (bacterial mats, authigenic carbonates, ice streamthroughs, etc.) (yellow dots). Where seeps as well as the seep indicators are present; they are indicated by red dots (after Judd and Hovland, 2007).

For the Dnepr paleo-delta (Black Sea), gas samples were taken with the submersible JAGO in October 2004 (as part of the EC-funded METROL project) at the -92 m seep site, directly at the seafloor. The initial gas composition of the bubbles was almost pure methane (80 to 90 %) of presumed microbial origin as indicated by the $\delta^{13}C_{CH_4}$ values (-62‰ to -68‰) (McGinnis et al., 2006). A similar observation was made for the -200 m seep site, as indicated by the $\delta^{13}C_{CH_4}$ values (-62‰ and -68‰) (Michaelis et al., 2002). Within these areas, gas-bearing layers have been seismically mapped up to a depth of 30 m below the seafloor. Thus gas generation in sediment layers occurs at least at 30 m subsurface depth (Fig. 3.9.). Measurements of the natural radiocarbon content of the methane ($^{14}C_{CH_4}$) show that most of it derives from radiocarbon-free sources (5.02±0.4 pMC, 24 ka) (Kessler et al., 2006). The released methane is thus assumed to represent a mixture of methane generated in organic-rich deltaic sediments deposited during various sealevel lowstands along the Dnepr paleo-delta and upward migrating radiocarbon-free methane from deeper strata. The most recent sealevel lowstands occurred at 9-10 ka ^{14}C B.P (Ivanova et al., 2007). For the -600 m seep site, heat-flow measurements and helium isotopes indicate a deeper source, originating from 200-300 m subsurface depth with a crustal helium overprint (Poort et al., 2007; Holzner et al., 2008).

At the Hikurangi Margin (SW Pacific), water samples taken at Faure Site and LM-3 obtained during ROV dives have $\delta^{13}C_{CH_4}$ values between -66 ‰ and -67 ‰, indicative of a microbial methane source (Faure et al., 2010). These values are very similar to the ones measured at e.g. Hydrate Ridge, another example of an accretionary margin with bubble-releasing seeps within the GHSZ (Heeschen et al., 2005). For both Faure Site and LM-3 no higher hydrocarbons were detected (Faure et al., 2010). Barnes et al. (2010) suggest that the substrate of exposed Cretaceous and Paleogene rocks or an eroded cover sequence of Miocene-Pliocene age acts as sources for the observed seeps and possible gas hydrates at the Rock Garden area. There is no indication that gas hydrates in the Rock Garden area are sources for the observed seepage. It rather seems that conduits through the GHSZ source the seeps from below the GHSZ (Crutchley et al., 2010; Crutchley et al., in press).

At the Posolsky Bank (Lake Baikal), gas samples from seeps were analyzed by Kalmychkov et al. (2006). They obtained a $\delta^{13}C_{CH_4}$ value of -66.6‰, with a C_1/C_{2+} ratio of 118, indicating a microbial-thermogenic origin for the released gasses. Organic matter in Lake Baikal comes from the input of the Selenga River and from primary production of phytoplankton (Vykhristyuk, 1980). Based on the seismic data, the gas-bearing layer feeding the seeps could be traced to below the BGHSZ. This indicates, together with the shallow depth occurrence of the seeps, that these seeps are not directly fed by the hydrates (Fig. 6.7.). The microbial-thermogenic origin also supports this assumption. The real thermogenic source could however not be determined. Sediment thickness in the SBB reaches up to 7.5 km and could therefore favor thermogenic methane production.

The previous paragraphs have shown that the released gas in the study areas has different sources and different compositions, albeit minor differences (Fig. 7.2.). The difference in source sediment and the nature of the associated fluids is strongly related to the present and past sedimentary environments of the seep areas. The tectonic setting partially determines the sedimentary environment but is rather a minor and indirect factor in relation to the fluid source and composition. Even though the three studied areas have the potential and established prove of thermogenic hydrocarbon production, none of the observed seeps have a clear thermogenic source, but rather a primarily microbial origin with merely a minor admixture of higher hydrocarbons. This conclusion can be made for a lot of the seep sites summarized in table 7.1. Regarding the overwhelming abundance of bubble-releasing seeps in the Dnepr paleo-delta (Black Sea), semi-enclosed (anoxic) basins with a high input of organic material can provide an enormous source for seepage (chapter 2-4). Other possible interesting anoxic basins to study seeps sites could be the anoxic Cariaco and Gotland Basins. Despite both having strong indications for shallow gas, no bubble-releasing

seeps have been observed until now (Piker et al., 1998; Wakeham et al., 2004).

7.2.2. Fluid migration modes, triggers and rates

First of all, it has to be stated that the 'normal' advective and diffusive flow of fluids, respectively related to pressure differences (Darcy's Law) or concentration differences (Fick's Law of diffusion), occurs everywhere and is a rather slow process (mm/yr) (Berndt, 2005; Judd and Hovland, 2007). This is related to the low solubility of gases (e.g. methane: 35 mg/l) and to the low permeability of normal marine sediments (10^{-8} - 10^{-9} m^2) (Judd and Hovland, 2007). It is only where fluid flow is focused, e.g. through permeable sandy layers (permeability: 10^{-2} - 10^{-5} m^2) or through cracks (permeability: 10^{-4} - 10^{-8} m^2), that advective fluid flow rates become much higher provided an excess of pressure at the depth. In this case the 'cubic law' and Poiseuille's Law come into play (Judd and Hovland, 2007). The occurrence of focused fluid flow can be witnessed, since it 'visibly' affects the geosphere, biosphere, hydrosphere and atmosphere. The studied release of bubbles into the water column, and the associated free gas migration through the sediment, is an ultimate example of focused fluid flow.

Focused fluid flow, which is often a result of compaction, is strongly depended on the sedimentation rate, the lithology and the stratigraphy (Berndt, 2005). Focused fluid flow will, for example, not occur in continuous sandy deposits because of its high permeability and hydraulic conductivity which leads to heterogeneous fluid flow. It is only where fluid flow is impeded by low-permeability stratigraphic horizons (e.g. clayey sediments with a permeability of 10^{-10} - 10^{-12} m^2, gas hydrates with a permeability 10^{-10} - 10^{-18} m^2) or by structural features (e.g. faults) that focused fluid can occur (Judd and Hovland, 2007).

In general, focused fluid migration through sediments has mainly two possible driving forces that can act separately or in combination; overpressure and buoyancy. Overpressure is generated at depth in location where pore pressure rises above hydrostatic pressure and approaches lithostatic pressure due to the increased compression and decreased permeability of sedimentary layers as a result of high sedimentation rates and/or tectonic loading (Judd and Hovland, 2007). In general, tectonic stress reaches values between 10-100 MPa, whereas hydrostatic pressure has a value of 10 MPa/km and lithostatic pressure reaches values of 20-30 MPa/km. These values indicate that tectonic stress can have a major impact on focused fluid flow and lead to overpressure situation in relatively shallow sediments, i.e. upper kilometers (Judd and Hovland, 2007). Therefore typical indications for overpressure and sediment underconsolidation, e.g. formations of subsurface diapirs or seabed mud volcanoes, can be found in tectonically active regions (Judd and Hovland, 2007; and references therein). Overpressure also occurs without the presence of tectonic loading, but due to sediment loading or in relation to gas hydrates (see section 7.2.3.).

Another important driving force for fluid migration is buoyancy, which acts where the concentration of gas dissolved in pore waters exceeds its solubility and free-gas bubbles form. The formation of free gas lowers the bulk density of a sediment body and can lead to a density inversion. In this way, buoyancy can lead to migration of sediments (whether or not initiated by overpressure) or instigates migration of pore waters containing microscopic bubbles even without the mobilization of sediments or makes bubbles rise through the sediments without the mobilization of sediments or pore waters.

The most effect way of gas to migrate through the sediments occurs in association with sediment mobilization. Whenever sediment mobilizations doesn't occur, the migration of gas through sediments is most effective by the movement of bubbles through the sediment pore spaces (Saunders et al., 1999). Depending on the grain size of the host sediment and the composition of the gas, bubble diameters can be too large in comparison with the pore spaces to facilitate bubble movement. Unless an overpressure situation is created, the gas can only migrate through the sediment by diffusive flow out of the bubble into the pore water. Where the space between the sediment grains

allows it, bubbles can form again. In this manner a chain of bubbles gets established that allows movement of gas through the sediments (Judd and Hovland, 2007).

For our studied seep areas, seismic data show a clear linkage between the presence of free gas in the subsurface and the release of bubbles into the water column, generally without clear indications for overpressure (e.g. subsurface deformation, strong thermal anomalies, mud volcanism, etc.). This suggests a mainly buoyancy-driven free gas migration in the upper sedimentary layers (Figs. 2.4., and 6.7.). At some locations however, buoyancy-driven fluid flow seems to occur in association with or is initiated by overpressure. Possible indication for overpressure forcing in our study areas are: i) the occurrences of submarine landslides near Faure Site (Hikurangi Margin) (Fig. 5.2.) and in the Dnepr paleo-delta at the -600 m seep site (Black Sea) (Figs. 3.5. and 3.11.); ii) the focused migration of free gas through the GHSZ at Faure Site and LM-3 (Hikurangi Margin) (Fig. 5.2.) (see section 7.2.3.) (Crutchley et al., 2010; Crutchley et al., in press); iii) breaching of the impermeable sediment cover on sedimentary ridges in the Dnepr paleo-delta (Fig. 3.10) (see section 7.2.4.). The presence of overpressure in an accretionary margin, like the Hikurangi Margin is often due to tectonic loading (Judd and Hovland, 2007). The Hikurangi accretionary prism is not an exception with overpressure reaching near-lithostatic pressure at about 2 km depth in near-shore and on-shore oil wells (Sibson and Rowland, 2003). The accretion and subduction cause significant dewatering, which is linked to the seep sites observed onshore and offshore (Lewis and Marshall, 1996; Barnes et al., 2010).

While buoyancy and overpressure are the main driving forces of fluid flow, in some cases additional triggers, such as earthquakes, can lead to enhanced fluid flow. This can lead to the release of bubbles at the seafloor due to enhanced fluid pressure, due to the reactivation of faults or by causing submarine landslides (Hovland et al., 2002; Kuscu et al., 2005; Judd and Hovland, 2007; Géli et al., 2008). Other environmental changes, like pressure changes by tides, by current changes or by storm waves are also known to regulate fluid flow and seep activity (see chapter 5) (Boles et al., 2001; Hovland et al., 2002; Torres et al., 2002; Judd and Hovland, 2007).

Lake Baikal and the Hikurangi Margin are seismically very active regions, nevertheless no direct relation between earthquakes and seepage has been established during our observations. But this doesn't rule out that seepage and fluid flow are always unrelated to earthquakes in these areas. For the seeps off New Zealand, there are strong indications that the seep activity is related to tides (Linke et al., 2010). In Lake Baikal and in the Black Sea there are no strong tidal variations, and thus seep activity can't be related to tides in these areas. In the Black Sea, strong current changes were observed by ADCP measurements, but no relation with seep activity was established (CRIMEA Project Team, 2006).

The fluid rates at which fluids can move through the sediments can strongly differ, depending on the observed fluid-flow system (i.e. with or without mobilization of sediments) and on the activity during the time of observation. Mud volcanoes, for example, are often characterized by repetitive fluid-flow activity with high flow rates. They are also associated with high thermal gradients which affect the stability of gas hydrates and results in enhanced fluid flow and in the release of bubbles into the water column (table 7.1.) (see section 7.2.3.). Fluid-flow rates of up to 4 m/year have been measured just below the seabed at the Håkon Mosby mud volcano, whereas at the Dvurechenskiy mud volcano fluid rates were less significant at 0.25 m/year at the center of the mud volcano (Aloisi et al., 2004; Feseker et al., 2008). The release of bubbles has been observed at both mud volcanoes, and seems to be independent of the release of other fluids, all or not associated with sediment movement or mud expulsions (table 7.1.) (Greinert et al., 2006; Sauter et al., 2006). The flux rates given here clearly represent a rather dormant period in the activity of the mud volcano without very active mud expulsions. Fluid rates related to the movement of free gas through the sediments have been measured for e.g. Hydrate Ridge, where rates varied between 0 to 10 m/year (Tryon et al., 2002).

For our study areas no subsurface fluid flow

rates were measured. Based on the relation between subsurface fluid flow rates and bubble-release rates in other areas, the bubble-release rates determined in our study areas can be used as an indication for the local fluid flow rates (table 5.1.). For the Håkon Mosby mud volcano for example, bubble release leads to methane flow rates of 4.8-21.6 mol/minute. At Hydrate Ridge flow rates were estimated to vary between 2.6-13 mol/minute. In our study areas, visual observations indicated methane flow rates of 0.2-7 mol/minute for Faure Site, whereas in the Dnepr paleo-delta flow rates of only 0.03 mol/minute were measured. This shows that at Faure Site, subsurface fluid flow rates are probably in the same order as at Hydrate Ridge. This indicates that at similar tectonic and sedimentary settings, comparable fluid flow systems with similar driving forces occur. In this case, an accretionary prism where probably overpressure is the main driving force allowing fluid flow though the GHSZ and bubble-release at the seafloor. Methane flow rates in the Dnepr paleo-delta point toward much lower subsurface fluid flow rates. This could indicate that the different tectonic and sedimentary environment of the Dnepr paleo-delta is associated with a different kind of fluid flow system with different driving forces. Buoyancy is probably the main driving force in the Dnepr paleo-delta, leading to lower fluid flow rates and more widespread occurrence of seeps (i.e. thousands) (Fig. 7.2.). Whereas, on the Hikurangi Margin, fluid flow rates are high and the number of seep sites is limited (i.e. dozens), as a result of enhanced focused fluid flow (Fig. 7.2.). The later is probably related to the presence of hydrates and the associated overpressure; hydrates limit the widespread occurrence of seeps and overpressure only leads to seepage where fluid flow is highly focused and passage through the GHSZ is possible.

For the Posolsky Bank, no fluid flow rates or bubble-release rates are known. But visual observations of bubbles reaching the lake surface and the relatively high amount of seeps occurring in a small and well-defined area indicate that fluid flow is probably relatively high (Fig. 6.5.). Fluid flow rates at the Posolsky Bank are probably higher than in the Dnepr paleo-delta and lower than in the Hikurangi Margin. This again shows that tectonic and sedimentary settings are associated with a particular fluid flow system that leads to different fluid flow focusing and fluid flow rates (Fig. 7.2.).

This section shows that fluid migration modes, rates and triggers differ in the different study areas and are strongly related to the geological setting of the studied area (Fig. 7.2.). The sedimentary environment and stratigraphic buildup of the study areas plays a major role, not only by providing adequate fluid sources (see section 7.2.1.), but also by providing stratigraphic conduits and seals that focus fluid flow. Conduits and seals can also be provided by structural features like faults, etc. (table 7.1.), but for our study areas stratigraphic conduits and seals are the most common (see section 7.2.3.-7.2.4.). With regard to the driving forces for focused fluid flow, buoyancy seems to be omnipresent in the shallow subsurface of all our study areas. But buoyancy-driven fluid flow sometimes occurs in association with overpressure leading to more enhanced focused fluid flow. Overpressure in our study areas is mainly related to stratigraphic seals, e.g. impermeable fine-grained or hydrate-bearing sediments, as was stated for buoyancy. This is also the case for an active tectonic environment as the Hikurangi Margin (see section 7.2.3.) (Crutchley et al., in press). This indicates that overpressure at gas-hydrate-bearing accretionary margins is not only related to tectonic loading with associated dewatering, but is also related to the sedimentary environment and associated stratigraphic buildup. The variety of driving forces, the complexity of the stratigraphy and the seismic activity makes accretionary prisms very interesting geological settings to study seeps with regard to driving forces and to fluid flow triggers. On the other hand, the amount of seeps detected in the Dnepr paleo-delta (Black Sea) is far greater than the amount of seeps detected on the Hikurangi Margin or any other accretionary prism, again pointing to the Black Sea as a unique seep environment. Concerning migrations rates, tectonically active compressional systems associated with strong overpressure indicated by active mud volcanism and -diapirism are

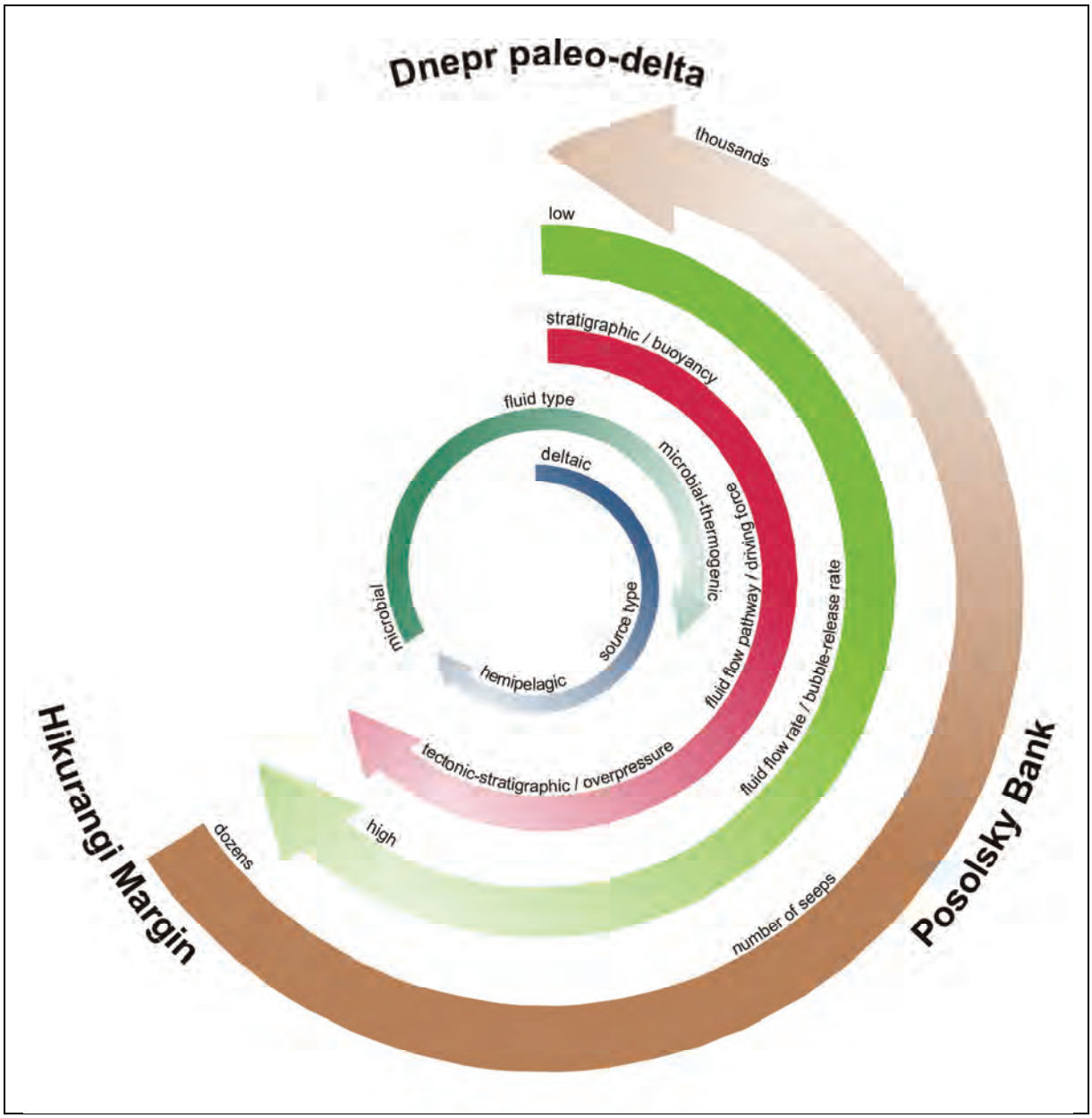

Figure 7.2. Overview of the fluid sources, the fluid types, the fluid pathways, the fluid flow rates and the numbers of seeps for the three study areas, shown relatively to each other as indicated by the arrows. The figure shows that the Hikurangi accretionary margin and the Dnepr paleo-delta are the two end-members for most fluid flow characteristics.

probably most interesting study areas.

In conclusion, the differences between our study areas indicate that fluid flow and bubble-release is primarily dependent on the sedimentary and stratigraphic environment. However, as was stated for fluid sources, the sedimentary environment and stratigraphic buildup is partially determined by the tectonic setting that therefore also influences the fluid migration mode and rates. That the tectonic setting does play a role is also indicated by the absence of seeps in the GHSZ of the Dnepr paleo-delta and the presence of seeps in the GHSZ of the Hikurangi Margin (see section 7.2.3.). Overpressure generated below the GHSZ, solely by the presence of gas hydrates, doesn't lead to fluid flow through the GHSZ as can be witnessed in the Dnepr paleo-delta. It is only where the tectonic setting enhances the overpressure due to tectonic loading and an

excess of fluids that fluid flow through the GHSZ occurs. The latter is demonstrated in the Hikurangi Margin and many other accretionary convergent margins (see section 7.2.3.).

7.2.3. Fluid migration within the gas-hydrate stability zone

With regard to the water depth, a division is made between seeps occurring within and seeps occurring outside of the theoretical gas-hydrate stability zone. The overview given in table 7.1. clearly shows that gas hydrates have been sampled at all seep sites occurring within the gas-hydrate stability zone, independent of the geological or tectonic setting. A large amount of these seeps occur at mud volcanoes in a compressional tectonic setting, or at accretionary prisms at active convergent margins, or in areas with diapiric sediment or salt movement. Often these deep seep sites correspond to locations with enhanced heat flow, indicating an upward flow of warmer fluids and/or sediments that affect the stability of hydrates present in the sediment. Deep bubble-releasing seeps can be sourced by these destabilized hydrates or by free gas that is able to migrate through the GHSZ at certain locations. This can also be the case for areas where saline fluids migrate towards the seabed.

Migration of free gas through the GHSZ is also witnessed at locations where gas hydrates should be thermodynamically stable given the temperature, the pressure and the presence of pore water with normal salinities, e.g. the Gulf of Mexico, the Cascadia Margin, Blake Ridge, Congo Basin, the Hikurangi Margin (Brooks et al., 1994; Tryon et al., 1999; Taylor et al., 2000; Gorman et al., 2002; Wood et al., 2002; Gay et al., 2007; Crutchley et al., 2010). Several mechanisms are proposed for the migration of free gas through the GHSZ. Torres et al. (2004) suggested that free gas can move freely through the GHSZ as long as the bubble pressure exceeds the overburden stress caused by the sediment load, resulting only in massive hydrate formation close to the seafloor as is observed at Hydrate Ridge and in the Congo Basin (Sahling et al., 2008). Flemings et al. (2003) suggest for Blake Ridge that rather the formation of massive hydrate layers at greater subsurface depth leads to overpressure generated by the build-up of free gas reservoirs beneath a low-permeable gas-hydrate cemented sediment layer. If the gas pressure of the gas reservoir exceeds the pressure exerted by the sediments above, a temporal conduit can be made allowing migrations of free gas through the GHSZ and the release of gas bubble into the water column. A high gas flux associated with rapid hydrate formation can lead to a depletion of pore water resulting in a high salinity of the residual pore waters or the formation of hydrate-coated veins that prevent interaction with the surrounding pore waters (Clennell et al., 1999; Flemings et al., 2003; Pecher et al., 2010). In both cases, further formation of hydrates may be impeded and this would allow the migration of free gas through the GHSZ. Alternatively, Ginsburg and Soloviev (1997) suggested that a diffusion barrier caused by a hydrate film at the gas-water interface may allow the free gas to migrate through the GHSZ.

Our study provides some interesting insights regarding the influence gas hydrate have on the migration of free gas through the GHSZ and on the associated distribution of seeps. Probably the most revealing observation is the almost complete absence of seeps in the GHSZ of the Dnepr paleo-delta, even though seismic data clearly indicated the presence of free gas in the sediments (Figs. 2.8. and 3.8.). The seismic data also show BSRs that indicate the presence of hydrates and free gas in the subsurface. Seismic inversion revealed that there is 38±10% hydrate in the pore space at BSR depth, where the porosity is 57% (Zillmer et al., 2005). For the Dnepr paleo-delta it seems to be clear that gas hydrates present in the sediments act as a buffer for upward migrating free gas and prevent the release of gas bubbles at the seafloor. Bubble-releasing seeps are only observed within the GHSZ of the Dnepr paleo-delta where the activity of a mud volcano allows to surpass this effective hydrate buffer (Kruglyakova et al., 2004). This almost complete absence of seeps within the GHSZ also suggests that the above proposed mechanisms for free gas migration through the GHSZ are not present or are unsuccessful in the Dnepr paleo-delta. For example, overpressure-related seepage that is

not related to mud volcanism, as is seen on many accretionary margins, doesn't seem to be effective in the Dnepr paleo-delta. This is true for the whole Black Sea, where bubble-releasing seeps occur exclusively outside of the GHSZ and only above mud volcanoes inside the GHSZ (Fig. 1.7.). The only exception is the Batumi seep area offshore Georgia, where seeps occur at gas hydrate-bearing circular structures associated with authigenic carbonates indicating focused fluid flow but without the presence of any mud extrusions or positive relief. Seepage at the Batumi seep area seems to be related to underlying mud diapirs which can however sometimes be precursors of mud volcanism (Klaucke et al., 2006).

Notwithstanding the different, geological and tectonic settings of the Black Sea and Lake Baikal, the seep distribution and the role of hydrates seems to be very similar. As for the Black Sea, bubble-releasing seeps in Lake Baikal's GHSZ are almost exclusively found at mud volcanoes, in spite of the widespread occurrence of active faults within the Baikal Basins (Figs. 1.7. and 1.11.) (Granin et al., in press). Within the Posolsky Bank study area free gas is observed on seismic recordings within the GHSZ and hydrates have been sampled by a submersible at the southwestern fault scarp of the Posolsky Bank (Figs. 6.3. and 6.7.). The absence of seeps in the GHSZ of the Posolsky study area and in Lake Baikal (excluding mud volcanoes) indicates that gas hydrates act as a seal for the upward migration of free gas and the release of free gas in the water column, as was observed in the Black Sea. The only differences between the Dnepr paleo-delta and the Posolsky Bank study area is that the seeps at the Posolsky Bank are partially sourced by gas coming from below the BGHSZ. Whereas in the Dnepr paleo-delta there are no indications that gas from below the BGHSZ is migrating along the sediment layers and is being released outside of the GHSZ (Figs. 2.8. and 3.8.). The geometry and the layering of the Posolsky Bank are probably a unique example allowing gas escape from below the BGHSZ without having to pass through the GHSZ. The only other known example are the seeps studied along the West Spitsbergen continental margin (Westbrook et al., 2009).

The only study area with a clear observation of fluid migration through the GHSZ that results in the release of bubbles into the water column is Rock Garden (LM-3 and Faure Site) (Fig. 5.2.). Numerous authors suggest that overpressure at the BGHSZ caused by rising bubbles or gas pockets allows the migration of fluids through the GHSZ at the Rock Garden seep sites (Pecher et al., 2005; Faure et al., 2006; Barnes et al., 2010; Crutchley et al., 2010; Crutchley et al., in press). Our study doesn't provide any data that sustains or contradicts these suggestions. But as was postulated in section 7.2.2., the overpressure generated at Rock Garden, and probably at a lot of hydrate-bearing accretionary prisms, is associated with the tectonic setting in combination with the sedimentary and stratigraphic buildup (i.e. presence of hydrates). Furthermore, Crutchley et al. (2010) show that for Faure Site migration through the GHSZ occurs along tilted permeable layers whereas at LM-3 faults control the fluid flow through the GHSZ (Fig. 5.12.). Our data and interpretation show that the difference in depth of LM-3 (-908 m) and Faure Site (-659 m) and the associated thickness of the underlying GHSZ (respectively 300 m and 35 m) has a strong influence on the bubble release and the seep environment (carbonates, fauna, etc.) at both seep sites. Crutchley et al. (in press) explains how a shallower BGHSZ is more strongly influenced by overpressure caused by underlying gas pockets allowing temporal migration of free gas through the GHSZ. The latter clearly shows up as strong differences in bubble release at LM-3 and Faure Site, as well as in the present seep fauna and authigenic carbonates (Fig. 5.12.). Overpressure can also have caused the submarine landslide at the Faure Site, changing and focusing fluid migration pathways towards the present bubble-releasing sites as was observed at the Dnepr paleo-delta and other seep sites in the world (Orange and Breen, 1992; Eichhubl et al., 2000; Kuscu et al., 2005).

This study has shown that gas hydrates play an important role in controlling the activity of bubble-releasing seeps, their distribution and associated manifestations on a basin-wide scale (Dnepr paleo-delta) and on smaller scales (Hikurangi Margin). The study of the seeps in the Dnepr paleo-delta clearly showed that gas hydrates can be regarded as buffers for upward

rising fluids, preventing bubble release at the seafloor. This was often suggested but never shown on such a scale. The Lake Baikal study also indicated gas hydrates as buffers, but the unique geometry and build-up of the Posolsky Bank allowed gas to escape from below the BGHSZ without migrating trough the GHSZ. Whereas at the Hikurangi Margin the overpressure typically associated with accretionary prisms allowed the migration of free gas through the GHSZ. In none of the studied areas gas hydrates have been inferred as direct sources for the released methane.

7.2.4. Fluid migration outside of the gas-hydrate stability zone

Fluid migration outside of the gas-hydrate stability zone, i.e. shallower water depths or greater subsurface depths, can be controlled by various types of conduits or seals which are also present in the GHSZ, but are often obscured by the presence of gas hydrates. Most important factors controlling fluid flow are overlying sediments layers (permeability, porosity, continuity, heterogeneity, etc.), the stratigraphic buildup of sedimentary strata, mud diapirs and the presence of (active) faults (see section 7.2.5.) (Judd and Hovland, 2007).

For the Dnepr paleo-delta, migration of gas in the upper 200 m is mainly controlled by stratigraphic and sedimentary factors, as revealed by the behavior of the gas front visible on high-resolution seismic reflection data (Figs. 3.6., 3.7. and 3.10.-3.12.). Along-strata and across-strata free gas migration seems to be important in the cut-and-fill delta deposits on the shelf and in stacked channel-levees on the continental slope. Near the seabed the occurrence of an overall-present fine-grained impermeable sediment cover, with a thickness up to 25 m, focuses fluids upslope to the margins of e.g. canyons or submarine landslides, where the cover is thinner or absent. These are the locations where free gas is released in the water column (Figs. 3.6. and 3.10-3.12.). On the shelf, filled paleo-channels and authigenic carbonates control and alter fluid migration pathways and lead to well-defined seep distributions on meter to kilometer scales (Figs. 3.6., 4.4. and 4.11.). At morphological highs, such as sediment ridges, gas generally accumulates near the top of the ridge, where overpressure or density inversion leads to breaching of the overlying stratigraphic cover and to bubble release (Figs. 3.10. and 3.12.). The available seismic data provides no evidence for the existence of faults which could act as conduits for upward fluid migration in the shallow subsurface of the Dnepr paleo-delta. However where faults were observed they were not related to bubble-releasing seeps. This does not rule out that deeper structures may be present. Structural pathways may be provided by: the large West-Crimean fault, diapiric structures on the slope, a normal fault along the shelf edge, and possible faults buried under channel-levee systems perpendicular to the slope at 300 m to 600 m below the seafloor (Lüdmann et al., 2004). Only for the -600 m seep site, helium isotopes indicate that the released gasses are possibly influenced by fluid advection from depth, possibly along deep-rooted faults (Fig. 3.13.) (Holzner et al., 2008). At this site, seismic data however indicates that the focusing and release of free gas at the seafloor is probably related and controlled by the underlying channel-levee systems (Fig. 3.7.), in a similar way as was observed in the Congo Basin (Gay et al., 2007). At the margin of the gas-hydrate stability zone, gas-hydrate recycling caused by paleoclimate-related temperature and pressure changes may also be a source for gas seeps although no direct evidence for this was observed (Poort et al., 2005). Gas-hydrate destabilization could however have lead to sliding of submarine sediments, resulting in new release paths for gas seepage (Fig. 3.11.).

As was already indicated in section 7.2.3., the controls on seepage in the Posolsky Bank study area are very similar to the ones in the Dnepr paleo-delta, i.e. stratigraphic and sedimentary controls (Figs. 6.7. and 6.10.). However across-strata migration seems to be almost absent at the Posolsky Bank where mainly focusing along the tilted sedimentary strata occurs. This focusing is probably a result of the angle and continuity of the layers and the presence of an overlying continuous fine-grained sediment layer that acts a seal (Fig. 6.10.). Gas release into the water column occurs where the gas-bearing

strata get cut off by a large fault, and not by erosional features like canyons or submarine landslides as observed in the Dnepr paleo-delta (Figs. 3.13. and 6.10.). The co-occurrence of the Posolsky Fault and the seeps could suggest that the fault acts as a conduit for fluid flow and seepage. However integration of the data counters this suggestion. Remarkable is the similarity of the controls on fluid flow and seep distribution between the Dnepr paleo-delta and the Posolsky Bank, notwithstanding the complete different geological setting (paleo-delta vs. tilted fault block) and the difference in tectonic activity between both settings.

On the Hikurangi Margin fluid migration below the GHSZ is mostly controlled by NW-dipping layers at LM-3 and by a permeability contrast at the BGHSZ at Faure Site (Crutchley et al., 2010). This implies that there is a difference in control of fluid migration for both seep sites, below as well as above the BGHSZ (see section 7.2.3.).

7.2.5. Faults versus sediments; which is the primary conduit/seal related to bubble-releasing seeps?

The previous two sections have shown that there are a lot of different controls on fluid migration in the shallow subsurface that lead to bubble release at the seafloor. However, these different controls are often not consistent with what could be expected from the geological and tectonic setting. Often it is a combination of sedimentary- and fault-controlled fluid flow even within a same area or at different subsurface depths below a certain seep site. For the Rock Garden seep sites on the Hikurangi Margin (Faure Site and LM-3), Crutchley et al (2010) showed that fluid migration can differ depending on the observed subsurface interval allowing sedimentary strata and faults to act as conduits for a same seep site (Fig. 5.12.). Gay et al.(2007) came to similar conclusions for the Congo Fan. At LM-3, for example, fluid flow below the GHSZ is stratigraphic-controlled by NW-dipping layers, whereas in the GHSZ fluid flow occurs along faults and by across-strata migration near the seafloor. The formation of MDACs and the activity of (seep) fauna near the seafloor at LM-3 act as an additional control on fluid flow and seep distribution (see section 7.3.1. and 7.3.2.). This change of migration mechanism is not fixed with depth or related to a certain driving force. Crutchley et al. (2010) show that the control of fluid flow below Faure Site is mainly stratigraphic-controlled, in as well as below the GHSZ. The type of fluid flow control is rather dependent on the local stratigraphic and structural setting below a seep site, even within a same study area. The example above indicates that it is very hard to predict whether sedimentary- or fault-controlled fluid flow occurs at a certain geological or tectonic setting, or at a certain depth interval

For our study areas, an integration was made of high-resolution seismic data with detailed and high amounts of seep-location data and other relevant datasets in order to understand the subsurface controls and the distribution of seeps. Variations in grain-size distribution and the consequent changes in permeability of the sediments in the upper hundreds of meters, all or not influenced by the presence of gas hydrates, seems to be the major control on fluid migration, on seep distribution and on seep activity, and this on meter to basin scale. This differs strongly from the general view that faults act as the primary conduit at most cold seep sites (Judd and Hovland, 2007; and references therein). We can't argue about the deep subsurface controls in our study areas since we don't always have the deep low-resolution seismic data. At the seafloor, often alignments of seeps were observed on different scales (Figs. 3.6., 3.10., 3.11., 4.1. and 5.9.). Without the integration of different high-resolution datasets these alignments could have been interpreted as related to underlying faults, although they are related to stratigraphic and sedimentary controls. It is clear that there is not a straightforward answer to the question raised in the title of this section; however our study indicates that stratigraphic and sedimentary factors in the shallow subsurface are probably very important for the distribution of bubble-releasing seeps (Fig. 7.3.). This conclusion can be extended to numerous other seep areas, since it is based on the study of seeps in three completely different geological settings.

7.3. Seafloor manifestations associated with bubble-releasing seeps

Bubble-releasing seeps are often associated with a multitude of seafloor manifestations which can be recognized even when seeps are not actively emitting bubbles into the water column. The three main types are: chemosynthetic communities, methane-derived authigenic carbonates and fluid-flow related seafloor morphologies. The presence of these seep indicators implies focused fluid flow and seepage but therefore not always seepage with bubble release. Only acoustic or visual observations can determine whether certain seep indicators are indeed associated with bubble-releasing seeps. The composition of fluids released can alter the biological and MDAC manifestations at a seeps site, seafloor morphology is however independent of the fluid composition.

7.3.1. Chemosynthetic communities

Chemosynthetic communities are probably the most striking and thus the most recognizable seepage indicators since they occur very localized and often strongly differ from other seafloor communities. Chemosynthetic communities thrive on diffusively released methane and sulfide which are available at seep sites and thus not directly on the methane that is present in bubbles. These communities are believed to be the base of complete chemosynthetic food web where higher non-chemosynthetic organism feed on chemosynthetic lower organisms (Judd and Hovland, 2007). Microbes are the foundation for chemosynthetic communities. They live in the sediments or are present as endosymbionts in seep megafauna. The main microbial groups involved are sulfate-reducing bacteria (SRB) and methanotrophic archaea that utilize methane and sulfate dissolved in the pore waters. This process is known as the anaerobic oxidation of methane (AOM) which results in the release of hydrogen sulfide and bicarbonate (Boetius et al., 2000). AOM and the associated chemosynthetic communities utilize most of the methane available at seep sites and can therefore be seen as an effective benthic filter (Boetius and Suess, 2004; Sommer et al., 2006). It is only where this seabed utilization of methane can't account for the entire methane flux or where fluid migration is highly focused that bubble release can occur.

In the Dnepr paleo-delta, two different chemosynthetic communities were observed: white bacterial mats at the -100 m seep site and black-pink bacterial mats covering up to 4-meter-high carbonate buildups at the -200 m seep site (Figs. 4.7. and 4.8.) (Michaelis et al., 2002; Blumenberg et al., 2004; Kruger et al., 2008). Whereas the bacterial-covered buildups are clearly associated with bubble release, the bacterial mats in the -100 m seep site show an inverse proportional relationship between the extent of the bacterial mats and the distribution and activity of the bubble-releasing seeps (see chapter 4). At the -100 m seep sites, methane-derived authigenic carbonates block fluid flow and bubble release whereas at the -200 m seep site the buildups are prolongations of the fluid-flow pathways. The occurrence of these two types of chemosynthetic communities and the chimney-like buildups is strongly related to the water depth and presence of anoxic water masses below -145 m in the Black Sea.

At the Hikurangi Margin, no bacterial mats were found at Faure Site and LM-3. They were, however, found at other seep sites at the Hikurangi Margin (Greinert et al., 2010a). As discussed in chapter 5, the difference in seep fauna observed at Faure Site and LM-3 is related to the difference in fluid release mode. At Faure Site, methane emission occurs mainly by bubble-release and only living ampheretid polychaetes were found. At LM-3 where methane is mainly released diffusively, living *Bathymodiolus* sp mussels and *Lamellibrachia* sp. tubeworms were observed on top of a carbonate platform. As for Faure Site, living ampheretid polychaetes were found near the bubble-releasing seeps at LM-3. These polychaetes are regarded as ecosystem engineers that facilitate the transition from a soft sediment environment with mainly bubble release to a hard substrate seep environment with associated fauna where AOM and diffusive methane transport prevail (Sommer et al., 2010;

Thurber et al., 2010). At both sites, high abundances of shells from dead *Calyptogena* sp. were found. We explained the difference in methane release and seep environment (chemosynthetic fauna and authigenic carbonates) by the depth of the underlying hydrate occurrence and the different tectonic histories of both sites (chapter 5).

At the Posolsky Bank, large bacterial mats where found near the hydrate site on the Posolsky Fault scarp during submersible observations (Oleg Khlystov, personal communication). Besides this, chemosynthetic fauna in Lake Baikal is mainly limited to microbial communities which can be found at gas-hydrate-bearing mud volcanoes, oil seeps and hydrothermal vents (Shubenkova et al., 2005; Namsaraev et al., 2006; Pavlova et al., 2008).

In the different study areas we observed a variety of chemosynthetic communities in completely different environments (anoxic, freshwater and sea water) and at different water depths ranging from -84 m to -908 m. For the Dnepr paleo-delta and Hikurangi margin, seep fauna's were indicative for locating the bubble-release sites even though bubble-release was more important where seep fauna was less abundant (see section 7.3.2.). For both study areas the water depth is an important factor controlling fluid flow, bubble release and the type of associated chemosynthetic fauna.

7.3.2. Methane-derived authigenic carbonates

Methane-derived carbonates (MDACs) are in most cases a result of AOM and are often formed by cemented seafloor sediments. Common carbonate minerals in these cements are high-magnesium calcite, aragonite and dolomite formed by Ca and/or Mg and the bicarbonate resulting from AOM present in the pore waters or bottom waters. Since they result from AOM, the carbonates are ^{13}C-depleted with $\delta^{13}C_{CH_4}$ values generally ranging from -60 to -20 ‰ (von Rad et al., 1996; Peckmann et al., 2001; Greinert et al., 2002a; Luff et al., 2005; Judd and Hovland, 2007). Other well-known MDACs are barites (Torres et al., 1996; Greinert et al., 2002b). MDACs occur in several forms (chimneys, plates, crusts, etc.). Their presence in the fossil record indicates that seepage and AOM were already important in earlier geological times (Luth et al., 1999; Díaz-del-Río et al., 2003; De Boever et al., 2006a; Judd and Hovland, 2007; Campbell et al., 2008).

In the Dnepr-paleo delta several MDACs are present at water depths ranging from -86 to -700 m. The carbonates occur often in association with bacterial mats and are ^{13}C-depleted with $\delta^{13}C_{CH_4}$ values generally ranging from -25.5 to -41.‰ (Fig. 4.7.) (Luth et al., 1999; Peckmann et al., 2001; Michaelis et al., 2002; Gulin et al., 2003; Reitner et al., 2005; CRIMEA Project Team, 2006). At the -100 m seep site, the MDACs are plate-like or form small buildups that are often covered by sediments (Fig. 4.7.). These MDACs control the locations of bubble-releasing seeps by clogging up, and eventually sealing, fluid pathways (chapter 4). This self-sealing process of seeps was previously suggested by Hovland (2002) for seeps in the North Sea. At the deeper seep sites, MDACs are present as chimney-like buildups which focus bubble release. These carbonate buildups are unique in the world due to anoxic water column of the Black Sea below -145 m water depth. Carbonate chimneys are normally formed within the anoxic environment present in the sediments and not within the water column (Díaz-del-Río et al., 2003; De Boever et al., 2006b). Peckmann et al. (2001) dated the carbonates from the -200 m seep site and concluded that the chimneys are made up from methane with an age of 19 ka BP. The real upper age limit of the microbial tower-like structures is given by the limnic-marine transition of the Black Sea and the subsequent development of a permanent anoxic water body about 8 ka BP ago (Pape et al., 2008). The presence of the MDACs indicates that seepage is long-lived at the Dnepr paleo-delta.

At the Hikurangi Margin, MDACs are present as a relatively large carbonate platform associated with live seep mega fauna at LM-3 and several smaller platforms without live seep megafauna near Faure Site. Carbonates from LM-3 had a $\delta^{13}C_{CH_4}$ value of -36.49 ‰ indicating the AOM-related formation of the MDACs (Campbell et al., 2010). As was observed in the

Dnepr paleo-delta, the carbonate platform at LM-3 focuses and relocates bubble-releasing seeps to an area just next to the area affected by massive carbonate precipitation. Near the bubble-releasing seeps of Faure Site, however, no MDACs were observed. This is remarkable for the Hikurangi Margin where most seep sites are associated with large carbonate structures, suggesting a longtime seepage history at this accretionary prism (Greinert et al., 2010a). The absence of MDACs indicates that seepage at Faure Site is rather recent, probably related to the presence of a submarine landslide.

At the Posolsky Bank, no sampling of carbonates was undertaken or observed. However, small MDACs do occur in Lake Baikal, notwithstanding the sulfate-poor freshwater environment. MDACs (siderites) have been sampled at several mud volcanoes where they occur in association with gas hydrates and are formed due to aceticlastic methanogenesis (Krylov et al., 2008a; Krylov et al., 2008b).

MDACs have been observed in the same water depth range as the chemosynthetic communities (-84 m to -908 m). Besides the visual observations, MDACs can be easily localized based on backscatter data from multibeam and side-scan sonar recordings making them strong seep indicators (chapter 4) (Greinert et al., 2010a). MDACs control the location and activity of bubble-releasing seeps, and therefore their presence doesn't always indicate active seepage. Vast occurrences of MDACs do, however, indicate that seepage is/was active over longer periods. Highly focused fluid flow can however also inhibit AOM and the formation of MDACs and chemosynthetic communities.

7.3.3. Seafloor morphology

In some cases bubble-releasing seeps occur at typical seafloor morphologies. The most common are seafloor depressions known as pockmarks or cone-shaped seafloor highs related to mud volcanism. Pockmarks are believed to be formed by blow-outs due to overpressure generated by gas trapped underneath an impermeable cohesive sealing layer. Mud volcanoes are formed by overpressured fluid and mud rising from great depths that extrude at the seafloor. (Judd and Hovland, 2007). Notwithstanding that both morphologies are very characteristic they are not always associated with bubble release. Acoustic and visual observations are needed to confirm if these features are actively bubbling.

In the Dnepr paleo-delta, bubble-releasing seeps occur at several seafloor morphologies: pockmarks, sedimentary ridges, scarps of submarine landslides and canyons (Figs. 3.5.-3.6. and 3.10.-3.12.). Probably only the pockmarks are a direct result of fluid flow and seepage. Whether they are formed by blow-outs is rather doubtful. Perhaps they are formed by the entrainment of sediment grains by bubbles over long time spans. The presence of MDACs in the deep pockmarks indicates such a longtime seepage. Visual observations at Faure Site clearly show that bubbles are capable of forming seafloor depressions by entrainment of sediment grains (Fig. 5.10.). The submarine landslides present in the Dnepr paleo-delta and near Faure Site are probably also related to fluid flow and/or seepage (Figs. 3.11. and 5.2.) (Pecher et al., 2005; Crutchley et al., in press). Whether in both cases bubble release was the cause or is rather the result of the mass movement is unclear. In the Dnepr paleo-delta, canyons are typically associated with bubble release. As for the submarine landslides, erosion of an impermeable cover exposes gas-bearing layers and leads to seepage. The formation and location of a canyon can be strongly controlled by fluid flow and seepage (Popescu et al., 2004). Furthermore, the alignment of seeps on the crests of sedimentary ridges is very common in the Dnepr paleo-delta, but such alignments are hardly observed anywhere else (Figs. 3.10. and 3.12.). This is maybe due to our detailed echosounder coverage and resulting seeps distribution. The presence of an impermeable top layer and the tendency of fluids to migrate towards the highest location in permeable reservoirs is probably the cause of this alignment. Whether overpressure helped to breach the cover layer at the crest of the ridges or whether the presence of MDACs have enhanced the ridge morphology is not clear.

As mentioned in the previous paragraph the seeps at Faure Site are associated with a

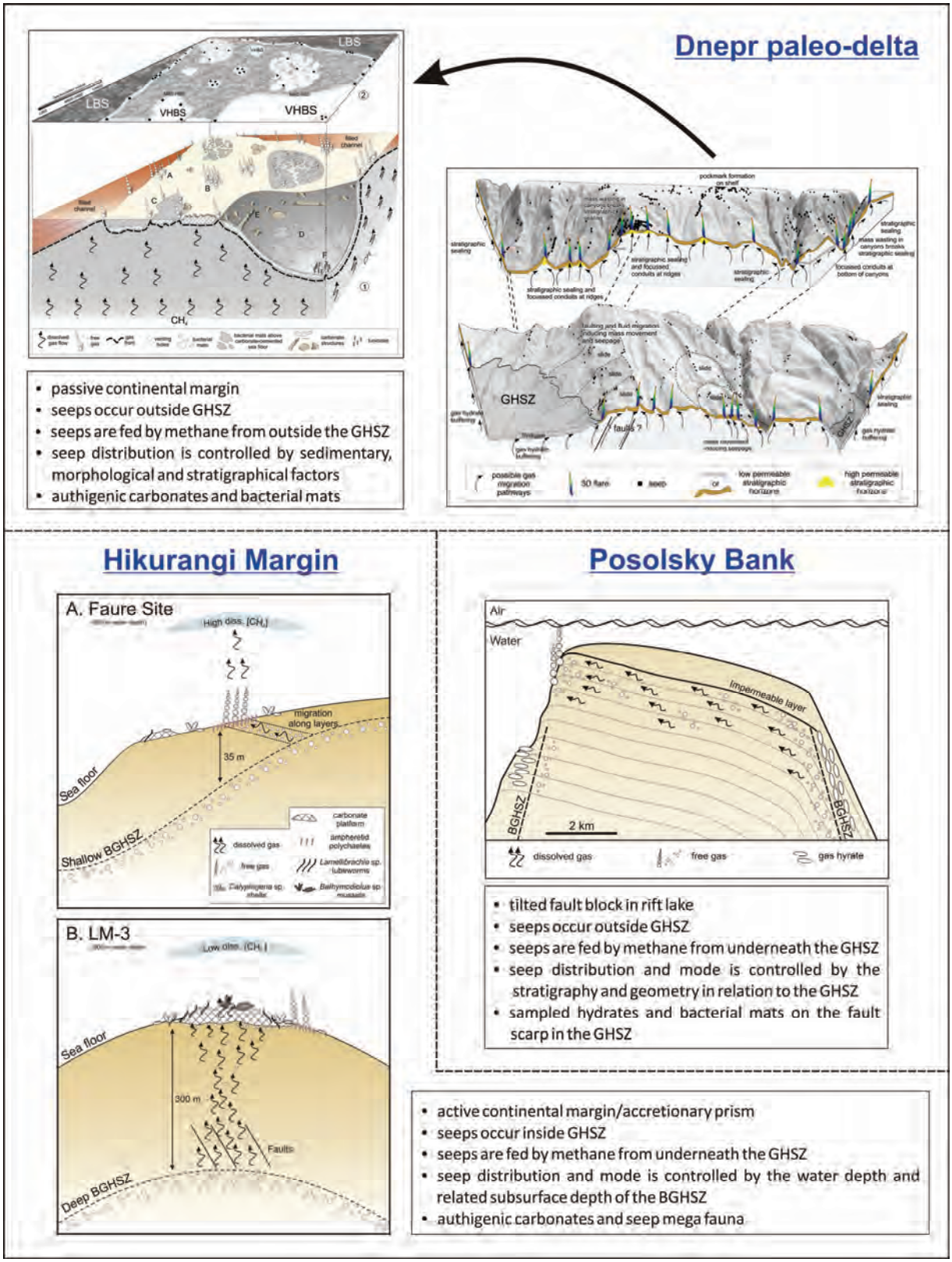

Figure 7.3. Overview of the models explaining fluid flow, the distribution of seeps and the associated seafloor/lake floor manifestations for the different study areas.

submarine landslide and with very small pockmarks formed by bubble release. At LM-3, no small-scale change in seafloor morphology is present at the seep site except for the presence of the carbonate platform. On a larger scale, seepage at Rock Garden and at the Hikurangi Margin is located on the crests of thrust-faulted ridges on the mid slope of the accretionary prism (Barnes et al., 2010).

At the Posolsky Bank, seeps occur where a major fault cuts off gas-bearing strata, whereas for the Dnepr paleo-delta and Faure site erosional features expose gas-bearing layers. Fault scarps seem to be the main seep location in the Posolsky Bank study area. One local pockmark was also observed at a fault scarp; however no bubble release was observed (Fig. 6.3.).

The previous has shown that seeps tend to occur at certain seafloor morphologies, but those seafloor morphologies are not always associated or caused by fluid flow or bubble release. Pockmarks are probably the most indicative for present or past seepage activity. However, in our study areas, the amount of pockmarks is rather small. Whether this is due to sediment type or fluid-flow activity is unclear. Locations where subsurface layers are exposed due to erosion or fault activity are particularly interesting to be associated with bubble-releasing seeps.

7.4. Fate of methane released at bubble-releasing seeps

Although it was not one of the main goals of this study, the fate of the methane released at bubble-releasing seeps is one of the key questions behind the conducted seep research and can therefore not be omitted from this discussion. Within the CRIMEA project (Black Sea), the main goal was to study and quantify the transfer of methane to the atmosphere emitted from bubble-releasing seeps. Several publications resulting from this project explained the mechanism controlling the release of methane from the seafloor, into the water column and potentially into the atmosphere (Durisch-Kaiser et al., 2005; Schmale et al., 2005; Greinert et al., 2006; Kourtidis et al., 2006; McGinnis et al., 2006; Schubert et al., 2006; Greinert, 2008; Greinert and McGinnis, 2009; Greinert et al., 2010b; Schmale et al., 2010). The main conclusion is that bubble-releasing seeps are only active over short periods, e.g. Faure Site (see table 5.1.), and are only effective in transferring methane into the atmosphere in shallow water depths (< 100 m). Even in these shallow water depths the resulting flux is rather limited. It is only where a widespread massive constant release of gas bubbles occurs, e.g. from destabilizing gas hydrates or from mud volcanoes, that bubble plumes can form and enable the release of significant volumes of methane into the atmosphere and influence regional atmospheric methane concentrations. In case of the mud volcanoes the duration of such outbursts is rather limited in time and thus less significant. Our observations at Faure Site also showed that bubble release is very transient and is controlled by different factors on different time scales (see section 5.5.2.). It seems that only very shallow and very active seeps, e.g. Coil Oil Point seeps, significantly contribute to atmospheric methane (Leifer et al., 2006b). Solomon et al. (2009) indicated however that deep oily seeps or seeps releasing large bubbles can have an important influence on atmospheric methane concentrations. It is clear that much more research needs to be conducted to understand the release of methane from bubble-releasing seeps. One of the main target study areas should be the shallow Arctic Shelf, where rapidly warming bottom waters are potentially affecting gas-hydrate stability and cause the thawing of permafrost. The release of the possible vast amounts of methane stored in the sediments and the shallow water depth could lead to enormous fluxes of methane into the atmosphere and could affect atmospheric methane concentrations and global climate in the near future (Shakhova and Semiletov, 2007; Greinert et al., 2010b).

References

Aloisi, G., Drews, M., Wallmann, K., Bohrmann, G., 2004. Fluid expulsion from the Dvurechenskii mud volcano (Black Sea) - Part I. Fluid sources and relevance to Li, B, Sr, I and dissolved inorganic nitrogen cycles. Earth Planet. Sci. Lett. 225, 347-363.

Baraza, J.s., Ercilla, G., 1996. Gas-charged sediments and large pockmark-like features on the Gulf of Cadiz slope (SW Spain). Mar. Pet. Geol. 13, 253-261.

Barnes, P.M., Lamarche, G., Bialas, J., Henrys, S., Pecher, I., Netzeband, G.L., Greinert, J., Mountjoy, J.J., Pedley, K., Crutchley, G., 2010. Tectonic and geological framework for gas hydrates and cold seeps on the Hikurangi subduction margin, New Zealand. Mar. Geol. 272, 26-48.

Bayon, G., Loncke, L., Dupré, S., Caprais, J.C., Ducassou, E., Duperron, S., Etoubleau, J., Foucher, J.P., Fouquet, Y., Gontharet, S., Henderson, G.M., Huguen, C., Klaucke, I., Mascle, J., Migeon, S., Olu-Le Roy, K., Ondréas, H., Pierre, C., Sibuet, M., Stadnitskaia, A., Woodside, J., 2009. Multi-disciplinary investigation of fluid seepage on an unstable margin: The case of the Central Nile deep sea fan. Mar. Geol. 261, 92-104.

Berndt, C., 2005. Focused fluid flow in passive continental margins. Philos. Trans. R. Soc. A-Math. Phys. Eng. Sci. 363, 2855-2871.

Blumenberg, M., Seifert, R., Reitner, J., Pape, T., Michaelis, W., 2004. Membrane lipid patterns typify distinct anaerobic methanotrophic consortia. Proc. Natl. Acad. Sci. USA 101, 11111-11116.

Boetius, A., Ravenschlag, K., Schubert, C.J., Rickert, D., Widdel, F., Gieseke, A., Amann, R., Jorgensen, B.B., Witte, U., Pfannkuche, O., 2000. A marine microbial consortium apparently mediating anaerobic oxidation of methane. Nature 407, 623-626.

Boetius, A., Suess, E., 2004. Hydrate Ridge: a natural laboratory for the study of microbial life fueled by methane from near-surface gas hydrates. Chem. Geol. 205, 291-310.

Bohrmann, G., Greinert, J., Suess, E., Torres, M., 1998. Authigenic carbonates from the Cascadia subduction zone and their relation to gas hydrate stability. Geology 26, 647-650.

Bohrmann, G., Ivanov, M., Foucher, J.P., Spiess, V., Bialas, J., Greinert, J., Weinrebe, W., Abegg, F., Aloisi, G., Artemov, Y., Blinova, V., Drews, M., Heidersdorf, F., Krabbenhoft, A., Klaucke, I., Krastel, S., Leder, T., Polikarpov, I., Saburova, M., Schmale, O., Seifert, R., Volkonskaya, A., Zillmer, M., 2003. Mud volcanoes and gas hydrates in the Black Sea: new data from Dvurechenskii and Odessa mud volcanoes. Geo-Mar. Lett. 23, 239-249.

Boles, J.R., Clark, J.F., Leifer, I., Washburn, L., 2001. Temporal variation in natural methane seep rate due to tides, Coal Oil Point area, California. Journal of Geophysical Research-Oceans 106, 27077-27086.

Brooks, J.M., Anderson, A.L., Sassen, R., Macdonald, I.R., Kennicutt, C., Guinasso, N.L., 1994. Hydrate Occurrences in Shallow Subsurface Cores from Continental-Slope Sediments. International Conference on Natural Gas Hydrates 715, 381-391.

Campbell, K.A., Francis, D.A., Collins, M., Gregory, M.R., Nelson, C.S., Greinert, J., Aharon, P., 2008. Hydrocarbon seep-carbonates of a Miocene forearc (East Coast Basin), North Island, New Zealand. Sediment. Geol. 204, 83-105.

Campbell, K.A., Nelson, C.S., Alfaro, A.C., Boyd, S., Greinert, J., Nyman, S., Grosjean, E., Logan, G.A., Gregory, M.R., Cooke, S., Linke, P., Milloy, S., Wallis, I., 2010. Geological imprint of methane seepage on the seabed and biota of the convergent Hikurangi Margin, New Zealand: Box core and grab carbonate results. Mar. Geol. 272, 285-306.

Clark, J.F., Leifer, I., Washburn, L., Luyendyk, B.P., 2003. Compositional changes in natural gas bubble plumes: observations from the Coal Oil Point marine hydrocarbon seep field. Geo-Mar. Lett. 23, 187-193.

Clennell, M.B., Hovland, M., Booth, J.S., Henry, P., Winters, W.J., 1999. Formation of natural gas hydrates in marine sediments. 1. Conceptual model of gas hydrate growth conditioned by host sediment properties. J. Geophys. Res. 104, 22985-23003.

Conti, A., Stefanon, A., Zuppi, G.M., 2002. Gas seeps and rock formation in the northern Adriatic Sea. Cont. Shelf Res. 22, 2333-2344.

CRIMEA Project Team, 2006. CRIMEA: Final Scientific Report: executive summary, Ghent University, Ghent.

Crutchley, G., Geiger, S., Pecher, I., Gorman, A., Zhu, H., Henrys, S., in press. The potential influence of shallow gas and gas hydrates on sea floor erosion of Rock Garden, an uplifted ridge offshore of New Zealand. Geo-Mar. Lett.

Crutchley, G.J., Pecher, I.A., Gorman, A.R., Henrys, S.A., Greinert, J., 2010. Seismic imaging of gas conduits beneath seafloor seep sites in a shallow marine gas hydrate province, Hikurangi Margin, New Zealand. Mar. Geol. 272, 114-126.

Dando, P.R., Bussmann, I., Niven, S.J., Ohara, S.C.M., Schmaljohann, R., Taylor, L.J., 1994. A Methane Seep Area in the Skagerrak, the Habitat of the Pogonophore Siboglinum-Poseidoni and the Bivalve Mollusk Thyasira-Sarsi. Mar. Ecol.-Prog. Ser. 107, 157-167.

De Batist, M., Klerkx, J., Van Rensbergen, P., Vanneste, M., Poort, J., Golmshtok, A.Y., Kremlev, A.A., Khlystov, O.M., Krinitsky, P., 2002. Active hydrate destabilization in Lake Baikal, Siberia? Terra Nova 14, 436-442.

De Boever, E., Swennen, R., Dimitrov, L., 2006a. Lower Eocene carbonate-cemented "chimney" structures (Varna, Bulgaria) - Control of seepage rates on their formation and stable isotopic signature. J. Geochem. Explor. 89, 78-82.

De Boever, E., Swennen, R., Dimitrov, L., 2006b. Lower Eocene carbonate cemented chimneys (Varna, NE Bulgaria): Formation mechanisms and the (a)biological mediation of chimney growth? Sediment. Geol. 185, 159-173.

Depreiter, D., Poort, J., Van Rensbergen, P., Henriet, J.P., 2005. Geophysical evidence of gas hydrates in shallow submarine mud volcanoes on the Moroccan margin. J. Geophy. Res., B, Solid Earth 110, 9 pp.-9 pp.

Díaz-del-Río, V., Somoza, L., Martínez-Frias, J., Mata, M.P., Delgado, A., Hernandez-Molina, F.J., Lunar, R., Martín-Rubí, J.A., Maestro, A., Fernández-Puga, M.C., León, R., Llave, E., Medialdea, T., Vázquez, J.T., 2003. Vast fields of hydrocarbon-derived carbonate chimneys related to the accretionary wedge/olistostrome of the Gulf of Cádiz. Mar. Geol. 195, 177-200.

Dimitrov, L., 2002. Contribution to atmospheric methane by natural seepages on the Bulgarian continental shelf. Cont. Shelf Res. 22, 2429-2442.

Dupre, S., Woodside, J., Foucher, J.P., de Lange, G., Mascle, J., Boetius, A., Mastalerz, V., Stadnitskaia, A., Ondreas, H., Huguen, C., Harmegnies, F.O., Gontharet, S., Loncke, L., Deville, E., Niemann, H., Omoregie, E., Roy, K.O.L., Fiala-Medioni, A., Dahlmann, A., Caprais, J.C., Prinzhofer, A., Sibuet, M., Pierre, C., Damste, J.S.S., Party, N.S., 2007. Seafloor geological studies above active gas chimneys off Egypt (Central nile deep sea fan). Deep-Sea Res. Part I-Oceanogr. Res. Pap. 54, 1146-1172.

Durisch-Kaiser, E., Klauser, L., Wehrli, B., Schubert, C., 2005. Evidence of intense archaeal and bacterial methanotrophic activity in the black sea water column. Appl Environ Microbiol 71, 8099-8106.

Egorov, V., Luth, U., Luth, C., Gulin, M.B., 1998. Gas seeps in the submarine Dnieper Canyon, Black Sea: acoustic, video and trawl data. In: U. Luth, C. Luth and H. Thiel (Editors), MEGASEEPS Gas Explorations in the Black Sea, Project Report. Zentrum für Meres- und Klimaforschung der Universität Hamburg, Hamburg, pp. 11-21.

Eichhubl, P., Greene, H.G., Naehr, T., Maher, N., 2000. Structural control of fluid flow: offshore fluid seepage in the Santa Barbara Basin, California. J. Geochem. Explor. 69, 545-549.

Etiope, G., 2009. Natural emissions of methane from geological seepage in Europe. Atmos. Environ. 43, 1430-1443.

Faure, K., Greinert, J., Pecher, I.A., Graham, I.J., Massoth, G.J., De Ronde, C.E.J., Wright, I.C., Baker, E.T., Olson, E.J., 2006. Methane seepage and its relation to slumping and gas hydrate at the Hikurangi margin, New Zealand. N. Z. J. Geol. Geophys. 49, 503-516.

Faure, K., Greinert, J., von Deimling, J.S., McGinnis, D.F., Kipfer, R., Linke, P., 2010. Methane seepage along the Hikurangi Margin of New Zealand: Geochemical and physical data from the water column, sea surface and atmosphere. Mar. Geol. 272, 170-188.

Feseker, T., Brown, K., Blanchet, C., Scholz, F., Nuzzo, M., Reitz, A., Schmidt, M., Hensen, C., in press. Active mud volcanoes on the upper slope of the western Nile deep-sea fan—first results from the P362/2 cruise of R/V Poseidon. Geo-Mar. Lett.

Feseker, T., Foucher, J.P., Harmegnies, F., 2008. Fluid flow or mud eruptions? Sediment temperature distributions on Hakon Mosby mud volcano, SW Barents Sea slope. Mar. Geol. 247, 194-207.

Feseker, T., Pape, T., Wallmann, K., Klapp, S.A., Schmidt-Schierhorn, F., Bohrmann, G., 2009. The thermal structure of the Dvurechenskii mud volcano and its implications for gas hydrate stability and eruption dynamics. Mar. Pet. Geol. 26, 1812-1823.

Flemings, P.B., Liu, X.L., Winters, W.J., 2003. Critical pressure and multiphase flow in Blake Ridge gas hydrates. Geology 31, 1057-1060.

Garcia-Gil, S., Vilas, F., Garcia-Garcia, A., 2002. Shallow gas features in incised-valley fills (Ria de Vigo, NW Spain): a case study. Cont. Shelf Res. 22, 2303-2315.

Gay, A., Lopez, M., Berndt, C., Seranne, M., 2007. Geological controls on focused fluid flow associated with seafloor seeps in the Lower Congo Basin. Mar. Geol. 244, 68-92.

Geletti, R., Del Ben, A., Busetti, M., Ramella, R., Volpi, V., 2008. Gas seeps linked to salt structures in the Central Adriatic Sea. Basin Res. 20, 473-487.

Géli, L., Henry, P., Zitter, T., Dupré, S., Tryon, M., Çagatay, M.N., de Lépinay, B.M., Le Pichon, X., Sengör, A.M.C., Görür, N., Natalin, B., Uçarkus, G., Özeren, S., Volker, D., Gasperini, L., Burnard, P., Bourlange, S., the Marnaut Scientific, P., 2008. Gas emissions and active tectonics within the submerged section of the North Anatolian Fault zone in the Sea of Marmara. Earth Planet. Sci. Lett. 274, 34-39.

Ghosh, R., Sain, K., 2008. Effective medium modeling to assess gas hydrate and free-gas evident from the velocity structure in the Makran accretionary prism, offshore Pakistan. Mar. Geophys. Res. 29, 267-274.

Ginsburg, G.D., Soloviev, V.A., 1997. Methane migration within the submarine gas-hydrate stability zone under deep-water conditions. Mar. Geol. 137, 49-57.

Gorman, A.R., Holbrook, W.S., Hornbach, M.J., Hackwith, K.L., Lizarralde, D., Pecher, I., 2002. Migration of methane gas through the hydrate stability zone in a low-flux hydrate province. Geology 30, 327-330.

Granin, N., Makarov, M., Kucher, K., Gnatovsky, R., in press. Gas seeps in Lake Baikal—detection, distribution, and implications for water column mixing. Geo-Mar. Lett.

Granin, N.G., Granina, L.Z., 2002. Gas hydrates and gas venting in Lake Baikal. Russian Geology and Geophysics 43, 589-597.

Greinert, J., 2008. Monitoring temporal variability of bubble release at seeps: The hydroacoustic swath system GasQuant. Journal of Geophysical Research-Oceans 113, 20.

Greinert, J., Artemov, Y., Egorov, V., De Batist, M., McGinnis, D., 2006. 1300-m-high rising bubbles from mud volcanoes at 2080m in the Black Sea: Hydroacoustic characteristics and temporal variability. Earth Planet. Sci. Lett. 244, 1-15.

Greinert, J., Bohrmann, G., Elvert, M., 2002a. Stromatolitic fabric of authigenic carbonate crusts: result of anaerobic methane oxidation at cold seeps in 4,850 m water depth. Int. J. Earth Sci. 91, 698-711.

Greinert, J., Bohrmann, G., Suess, E., 2001. Gas hydrate-associated carbonates and methane-venting at Hydrate Ridge: Classification, distribution, and origin of authigenic lithologies. In: C.K. Paull and W.P. Dillon (Editors), Natural Gas Hydrates: Occurrence, Distribution, and Detection, Geophysical Monograph. American Geophysical Union, pp. 99-113.

Greinert, J., Bollwerk, S.M., Derkachev, A., Bohrmann, G., Suess, E., 2002b. Massive barite deposits and carbonate mineralization in the Derugin Basin, Sea of Okhotsk: precipitation processes at cold seep sites. Earth Planet. Sci. Lett. 203, 165-180.

Greinert, J., Lewis, K.B., Bialas, J., Pecher, I.A., Rowden, A., Bowden, D.A., De Batist, M., Linke, P., 2010a. Methane seepage along the Hikurangi Margin, New Zealand: Overview of studies in 2006 and 2007 and new evidence from visual, bathymetric and hydroacoustic investigations. Mar. Geol. 272, 6-25.

Greinert, J., McGinnis, D.F., 2009. Single bubble dissolution model - The graphical user interface SiBu-GUI. Environmental Modelling & Software 24, 1012-1013.

Greinert, J., McGinnis, D.F., Naudts, L., Linke, P., De Batist, M., 2010b. Atmospheric methane flux from bubbling seeps: Spatially extrapolated quantification from a Black Sea shelf area. J. Geophys. Res. 115, 1-18.

Gürgey, K., Philp, R.P., Clayton, C., Emiroglu, H., Siyako, M., 2005. Geochemical and isotopic approach to maturity/source/mixing estimations for natural gas and associated condensates in the Thrace Basin, NW Turkey. Appl. Geochem. 20, 2017-2037.

Gulin, S.B., Polikarpov, G.G., Egorov, V.N., 2003. The age of microbial carbonate structures grown at methane seeps in the Black Sea with an implication of dating of the seeping methane. Mar. Chem. 84, 67-72.

Haeckel, M., Suess, E., Wallmann, K., Rickert, D., 2004. Rising methane gas bubbles form massive hydrate layers at the seafloor. Geochim. Cosmochim. Acta 68, 4335-4345.

Heeschen, K.U., Collier, R.W., de Angelis, M.A., Suess, E., Rehder, G., Linke, P., Klinkhammer, G.P., 2005. Methane sources, distributions, and fluxes from cold vent sites at Hydrate Ridge, Cascadia Margin. Global Biogeochem. Cycles 19.

Holbrook, W.S., 2001. Seismic studies of the Blake Ridge: implications for hydrate distribution, methane expulsion and free gas dynamics. In: C.K. Paull and W.P. Dillon (Editors), Natural Gas Hydrates: Occurrence, Distribution and Detection. Geophysical Monographs. American Geophysical Union, pp. 235-256.

Holzner, C.P., McGinnis, D.F., Schubert, C.J., Kipfer, R., Imboden, D.M., 2008. Noble gas anomalies related to high-intensity methane gas seeps in the Black Sea. Earth Planet. Sci. Lett. 265, 396-409.

Hovland, M., 2002. On the self-sealing nature of marine seeps. Cont. Shelf Res. 22, 2387-2394.

Hovland, M., 2007. Discovery of prolific natural methane seeps at Gullfaks, northern North Sea. Geo-Mar. Lett. 27, 197-201.

Hovland, M., Curzi, P.V., 1989. Gas Seepage and Assumed Mud Diapirism in the Italian Central Adriatic Sea. Mar. Pet. Geol. 6, 161-169.

Hovland, M., Gardner, J.V., Judd, A.G., 2002. The significance of pockmarks to understanding fluid flow processes and geohazards. Geofluids, 127-136.

Huguen, C., Foucher, J.P., Mascle, J., Ondreas, H., Thouement, M., Gontharet, S., Stadnitskaia, A., Pierre, C., Bayon, G., Loncke, L., Boetius, A., Bouloubassi, I., de Lange, G., Caprais, J.C., Fouquet, Y., Woodside, J., Dupre, S., Party, N.S., 2009. Menes caldera, a highly active site of brine seepage in the Eastern Mediterranean sea: "In situ" observations from the NAUTINIL expedition (2003). Mar. Geol. 261, 138-152.

Iglesias, J., Garcia-Gil, S., 2007. High-resolution mapping of shallow gas accumulations and gas seeps in San Simon Bay (Ria de Vigo, NW Spain). Some quantitative data. Geo-Mar. Lett. 27, 103-114.

Ivanova, E.V., Murdmaa, I.O., Chepalyga, A.L., Cronin, T.M., Pasechnik, I.V., Levchenko, O.V., Howe, S.S., Manushkina, A.V., Platonova, E.A., 2007. Holocene sea-level oscillations and environmental changes on the Eastern Black Sea shelf. Palaeogeogr. Palaeoclimatol. Palaeoecol. 246, 228-259.

Jeong, K.S., Cho, J.H., Kim, S.R., Hyun, S., Tsunogai, U., 2004. Geophysical and geochemical observations on actively seeping hydrocarbon gases on the south-eastern Yellow Sea continental shelf. Geo-Mar. Lett. 24, 53-62.

Jerosch, K., Schluter, M., Foucher, J.-P., Allais, A.-G., Klages, M., Edy, C., 2007. Spatial distribution of mud flows, chemoautotrophic communities, and biogeochemical habitats at Hakon Mosby Mud Volcano. Mar. Geol. 243, 1-17.

Joye, S.B., Boetius, A., Orcutt, B.N., Montoya, J.P., Schulz, H.N., Erickson, M.J., Lugo, S.K., 2004. The anaerobic oxidation of methane and sulfate reduction in sediments from Gulf of Mexico cold seeps. Chem. Geol. 205, 219-238.

Judd, A., Croker, P., Tizzard, L., Voisey, C., 2007. Extensive methane-derived authigenic carbonates in the Irish Sea. Geo-Mar. Lett. 27, 259-267.

Judd, A., Hovland, M., 2007. Seabed fluid flow: the impact on geology, biology and the marine environment. Cambridge University Press, Cambridge. 475 pp.

Kalmychkov, G., Egorov, A., Kuz'min, M., Khlystov, O., 2006. Genetic types of methane from Lake Baikal. Doklady Earth Sciences 411, 1462-1465.

Kessler, J.D., Reeburgh, W.S., Southon, J., Seifert, R., Michaelis, W., Tyler, S.C., 2006. Basin-wide estimates of the input of methane from seeps and clathrates to the Black Sea. Earth Planet. Sci. Lett. 243, 366-375.

Kida, M., Khlystov, O., Zemskaya, T., Takahashi, N., Minami, H., Sakagami, H., Krylov, A., Hachikubo, A., Yamashita, S., Shoji, H., Poort, J., Naudts, L., 2006. Coexistence of structure I and II gas hydrates in Lake Baikal suggesting gas sources from microbial and thermogenic origin. Geophys. Res. Lett. 33.

Klaucke, I., Sahling, H., Weinrebe, W., Blinova, V., Burk, D., Lursmanashvili, N., Bohrmann, G., 2006. Acoustic investigation of cold seeps offshore Georgia, eastern Black Sea. Mar. Geol. 231, 51-67.

Kourtidis, K., Kioutsioukis, I., McGinnis, D.F., Rapsomanikis, S., 2006. Effects of methane outgassing on the Black Sea atmosphere. Atmos. Chem. Phys. 6, 5173-5182.

Kruger, M., Blumenberg, M., Kasten, S., Wieland, A., Kanel, L., Klock, J.H., Michaelis, W., Seifert, R., 2008. A novel, multi-layered methanotrophic microbial mat system growing on the sediment of the Black Sea. Environ. Microbiol. 10, 1934-1947.

Kruglyakova, R.P., Byakov, Y.A., Kruglyakova, M.V., Chalenko, L.A., Shevtsova, N.T., 2004. Natural oil and gas seeps on the Black Sea floor. Geo-Mar. Lett. V24, 150-162.

Krylov, A., Khlystov, O., Zemskaya, T., Minami, H., Hachikubo, A., Nunokawa, Y., Kida, M., Shoji, H., Naudts, L., Poort, J., Pogodaeva, T., 2008a. First discovery and formation process of authigenic siderite from gas hydrate-bearing mud volcanoes in fresh water: Lake Baikal, Eastern Siberia. Geophys. Res. Lett. 35.

Krylov, A., Khlystov, O., Zemskaya, T., Minami, H., Hachikubo, A., Shoji, H., Kida, M., Pogodaeva, T., Naudts, L., Poort, J., 2008b. Crystallization of authigenic carbonates in mud volcanoes at Lake Baikal. Geochem. Int. 46, 985-995.

Kuscu, I., Okamura, M., Matsuoka, H., Gokasan, E., Awata, Y., Tur, H., Simsek, M., Kecer, M., 2005. Seafloor gas seeps and sediment failures triggered by the August 17, 1999 earthquake in the Eastern part of the Gulf of Izmit, Sea of Marmara, NW Turkey. Mar. Geol. 215, 193-214.

Kutas, R., Poort, J., 2008. Regional and local geothermal conditions in the northern Black Sea. Int. J. Earth Sci. 97, 353-363.

Kvenvolden, K.A., Dillon, W.P., 1981. Natural-Gas Hydrates of Blake Ridge Region, Atlantic Continental-Margin. Aapg Bulletin-American Association of Petroleum Geologists 65, 1665-1665.

Leifer, I., Luyendyk, B., Broderick, K., 2006a. Tracking an oil slick from multiple natural sources, Coal Oil Point, California. Mar. Pet. Geol. 23, 621-630.

Leifer, I., Luyendyk, B.P., Boles, J., Clark, J.F., 2006b. Natural marine seepage blowout: Contribution to atmospheric methane. Global Biogeochem. Cycles 20, -.

Lewis, K.B., Marshall, B.A., 1996. Seep faunas and other indicators of methane-rich dewatering on New Zealand convergent margins. N. Z. J. Geol. Geophys. 39, 181-200.

Linke, P., Sommer, S., Rovelli, L., McGinnis, D.F., 2010. Physical limitations of dissolved methane fluxes: The role of bottom-boundary layer processes. Mar. Geol. 272, 209-222.

Logan, G.A., Jones, A.T., Kennard, J.M., Ryan, G.J., Rollet, N., 2010. Australian offshore natural hydrocarbon seepage studies, a review and re-evaluation. Mar. Pet. Geol. 27, 26-45.

Ludmann, T., Wong, H.K., 2003. Characteristics of gas hydrate occurrences associated with mud diapirism and gas escape structures in the northwestern Sea of Okhotsk. Mar. Geol. 201, 269-286.

Lüdmann, T., Wong, H.K., Konerding, P., Zillmer, M., Petersen, J., Flüh, E., 2004. Heat flow and quantity of methane deduced from a gas hydrate field in the vicinity of the Dnieper Canyon, northwestern Black Sea. Geo-Mar. Lett. V24, 182-193.

Luff, R., Greinert, J., Wallmann, K., Klaucke, I., Suess, E., 2005. Simulation of long-term feedbacks from authigenic carbonate crust formation at cold vent sites. Chem. Geol. 216, 157-174.

Luth, C., Luth, U., Gebruk, A.V., Thiel, H., 1999. Methane gas Seeps Along the Oxic/Anoxic Gradient in the Black Sea: Manifestations, Biogenic Sediment Compounds and Preliminary Results on Benthic Ecology. Mar. Ecol. 20, 221-249.

MacDonald, I.R., Leifer, I., Sassen, R., Stine, P., Mitchell, R., Guinasso, N., 2002. Transfer of hydrocarbons from natural seeps to the water column and atmosphere. Geofluids 2, 95-107.

MacDonald, I.R., Sager, W.W., Peccini, M.B., 2003. Gas hydrate and chemosynthetic biota in mounded bathymetry at mid-slope hydrocarbon seeps: Northern Gulf of Mexico. Mar. Geol. 198, 133-158.

McGinnis, D.F., Greinert, J., Artemov, Y., Beaubien, S.E., Wuest, A., 2006. Fate of rising methane bubbles in stratified waters: How much methane reaches the atmosphere? J. Geophys. Res., Oceans 111.

Michaelis, W., Seifert, R., Nauhaus, K., Treude, T., Thiel, V., Blumenberg, M., Knittel, K., Gieseke, A., Peterknecht, K., Pape, T., Boetius, A., Amann, R., Jorgensen, B.B., Widdel, F., Peckmann, J., Pimenov, N.V., Gulin, M.B., 2002. Microbial Reefs in the Black Sea Fueled by Anaerobic Oxidation of Methane. Science 297, 1013-1015.

Namsaraev, B.B., Dagurova, O.P., Zemskaya, T.I., Golobokova, L.P., 2006. The functioning of the microbial community in bottom sediments of Lake Baikal, with special regard to hydrothermal and gas hydrate regions. Hydrobiologia 568, 83-85.

Naudts, L., De Batist, M., Greinert, J., Artemov, Y., 2009. Geo- and hydro-acoustic manifestations of shallow gas and gas seeps in the Dnepr paleodelta, northwestern Black Sea. The Leading Edge 28, 1030-1040.

Naudts, L., Greinert, J., Artemov, Y., Beaubien, S.E., Borowski, C., De Batist, M., 2008. Anomalous sea-floor backscatter patterns in methane venting areas, Dnepr paleo-delta, NW Black Sea. Mar. Geol. 251, 253-267.

Naudts, L., Greinert, J., Artemov, Y., Staelens, P., Poort, J., Van Rensbergen, P., De Batist, M., 2006. Geological and morphological setting of 2778 methane seeps in the Dnepr paleo-delta, northwestern Black Sea. Mar. Geol. 227, 177-199.

Naudts, L., Greinert, J., Poort, J., Belza, J., Vangampelaere, E., Boone, D., Linke, P., Henriet, J.P., De Batist, M., 2010. Active venting sites on the gas-hydrate-bearing Hikurangi Margin, Off New Zealand: Diffusive- versus bubble-released methane. Mar. Geol. 272, 233-250.

Naudts, L., Khlystov, O., Granin, N., Chensky, A., Poort, J., De Batist, M., submitted. Stratigraphic and structural controls on the location of active methane seep on Posolsky Bank, Lake Baikal. Mar. Pet. Geol.

Niemann, H., Elvert, M., Hovland, M., Orcutt, B., Judd, A., Suck, I., Gutt, J., Joye, S., Damm, E., Finster, K., Boetius, A., 2005. Methane emission and consumption at a North Sea gas seep (Tommeliten area). Biogeosciences 2, 335-351.

Niemann, H., Losekann, T., de Beer, D., Elvert, M., Nadalig, T., Knittel, K., Amann, R., Sauter, E.J., Schluter, M., Klages, M., Foucher, J.P., Boetius, A., 2006. Novel microbial communities of the Haakon Mosby mud volcano and their role as a methane sink. Nature 443, 854-858.

Nikolovska, A., Sahling, H., Bohrmann, G., 2008. Hydroacoustic methodology for detection, localization, and quantification of gas bubbles rising from the seafloor at gas seeps from the eastern Black Sea. Geochem. Geophys. Geosyst. 9.

Olu-Le Roy, K., Caprais, J.C., Fifis, A., Fabri, M.C., Galeron, J., Budzinsky, H., Le Menach, K., Khripounoff, A., Ondreas, H., Sibuet, M., 2007. Cold-seep assemblages on a giant pockmark off West Africa: spatial patterns and environmental control. Mar. Ecol. 28, 115-130.

Omoregie, E.O., Niemann, H., Mastalerz, V., de Lange, G.J., Stadnitskaia, A., Mascle, J., Foucher, J.P., Boetius, A., 2009. Microbial methane oxidation and sulfate reduction at cold seeps of the deep Eastern Mediterranean Sea. Mar. Geol. 261, 114-127.

Orange, D.L., Breen, N.A., 1992. The Effects of Fluid Escape on Accretionary Wedges. 2. Seepage Force, Slope Failure, Headless Submarine Canyons, and Vents. J. Geophys. Res. Solid Earth 97, 9277-9295.

Orange, D.L., Yun, J., Maher, N., Barry, J., Greene, G., 2002. Tracking California seafloor seeps with bathymetry, backscatter and ROVs. Cont. Shelf Res. 22, 2273-2290.

Orphan, V.J., Ussler, W., Naehr, T.H., House, C.H., Hinrichs, K.U., Paull, C.K., 2004. Geological, geochemical, and microbiological heterogeneity of the seafloor around methane vents in the Eel River Basin, offshore California. Chem. Geol. 205, 265-289.

Panieri, G., 2006. Foraminiferal response to an active methane seep environment: A case study from the Adriatic Sea. Mar. Micropaleontol. 61, 116-130.

Pape, T., Blumenberg, M., Seifert, R., Bohrmann, G., Michaelis, W., 2008. Marine Methane Biogeochemistry of the Black Sea: A Review. Links between Geological Processes, Microbial Activities & Evolution of Life: Microbes and Geology 4, 281-311
348.

Pavlova, O.N., Zemskaya, T.I., Gorshkov, A.G., Kostornova, T.Y., Khlystov, O.M., Parfenova, V.V., 2008. Comparative characterization of microbial communities in two regions of natural oil seepage in Lake Baikal. Biol. Bull 35, 287-293.

Pecher, I.A., Henrys, S.A., Ellis, S., Chiswell, S.M., Kukowski, N., 2005. Erosion of the seafloor at the top of the gas hydrate stability zone on the Hikurangi Margin, New Zealand. Geophys. Res. Lett. 32.

Pecher, I.A., Henrys, S.A., Wood, W.T., Kukowski, N., Crutchley, G.J., Fohrmann, M., Kilner, J., Senger, K., Gorman, A.R., Coffin, R.B., Greinert, J., Faure, K., 2010. Focussed fluid flow on the Hikurangi Margin, New Zealand -- Evidence from possible local upwarping of the base of gas hydrate stability. Mar. Geol. 272, 99-113.

Peckmann, J., Reimer, A., Luth, U., Luth, C., Hansen, B.T., Heinicke, C., Hoefs, J., Reitner, J., 2001. Methane-derived carbonates and authigenic pyrite from the northwestern Black Sea. Mar. Geol. 177, 129-150.

Perez-Garcia, C., Feseker, T., Mienert, J., Berndt, C., 2009. The Håkon Mosby mud volcano: 330 000 years of focused fluid flow activity at the SW Barents Sea slope. Mar. Geol. 262, 105-115.

Piker, L., Schmaljohann, R., Imhoff, J.F., 1998. Dissimilatory sulfate reduction and methane production in Gotland Deep sediments (Baltic Sea) during a transition period from oxic to anoxic bottom water (1993-1996). Aquat Microb Ecol 14, 183-193.

Poort, J., Kutas, R., Klerkx, J., Beaubien, S., Lombardi, S., Dimitrov, L., Vassilev, A., Naudts, L., 2007. Strong heat flow variability in an active shallow gas environment, Dnepr palaeo-delta, Black Sea. Geo-Mar. Lett. 27, 185-195.

Poort, J., Vassilev, A., Dimitrov, L., 2005. Did postglacial catastrophic flooding trigger massive changes in the Black Sea gas hydrate reservoir? Terra Nova 17, 135-140.

Popescu, I., Lericolais, G., Panin, N., Normand, A., Dinu, C., Le Drezen, E., 2004. The Danube submarine canyon (Black Sea): morphology and sedimentary processes. Mar. Geol. 206, 249-265.

Reitner, J., Peckmann, J., Blumenberg, M., Michaelis, W., Reimer, A., Thiel, V., 2005. Concretionary methane-seep carbonates and associated microbial communities in Black Sea sediments. Palaeogeogr. Palaeoclimatol. Palaeoecol. 227, 18-30.

Riedel, M., Tréhu, A., Spence, G., in press. Characterizing the thermal regime of cold vents at the northern Cascadia margin from bottom-simulating reflector distributions, heat-probe measurements and borehole temperature data. Mar. Geophys. Res.

Rise, L., Saettem, J., Fanavoll, S., Thorsnes, T., Ottesen, D., Boe, R., 1999. Sea-bed pockmarks related to fluid migration from Mesozoic bedrock strata in the Skagerrak offshore Norway. Mar. Pet. Geol. 16, 619-631.

Rollet, N., Logan, G.A., Kennard, J.M., O'Brien, P.E., Jones, A.T., Sexton, M., 2006. Characterisation and correlation of active hydrocarbon seepage using geophysical data sets: An example from the tropical, carbonate Yampi Shelf, Northwest Australia. Mar. Pet. Geol. 23, 145-164.

Rollet, N., Logan, G.A., Ryan, G., Judd, A.G., Totterdell, J.M., Glenn, K., Jones, A.T., Kroh, F., Struckmeyer, H.I.M., Kennard, J.M., Earl, K.L., 2009. Shallow gas and fluid migration in the northern Arafura Sea (offshore Northern Australia). Mar. Pet. Geol. 26, 129-147.

Sahling, H., Bohrmann, G., Spiess, V., Bialas, J., Breitzke, M., Ivanov, M., Kasten, S., Krastel, S., Schneider, R., 2008. Pockmarks in the Northern Congo Fan area, SW Africa: Complex seafloor features shaped by fluid flow. Mar. Geol. 249, 206-225.

Sahling, H., Galkin, S.V., Salyuk, A., Greinert, J., Foerstel, H., Piepenburg, D., Suess, E., 2003. Depth-related structure and ecological significance of cold-seep communities - a case study from the Sea of Okhotsk. Deep-Sea Res., Part I 50, 1391-1409.

Saunders, D.F., Burston, K.R., Thompson, C.K., 1999. Model for hydrocarbon microseepage and related near-surface alterations. American Association of Petroleum Geologists, 170-185.

Sauter, E.J., Muyakshin, S.I., Charlou, J.L., Schluter, M., Boetius, A., Jerosch, K., Damm, E., Foucher, J.P., Klages, M., 2006. Methane discharge from a deep-sea submarine mud volcano into the upper water column by gas hydrate-coated methane bubbles. Earth Planet. Sci. Lett. 243, 354-365.

Schmale, O., Beaubien, S.E., Rehder, G., Greinert, J., Lombardi, S., 2010. Gas seepage in the Dnepr paleo-delta area (NW-Black Sea) and its regional impact on the water column methane cycle. J. Mar. Syst. 80, 90-100.

Schmale, O., Greinert, J., Rehder, G., 2005. Methane emission from high-intensity marine gas seeps in the Black Sea into the atmosphere. Geophys. Res. Lett. 32.

Schubert, C.J., Durisch-Kaiser, E., Holzner, C.P., Klauser, L., Wehrli, B., Schmale, O., Greinert, J., McGinnis, D.F., De Batist, M., Kipfer, R., 2006. Methanotrophic microbial communities associated with bubble plumes above gas seeps in the Black Sea. Geochem. Geophys. Geosyst. 7.

Shakhova, N., Semiletov, I., 2007. Methane release and coastal environment in the East Siberian Arctic shelf. J. Mar. Syst. 66, 227-243.

Shoji, H., Soloviev, V., Matveeva, T., Mazurenko, L., Minami, H., Hachikubo, A., Sakagami, H., Hyakutake, K., Kaulio, V., Gladysch, V., Logvina, E., Obzhirov, A., Baranov, B., Khlystov, O., Biebow, N., Poort, J., Jin, Y.K., Kim, Y., 2005. Hydrate-Bearing Structures in the Sea of Okhotsk. Eos Trans. Am. Geophys. Union 86, 13-18.

Shubenkova, O.V., Zemskaya, T.I., Chernitsyna, S.M., Khlystov, O.M., Triboi, T.I., 2005. The first results of an investigation into the phylogenetic diversity of microorganisms in southern Baikal sediments in the region of subsurface discharge of methane hydrates. Microbiology 74, 314-320.

Sibson, R.H., Rowland, J.V., 2003. Stress, fluid pressure and structural permeability in seismogenic crust, North Island, New Zealand. Geophys. J. Int., 584-594.

Solomon, E.A., Kastner, M., MacDonald, I.R., Leifer, I., 2009. Considerable methane fluxes to the atmosphere from hydrocarbon seeps in the Gulf of Mexico. Nature Geosci 2, 561-565.

Sommer, S., Linke, P., Pfannkuche, O., Niemann, H., Treude, T., 2010. Benthic respiration in a seep habitat dominated by dense beds of ampharetid polychaetes at the Hikurangi Margin (New Zealand). Mar. Geol. 272, 223-232.

Sommer, S., Pfannkuche, O., Linke, P., Luff, R., Greinert, J., Drews, M., Gubsch, S., Pieper, M., Poser, M., Viergutz, T., 2006. Efficiency of the benthic filter: Biological control of the emission of dissolved methane from sediments containing shallow gas hydrates at Hydrate Ridge. Global Biogeochem. Cycles 20.

Taylor, M.H., Dillon, W.P., Pecher, I.A., 2000. Trapping and migration of methane associated with the gas hydrate stability zone at the Blake Ridge Diapir: new insights from seismic data. Mar. Geol. 164, 79-89.

Thurber, A.R., Kröger, K., Neira, C., Wiklund, H., Levin, L.A., 2010. Stable isotope signatures and methane use by New Zealand cold seep benthos Mar. Geol. 272, 260-269.

Torres, M.E., Bohrmann, G., Suess, E., 1996. Authigenic barites and fluxes of barium associated with fluid seeps in the Peru subduction zone. Earth Planet. Sci. Lett. 144, 469-481.

Torres, M.E., McManus, J., Hammond, D.E., de Angelis, M.A., Heeschen, K.U., Colbert, S.L., Tryon, M.D., Brown, K.M., Suess, E., 2002. Fluid and chemical fluxes in and out of sediments hosting methane hydrate deposits on Hydrate Ridge, OR, I: Hydrological provinces. Earth Planet. Sci. Lett. 201, 525-540.

Torres, M.E., Wallmann, K., Trehu, A.M., Bohrmann, G., Borowski, W.S., Tomaru, H., 2004. Gas hydrate growth, methane transport, and chloride enrichment at the southern summit of Hydrate Ridge, Cascadia margin off Oregon. Earth Planet. Sci. Lett. 226, 225-241.

Tryon, M.D., Brown, K.M., Torres, M.E., 2002. Fluid and chemical flux in and out of sediments hosting methane hydrate deposits on Hydrate Ridge, OR, II: Hydrological processes. Earth Planet. Sci. Lett. 201, 541-557.

Tryon, M.D., Brown, K.M., Torres, M.E., Trehu, A.M., McManus, J., Collier, R.W., 1999. Measurements of transience and downward fluid flow near episodic methane gas vents, Hydrate Ridge, Cascadia. Geology 27, 1075-1078.

Van Dover, C.L., Aharon, P., Bernhard, J.M., Caylor, E., Doerries, M., Flickinger, W., Gilhooly, W., Goffredi, S.K., Knick, K.E., Macko, S.A., Rapoport, S., Raulfs, E.C., Ruppel, C., Salerno, J.L., Seitz, R.D., Sen Gupta, B.K., Shank, T., Turnipseed, M., Vrijenhoek, R., 2003. Blake Ridge methane seeps: characterization of a soft-sediment, chemo synthetically based ecosystem. Deep-Sea Res. Part I-Oceanogr. Res. Pap. 50, 281-300.

Van Rensbergen, P., De Batist, M., Klerkx, J., Hus, R., Poort, J., Vanneste, M., Granin, N., Khlystov, O., Krinitsky, P., 2002. Sublacustrine mud volcanoes and methane seeps caused by dissociation of gas hydrates in Lake Baikal. Geology 30, 631-634.

Van Rooij, D., Depreiter, D., Bouimetarhan, I., De Boever, E., De Rycker, K., Foubert, A., Huvenne, V., Réveillaud, J., Staelens, P., Vercruysse, J., Versteeg, W., Henriet, J.P., 2005. First sigthing of active fluid venting in the Gulf of Cadiz. Eos Trans. AGU 86, 509-511.

von Rad, U., Berner, U., Delisle, G., Doose-Rolinski, H., Fechner, N., Linke, P., Lückge, A., Roeser, H.A., Schmaljohann, R., Wiedicke, M., Parties, S.S., Block, M., Damm, V., Erbacher, J., Fritsch, J., Harazim, B., Poggenburg, J., Scheeder, G., Schreckenberger, B., von Mirbach, N., Drews, M., Walter, S., Ali Khan, A., Inam, A., Tahir, M., Tabrez, A.R., Cheema, A.H., Pervaz, M., Ashraf, M., 2000. Gas and fluid venting at the Makran accretionary wedge off Pakistan. Geo-Mar. Lett. 20, 10-19.

von Rad, U., Rosch, H., Berner, U., Geyh, M., Marchig, V., Schulz, H., 1996. Authigenic carbonates derived from oxidized methane vented from the Makran accretionary prism off Pakistan. Mar. Geol. 136, 55-77.

Vykhristyuk, L.L., 1980. Organic Matter of Bottom Sediments of Lake Baikal (in Russian). Nauka, Novosibirsk, Russia. 80 pp.

Wakeham, S.G., Hopmans, E.C., Schouten, S., Sinninghe Damsté, J.S., 2004. Archaeal lipids and anaerobic oxidation of methane in euxinic water columns: a comparative study of the Black Sea and Cariaco Basin. Chem. Geol. 205, 427-442.

Westbrook, G.K., Thatcher, K.E., Rohling, E.J., Piotrowski, A.M., Pallike, H., Osborne, A.H., Nisbet, E.G., Minshull, T.A., Lanoiselle, M., James, R.H., Hohnerbach, V., Green, D., Fisher, R.E., Crocker, A.J., Chabert, A., Bolton, C., Beszczynska-Moller, A., Berndt, C., Aquilina, A., 2009. Escape of methane gas from the seabed along the West Spitsbergen continental margin. Geophys. Res. Lett. 36, L15608.

Wever, T.F., Abegg, F., Fiedler, H.M., Fechner, G., Stender, I.H., 1998. Shallow gas in the muddy sediments of Eckernforde Bay, Germany. Cont. Shelf Res. 18, 1715- 1739.

Whiticar, M.J., 1999. Carbon and hydrogen isotope systematics of bacterial formation and oxidation of methane. Chem. Geol. 161, 291-314.

Wood, W.T., Gettrust, J.F., Chapman, N.R., Spence, G.D., Hyndman, R.D., 2002. Decreased stability of methane hydrates in marine sediments owing to phase-boundary roughness. Nature 420, 656-660.

Zillmer, M., Flueh, E.R., Petersen, J., 2005. Seismic investigation of a bottom simulating reflector and quantification of gas hydrate in the Black Sea. Geophys. J. Int. 161, 662-678.

Zitter, T.A.C., Henry, P., Aloisi, G., Delaygue, G., Çagatay, M.N., Mercier de Lepinay, B., Al-Samir, M., Fornacciari, F., Tesmer, M., Pekdeger, A., Wallmann, K., Lericolais, G., 2008. Cold seeps along the main Marmara Fault in the Sea of Marmara (Turkey). Deep Sea Research Part I: Oceanographic Research Papers 55, 552-570.

CHAPTER 8

Conclusions

Based on the study of bubble-releasing methane seeps at three different geological and plate-tectonic settings, this study provides a broader insight in the geological factors controlling the distribution of methane seeps and the processes associated with them. Gas seepage was studied by making an integration of hydro-acoustic investigations (single- and multibeam echosounding, side scan sonar, seismics), seafloor observations (ROV, submersible, TV-sled) and grainsize-, geochemical- and geothermal analyses. The three study areas were: the Dnepr paleo delta on a passive continental margin in the Black Sea; the Hikurangi Margin, an active continental margin in SW Pacific Ocean; and the Posolsky Bank, a tilted fault block, in the Lake Baikal rift.

On a regional or basin-wide scale, the occurrence of gas hydrates seems to play a very important role in determining the distribution of and the processes associated with bubble-releasing seeps. In the Dnepr-paleo delta and in Posolsky Bank area almost no seeps were detected within the gas-hydrate stability zone (GHSZ), indicating that gas hydrates, where stable, can act as an effective seal and prevent upward migrating methane gas to be released as bubbles into the water column. Whereas on the Hikurangi Margin seepage mainly occurs in the GHSZ in relation with overpressure and large-scale fracture zones, associated with the sedimentary and plate-tectonic setting of this accretionary prism. The depth of the base of the GHSZ, related to the water depth, and the tectonic history of the two seep sites studied on Hikurangi Margin (Faure Site and LM-3) strongly influence the methane-releasing mechanism and the resulting seep environments. At LM-3, methane is mainly released diffusively allowing authigenic carbonate formation and sustaining seep-related mega fauna, whereas at Faure Site, methane is mainly released as bubbles and the presence of authigenic carbonates and seep fauna is limited. The released methane, at the Hikurangi Margin or at the other study areas, doesn't seem to be sourced by destabilizing gas hydrates.

In addition to gas hydrates, the presence of fine-grained low-permeability stratigraphic horizons, present at various subsurface depths, is also very important in focusing or preventing shallow gas migration and gas-bubble release on various spatial scales. The latter was clearly visible in the Dnepr paleo-delta and on the Posolsky Bank where the occurrence of free gas in the subsurface is controlled by the occurrence of certain stratigraphic horizons. It is only where these horizons were absent or had a negligible thickness that fluid flow towards the seafloor or lakebed is possible and that bubble-releasing seeps were observed. These locations are often characterized by erosional features associated with typical seafloor/lake floor morphologies such as canyons, sedimentary ridges, submarine landslides, pockmarks or fault scarps, which alter fluid-flow pathways and enhanced bubble release. In general, seepage in our study areas is associated with morphologically or stratigraphically controlled fluid flow in the shallow subsurface, rather than fluid flow driven by regional or local faulting. However, seismic data from the Hikurangi margin indicated that controls on fluid migration can differ depending on the observed subsurface interval allowing sedimentary and fault controlled fluid flow at one seep site.

On small spatial scales, the activity of seep fauna and the formation of methane-derived authigenic carbonates, both related to the anaerobic oxidation of methane, play an important role in the distribution and activity of seeps. In the Dnepr paleo delta and in LM-3, the formation of authigenic carbonates in the subsurface has led to (self-)sealing of fluid flow pathways by carbonate clogging, followed by a relocation of the fluid pathways and gas seep locations around these carbonate-cemented impermeable areas. For the Dnepr paleo-delta, the established relation between seep density and the degree of authigenic carbonate precipitation indicates that methane flux calculations can be performed using backscatter-based estimations of seep densities.

The presence of seep fauna, e.g. ampheretid

polychaetes and bacterial mats, also influences seep activity and distribution as was observed on the Hikurangi Margin and in the Dnepr paleo-delta. These fauna facilitate the transition from a soft sediment environment with mainly bubble release to a hard substrate seep environment with associated seep megafauna where AOM and diffusive methane transport prevail.

In addition to these local controls on seep distribution and activity, bubble release was very variable over periods of minutes to hours, as indicated by seafloor observations in the Dnepr paleo-delta and at Faure Site. These variations are attributed to external changes (e.g. tides, current changes, etc.) or internal changes related to the fluid-flow/seep system (e.g. gas supply).

As a final conclusion, this study has shown that integration of high-resolution datasets are needed, in addition to low-resolution datasets, to understand the distribution and manifestations of bubble-releasing methane seeps and the associated fluid-flow systems.

Future perspectives

Besides the obtained results and conclusions, this study raises some questions that could guide future research activities related to bubble-releasing methane seeps.

First of all, it is important to know the basics of subsurface fluid flow to understand the resulting release of gas and its associated seafloor manifestations. This study gave strong indications about controls of fluid flow in the shallow subsurface, but a more quantitative approach based on the integration of analog sandbox modeling, numerical modeling and data from fossil seep structures can help to better understand the present-day seep and fluid-flow systems. Such integrations would help to better interpret data from present-day seeps gathered by remote sensing, e.g. seismic data. Seep areas should be better imaged using ROVs, AUVs and high-resolution acoustic methods to better understand and know the extent of associated sea-floor manifestations. A better understanding of fluid flow and seepage would allow better risk assessments for offshore operations, e.g. pockmark formation near pipelines, etc.

This study and other studies often have problems indicating the main source of the released fluids. Again a better integration of different kinds of geophysical data (e.g. high- and low-resolution seismic data, heat flow data, etc.) and geochemical data should provide better insights in the origin of the fluids and the influence these fluids have on seep-related seafloor manifestations. For the exploration of new hydrocarbon resources based on seep occurrence, a correct constraint of the fluid-flow source is highly necessary.

Despite the research done during the CRIMEA project and other projects, it is still unclear how important methane seeps are as sources of atmospheric methane and what their influence is on global climate. As shown by Greinert et al. (2010), an integration of spatial and temporal datasets is needed and results in good methane flux estimates. Similar research strategies should be used in other known and yet unknown seep areas occurring at different geological settings and this over larger areas and during longer observations periods. To achieve global estimates of methane release from the seafloor and oceans, it is essential to make correct assessment of the activity and the amount of seeps present at the seafloor. New multibeam systems that provide water column imaging can help to find new seep provinces, not only in pioneer areas like the Arctic or Antarctic but also in basins known for seepage. The Black Sea, for example, has probably the highest amount of detected seeps in the world. But this is only based on a handful of seep provinces. Seepage is most certainly much more widespread. It is clear that in addition to very local and detailed studies focusing on known seep sites, there is also big need to do more extended surveying to find new seep areas to better understand all processes involved.

Furthermore, it is important to better understand the role gas hydrates play as a source for methane release and atmospheric methane. How does global warming and associated rising temperature of bottom waters affect gas-hydrate stability and on what time scales? Does abundant gas release resulting from destabilized gas hydrates alter fluid-flow pathways? Does this lead to the observed widespread occurrences of submarine landslides

in gas-hydrate and seep areas? Again better constraints of the natural environment by integration of new techniques like 3D seismics, controlled source electromagnetic measurements, etc. should help answering these questions.

This study, as well as previous studies, has shown that integration of different datasets and the collaboration of geoscientist with different backgrounds are needed to enhance our knowledge of bubble-releasing seeps and the influence they have on the geosphere, biosphere, hydrosphere and atmosphere.

APPENDIX A – LIST OF PUBLICATIONS

Publications in journals or books with peer review

Published

GREINERT, J., MCGINNIS, D.F., **NAUDTS, L.**, LINKE, P., AND DE BATIST, M., 2010. Atmospheric methane flux from bubbling seeps: Spatially extrapolated quantification from a Black Sea shelf area. *Journal of Geophysical Research – Oceans*, 115, 1-18. doi:10.1029/2009JC005381

HUS, R., POORT, J., CHARLET, F., **NAUDTS, L.**, KHLYSTOV, O., KLERKX, J., DE BATIST, M., 2010. Lake Baikal. In: Bally, A.W. & Roberts, D.G. (Eds.) Phanerozoic Geology Regional Geology of the World. *Elsevier Publications.*

KIDA, M., KHLYSTOV, O., ZEMSKAYA, T., TAKAHASHI, N., MINAMI, H., SAKAGAMI, H., KRYLOV, A., HACHIKUBO, A., YAMASHITA, S., SHOJI, H., POORT, J., **NAUDTS, L.**, 2006. Coexistence of structure I and II gas hydrates in Lake Baikal suggesting gas sources from microbial and thermogenic origin. *Geophysical Research Letters,* 33, doi: 0.1029/2006GL028296

KRYLOV, A., KHLYSTOV, O.M., ZEMSKAYA, T.I., MINAMI, H., HACHIKUBO, A., SHOJI, H., KIDA, M., POGODAEVA, T.P., **NAUDTS, L.**, POORT, J., 2008. Crystallization of authigenic carbonates in mud volcanoes of Lake Baikal. *Geochemistry International,* 46, 985-995. doi: 10.1134/S0016702908100030

KRYLOV, A., KHLYSTOV, O., ZEMSKAYA, T., MINAMI, H., HACHIKUBO, A., NUNOKAWA, Y., KIDA, M., SHOJI, H., **NAUDTS, L.**, POORT, J., POGODAEVA, T., 2008. First discovery and formation process of authigenic siderite from gas hydrate-bearing mud volcanoes in fresh water: Lake Baikal, eastern Siberia. *Geophysical Research Letters*, 35. doi:10.1029/2007GL032917

MERTENS, K.N., RIBEIRO, S., BOUIMETARHAN, I., CANER, H., NEBOUT, N.C., DALE, B., DE VERNAL, A., ELLEGAARD, M., FILIPOVA, M., GODHE, A., GOUBERT, E., GROSFJELD, K., HOLZWARTH, U., KOTTHOFF, U., LEROY, S.A.G., LONDEIX, L., MARRET, F., MATSUOKA, K., MUDIE, P.J., **NAUDTS, L.,** PENA-MANJARREZ, J.L., PERSSON, A., POPESCU, S.M., POSPELOVA, V., SANGIORGI, F., VAN DER MEER, M.T.J., VINK, A., ZONNEVELD, K.A.F., VERCAUTEREN, D., VLASSENBROECK, J., LOUWYE, S., 2009. Process length variation in cysts of a dinoflagellate, Lingulodinium machaerophorum, in surface sediments: Investigating its potential as salinity proxy. *Marine Micropaleontology,* 70, 54-69. doi: 10.1016/j.marmicro.2008.10.004

NAUDTS, L., GREINERT, J., ARTEMOV, Y., STAELENS, P., POORT, J., VAN RENSBERGEN, P., DE BATIST, M., 2006. Geological and morphological setting of 2778 methane seeps in the Dnepr paleo-delta, northwestern Black Sea. *Marine Geology,* 227, 177-199. doi: 10.1016/j.margeo.2005.10.005

NAUDTS, L., GREINERT, J., ARTEMOV, Y., BEAUBIEN, S. E., BOROWSKI, C., DE BATIST, M., 2008. Anomalous sea-floor backscatter patterns in methane venting areas, Dnepr paleo-delta, NW Black Sea. *Marine Geology,* 251, 253-267. doi: 10.1016/j.margeo.2008.03.002

NAUDTS, L., DE BATIST, M., GREINERT, J. & ARTEMOV, Y., 2009. Geo- and hydro-acoustic manifestations of shallow gas and gas seeps in the Dnepr paleo-delta, northwestern Black Sea. *The Leading Edge*, 28(9), 1030-1040. doi:10.1190/1.3236372

NAUDTS, L., GREINERT, J., POORT, J., BELZA, J., VANGAMPELAERE, E., BOONE, D., LINKE, P., HENRIET, J.P. & DE BATIST, M., 2010. Active venting sites on the gas-hydrate-bearing Hikurangi Margin, off New Zealand: Diffusive- versus bubble-released methane. *Marine Geology*, 272, 233-250. doi: 10.1016/j.margeo.2009.08.002

PIRLET, H., WEHRMANN, L.M., BRUNNER, B., FRANK, N., DEWANCKELE, J., VAN ROOIJ, D., FOUBERT, A., SWENNEN, R., **NAUDTS, L.**, BOONE, M., CNUDDE, V., HENRIET, J.-P., 2010. Diagenetic formation of gypsum and dolomite in a cold-water coral mound in the Porcupine Seabight, off Ireland. *Sedimentology*, 57, 786-805. doi: 10.1111/j.1365-3091.2009.01119.x

POORT, J., KUTAS, R., KLERKX, J., BEAUBIEN, S., LOMBARDI, S., DIMITROV, L., VASSILEV, A., **NAUDTS, L.**, 2007. Strong heat flow variability in an active shallow gas environment, Dnepr palaeo-delta, Black Sea. *Geo-Marine Letters*, 27, 185-195. doi: 10.1007/s00367-007-0072-4

In press

KRYLOV, A.A., KHLYSTOV, O.M., HACHIKUBO, A., MINAMI, H., NUNOKAWA, Y., SHOJI, H., ZEMSKAYA, T.I., **NAUDTS, L.**, POGODAEVA, T.V., KIDA, M., KALMYCHKOV, G.V. & POORT, J., (submitted). Isotopic composition of dissolved carbon in the subsurface sediments of gas hydrate-bearing mud volcanoes, Lake Baikal: implications for methane and carbonate origin. *Geo-Marine Letters*. doi: 10.1007/s00367-010-0190-2

Submitted

NAUDTS, L., KHLYSTOV, O., GRANIN, N., CHENSKY, A., POORT, J., DE BATIST, M., (submitted). Stratigraphic and structural controls on the location of active methane seep on Posolsky Bank, Lake Baikal. *Marine and Petroleum Geology.*

NAUDTS, L., KHLYSTOV, O.M., KHABUEV, A.V., SEMINSKIY, I., CASIER, R., CUYLAERTS, M., GENERAL'CHENKO, P., SYNAEVE, J., VLAMYNCK, N., DE BATIST, M., GRACHEV, M.A. (submitted). Newly collected multibeam swath bathymetry data herald a new phase in gas-hydrate research on Lake Baikal. *EOS Ttransactions.*

POORT, J., KHLYSTOV, O., **NAUDTS, L.**, DUCHKOV, A., SHOJI, H., NISHIO, S., DE BATIST, M., HACHIKUBO, A., KIDA, M., MINAMI, H., MANAKOV, A.Y., KULIKOVA, M.V., KRYLOV, A.A., submitted. Low thermal anomalies associated with double structure gas hydrates in K-2 mud volcano, Lake Baikal. *Geochemistry Geophysics Geosystems.*

SASTRE, V., LOIZEAU, J.L., GREINERT, J., **NAUDTS, L.**, ARPAGAUS, P., ANSELMETTI, F. & WILDI, W., (submitted). Morphology and recent history of the Rhone River delta in Lake Geneva (Switzerland). *Eclogae geologicae Helvetiae.*

Abstracts of presentations

NAUDTS, L., KHLYSTOV, O.M., KHABUEV, A.V., SEMINSKIY, I., CASIER, R., CUYLAERTS, M., GENERAL'CHENKO, P., SYNAEVE, J., VLAMYNCK, N., DE BATIST, M., GRACHEV, M.A., 2009. Newly collected multibeam swath bathymetry data herald a new phase in gas-hydrate research on Lake Baikal. AGU 2009 Fall Meeting, 14-18th December 2009, San Francisco, USA.

PIRLET, H., WEHRMANN, L.M., BRUNNER, B., FRANK, N., DEWANCKELE, J., VAN ROOIJ, D., FOUBERT, A., SWENNEN, R., **NAUDTS, L.,** BOONE, M., CNUDDE, V., HENRIET, J.P., 2009. Diagenetic formation of gypsum and dolomite in a cold-water coral mound in the Porcupine Seabight, off Ireland. AGU 2009 Fall Meeting, 14-18th December 2009, San Francisco, USA.

SASTRE, V., LOIZEAU, J.-L., GREINERT, J., **NAUDTS, L.**, ARPAGAUS, P., ANSELMETTI, F., WILDI, W., 2009. Morphology and recent history of the Rhone River Delta in Lake Geneva (Switzerland and France). 7th Swiss Geoscience Meeting, 20-21th November, Neuchâtel, Switserland.

NAUDTS, L., GREINERT, J., POORT, J., DE BATIST, M., 2009. Geological characterization of methane seeps in the Black Sea, in the SW Pacific Ocean and in Lake Baikal. International Workshop on "Geological and bio(geo)chemical processes at cold seeps – Challenges in recent and ancient systems", 28-30th September 2009, Varna, Bulgaria.

NAUDTS, L., GREINERT, J., POORT, J., DE BATIST, M., 2009. Geological characterization of methane seeps in the Black Sea, in the SW Pacific Ocean and in Lake Baikal. 3rd International Conference Geologica Belgica "Challenges for the Planet: Earth Science's perspective", 14-15th September 2009. Gent, Belgium.

NAUDTS, L., GREINERT, J., POORT, J., BELZA, J., VANGAMPELAERE, E., BOONE, D., LINKE, P., HENRIET, J.P., DE BATIST, M., 2009. Active Venting Sites On The Gas-hydrate-bearing Hikurangi Margin, Off New Zealand: Diffusive- Versus bubble-released Methane. 11-15th August AOGS 2009, Singapore.

NAUDTS, L., DE BATIST, M., 2009. Massive methane release on the gas-hydrate-bearing Hikurangi Margin, off New Zealand: diffusive- versus bubble-released methane. Doctoraatssymposium Faculteit Wetenschappen, 28th April 2009, Gent, Belgium.

GREINERT, J., FAURE, K., **NAUDTS, L.**, DE BATIST, M., BIALAS, J., LINKE, P., PECHER, I., ROWDEN, R., 2009. An overview of gas hydrate and cold seep research along the Hikurangi Margin, New Zealand (2006 & 2007). *Geoph. Res. Abstracts*, 11, EGU2009-8588.

NAUDTS, L., GREINERT, J., POORT, J., DE BATIST, M., 2009. Geological characterization of methane seeps in the Black Sea, in Lake Baikal and in the SW Pacific Ocean, International workshop on "Developing Long Term International Collaboration on Methane Hydrate Research and Monitoring in the Arctic Region". 18-20th February 2009, Den Burg, The Netherlands

NAUDTS, L., GREINERT, J., POORT, J., BELZA, J., VANGAMPELAERE, E., BOONE, D., LINKE, P., HENRIET, J.P., DE BATIST, M., 2008. Submeter mapping of methane seeps by ROV observations and Measurements at the Hikurangi Margin, New Zealand. *EOS Transactions*, 89(53), OS33A-1304

NAUDTS, L., GREINERT, J., POORT, J., BELZA, J., VAN GAMPELAERE, E., BOONE, D., LINKE, P., HENRIET, J.P., DE BATIST, M., 2008. Submeter mapping of methane seeps by ROV observations and measurements at the Hikurangi Margin, New Zealand. Geosciences '08, 23-26th November 2008, Wellington, New Zealand.

NAUDTS, L., GREINERT, J., POORT, J., BELZA, J., VANGAMPELAERE, E., BOONE, D., LINKE, P., HENRIET, J.P. & DE BATIST, M., 2008. Submeter mapping of methane seeps by ROV observations and measurements at the Hikurangi Margin, New Zeeland. 9th International Conference on Gas in Marine Sediments, 15-19th September 2008, Bremen, Germany.

NAUDTS, L., GREINERT, J., ARTEMOV, Y., BEAUBIEN, S.E., BOROWSKI, C. & DE BATIST, M., 2008. Anomalous sea-floor backscatter patterns in methane venting areas, Dnepr paleo-delta, NW Black Sea. 9th International Conference on Gas in Marine Sediments, 15-19th September 2008, Bremen, Germany.

NAUDTS, L., GRANIN, N., KHLYSTOV, O., CHENSKY, A.G., POORT, J., DE BATIST, M., 2009. What is controlling shallow active methane seeps in Lake Baikal? Posolsky Bank case-study. 9th International Conference on Gas in Marine Sediments, 15-19th September 2009, Bremen, Germany.

GREINERT, J., MCGINNIS, D., **NAUDTS, L.**, LINKE, P. & DE BATIST, M., 2008. Spatial methane-bubble flux quantification from seeps into the atmosphere on the Black Sea shelf. 9th International Conference on Gas in Marine Sediments, 15-19th September 2008, Bremen, Germany.

POORT, J., KHLYSTOV, O., KULIKOVA, M., NAUDTS, L., SHOJI, H., NISHIO, S., DE BATIST, M., Thermal features and gas hydrate formation in Lake Baikal mud volcanoes and other deep-sea seepage areas. 9th International Conference on Gas in Marine Sediments, 15-19th September 2008, Bremen, Germany.

GREINERT, J., MCGINNIS, D., **NAUDTS, L.**, LINKE, P., DE BATIST, M., 2008. Spatial methane-bubble flux quantification from seeps into the atmosphere on the Black Sea shelf. ESF Magellan Workshop on "Ocean Drilling for Seismic Hazard in European Geosystems, 18-20th August 2008, Luleå, Sweden.

GREINERT, J., **NAUDTS, L.**, MCGINNIS, D., 2008. Monitoring of temporally and spatially transient bubble release and the spatial extrapolation of methane fluxes: Use of hydroacoustic methods in the Black Sea. 6th International Workshop on Methane Hydrate Research and Development, 13-15th May 2008, Bergen, Norway.

NAUDTS, L., GRANIN, N., KHLYSTOV, O., CHENSKY, A.G., POORT, J. & DE BATIST, M., 2008. What is controlling shallow active methane seeps in Lake Baikal? Posolsky Bank case-study. *Geoph. Res. Abstracts*, 10, 02119.

NAUDTS, L., GREINERT, J., ARTEMOV, Y., BEAUBIEN, S.E., BOROWSKI, C. & DE BATIST, M., 2008. Abnormally high acoustic sea-floor backscatter patterns in active methane venting areas, Dnepr paleo-delta, northwestern Black Sea. *Geoph. Res. Abstracts*, 10, 02114.

NAUDTS, L., GREINERT, J., POORT, J., BELZA, J., VANGAMPELAERE, E., BOONE, D., LINKE, P., HENRIET, J.P. & DE BATIST, M., 2008. Submeter mapping of methane seeps by ROV observations and

measurements at the Hikurangi Margin, New Zeeland. *Geoph. Res. Abstracts*, 10, 02107.

GREINERT, J., **NAUDTS, L.**, MCGINNIS, D., 2008. Monitoring of temporally and spatially transient bubble release and the spatial extrapolation of methane fluxes: Use of hydroacoustic methods in the Black Sea. *Geoph. Res. Abstracts*, 10, 02078

NAUDTS, L., POORT, J., BOONE, D., LINKE, P., GREINERT, J., DE BATIST, M., HENRIET, J.P., 2007. Active venting sites on the gas-hydrate-bearing Hikurangi Margin, off New Zealand: ROV measurements and observations. Eos Trans., 88(52), B43E-1655.

DE BATIST, M., KLERKX, J., **NAUDTS, L.**, POORT, J., KHLYSTOV, O., GOLMSHTOK, A., KREMLEV, A., DUCHKOV, A., GRANIN, N., THE SONIC TEAM, INTAS PROJECTS 1915 AND 2309 PARTNERS, 2007. A reassessment of gas hydrate occurrences in Lake Baikal. Eos Trans., 88(52), OS23A-1053

DE BATIST, M., KLERKX, J., **NAUDTS, L.**, POORT, J., KHLYSTOV, O., GOLMSHTOK, A., KREMLEV, A., DUCHKOV, A.D., GRANIN, N., SONIC TEAM, INTAS PROJECTS 1915 AND 2309 PARTNERS. Gas hydrates, mud volcanoes and gas seeps in Lake Baikal - A review. International Conference on "Gas Hydrates", 3-8th September 2007, Listvyanka, Russian Federation.

NAUDTS, L., GREINERT, J., ARTEMOV, Y., BEAUBIEN, S., BOROWSKI, C., DE BATIST, M. Quantitative assessment of methane seep distribution in the Dnepr paleo-delta region, NW Black Sea. International Conference on "Gas Hydrates", 3-8th September 2007, Listvyanka, Russian Federation.

NAUDTS, L., POORT, J., BOONE, D., LINKE, P., GREINERT, J., DE BATIST, M., HENRIET, J.P., 2007. Active venting sites on the gas-hydrate-bearing Hikurangi Margin, off New Zealand: ROV measurements and observations. International Conference on "Gas Hydrates", 3-8th September 2007, Listvyanka, Russian Federation.

POORT, J., KHLYSTOV, O., KULIKOVA, M., **NAUDTS, L.**, SHOJI, H., NISHIO, S., DE BATIST, M. Thermal features of seep activity and gas hydrate occurrence in Lake Baikal and other deep-sea seepage areas. International Conference on "Gas Hydrates", 3-8th September 2007, Listvyanka, Russian Federation.

NAUDTS, L., GRANIN, N., KHLYSTOV, O., CHENSKY, A.G., POORT, J., DE BATIST, M. What is controlling shallow active methane seeps in Lake Baikal? Posolsky Bank case-study. International Conference on "Gas Hydrates", 3-8th September 2007, Listvyanka, Russian Federation.

KRYLOV, A., KHLYSTOV, O., ZEMSKAYA, T., MINAMI, H., HACHIKUBO, A., NUNOKAWA, Y., AYUTA, K., TAKAHASHI, N., SHOJI, H., **NAUDTS, L.**, POORT, J. Formation of authigenic carbonates in mud volcanoes in Lake Baikal. International Conference on "Gas Hydrates", 3-8th September 2007, Listvyanka, Russian Federation.

KULIKOVA, M., POORT, J., MATVEEVA, T., MAZURENKO, L., **NAUDTS, L.** The features of temperature and acoustic fields related to the gas hydrate formation at the fluid discharge structures. International Conference on "Gas Hydrates", 3-8th September 2007, Listvyanka, Russian Federation.

DE BATIST, M., **NAUDTS, L.**, CRIEL, W., KLERKX, J., POORT, J., GRANIN, N., GNATOVSKY, R., KHLYSTOV, O., THE SONIC TEAM, INTAS PROJECTS 2309 PARTNERS. Relationships between gas hydrates, mud volcanoes and gas seeps. Can Lake Baikal be used as a model for continental margin hydrate provinces? AOGS2007, 30th July-4th August 2007, Bangkok, Thailand.

POORT, J., KHLYSTOV, O., SHOJI, H., NISHIO, S., KIDA, M., GRANIN, N., **NAUDTS, L**., DE BATIST, M. Baikal mud volcanoes: thermal features of dynamic gas hydrate systems. AOGS2007, 30th July-4th August 2007, Bangkok, Thailand.

NAUDTS, L., GRANIN, N., KHLYSTOV, O., CHENSKY, A.G., POORT, J., DE BATIST, M. What is controlling shallow active methane seeps in Lake Baikal? Posolsky Bank case-study. 4th International Limnogeology Congress (ILIC 2007), 11-14th July 2007, Barcelona, Spain.

KHLYSTOV, K. , POORT, J., **NAUDTS, L.**, DE BATIST, M., KRYLOV, A., SHOJI, H., KIDA, M., NISHIO, S. Geophysical prospecting of near-surface gas hydrates in Lake Baikal mud volcanoes. 4th International Limnogeology Congress (ILIC 2007), 11-14th July 2007, Barcelona, Spain.

SHERSTYANKIN, P.P., DE BATIST, M., CANALS, M., HUS, R., CHARLET, F., **NAUDTS, L.**, IVANOV, V.G., KUIMOVA, L.N., CASAMOR, J.L., KOLOTILO, L.G. Digital bathymetric map of Lake Baikal and its applications in

lacustrine geology. 4th International Limnogeology Congress (ILIC 2007), 11-14th July 2007, Barcelona, Spain.

NAUDTS, L. Acoustic sea-floor backscatter as a proxy for active methane seep distribution. Doctoraatssymposium Faculteit Wetenschappen, Ghent University, 24th March 2007, Ghent, Belgium.

DEPREITER, D., **NAUDTS, L.**, FOUBERT, A., HENRIET, J.P., 2007. Externally driven subsurface pumping and consequences. *Geoph. Res. Abstracts*, 9, 06128.

POORT, J., KHLYSTOV, O., SHOJI, H., NISHIO, S., KIDA, M., GRANIN, N., **NAUDTS, L.**, DE BATIST, M., 2007. Baikal mud volcanoes: thermal features of dynamic gas hydrate systems. *Geoph. Res. Abstracts*, 9, 09541.

BIALAS, J., DE BATIST, M., **NAUDTS, L.**, POORT, J., TALUKDER, A.R., KLAESCHEN, D., 2006. Fluid Migration Observed From Seismic Evidence in Different Hydrate Provinces – Nicaragua vs. Black Sea, Eos. Trans. AGU, **87 (52)**, Fall Meet. Suppl.

NAUDTS L., DE BATIST M., CRIEL W., POORT J., VAN RENSBERGEN P., THE SONIC TEAM, KLERKX J., GRANIN N., KHLYSTOV O., DUCHKOV A.D., DUCHKOV A.A., OBZHIROV A., CHENSKY A., KAPITANOV V., WUEST A., MCGINNIS D., THE INTAS PROJECT 01-2309 MEMBERS, 2006. Gas hydrates, mud volcanoes and gas seeps in Lake Baikal. 5th International Workshop on Methane Hydrate Research and Development, 9-12th October 2006, Edinburgh, Scotland.

NAUDTS L., GREINERT J., ARTEMOV Y., DE BATIST M., 2006. Characterization of methane seep areas based on acoustic seafloor backscatter measurements. 5th International Workshop on Methane Hydrate Research and Development, 9-12th October 2006, Edinburgh, Scotland.

NAUDTS L., GREINERT J., ARTEMOV Y., DE BATIST M. Geological and morphological setting of 2778 methane seeps in the Dnepr paleo-delta, northwestern Black Sea. 5th International Workshop on Methane Hydrate Research and Development, 9-12th October 2006, Edinburgh, Scotland.

NAUDTS L., GREINERT J., ARTEMOV Y., DE BATIST M. The use of acoustic seafloor backscatter measurements for quantitative and qualitative characterization of methane seep areas. 2nd Belgian Geological Congress, 07-08th September 2006, Liège, Belgium.

NAUDTS L., DE BATIST M., CRIEL W., POORT J., VAN RENSBERGEN P., THE SONIC TEAM, KLERKX J., GRANIN N., KHLYSTOV O., DUCHKOV A.D., DUCHKOV A.A., OBZHIROV A., CHENSKY A., KAPITANOV V., WUEST A., MCGINNIS D., THE INTAS PROJECT 01-2309 MEMBERS. Gas hydrates, mud volcanoes and gas seeps in Lake Baikal. 2nd Belgian Geological Congress, 07-08th September 2006, Liège, Belgium.

NAUDTS L., GREINERT J., ARTEMOV Y., DE BATIST M. Geological and morphological setting of 2778 methane seeps in the Dnepr paleo-delta, northwestern Black Sea. 2nd Belgian Geological Congress, 07-08th September 2006, Liège, Belgium.

DE BATIST M., ARTEMOV Y., BEAUBIEN S., GREINERT J., HOLZNER C., KIPFER R., LOMBARDI S., MCGINNIS D., **NAUDTS L.**, SCHMALE O., SCHUBERT C., VAN RENSBERGEN P., ZUPPI G.M., THE CRIMEA PROJECT MEMBERS. The "Clathrate Gun" did not fire bubbles… 2nd Belgian Geological Congress, 07-08th September 2006, Liège, Belgium.

NAUDTS, L., GREINERT, J., ARTEMOV, Y., DE BATIST, M. Characterization of methane seep areas based on acoustic seafloor backscatter measurements. 17th International Sedimentological Congress, 27th August-1st September 2006, Fukuoka, Japan.

NAUDTS, L., GREINERT, J., ARTEMOV , Y., DE BATIST, M. Characterization of methane seep areas based on acoustic seafloor backscatter measurements. 3rd International Conference on "Minerals of the Ocean – Future developments, 19-23th June 2006, St. Petersburg, Russia.

POORT, J., NOLMANS, M., **NAUDTS, L.**, KHLYSTOV, O., SHOJI, H. Thermal features from the gas hydrate containing Kukuyu mud volcano, Lake Baikal. 3rd International Conference on "Minerals of the Ocean – Future developments, 19-23th June 2006, St. Petersburg, Russia.

NAUDTS, L., GREINERT, J., ARTEMOV, Y., DE BATIST, M., 2006. The use of acoustic seafloor backscatter measurements for quantitative and qualitative characterization of methane seep areas. *Geoph. Res. Abstracts*, 8, 09411.

NAUDTS, L., DE BATIST, M., GRANIN, N., KHLYSTOV, O., VAN RENSBERGEN, P., POORT, J., CRIEL, W., KLERKX, J., SONIC TEAM. Distribution of lacustrine gas seeps and mud volcanoes in Lake Baikal, Siberia. 4th Vereshchagin Baikal Conference, 04-09th October 2005, Irkutsk, Russia.

DE BATIST, M., HUS, R., CHARLET, F., **NAUDTS, L.**, SHERSTYANKIN, P., CANALS, M., CASAMOR, J.L., ALEKSEEV, S., THE INTAS 99-1669 PROJECT MEMBERS. New views on the morphology of the bottom of Lake Baikal. 4th Vereshchagin Baikal Conference, 04-09th October 2005, Irkutsk, Russia.

DE BATIST, M., **NAUDTS, L.**, CRIEL, W., KLERKX, J., POORT, J., VAN RENSBERGEN, P., GRANIN, N., CHENSKY, A., GNATOVSKY, R., KHLYSTOV, O., SONIC TEAM, INTAS PROJECT 2309 PARTNERS. Mud volcanoes, gas seeps and gas hydrates in Lake Baikal - A review. 4th Vereshchagin Baikal Conference, 04-09th October 2005, Irkutsk, Russia.

GREINERT, J., ARTEMOV, Y., MCGINNIS, D., **NAUDTS, L**. Bubble detection, monitoring and spatial flux quantification with multi and single beam systems: Case study from the shallow Black Sea. Annual Symposium of the Geophysical Society of New Zealand, 27-28th September 2005, Lower Hutt, New Zealand.

NAUDTS, L., DE BATIST, M. Reconstructing lake-level fluctuations based on seismic-stratigraphic analysis of stacked delta-lobe deposits in Lake Issyk-Kul, Kyrghyz Republic. Astrakhan Workshop, 18-21th September 2005, Astrakhan, Russia.

NAUDTS, L., GREINERT, J., ARTEMOV, YU.G., DE BATIST, M. Subsurface and morphologic setting of 2778 methane seeps in the Dnepr paleo-delta, northwestern Black Sea. VIIIth International Conference on "Gas in Marine Sediments", 05-10th September 2005, Vigo, Spain.

DE BATIST, M., ARTEMOV, Y., BEAUBIEN, S., GREINERT, J., HOLZNER, C., KIPFER, R., LOMBARDI, S., MCGINNIS, D., **NAUDTS, L.**, SCHMALE, O., SCHUBERT, C., VAN RENSBERGEN, P., ZUPPI, G.M., THE CRIMEA PROJECT MEMBERS. The clathrate gun did not fire bubbles… . VIIIth International Conference on "Gas in Marine Sediments", 05-10th September 2005, Vigo, Spain.

DE BATIST, M., **NAUDTS, L.**, CRIEL, W., POORT, J., VAN RENSBERGEN, P., THE SONIC TEAM, KLERKX, J., GRANIN, N., KHLYSTOV, O., DUCHKOV, A., DUCHKOV, A., OBZHIROV, A., CHENSKY, A., KAPITANOV, V., WUEST, A., MCGINNIS, D., THE INTAS PROJECT 01-2309 MEMBERS. Gas hydrates, mud volcanoes and gas seeps in Lake Baikal. VIIIth International Conference on "Gas in Marine Sediments", 05-10th September 2005, Vigo, Spain.

GREINERT, J., ARTEMOV, Y., MCGINNIS, D., **NAUDTS L**. Case studies of detection, flux quantification and modelling of methane bubble release at 90 to 2050 m deep cold seeps in the Black Sea. VIIIth International Conference on "Gas in Marine Sediments", 05-10th September 2005, Vigo, Spain.

NAUDTS, L., GREINERT, J., ARTEMOV, Y., DE BATIST, M., POORT, J., AND VAN RENSBERGEN P. Subsurface and morphologic setting of 2778 methane seeps in the Dnepr paleo-delta, northwestern Black Sea. International Workshop on Methane in sediments and water column of the Black Sea: Formation, transport pathways and the role within the carbon cycle, 17-22th May 2005, Sevastopol, Ukraine.

ZILLMER, M., BIALAS, J., IVANOVA, A., FLUEH, E.R., PLANERT, L., VON GRONEFELD, G., KRABBENHOEFT, A., MIDDAG, C., **NAUDTS, L.** Acoustic imaging of the Dvurechenskii mud volcano in the Black Sea. International Workshop on Methane in sediments and water column of the Black Sea: Formation, transport pathways and the role within the carbon cycle, 17-22th May 2005, Sevastopol, Ukraine.

NAUDTS, L., GREINERT, J., ARTEMOV, Y., DE BATIST, M. Subsurface and morphologic setting of 2778 methane seeps in the Dnepr paleo-delta northwestern Black Sea. IVth International Methane Hydrates Workshop, 9-11th May 2005, Victoria, Canada.

NAUDTS, L. Massive methane bubble release in the Dnepr paleo-delta, northwestern Black Sea: the geological and morphological context. Doctoraatssymposium Faculteit Wetenschappen, Ghent University, 3rd May 2005, Ghent, Belgium.

NAUDTS, L., GREINERT, J., ARTEMOV, YU.G., DE BATIST, M. Subsurface and morphologic setting of 2778 methane seeps in the Dnepr paleo-delta, northwestern Black Sea. *Geoph. Res. Abstracts*, 7, 06455.

GREINERT, J., ARTEMOV, Y., MCGINNIS, D.F., **NAUDTS, L**., LINKE, P. Methane fluxes from a high intensity seep area west of Crimea, Black Sea. *Geoph. Res. Abstracts*, 7, 03035.

NAUDTS, L., DE BATIST, M., GRANIN, N., KHLYSTOV, O., VAN RENSBERGEN, P., POORT, J., CRIEL, W., KLERKX, J., Sonic Team. Distribution of lacustrine gas seeps and mud volcanoes in Lake Baikal, Siberia. *Geoph. Res. Abstracts*, 7, 06636.

ZILLMER, M., BIALAS, J., IVANOVA, A., FLUEH, E.R., PLANERT, L., VON GRONEFELD, G., MIDDAG, C., **NAUDTS, L**. Acoustic imaging of the Dvurechenskii mud volcano in the Black Sea. *Geoph. Res. Abstracts*, 7, 02238.

VAN RENSBERGEN, P., **NAUDTS, L.**, GREINERT, J., ARTEMOV, Y., POORT, J., POPESCU, I., DE BATIST M., 2004. The role of gas hydrates and gas seeps in shaping the NW Black Sea margin. 32nd IGC Abs. Vol., part 2, Abstract 282-12, 1249.

GREINERT, J., ARTEMOV, Y., **NAUDTS, L.**, DE BATIST, M., CRIMEA PROJECT MEMBERS. Hydroacoustic manifestations of methane 'bubble' seeps in the Black Sea and approaches for a hydroacoustic methane flux determination. 7th European Conference on Underwater Acoustics, 5-8th July 2004, Delft, the Netherlands.

NAUDTS, L., GREINERT, J., ARTEMOV, Y., DE BATIST, M., 2004. Seismic and hydro-acoustic evidence for subsurface controls of methane seepage in the Dnepr paleo-delta, Black Sea. *Geoph. Res. Abstracts*, 6, 02591.

GREINERT, J., ARTEMOV, Y., **NAUDTS, L.**, DE BATIST, M., CRIMEA PROJECT MEMBERS. High Intensity Methane Seeps in the Black Sea: Hydroacoustic Manifestations. Oceanology International 2004, 16-19th March 2004, London, United Kingdom.

NAUDTS, L., GREINERT, J., ARTEMOV, Y., DE BATIST, M. Seismic and hydro-acoustic evidence for subsurface controls of methane seepage in the Dnepr paleo-delta, Black Sea. Informal conference on 'Methane seepage, mud volcanoes and gas hydrates in the Black Sea', 6th February 2004, Kiel, Germany.

BIALAS, J., IVANOVA, A., ZILLMER, M., V. GRONEFELD, G., PLANERT, L., FLUEH, E.R., **NAUDTS, L.**, MIDDAG, C. Wide angle seismic data experiments at active vent sites in the Black Sea. Informal conference on 'Methane seepage, mud volcanoes and gas hydrates in the Black Sea', 6th February 2004, Kiel, Germany.

APPENDIX B – LIST OF RESEARCH EXPEDITIONS

01.01.2010 - 02.03.2010	ROV expedition in Antarctica R.V.I.B. Nathaniel B. Palmer (10-01) Punta Arenas (CHL) – Punta Arenas (CHL)
15.06.2009 - 15.08.2009	Multibeam and submersible expedition on Lake Baikal R.V. TITOV/MIR-2 Listvyanka (RUS) – Listvyanka (RUS)
13.03.2009	Multibeam and seismic expedition on Belgian Continental Shelf R.V. BELGICA (2009/04) Zeebrugge (BEL) – Zeebrugge (BEL)
02.08.2008 - 11.08.2008	Heat flow and coring expedition on Lake Baikal R.V. VERESHCHAGIN Listvyanka (RUS) – Listvyanka (RUS)
01.03.2008 - 30.03.2008	Heat flow and coring ice-expedition on Lake Baikal Listvyanka (RUS) – Listvyanka (RUS)
26.01.2008 - 08.02.2008	Multibeam expedition on Lake Geneva R.V. LA LICORNE Versoix (CH) – Versoix (CH)
11.01.2007 – 23.03.2007	ROV, heatflow and coring expedition on Hikurangi Margin R.V. SONNE (191/3) Napier (NZ) – Auckland (NZ)
03.07.2006 – 06.07.2006	Seismic expedition on Belgian Continental Shelf R.V. BELGICA (2006/14) Zeebrugge (BEL) – Zeebrugge (BEL)
24.03.2006	Multibeam and seismic expedition on Belgian Continental Shelf R.V. R.V. BELGICA (2006/05B) Zeebrugge (BEL) – Zeebrugge (BEL)
17.09.2005 – 23.09.2005	Heat flow and coring expedition on Lake Baikal R.V. VERESHCHAGIN Listvyanka (RUS) – Listvyanka (RUS)
22.06.2005 – 24.06.2005	Multibeam expedition on Belgian Continental Shelf R.V. BELGICA (2005/15) Zeebrugge (BEL) – Zeebrugge (BEL)
28.02.2005 – 04.03.2005	Seismic expedition on Belgian Continental Shelf R.V. BELGICA (2005/04B) Zeebrugge (BEL) – Zeebrugge (BEL)
01.10.2004 – 06.10.2004	Bathymetry and coring expedition on Lake Baikal R.V. VERESHCHAGIN Listvyanka (RUS) – Listvyanka (RUS)

25.05.2004 – 23.06.2004	Multibean, heat flow and coring expedition on Black Sea R.V. Vodyanitskiy (60) Istanbul (TUR) – Istanbul (TUR)
25.05.2003 – 23.06.2003	Seismic, multibean, heat flow and coring expedition on Black Sea R.V. Vodyanitskiy (58) Istanbul (TUR) – Istanbul (TUR)

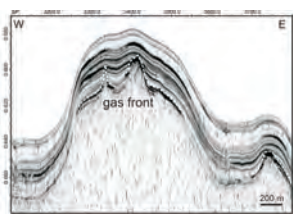
W
E
gas front
200 m

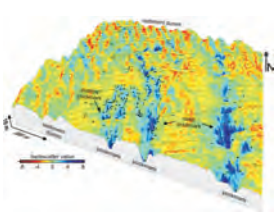

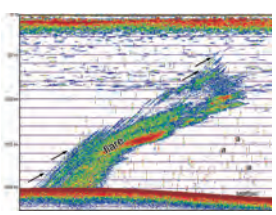
flare